MODELING AND OBSERVATIONAL STUDY OF THE DAYTIME EVOLUTION EAST OF THE CREST OF THE COLORADO ROCKIES

by

Paul G. Wolyn

Thomas B. McKee

Research was supported by
ARO Grant #DAAL03-86-K-0175
and NSF Grant #ATM-8713652.

Department of Atmospheric Science
Colorado State University
Fort Collins, Colorado
80523

April 1992

Atmospheric Science Paper No. 496

Climatology Report No. 92-1

ABSTRACT

MODELING AND OBSERVATIONAL STUDY OF THE DAYTIME EVOLUTION EAST OF THE CREST OF THE COLORADO ROCKIES

The west-east nature of the daytime evolution east of the Front Range of the Colorado Rockies in the vicinity of Fort Collins, Colorado is examined for conditions of clear skies, little change to the synoptic-scale wind and thermal fields, and light ambient winds with a westerly component (around $5ms^{-1}$). The observations mainly consist of airsondes launched at every 2-3 hours at sites on the eastern plains and on the east slope of the mountain barrier. A variety of two-dimensional simulations using the CSU RAMS are run with varying initial conditions that change the surface heating, ambient winds, ambient thermal structure, and barrier height. A full nighttime phase is simulated before the daytime phase.

From the observations and simulations a conceptual model of the daytime is developed. The sunrise state includes a strong jet down the east side of the barrier and a deep layer of stability to the east of the barrier. Phase 1 of the evolution lasts until 3-4 hours after sunrise and results from the weakening nocturnal flow interacting with the early daytime heating. Phase 2 has a solenoid which is not symmetric horizontally and which does not develop uniformly with time. Phase 3 is characterized by a solenoid which migrates eastward.

The variety of simulations show how the daytime evolution changes for the various initial conditions. Generally, the solenoid in phases 2 and 3 is weaker and shallower for moister soil (less surface sensible heat flux) on the plains east of the barrier, moister soil west of barrier crest, days closer to the winter solstice, stronger ambient winds, and a lower convective boundary layer (CBL) the previous day. The solenoid is generally deeper and stronger for less ambient stability and days closer to the summer solstice.

The usefulness of vertical integrals of heating and mass flux in the analysis of simulations and observations is explored in this study. These vertical integrals quantify the movement of energy and mass at different heights by the circulations, and they are very useful for comparing the strength and depth of the circulations among simulations and between the simulations and observations.

ACKNOWLEDGEMENTS

The authors would like to thank Dr. Richard Johnson, Dr. Jon Peterka, and Dr. Roger Pielke for their helpful comments with this manuscript. Special thanks to Odie Bliss for her enormous help with the preparation of this document. The figures were expertly drafted by Judy Sorbie-Dunn.

Numerous people have helped with the collection of field data. Thanks to Dr. David Changnon, Bernie Connell, Chris Cornwall, Dr. Steve Cox, Nolan Doesken, Chris Johnson-Pasqua, Jimmy Keener, John Kleist, Georg Mayr, Tom Merrill, Brad Nichols, Tye Parzybok, and Dr. Gene Wooldridge. Also, sincere thanks to the many people who have helped with the used of the CSU RAMS. These people include Dr. Jim Bossert, Keeley Costigan, Dr. Jennifer Cram, Tsengdar John Lee, Mike Meyers, Mike Moran, Dr. Craig Tremback, Dr. Bob Walko, and Dr. Doug Wesley. (Our apologies to anyone who helped with the observations and model that may have been overlooked). Special thanks to John Kleist for all his help with learning about the use of computers.

Paul Wolyn would like to extend a special thanks to his wife, Kathy, for her patience and support and for her help in editing the manuscript.

The CSU RAMS and its analysis package are run on the CRAY-YMP at NCAR. NCAR is supported by the National Science Foundation. The CLASS sounding system from NCAR was used to obtain the soundings in the Fall 1987 and Summer 1988. This work has been supported by ARO grant # DAAL03-86-K-0175 and NSF grant # ATM-8713652.

TABLE OF CONTENTS

CHAPTER 1.
INTRODUCTION

The diurnal evolution of the atmosphere east of the crest of the Front Range of the Colorado Rockies is very complex. Figure 1.1 shows a topography map of the Front Range of northeast Colorado and the eastern plains near Fort Collins, Colorado. The Front Range is a north-south barrier which frequently crests above 3600m mean sea level (MSL). Over a horizontal distance of 50 to 65km the barrier slopes downward to about 1500m MSL at the base of the barrier. On the eastern plains two east-west ridges are present. To the north the Cheyenne Ridge rises to over 1800m MSL, and to the south the Palmer Divide rises to over 2200m. The eastern plains gradually slope downward towards the east. The Cache la Poudre River flows southeastward out of Fort Collins and intersects the South Platte River at Greeley.

The diurnal evolution of the atmosphere in this region has profound influences on the horizontal and vertical movement of low level moisture involved in thunderstorm development. Air pollution in the major cities immediately east of the base of the Front Range of the Colorado Rockies is affected by the diurnal evolution. The wind and thermal patterns influence the movement and dispersion of potentially hazardous aerosols and gases associated with air pollution.

Many factors influence the daytime evolution of the airflow east of the crest of the Front Range of the Colorado Rockies. Air flowing over the Front Range can induce mountain waves and downslope windstorms. The daytime heating of the large north-south mountain barrier can induce circulations that extend far east of the barrier. Different patterns of surface heating due to snow cover or moisture differences (Segal et al, 1991, for

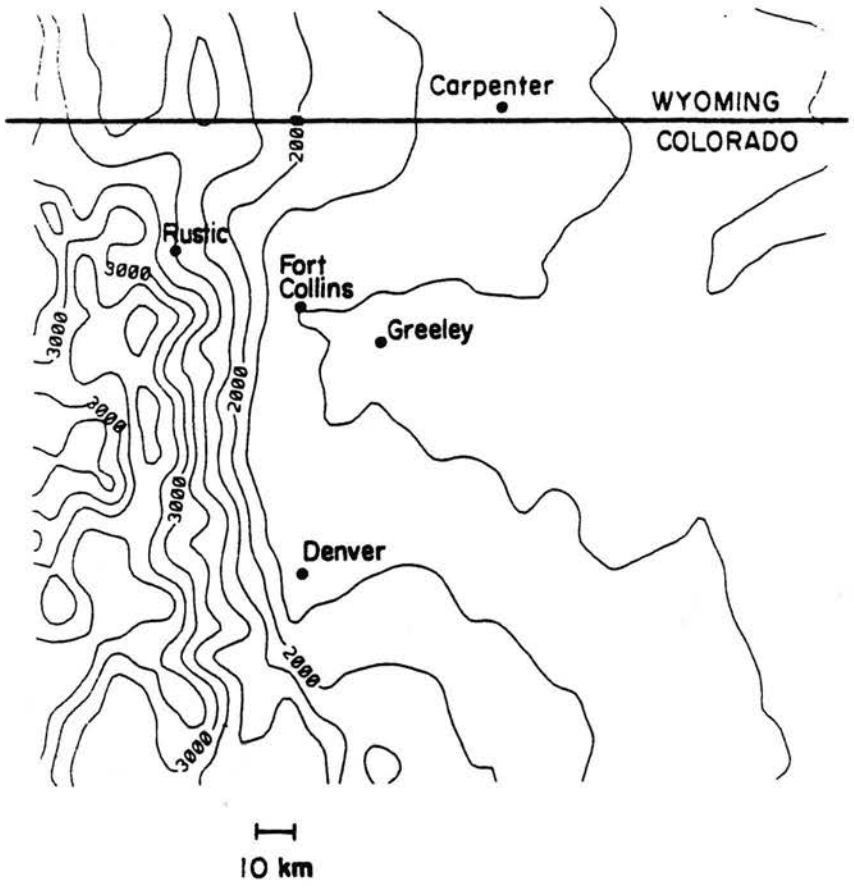

Figure 1.1. Topography map of northeast Colorado. Contour interval is 250m.

example) can cause circulations similar to sea breezes on the eastern plains. The daytime heating of the Cheyenne Ridge and Palmer Divide and air flowing over these ridges can further complicate the daytime evolution creating features such as the Denver cyclone (Crook, et al, 1991, for example), which is a mesoscale cyclonic circulation in the Denver area.

This present study will examine west-east structure of the daytime evolution of the atmosphere in the vicinity of Fort Collins, Colorado. The evolution is studied under weather conditions of clear skies, light westerly winds with a westward component of around $5ms^{-1}$, and little change in time and space of the synoptic-scale wind and thermal fields. These weather conditions are very unlikely to produce severe weather events such as strong thunderstorms, downslope windstorms, or snowstorms. The mountain-plains circulation generated by the heating/cooling of the large mountain barrier and gently sloping plain, interacting with the ambient flow, is the focus of this present study. The influence of the Cheyenne Ridge, Palmer Divide, and other north-south variations in topography are not taken into account in this study. The heating/cooling of the north-south barrier gently sloping eastern plains is the predominate forcing in the daytime evolution under most situations including the weather conditions in this study.

Two-dimensional simulations using the CSU RAMS (Colorado State University Regional Atmospheric Modeling System) and observations, mainly consisting of frequent airsonde launches, are used in this study. The CSU RAMS is run with a nighttime phase before the daytime phase is simulated. In the model runs condensation and precipitation are not allowed to occur, and a subgrid scale closure scheme for scalars and momentum is used that works well for the nighttime phase. A variety of simulations are run for many different initial conditions showing how different ambient winds, thermal structures, surface heating, and barrier height can affect the west-east nature of the daytime evolution. The simulations

are compared to the observations to examine how well the simulated evolution matches the observed evolution. In the comparison between simulations the usefulness of using vertical integrals of thermal and wind quantities is explored. The utility of frequent airsonde launches as an observational method and for the comparison of observations to simulations is also examined.

This dissertation has a literature review in chapter 2. In chapter 3 a "baseline" simulation is discussed in detail. Vertical integrals of thermal and wind fields are derived to provide insight into the evolution of the flow. After the evolution is discussed in detail for one simulation the evolution for many other simulations with differing thermal structures, wind speeds, surface heat flux, barrier height, and absence of nighttime phase is discussed in chapter 4. Chapter 4 uses several quantities derived from the vertical integrals to quantitatively compare the evolution in the different simulations. Chapter 5 discusses the observations of the daytime evolution and compares the simulations to the observations qualitatively and quantitatively. Using the observations and simulations, a conceptual model of the west-east nature of the daytime evolution east of the Front Range of the Colorado Rockies is presented in chapter 6. Chapter 7 summarizes the results and discuss avenues for future research. While this study concentrates on the daytime evolution in the vicinity of Fort Collins, Colorado, the results may be applicable to north-south mountain barriers of similar dimension.

CHAPTER 2.
LITERATURE REVIEW

2.1 Introduction

The daytime evolution of the atmosphere east of the Front Range of the Colorado Rockies in the vicinity of Fort Collins, Colorado involves both thermally driven flows and dynamically induced circulations. The nighttime cooling and daytime heating of the complex terrain leads to thermally driven flows. Circulations induced by air flowing over the barrier are important as well since the barrier height is over 2.0km. There have been many observational and modeling studies of the circulations in the mountains and the northeast plains of Colorado because of the interesting phenomenon which occur in this region and partly due to the large number of research meteorologists who live in this area.

Some of the past research on thermally induced flows in complex terrain is discussed in section 2.2. Section 2.3 describes some aspects of the dynamically induced circulations caused by flow over complex terrain. In section 2.4 observational studies of the diurnal evolution of the atmosphere over and east of a large mountain is presented. Section 2.4 first discusses studies which only examine surface and near surface observations, then observational studies which examine the evolution well above the surface are presented. Computer simulations of the diurnal evolution over and east of mountains are given in section 2.5. In section 2.6 the plateau circulations, which show the diurnal and seasonal influences of large mountain ranges on scales approaching the synoptic scale, are discussed. Section 2.7 mentions other influences of mountain barriers on the atmosphere. Finally, section 2.8 summarizes the main results of the literature reviews and lists how this present study contributes to the

understanding of the west-east nature of the daytime evolution east of the crest of the Colorado Rockies.

2.2 Slope and Valley Flows

The diurnal heating of complex terrain can induce flows which move in opposite directions during the daytime and nighttime. One group of thermally driven flows in complex terrain is slope flows. Atkinson (1981) provides a clear presentation of the basic theory of thermally driven slope flows describing the mechanism that occurs on the smallest of scales. The heating of sloping terrain occurs creates lower pressure at the same height than the unheated air away from the slope. This creates a horizontal pressure gradient that induces the air to move up the slope. At the same time, the heated air is not in hydrostatic equilibrium with the surrounding air and has a tendency to rise. The combination of the horizontal pressure gradient along the slope and the vertical pressure force induces the air to rise up along the barrier. The opposite occurs at night due to surface cooling. The magnitude of horizontal pressure gradient driving the upslope/downslope flow is proportional to the slope of the terrain and the magnitude of the heating (or cooling) of the air at the surface compared to the heating (or cooling) of the ambient air away from the slope.

Mahrt (1982) does a unified scale analysis for gravity/drainage flows. He performs a scale analysis of the equations of motion for nocturnal drainage flows along a slope. Using this scale analysis, he shows under what conditions the different terms are important, and he identifies eight regions in which different regimes for stationary flows can exist.

The detailed structure of shallow nocturnal drainage flows is important for dispersion of surface releases of pollutants. Rao and Snodgrass (1981) model the nocturnal drainage flow down a large homogeneous plane with a constant slope. This model uses a turbulent kinetic energy (TKE) based subgrid scale closure scheme which can produce vertical mixing

in stable conditions if the wind shear is sufficiently strong. The TKE is strongest at the surface, reaches a local minimum at the nose of the drainage flow jet and a secondary maximum above the jet, and goes to zero above this maximum. Their sensitivity analysis shows that as the slope of the terrain increases the temperature deficit in the jet increases, the wind maximum occurs at a greater height, and the winds above the wind speed maximum become faster. As the surface temperature deficit increases the wind at all levels becomes faster, the speed of the wind maximum increases, and the flow becomes deeper. The speed of the wind maximum varies directly with the magnitude of the surface cooling. As the surface roughness increases the maximum wind speed and depth of the flow decrease, and the atmospheric temperature deficit decrease.

Arritt and Pielke (1986) use a two-dimensional numerical model to study the interaction of ambient winds with nocturnal slope flows. Their model also uses TKE to calculate vertical diffusion. The speed of the drainage flow is larger for an imposed ambient $2ms^{-1}$ flow in the direction of the drainage flow than a $2ms^{-1}$ flow ambient flow in the opposite direction. The difference of the jet speed from the ambient flow, however, is larger for the imposed $2ms^{-1}$ wind against the drainage flow, because the shear is less for this case resulting in is less dissipation at the surface. Their paper states that the ambient winds cannot simply be added to the thermally driven nocturnal drainage flows to get the proper drainage flow speed and that the diffusion of TKE is important for allowing transport across the jet despite the vertical wind shear being zero at the wind speed maximum.

Another aspect of thermally induced upslope and downslope flow in complex terrain is the diurnal flows in mountain valleys. Defant (1952) shows a basic conceptual diagram of the evolution of thermally induced flows in mountain valleys. The mountain valleys have two related flows. One flow is up or down the sides of the valley and is called the sidewall flows. The second major flow is up or down the valley axis and is called the along valley flows.

During the night the sidewall flows are down the side slopes of the valley, and the along valley flow is down the valley axis. As the daytime heating begin the sidewall flows first flow up the slope. As the heating continues the along valley flow reverses to up the axis of the valley. The transition form the daytime to nighttime circulation has the sidewall flows become down the sidewalls of the valley before the along valley flow becomes down the valley axis.

The flows up and down the side slope of the valley influence the daytime and nighttime thermal and wind structure of the valley. For the daytime Whiteman (1980) and Whiteman and McKee (1982) show that the developing sidewall flows move from the bottom of the valley up the sidewalls. The inversion in a deep mountain valley is destroyed by both heating of air at the surface and the movement of the air up the sidewalls which causes the pool of cold air in the valley to sink. Bader and McKee (1983) simulate the upslope flow in a deep mountain valley. The flow up the sidewalls initially does not extend throughout the depth of the valley. As parcels heated near the surface rise up the sidewalls, the heating from the side slope can not compensate the adiabatic cooling, and the parcels became negatively buoyant. These parcels leave the sidewalls and flow towards the center of the valley. As the heating continues the sidewall flows become continuous up the side slopes of the valley.

McNider (1981) and McNider and Pielke (1984) model the nighttime flows in deep mountain valleys. Their simulations show that the down valley flow is a secondary flow which results from the drainage winds along the sidewalls of the valley. Cold air fills the valley to near valley top, and this cold air creates the pressure gradients that drives the down valley flow. The cold air fills the valley through lifting caused by convergence of the flows down the two opposing sides of the valley.

2.3 Dynamically Induced Circulations by Flow over Mountains

As air passes over a mountain its motion is influenced by the topography. With stable static stability, as the air ascends over the barrier it tends to return to its original height after it passes over the barrier. Smith (1979), in this review article, shows the development of the basic equations for two-dimensional flow over mountainous terrain using a steady state, adiabatic set of equations. The equations are solved for perturbation quantities in a hydrostatic, steady state which only varies with height. If the Bousinesq approximation is made, the equation for mountain waves becomes:

$$\frac{\partial^2 w}{\partial x^2} + \frac{\partial^2 w}{\partial z^2} + l^2 w = 0. \tag{2.1}$$

$$l^2 = \frac{N^2}{U^2} + \frac{1}{U}\frac{\partial^2 U}{\partial z^2} \tag{2.2}$$

where l^2 is the Scorer parameter. The Scorer parameter is the fundamental factor which determines whether mountain waves will exist.

Gill (1982) lists several different flow types depending on the Scorer parameter and the wavelength of the topography. The flows are given for an atmosphere with a vertically uniform wind speed (du/dz=0) and vertically uniform stability (N constant with height) flowing over a Witch of Agnesi mountain. The Witch of Agnesi mountain is given by:

$$h(x) = \frac{h_m a^2}{(x^2+a^2)} \tag{2.3}$$

where h(x) is the height, h_m is the maximum height of the mountain, and a is a measure of the mountain's width. The equation for the mountain has a Fourier transform of:

$$\frac{1}{\pi}\int_{-\infty}^{\infty} \frac{h_m a^2}{(x^2+a^2)} e^{-ilx}\, dx = h_m a\, e^{-la} \tag{2.4}$$

For **a/l** significantly less than 1 potential flow occurs and mountain waves do not exist. For **a/l** ~ 1 non-hydrostatic mountain waves occur. For **a/l** significantly larger than 1 hydrostatic mountain waves exist. Hydrostatic mountain waves commonly occur for air flowing over large mountain barrier and are the basis for studying many mountain wave phenomenon including downslope wind storms. The vertical wavelength of hydrostatic mountain waves is $\frac{2\pi}{l}$.

Downslope windstorms are an important consequence of flow over large mountain barriers. There are three prominent theories for downslope wind storms. One theory is related to hydrostatic mountain waves and layers of differing stability in the atmosphere. Klemp and Lilly (1975) use a three layer atmosphere to study the influence of differing stability and wind shears in each layer on downslope windstorms. The lowest layer extends to just above mountain top, the second layer extends to the tropopause, and the third layer is above the tropopause. Using linear theory and no shear they found that the atmosphere is "tuned" for downslope wind storms when the vertical depth of the lowest two layers is 1/4 a vertical wavelength of the mountain wave. The speed and location of the wind maximum is very sensitive to the depth of the lower layer and less sensitive to the depth of the middle layer because this layer is deeper. They also examine the effects of vertical wind shear. Shear has little influence on the wind maximum, and shear subtly changes the optimum depth of the layers for maximum wind. They use a three layer model for 51 observed windstorm cases and found fairly good agreement between the model and observations. The model overpredicts the wind maximum for winds greater than 40ms^{-1}. They comment that since the

model has isentropes into the surface, non-linear influences must also be taken into account when studying windstorms.

The second theory for the existence of downslope windstorms is most recently described in Clark and Farley (1984). The breaking of waves create adiabatic regions through which waves cannot vertically propagate. This layer reflects energy from the surface back towards the surface amplifying the speed of the winds. They use a nested grid model with a deformation subgrid scale closure scheme to perform two-dimensional and three-dimensional simulations. The three-dimensional simulations have two-dimensional topography (the same in the cross barrier direction) and cyclic boundary conditions in the cross barrier direction. These simulations allow for turbulence to exist in three dimensions. The two-dimensional and three-dimensional simulations, which have the same topography and initial conditions, agree well until breaking of waves begin. The breaking of the waves produces gustiness in the surface wind half to three-quarters down the eastern side of the barrier. The gustiness is produced by the build up of a region of convective instability with the subsequent breaking down of the instability through convective motions, and this process causes the leading edge of the steep isentropes to move back and forth. The model produces a 15 minute variation in winds similar to observation but not the 1 minute variation seen in the observations. Winds gusts are 15-20ms^{-1} greater than the observations, and other factors such as moisture, 3-D nature of the barrier, and spatial resolution can cause the differences between the simulations and observations.

The third major theory for downslope windstorms is most recently described in Durran (1986). He performs simulations of a two layer fluid over a relatively high "Witch of Agnesi Mountain" with a more stable layer of air to just above barrier top and a less stable layer above it. The flow in the lower layer continues to accelerate as it passes over the mountain, similar to a hydraulic jump. A hydraulic jump in a fluid, such as water, occurs when the flow

goes from supercritical to subcritical as it passes over the barrier. As the air passes over the barrier, it constantly converts potential to kinetic energy a causing the strong wind acceleration.

Richard et al (1988) uses a two-dimensional hydrostatic model with TKE based subgrid scale K closure, bell shaped mountain, and no surface heat flux to simulate the Jan. 11, 1972 Boulder windstorm. This study examines the influence of surface friction on the windstorm. With surface friction the development of the strong winds along the lee slope is delayed, and the "jumplike" structure remains stationary. With no friction this structure propagates down the slope. Inclusion of friction makes the simulations agree better with data. The model shows two areas of TKE production: near the ground above the lee slope and a few kilometers downstream of the crest. The main production of TKE is at 6km mean sea level (MSL) and is due to shear. Buoyancy production is small and mainly negative. Increasing roughness length delays the amplification, but has little influence on the final state.

Lee et al (1989) model the effects that a cold pool east of a 2km high barrier with a half width of 20km has on mountain waves. In a simulation without a cold pool wave overturning occurs and a strong windstorm is present east of the barrier. When a cold pool is inserted east of the barrier crest with a wind speed in the cold pool of $10ms^{-1}$ towards the barrier, the mountain wave has a smaller amplitude and no windstorm occurs. When the cold pool is replaced by topography of the same height, the simulation is very similar to when the cold pool is present. In the simulation with the cold pool turbulence is not sufficiently strong to erode the cold pool from the top. In fact, the turbulence strengthens the inversion at the top of the cold pool. With winds of $5ms^{-1}$ towards the barrier in the cold pool some eroding of the cold pool occurs, but the stronger winds do not erode through to the surface.

Mountain waves and downslope windstorms are examples of dynamically induced flows affecting the atmosphere over and to the east of barriers. Smith (1989) further examines

hydrostatic flow over a three-dimensional bell shaped mountain. He includes barrier shape as well as barrier height, wind speed, and stability to determine the flow type. Besides investigating the conditions under which potential flow (no mountain waves) and mountain waves exist, he examines the conditions under which wave breaking and flow splitting occurs. Wave breaking and flow splitting are not accounted for in linear theory. As the aspect ratio of the mountain (the length of the barrier perpendicular to the flow divided by the length parallel to the flow) increases, wave breaking occurs for lower barrier height, weaker stability, and stronger winds.

Smolarkiewicz and Rotunno (1989) examine inviscid, uniformly stratified, non-rotating flow past a three-dimensional bell-shaped mountain using the model of Clark and Farley (1984) with special concern for where the Froude number is less than one and linear theory does not apply. The main impetus for the study is the lee vortices observed in Hawaii. Smolarkiewicz and Rotunno (1990) continue the study using the same model with bell shaped topography with an elliptic horizontal cross-section. These studies examine the flow for atmospheric conditions where linear theory does not apply. Smolarkiewicz and Rotunno (1989) discover that lee vortices appear as the Froude number decreases from 2.2. Flow stagnation occurs when the Froude number reaches 0.5, and for very small Froude numbers the flow becomes nearly horizontal. As the Froude number is decreased from 1.0, Smolarkiewicz and Rotunno (1990) show that linear theory and the model agreed on the location of the stagnation point despite linear theory being invalid. As the cross flow axis of the mountain becomes larger, the lee vortices become larger and displace downstream and toward the lateral edges. Furthermore, as the cross flow axis of the mountain becomes larger the decelerated flow extends further upstream, and the vertically propagating gravity waves upstream of the obstacle tilt more vertically.

2.4 Observations of the Diurnal Evolution Over and East of Mountains

The discussion of the observational studies of the diurnal evolution of the flow over and east of mountains is divided into two sections. The first section presents studies of the observed evolution at the surface or near surface. This section concentrates on the observed evolution in northeast Colorado which has the PROFS network of over 10 surface stations and the 300m high BAO tower. The second section presents studies with observations taken above the surface, mainly using airsondes or aircraft data.

2.4.1 Surface and Near Surface Observations

Several studies of the surface and near surface evolution of the atmosphere on the plains of northeast Colorado use the BAO tower or the PROFS mesonet stations. Hahn (1981) studies the wind and thermal structure at the BAO tower for 8 days without clouds or strong winds. On days with light geostrophic winds, the winds shift to westerly shortly after sunset. The maximum speed occurs at around 50m above ground level (AGL), and the maximum never occurs above 100m. Throughout the night the v-component has weak southerly flow. The air above 100m does not cool until shortly after midnight which she suggests is due to shear inducing the cold air to mix upward.

On days with easterly geostrophic winds a drainage flow develops after sunset. Strong shear is present above the drainage flow, and the Richardson numbers are 0.1 at 100-150m AGL. Later in the evening the easterly and westerly flow weaken due to strong mixing, and a near a adiabatic layer is present above 50m. The hodograph of the 300m AGL winds suggests an inertial oscillation is present. On days with southerly geostrophic winds the 300m hodograph shows a large and rapid increase in wind speeds before sunset, rapid clockwise rotation until midnight, then counterclockwise rotation until noon. The winds at different layers are decoupled and are significantly influenced by other forces besides the coriolis force.

Hootman and Blumen (1983) use the BAO tower and data from the Boulder wind network, which includes five locations that measure the wind at 7m AGL (except 28m at NOAA-ERL), to study the nighttime drainage flow on undisturbed nights. The drainage flow reaches the BAO tower 83% of the time when drainage flow is observed at a site very close to the foothills, and there is some correlation between the speed of the flow at the near-foothills site and whether the drainage flow reaches the BAO tower. The leading edge of the drainage flow passes the BAO tower like a front with an increase in the speed of the westerly flow in the lowest 150m, a temperature drop of 5.5°C in 10 minutes at 10m, and the leading edge of the flow sloping upward and to the west. After the drainage flow front passes there is significant temperature fluctuations at 10m with less fluctuation above 10m. A well defined turbulent boundary is seen for 20 minutes after the front passes, and little turbulence is observed above 150m throughout this period. A steady state is reached 30-90 minutes after the passage of the front at the BAO tower.

Smith and McKee (1983) examine the PROFS temperature and wind data for three days in the Autumn of 1981. At sunrise there is general drainage flow down the east side of the high mountains to the west, as well as flow away from the crest of the Cheyenne Ridge and Palmer Divide. During the morning the upslope winds first begin along the foothills and expand eastward onto the plains. Upslope flow develops along the Cheyenne Ridge, and downslope winds still are present along the north side of the Palmer Divide because the synoptic scale winds opposes the development of upslope flow. By six hours after sunrise upslope flow occurs everywhere in the region except the extreme eastern plains.

The nighttime evolution has downslope winds in the mountains, foothills, and the northern side of the Palmer Divide by one hour after sunset. By three hours after sunset drainage winds occur at all sites except the lowest parts of the South Platte River Valley. When the 0500 Mountain Standard Time (MST) temperatures at the PROFS stations are

compared to the Denver sounding, the change in temperature of the PROFS stations with elevation agrees well with the change of the Denver sounding temperature with height. The PROFS temperatures generally are cooler than the Denver sounding temperature at the same height.

The warmest PROFS temperatures occurred at about 1829m (6000 feet) MSL. The daytime maximum temperatures generally occur between 1330 and 1500 MST on the plains and in the foothills, and the high mountain stations have a maximum temperature close to noon. The maximum temperatures are not correlated with elevation below 1829m and are well correlated with elevation above 1829m with a linear decrease of 8.2°C/km (4.5°F/1000 feet).

Toth and Johnson (1984) evaluate vector averaged winds for July 1981 from the National Weather Service and PROFS stations on the eastern plains of Colorado with winds that differed by more than two standard deviations removed from the average. The vector averaged winds have drainage flow from 0200 to 0500 MST with confluence in the South Platte River Valley and diffluence over Cheyenne Ridge and Palmer Divide. At 0800 MST upslope develops at the western stations but not at the high altitude stations. By 1100 MST upslope is present at all locations except the highest stations, and by 1300 MST upslope also occurs at the highest stations. At 1600 MST there is an indication of reversal to downslope winds at the most western stations which are located high in the mountains. At 1700 MST the westerly downslope flow expands eastward to just east of the base of the foothills. By 2000 MST the confluence associated with the westerly flow meeting the easterly flow moves east of Keensberg. At night southerly flow is seen well east of the barrier.

The change from upslope to downslope and visa versa moves eastward from the foothills and the upslope to downslope transition takes 4-5 hours while the transition from downslope to upslope takes about 3 hours. The only significant difference the synoptic winds

have on the evolution is that the upslope to downslope transition begins 1-2 hours earlier for westerly synoptic winds. The convergence zone, seen in the vector averaged winds, which moves off of the mountains late in the afternoon matches the climatological secondary maximum in thunderstorms in the High Plains. Several stations, especially those in the South Platte Valley, have a prominent clockwise turning of the wind.

2.4.2 Deeper Atmospheric Observations

The studies discussed in the previous section mainly concentrate on the surface or near surface diurnal evolution of the atmosphere east of the Colorado Rockies. In this section studies of the diurnal evolution over greater depths of the troposphere are given and several of these studies do not occur in northeast Colorado.

One of the earliest reports of the deeper atmospheric thermally induced circulations near large terrain features is presented in Defant (1952). His article describes the thermally driven circulation near the Alps. During the daytime heating causes air to flow up the slope of the Alps, and air over nearby flatter terrain also flows towards the Alps. Above the upslope flow return flow away from the Alps occurs. Sinking motion over the flatter terrain near the Alps completes the circulation. During the night cooling induces flow away from the Alps near the surface producing a circulation in an opposite direction to the daytime flows.

Braham and Draginis (1960) report on the morning evolution of a convective core over the Santa Catalina Mountains north of Tuscon using research aircraft data. The mountains rise to over 2743m (9,000 feet) from surrounding terrain of 914m to 1219m (3,000 to 4,000 feet). By 1000 MST a 2 mile wide convective core appears which extends to 4267m (14,000 feet) MSL. The convective core is warmer and moister than the surrounding air at 3048m (10,000 feet). At 3353m (11,000 feet) the convective core has a colder temperature

(actual and virtual) than the warmer air in the apparent region of downward motion around the core. At 3658m, 3962m, and 4267m (12,000, 13,000, and 14,000 feet, respectively) the convective core is colder than the undisturbed surrounding air. Assuming conservation of moisture, they calculate that the air ascends 2.0-2.6km up the slope before rising into the cold core. The upwind edge of the cold core is "sharp" while the downwind edge is more diffuse with an irregular pattern of potential temperature and mixing ratio downwind of the cold core.

By 1040 MST the air in the convective core is heated 3-4 K from its source region along the slopes of the mountain. (The source region is identified assuming conservation of mixing ratio). Their explanation for the development of the cold core is that air heated along the slopes remains close to the mountain until it reaches mountain top. The heated air is buoyant until about 3658m (12,000 feet) because of its higher virtual temperature. The heated air continues to rise above the layer where it is positively buoyant, because the heated air cannot spread out quickly enough. The overshooting air creates a core of air colder than the ambient atmosphere.

Raymond and Wilkening (1980) also study dry or nearly dry convection over mountains using aircraft data. Their observations are made in New Mexico over the San Mateo Mountains, which rise 1km above a plain that is 2km MSL. The convergence near and below barrier top is $5 \times 10^{-4} s^{-1}$, and the divergence in the upper levels is about half as large. A mean updraft speed of $0.5 ms^{-1}$ is obtained from the convergence and divergence. The inflow is nearly circular while the outflow above it takes the form of a wake. The mesoscale updraft is 10-20km wide and about 2-3km deep, and it does not resemble a plume. The wavelength of the vertical circulations in the convective core over the mountain is 3-4km. The inflow air is about 2°C warmer and $1.5 gkg^{-1}$ moister than the outflow air. The aircraft shows that the vertical turbulent heat flux is negative in the upper levels, and in the lower

layers it is as strong but positive. The vertical turbulent latent heat flux increases with height. Their observations show that moderate ($5ms^{-1}$) low level winds can suppress the type of flow discussed, and stronger winds well above the peak have little effect except to modify the form of the outflow.

Tyson and Preston-White (1972) examine the daytime and nighttime flows along Natal, which is a province of South Africa that borders on the Indian Ocean. The study region has a 3000m high escarpment which slopes downward to the Indian Ocean 200km to the east. There are imbedded river canyons which frequently are greater than 500m deep. When local valleys do not have the same orientation as the general slope, the regional-scale mountain-plains flow is still more a function of the overall slope than the local slopes in the valleys. A common night flow pattern has local drainage flows present beneath the more regional mountain-plains circulation. They comment that the flow is very similar to the flow east of the Rocky Mountains with a low-level nocturnal jet along the coast.

Wetzel (1973) uses sounding data from the National Hail Research Experiment (NHRE) and other data to study the daytime evolution in northeast Colorado east of the continental divide between the Cheyenne Ridge and Palmer Divide. The sounding data is averaged by levels and is divided into one-third dry days, one-third moderate precipitation days, and one-third wet days. Discontinuities in winds occur at 740mb and 540mb. The low level winds (surface to 740mb) have diurnal direction changes of 60-150 degrees. On dry days the winds are west to northwest in the day, and not until late in the afternoon are they weak easterly. On moderate precipitation days a mountain-plains solenoid occurs with the winds near the surface being of equal strength in the morning and afternoon. On the wet days east to southeast winds persist throughout the day and the speeds are stronger.

In the middle layer (740 to 540mb) the greatest shear occurs on moderate precipitation days. The shear may result from mechanical mixing as the air passes over the

mountain, air accelerating into low pressure in the east, or warm air advection from the west producing veering of the wind with height (as seen in the thermal wind). In the upper layer (540mb and above) the winds have little diurnal change and are stronger on wet days.

Temperature discontinuities also occur at the levels of the wind discontinuities. The top of the nocturnal inversion exists at about 740mb. During the day a noticeable inversion or temperature discontinuity exists at 540mb. The moisture fields show drying in the middle layer in the morning and moistening in the afternoon. Above 540mb the moisture is constant until midafternoon, and a strong jump in the moisture occurs up to one hour before storm time.

From analysis of the sounding data he concludes that the 740mb level, which is 1.25km above the surface on the high plains, may be the top of the convective boundary layer (CBL). The 540mb level, which is 1km above barrier top, is the top of a layer which likely is frictionally mixed as it crosses the barrier. The increased moisture in this layer results from evaporation on the mountain slopes. The near neutral lapse rate in the middle layer may be due to mechanical mixing as the air passes over the mountains. On two-thirds of the days a solenoid circulation is present.

Banta and Cotton (1981) study the daytime evolution in the South Park area of Colorado in July and August 1977 using tethersondes and PAM (Portable Automated Mesonet) station data taken during the South Park Area Cumulus Experiment (SPACE). The barrier is about 1.0km higher than the bottom of South Park. They closely study 2 dry days in August, and three regimes in the wind patterns appear. On August 8 nocturnal drainage flow occurs until about 0830MST when the daytime upslope begins. Dewpoints increase by 1-2°C near the surface as the cooler, moister air advects into the region from the east. At 1000MST a westerly gradient wind appears. Associated with the appearance of the gradient wind is a decrease in the dewpoint and a "leveling off" of the temperature. Similar

events occur on another day but the changes occur later. On August 7 tethersondes launches show a 250m deep inversion with drainage flow at sunrise, and above the inversion an adiabatic layer containing synoptic-scale winds is evident. One hour later, the surface winds are upslope. Later in the morning a shallow CBL appears in the colder air at the surface, and the winds turn more up valley than upslope. When the surface inversion is finally eroded, the westerly winds that are above the inversion reach the surface, and a deep neutral layer is present.

Banta (1984) further analyzes the observational data of the daytime evolution in South Park. In the early morning the isentropes near the surface tend to slope along the mountain, while beginning at 1.0km above mountain top the isentropes are nearly horizontal. On most days the initiation of the upslope flow occurs at nearly the same time at sites on the slope and in the valley. On some mornings the upslope flow appears to expand up the slope. He develops a four phase conceptual model of the evolution. Phase 1 has a cold pool in the valley with a neutral layer above it. Along the east side of the barrier the isentropes near the surface are nearly parallel to the sloping terrain. In phase 2 daytime heating generates upslope flow in the cold pool with cold air advection in the upslope flow. Phase 3 has a deepening CBL in the cold pool. A convergence zone is evident where the wind changes from upslope to downslope. To the west of the convergence zone the CBL is much deeper, while to the east the CBL developing in the cold pool is much shallower. This convergence zone moves eastward during this phase. In phase 4 the cold pool is completely dissolved, and potential temperature gradients of about 1K exist between the deep CBL over the ridge and over the plains.

Hahn (1980) examines the turbulence in the boundary layer over South Park as well as thermal, moisture, and wind fields from aircraft data, supplemented by other data taken in SPACE of 1977. He studies two days with vigorous convection and two days with

suppressed cumulus activity and westerly flow reaching the ground. The "dry" days have stronger winds (17ms^{-1}) at 500mb with strong inversions around 450-490mb which delays the development of the convection. During the morning the warmest location is on Sheep Ridge which is a 400m high ridge on the west side of South Park and east of the 1000m high barrier. Stronger vertical motions are present around this higher barrier due to the strong ambient flow passing across the barrier. On the dry or windy days a wave is seen over this barrier. The aircraft turbulence data shows that shear production, and not buoyancy, is the largest source of TKE at higher levels. This is opposite to a CBL over flat terrain where buoyancy is the greatest source of TKE. With daytime heating upslope motion occurs in South Park with rising motion over Sheep Ridge, and through these circulations the air is able to mix through the cold pool later in the day. Westerly flow reaches the surface when the potential temperature of the air near the surface obtains the potential temperature of the air above it.

Cotton et al (1982) discuss an evolving thunderstorm in South Park during SPACE of 1977. Thunderstorm evolution first occurs in favored locations. By 1530 MST drier upslope air from the plains enters the region indicating that the South Park region has created a thermal low. The convergence lines in South Park are influenced by the outflow of cooler air from thunderstorms to the north. The line moves across the valley and by 1830 MST one main thunderstorm is present.

Cotton et al (1983) study the generation of a mesoscale convective complex (MCC) on August 4, 1977 using SPACE data. The main synoptic features include a cold front stalled over Colorado with the easterly flow not being able to make it over the Front Range, upper level moisture advection from the west, and warm air advection based on the 500-850mb thickness. Upslope winds develop in South Park after sunrise and are about 3ms^{-1} making the stability fairly uniform laterally. Unlike Banta (1981) the westerly winds do not appear to mix down toward the surface. Before the first convection begins the tethersonde launches show

a shallow, moister CBL which is cooler than the ridge top temperatures. The first convection does not appear until 1100 MST, with the tethersonde profiles showing a well mixed profile. The moisture that forms the first thunderstorms is residual moisture that remains in South Park from the previous night.

Schneider (1991) examines instrumented aircraft, micrometeorological tower, and surface network data in her study the daytime CBL evolution over the eastern plains of Colorado near Boulder. The data is taken during the PHOENIX II field project. The observations are taken from 1200 to about 1800 MST and the data analysis concentrates on June 17 and June 22, 1984. The mountains strongly influence the CBL development, and the CBL structure is complicated by gravity waves above the CBL. The CBL is capped by a 500m to 1000m deep layer of weak stability instead of a capping inversion. This layer has significant vertical wind shear with turbulence and waves. Warming in the CBL is not associated with local surface heating. The mountains are believed to have acted as an elevated heat source with a horizontal temperature gradient of $0.015 Km^{-1}$ occurring with easterly winds at the surface. Because of the heating over the mountain, there is sustained shear in the lowest 4km. The cumulus present do not appear to be associated with the lower boundary layer.

2.5 Simulated Evolution Over and East of Mountains

The observations of the diurnal evolution of the atmosphere over and east of mountains show a very complicated evolution resulting from the thermal heating interacting with the ambient winds and thermal fields. With this complex evolution computer models have been used to further understand the evolution of the atmosphere near large mountains. This section discusses modeling and combined model and observational studies of the diurnal evolution near large mountains.

Orville (1964), using a two dimensional, vorticity, incompressible model, examines the daytime development of the atmosphere along a 1km high, 2km wide mountain. He simulates the evolution with a neutral stability and with $d\theta/dz$ of $1Kkm^{-1}$. For the neutral case a thermal bubble forms over the mountain top lifting the isentropes. The vortex rises up the slope throughout the day, with the center of vortex moving away from the barrier. For the more stable case, the development is less regular. A solenoid initially develops over the lower portion of the slope of the mountain. As the heating continues another circulation center develops higher on the slope, and the center of the circulation "jumps" up the slope of the mountain as the circulation center over the lower portion of the slope dissipates. The center of the vortex does not move away from the barrier, and the stable case develops one-third to one-half as fast as the neutral case.

Orville (1965) adds moisture, a sinusoidal evaporation function, and a sinusoidal heating function to the model in Orville (1964). He simulates five cases: case (a) has the same stability as in the slightly stable run in Orville (1964) (similar to what Brahm and Draginis (1960) observed); case (b) has temperature and water vapor typical for a rainy day near Tuscon, Arizona; case (c) changes the mountain slope from 45 to 26 degrees; case (d) has no evaporation at the surface; and case (e) has a larger eddy diffusion coefficient and otherwise is the same as case (b). In case (a) the circulation develops 30% faster than Orville (1964). The trajectory of the circulation center, amount of vorticity, temperature excesses, and slope winds are almost the same as in the previous paper. He attributes 20 to 25% of the increase in speed of development to moisture buoyancy effects. At the top of the barrier there is a mushroom shaped region of moisture. Case (b) has greater stability and water content than case (a). A cloud forms at barrier top later than case (a) and a second surge in cloud growth occurs. The center of the vortex is closer to the mountain top than the other cases. Case (c) does not differ much from case (a). The magnitude of the stream function

is slightly less than case (a) and the cloud forms 100m lower. In case (d) the stream function is 10-15% greater than the "dry case" in Orville (1964) and lags case (a) by the same percentage. In case (e) clouds form 30 minutes later and there is broader upslope flow than case (b).

Orville (1968), using a similar model to the two previous studies, examines the effects of wind and wind shear on the daytime evolution east of a 1km high, 2km wide mountain. The simulations have $d\theta/dz$ of $2.8°Ckm^{-1}$. In a simulation with no initial winds, the surface air over the mountain is warmer than over the plains. A cold core, which is similar to the convective core in Brahm and Draginis (1960), develops over the mountain, and there is subsidence on either side of the mountain over the flat terrain. The vorticity increases with heating and continues to increase as long as the surface heating is greater than the cooling of the air above it. Another simulation has a linear wind shear of $2.5ms^{-1}km^{-1}$ above barrier top with no winds below barrier top. The development of the downwind circulation is quicker than the no wind case, and on the upwind side of the barrier the wind speeds increase. The maximum in potential temperature and moisture have less areal extent than the no wind case, and the maximums are shifted downwind. Cloud development is slower than the no wind case, and he hypothesizes the slower development may be due to shear tilting updrafts, the upper boundary conditions increasing shear as convection squeezes flow between cloud and model top, or packing of isentropes above cloud top creating a very stable atmosphere which further restricts cloud growth. Comparison of several simulations show that the shear is the main factor for slowing the cloud growth. In a simulation with a mountain wave the cloud development is quicker than the previous cases and no cold core is evident above the mountain top. The circulation cells experience strong vertical shear near barrier top and cannot penetrate far above the ridge top. Increased moisture appears to be flowing over the eastern plains above barrier top with a moisture inversion present below barrier top.

Dirks (1969) models the evolution east of a 1.75km high and 35km wide triangular-shaped mountain. A sinusoidal surface heating function and vertical turbulence parameterizations based solely on grid spacing are used. Slight differences appear between a simulation with calm winds and an adiabatic lapse rate and a simulation with calm winds and $d\theta/dz$ of $1Kkm^{-1}$. Both simulations produce upslope flow on the east side of the barrier with a region of subsidence over the plain to the east. For the weak stability case the magnitude of the sinking motion over the plains is less, and it extends to 50-75km eastward from the base of the slope. For the adiabatic simulation the flow only extends 15-20km east of the base of the slope. In a simulation with $d\theta/dz$ of $2.5Kkm^{-1}$ the movement of the vortex center up the slope is much less than the previous cases, and stronger sinking over the eastern plains occurs. The intensity of the low level circulation remains the same as the two previous cases. In a simulation with weak stability ($d\theta/dz$ of $1Kkm^{-1}$) and a wind shear of $2ms^{-1}km^{-1}$, the vertical movement of the solenoid up the slope is greater than in the other simulations, and the shear enhances the strength of the solenoid. A simulation of the nocturnal evolution with wind shear shows that sinking motion develops over the barrier with the westerly surface flow existing at least 75km east of the base of the barrier.

Liu and Orville (1969) use a similar model as Orville (1968) with approximations for cloud shading and precipitation to model the daytime evolution in the vicinity of a 1km high mountain with slopes of 45 degrees. The model has a domain 7km wide and 3.5km high. Before clouds develop there is a slight suppression of the CBL east of the barrier with increased moisture to the east of the barrier near barrier top. One cloud forms and moves east. A second cloud, which is shallower and has a weaker updraft, develops over the ridge, and the shading of the clouds weakens the thermal circulation. The weakened circulation allows the westerly winds to influence the lower part of the model, creates tilting to the clouds, and causes the clouds to move out of the domain more quickly. With no ambient

winds two clouds develop and dissipate fairly quickly, and later in this simulation shading from the other clouds that develop creates a reverse thermal circulation over the mountain.

Orville and Sloan (1970) have a 1km high mountain in the middle of a 10km wide domain with specified surface temperature and moisture. At 95 minutes into the simulation upslope flow is present and the first clouds appear. At 126 minutes one cloud forms upwind of the mountain, and another cloud forms downwind of the mountain. The model simulates a cumulus stage, mature stage, and dissipation stage of a thunderstorm drifting over the eastern plain.

Orville and Kopp (1977) in a "sequel" to Orville and Sloan (1970) incorporates detailed microphysical and hail growth into the model to simulate the "Fleming Storm" in NHRE. Early stages of the convection occur west of the mountain ridges. The clouds grow and weaken as they impinge on the midlevel inversion. Several clouds form and weaken until a cloud develops which remains organized as it moves east of the barrier crest. Their main conclusion is that the sloping updraft is important, because it allows precipitation to fall outside of the updraft. A propagating gust front allows the thunderstorm to obtain more warm and moist air from the east.

Mahrer and Pielke (1975) simulate the flow over a 2.0km high bell-shaped mountain with a lapse rate (-dT/dz) of 6.5°Ckm^{-1} and winds of 15ms^{-1} using a primitive equation model described in Pielke (1974). Compared to a case without surface heating, the daytime winds near the surface in a simulation with prescribed surface heating are stronger on the windward side, weaker on the leeward side, and about the same at mountain top. During the night the opposite differences, when compared to the no wind case, occurs. A pressure minimum is present at barrier top during the day which tends to slow the flow. At night a pressure maximum at the same location occurs which tend to accelerate the flow. At 0800 LST the height of the CBL at 30km downwind of the crest is much lower than the same distance

upwind of the crest. By 1400 LST the difference is less, and by 1800 LST the heights are the same as 0800 LST.

Hughes (1978) simulates the daytime evolution in eastern Colorado using a three-dimensional model with prescribed surface heating. The initial conditions are nearly dry adiabatic to 500mb, moist adiabatic to 400mb, and more stable above 400mb. Weak northwest winds are present near the surface with the winds backing with height becoming west-southwest at $10ms^{-1}$. At 0630 MST there is a region of sinking motion in a line east of Fort Collins and Denver, and the region of sinking motion expands and moves eastward with time. During the day a general increase in divergence occurs over the mountains, except for over the peaks. This divergence pattern results from heating occurring sooner over lower elevations. The upward motion in a line west of Fort Collins and Denver induce a series of lines of upward and downward motions on the eastern plains.

Hughes runs another simulation with winds increasing to 18m/s aloft, with the 500-300mb layer being less stable than the previous simulation, and with greater stability above 300mb. By 1300 MST a line of sinking motion from east of Denver to east of Fort Collins develops which moves eastward with time and weakens. By 1500 MST rising motion dominates the eastern plains.

Banta (1986) models the daytime evolution in South Park (Banta and Cotton, 1981, Banta, 1984) using a primitive equation model which is an earlier version of the CSU RAMS. The simulations have horizontal and vertical grid spacings of 100m, a deformation-based subgrid scale closure for scalars and momentum, and a prescribed sinusoidal surface heating. The terrain is a hill about 450m high. This terrain is similar to the Mosquito Range, but it is steeper than the topography in South Park. The model is initialized with soundings typical of "dry days".

Nine simulations are performed to determine the physical processes important to the evolution and to study the sensitivity of the evolution to different ambient conditions. With no ambient winds a convergence zone that develops over the hill moves toward the gentler slope (eastern side), and with $4ms^{-1}$ ambient winds the convergence zone also moves eastward. The pressure fields show high pressure over the hill top and on the west side of the convergence zone, and to the east of the convergence zone there is an upslope pressure gradient. In the $8ms^{-1}$ ambient winds simulation the convergence zone moves out of the domain in half the time as the $4ms^{-1}$ simulation. In the $12ms^{-1}$ ambient wind simulation the convergence zone moves out of the domain four times faster than the $4ms^{-1}$ simulation, and the upslope flow is weaker than in the $4ms^{-1}$ and $8ms^{-1}$ simulations.

A simulation without a cold pool does not have any upslope flow. Similarly, a simulation without a cold pool and without surface heating does not have any upslope flow the lee of the hill. In a simulation with a cold pool and without surface heating, weak and disorganized upslope flow appears beneath the inversion. The updraft has a speed of $1.5ms^{-1}$, and no steady state is ever reached.

Banta (1982) includes simulations with a 1.0km high barrier with a half width of 10km. The cold pool is deeper than in the simulations with a 450m high hill (Banta, 1986). As the daytime heating begins a CBL develops in the cold pool. With continued heating a vortex develops with its center located in a low pressure trough. He divides the evolution into three phases. The first phase occurs in the first half hour of the simulation. The second phase has the development of a shallow CBL and upslope flow. The third phase has flow dominated by the large scale vortex which moves eastward at around $2ms^{-1}$. The movement of the vortex eastward is the main process for the changing of the winds from easterly to westerly at the base of the highest terrain. This is different from the smaller terrain simulations where the vertical diffusion of momentum is the main process for changing the winds from east to west.

He states that the height of the mountain to the west allows for the generation of the pressure patterns needed for the vortex to exist.

Abbs and Pielke (1986) uses the model of Pielke (1974), Mahrer and Pielke (1977), and McNider and Pielke (1981) to study the influence of different synoptic scale winds and cloud shading on the thermally driven surface flows on the plains of northeast Colorado. After a six hour initialization the surface heating is initiated at sunrise. For very weak synoptic winds ($0.5ms^{-1}$) the most unstable air is over the Palmer Divide. By the evening, a convergence zone develops in the South Platte River Valley, and a southerly jet develops east of the main barrier. Simulations are performed for synoptic scale winds of $2.5ms^{-1}$ from north, east, southeast, south, and west. The southeast and south wind cases are similar. With imposed flow from the southeast to west, cyclonic motion occurs in the Denver area in the morning because the higher terrain blocks the flow. Except for the simulation with imposed southerly flow, a well defined confluence along the Palmer and Cheyenne Ridges occurs by the midafternoon. In the evening cooling creates drainage flows with convergence in the South Platte River Valley, and a southerly nocturnal jet develops.

Other simulations are run with low level easterly and westerly flow and a constant wind shear well above the CBL. When compared to the westerly wind simulation without shear, the westerly wind simulation with shear has weaker upslope along Front Range, the convergence zone 20km further east, and a weaker nocturnal southerly jet. Compared to simulation without shear, during the night the low level east wind simulation with shear has a stronger southerly jet and a stronger convergence zone in the South Platte Valley resulting from stronger drainage off of the Palmer Divide. Cyclonic vorticity appears near the Front Range. Cloud shading effects are minimal during most the daytime becoming more important later in the day, and at 1800 MST the eastern slopes of the mountains are 1-2°C cooler with drainage flow at this location beginning 1 hour earlier.

Pielke et al (1987) simulates the daytime to nighttime transition in the vicinity of Denver, Colorado. The simulations show a near surface jet flowing down the barrier to the west of Denver. The near surface jet extends eastward of the barrier being present over the flatter terrain in the Denver area. Observations taken in the vicinity of Denver qualitatively agree well with the simulations showing the presence of the near surface jet in the evening.

Wilczak and Glendening (1988) present observations and simulations of the Denver Cyclone. The observations are from August 1, 1985, and the simulations use a mixed layer model. The observations show a tongue of warm air moving northward with northerly flow along the base of the foothills at 0500 MST. A northeast to southwest orientated convergence zone exists just north of Denver, and this convergence zone has moved southward along the Front Range. At 0800 MST a well developed Denver cyclone is present with southeast flow on the plains, northerly flow along the foothills, and southwesterly flow over the Palmer Divide.

In the model the horizontal grid sizes are 7.1km by 7.4km and, the domain covers 360km by 437km. The simulation match the observed winds and the soundings taken near the BAO tower, and the simulations and observations both have the northward moving warm tongue of air. Vorticity analysis shows that the two largest sources of vorticity are the baroclinic slope term, which relates the temperature gradient and the slope of the terrain, and the stretching term in the convergent part of the cyclone. Their non-dimensional vorticity equation shows that varying the Rossby number has little influence on the cyclone, increasing surface drag decreases the gyre, the baroclinic depth term (which relates temperature gradient to the gradient of CBL height) is an important sink for the gyre, the baroclinic slope term is an important source term for the gyre, and diffusion is implicit to the model and cannot be easily changed.

Tripoli and Cotton (1989a) run two-dimensional simulations of the orogenic development of MCC's using grid spacing of 1.08km horizontally and 250 to 750m vertically. These simulations have a deformation based subgrid scale closure and a barrier over 2km high sloping downward to the east. The nighttime phase is simulated before the daytime evolution is studied in detail. At sunrise downslope motion on the east side of the barrier associated with a mountain wave system occurs. By 0800 LST the flow down the east side of the barrier weakens. The weakened flow is likely a combined upslope and downslope flow in the lowest layer, and the coarse vertical resolution cannot identify a shallow upslope layer at this location. Convection in the simulation begins one hour later than the observed start of the convection, and they attribute this difference to the elimination of "hot spots" (Henz, 1974) in the highly smooth model topography.

The first convection occurs near the crest of the barrier. A second convection region forms 60km east of the crest of the mountain where the axis of upward motion in the mountain wave intersects the surface. The primary moisture for both regions of convection is from west of the barrier crest. The upslope flow below the plains inversion has cold air advection, and subsidence warms the air above the upslope flow. The cooling in the upslope flow and warming from the subsidence intensify the plains inversion. By 1300 LST the convection over the mountain intensifies, and the convection 60km to the east of the barrier crest weakens because of subsidence from the convection to the west. At 1500 LST the convection to the east of the barrier drifts eastward and continues to weaken. The weakening from the convection moving away from the upward motion in the mountain wave and not being coupled with the moist air below the plains inversion.

They derive a conceptual model of the orogenic MCC development and structure from the results in this paper and the second part of this study (Tripoli and Cotton, 1989b). In the first stage a dry solenoid exists. The surface heating produces cold air advection in the

upslope layer and warm air advection above the upslope flow due to subsidence. The first cumulus appear in this phase, and the mountain wave and solenoid convergence zone remain stationary. The second stage has deep convection developing immediately west of the crest of the barrier and 60km to the east of the barrier. The convection to the east of the crest results from convergence of the mountain wave circulations and daytime solenoid. The third phase is linkage where the convection immediately west of the barrier reaches the upward motion in convergence zone resulting from the solenoid and mountain wave. When the convection reaches the upward motion, it explosively grows. The fourth stage is the meso-beta breakdown phase where the thunderstorms weaken. The weakening results from the incorporation of cooler θ_e air into the storm and from less surface convergence immediately east of the plains-foothills boundary. In the fifth stage a meso-alpha component grows from the weakening meso-beta component resulting in less suppression of the convective core. The meso-beta component breaks down about every two hours creating gravity waves which radiatively propagate outward weakening the meso-alpha circulation. As this phase progresses the up branch of the convection is supported more by the meso-alpha circulation, and the break down of the meso-beta component weakens the up branch less. In the sixth stage trapped meso-beta waves assist in strengthening the convection.

In Tripoli and Cotton (1989b) other sensitivity runs are discussed. In a run which includes virtual temperature effects but does not have condensation and precipitation, the meso-alpha scale mountain plains circulation extends to above 5km but not to the tropopause as in their main simulation discussed previously. The mountain wave convergence zone remains stationary and does not propagate eastward as in the main simulation. In another simulation no precipitation is allowed to form, and it is similar to the main simulation. In a simulation without cloud induced longwave cooling, the difference from the main simulation occurs after sunset when the growth of the convection is less. In a simulation with one-half

the ambient wind speed, the mountain wave convergence zone is half way between the barrier crest and the location of the convergence zone in the main simulation. The advection of moisture from the west side of the barrier is less, and the MCC moves eastward at about half the speed. In a no wind simulation there is a weakened plains inversion and possibly weaker convection which is caused by the absence of mountain wave subsidence.

2.6 Plateau Circulations

The heating and cooling of large regions of elevated terrain, such as the Rocky Mountains or the Tibetan Plateau, can influence the atmosphere for many hundreds of kilometers. Tang and Reiter (1984) uses the National Weather Service (NWS) radiosonde system, augmented by stations which measure surface pressure between 840 and 860mb, to study the plateau monsoon induced by the Rockies for the entire year. The pressure 850mb pressure patterns shows general high pressure over the intermountain west in the winter. From March to June these high pressure regions are replaced by low pressure. In July and August low pressure centers are in the major "bowls" of the intermountain west. The transition back to the winter pattern occurs during September and October.

To analyze the wind they divide the atmosphere into three layers with the lowest being 500m thick or less, the middle layer being dominated by the monsoon, and the upper layer being dominated by planetary circulations. The middle layer is semicircular as it envelops the west, south, and north side of the plateau. In this layer wind shifts of greater than 120 degrees occur between January and July. The east-west diameter of the middle layer is 3000km, and the east side slopes more gently than the west side. The highest elevation of the middle (or monsoon) layer is 2.5km. Its thickness is about 1km on the edge of the plateau, and it thins rapidly away from the plateau. The low level jet appears to be

part of the monsoon circulation and may be partly caused by a monsoon circulation. They identify five major regimes which affect the seasonality of the precipitation.

Reiter and Tang (1984) study the daytime and nighttime boundary layer structure in the intermountain region during July, which is the time of strongest summer monsoon. The daytime has low pressure develop over Colorado and Wyoming, slightly east of the Continental Divide, and over Nevada. In the evening the low over Colorado moves into Utah. The nighttime phase has an anticyclonic system over Colorado and New Mexico with an extension into Nevada. The anticyclones reach their maximum development at 0500 MST, which is shortly before sunrise. The times of early thunderstorm development during the day match well with the locations of the lows which develop over the mountains. The longitudinal extent of the plateau circulation is 100km away from the "hub" of the circulation. At night there is a ring of cyclonic flow around the anticyclonic flow emanating from the plateau. Using a friction velocity they calculate the mean upward motion from 1400 to 1700 MST of $1.2cms^{-1}$ and about $-0.6cms^{-1}$ at 0500 MST. The 850mb and 700mb levels are lower during the day and are higher during the night, and the opposite occurs for 500 and 100mb levels. The level of zero vorticity is about 675mb, which is not synonymous with the top of the mixed layer.

Sang and Reiter (1982) use a linearized system of equations in cylindrical coordinates to study the thermally induced flow around a plateau. This article focuses on the Tibetan Plateau and uses a sinusoidal heating function with a 24 hour period. During the day the height of the pressure levels decrease in the lower layers while the opposite occurs in the upper layers. At night the pattern is reversed. Tangential motion is counter clockwise for inflow and clockwise for outflow, and the tangential flow has a maximum amplitude about 6 hours later than the radial velocity. Their system of equations show relationships between the heating, winds, and pressure. If the thermal forcing is the same at all levels or increases

with height, then low pressure and inflow occur at all levels. If the heating decreases with height, low pressure and inflow occurs in the lower layers and high pressure and outflow occurs at the higher layers. For a stronger the vertical gradient of heating, the height where the pressure change changes is lower. The equations show that stability does not have as much of an influence on the circulation as structure of heating does.

Egger (1987) uses a cylinder with slices removed to simulate diurnal plateau circulation with valleys. The model is written in cylindrical coordinates, and it has four levels vertically and two grid points horizontally emanating out of the center of the grid. Since the valleys carved out of the cylinder are equally spaced apart, it is necessary to consider only one sector of the cylinder. The wind intensity and moisture well above the plateau is enhanced if valleys are present. The model terms show that advection tends to reduce moisture and increase temperature in the valleys while the reverse is true for upper levels. In his simulations neutral stability strengthens the circulation, and neglecting the coriolis force has little effect. If the turbulent coefficients of heat and momentum are larger near the surface than aloft, the circulation is slightly more intense.

2.7 Other Mountain Influences

Beside the thermally induced circulations over and immediately to the east of the barrier, complex terrain has other effects on the atmosphere. Using rawindsonde data Bonner (1968) identifies the nocturnal low level jet which is related to the nocturnal thunderstorm maximum in the Great Plains. McNider and Pielke (1981) run two-dimensional simulations with a terrain slope of 0.0018, which is the slope of the Great Plains without the sudden rise of the Rocky Mountains. The daytime heating creates lower pressure over the higher terrain, which creates a southerly geostrophic wind over the Great Plains. The nighttime cooling affects the pressure gradient in the lower levels, but the gradient in the upper layers is not

significantly affected by the cooling which allows the strong southerly flow to continue. When the friction in the flow rapidly decreases during the evening, the southerly flow overshoots to try to achieve geostrophic balance. The overshooting of the flow creates an inertial oscillation which causes the low level jet. Doubling the terrain slope creates a stronger jet. At a lower latitude the low level jet occurs later because of a longer inertial oscillation time scale.

Fast and McCorcle (1990) examine the influence of latitude and surface heating on the Great Plains low level jet using a two-dimensional model in which terrain rises 1.2km over a horizontal distance of 960km. The peak speed of the jet occurs earlier for higher latitudes because the frequency of the inertial oscillation increases. The speed of the jet decreases with latitude due to less daytime heating. Uniformly wetter soil also decreases the speed of the jet, because the daytime surface heating is less. With wet soil at higher elevations and dry soil at lower elevations, the speed of the upslope flow is greatly altered; a convergence zone develops in the middle of the domain; and an ageostrophic wind develops which opposes the low level jet. For this simulation the jet is further to the east than the simulation with homogeneous soil moisture. With dry soil at the higher elevations and wet soil at the lower elevations, the pressure gradient increases resulting in an ageostrophic flow which enhances the low level jet, and the jet is further west than in the homogeneous soil moisture case.

Bossert et al (1989) study the diurnal evolution over the mountains of Colorado from data taken over four summers (1984-1987) during ROMPEX (Rocky Mountain Peaks Experiment). The days examined have quiescent synoptic condition, are dry, and have strong solar forcing. During the daytime the mountain peaks show a general upslope flow, and general downslope flow occurs at night. The flow at stations east of the continental divide are generally opposite to stations west of the continental divide for the entire day. Stations on the east side of the continental divide that are near the divide sometimes do not have

upslope flow during the day while lower elevation stations have upslope flow. During the night, jets of easterly winds well above valley bottom occur west of the continental divide.

Bossert (1990) studies this shallow easterly flow, which was not related to the synoptic flow, observed in the evening over the western slope of Colorado. Numerical simulations, using the CSU RAMS, show that the shallow easterly flow is a gravity current flow down the west side of the mountains. This gravity flow originates with the daytime upslope flow on the east side of the barrier. During the daytime a convergence zone forms where the thermally induced flow up the east side and the west side of the mountains meet. This convergence zone moves west of the continental divide in the afternoon. In the evening the low level easterly flow west of the continental divide continues as a gravity flow which is about 500m deep. During the night the gravity flow continues to move west and turns more towards the north because of the terrain west of the Front Range. The simulations show that the nighttime gravity current over the western Colorado is stronger with easterly ambient winds and occurs with westerly ambient winds up to $3ms^{-1}$. The gravity flow develops with all thermal stratifications, and the daytime upslope flow is stronger for weaker stability. The westward propagation of the gravity flow during the evening is stronger for isothermal stability. Dry soil in western Colorado and moist soil in eastern Colorado provides the most favorable conditions for the development of the nocturnal gravity flow in western Colorado.

The air motions on and around the island of Hawaii are highly influenced by the thermal circulations created by the high mountains in the island. Lavoie (1967) states that air motions over the island of Hawaii are influenced by four main factors: large scale synoptic wind field, mountain barrier height and configuration, intensity and height of trade inversion, and diurnal heating and cooling of the land. A composite sounding, compiled from soundings taken four times a day from July 11 to August 25, 1965, shows that the mountain/sea breeze circulation extends up to 3.0km (when the mean wind is subtracted from the sounding winds).

The lower branch of the sea breeze circulation is 1km deep, and the upper branch is twice as deep and half as strong as the lower branch. The maximum return flow is immediately below the base of the trade inversion. Mylar balloons show a three layer structure at 1315 LST. Near the coast the balloons nearly parallel the terrain contours. Further up the mountain the balloons travel up the terrain slope, and even higher up the mountain the balloons again travel parallel to the contours. The explanation for the three layer structure is that the first layer is blocked by the mountain and is not in the sea breeze/upslope flow. The second layer is closer to the slope and is in the sea breeze/upslope flow. The third layer is in the cloud updraft and is carried away by the updraft.

Garrett (1980) uses eight sites along the east side of Mauna Loa to observe the daytime evolution. The research supports Lavioe's (1974) four main factors controlling the winds. In Garrett's conceptual model, as the air rises up Mauna Loa it becomes nearly saturated and can form clouds, while the subsidence produced by this flow occurs over the coast and ocean. Stronger winds can somewhat alter this circulation. During the night, a drainage flow develops, and the presence of a secondary inversion at 975m (3200 feet) prevents the drier air from reaching the coast. A line of shallow cumulus with tops at the trade inversion form off shore because of convergence of the land breeze with the trade winds. The speed of the upslope and downslope winds average less than $5ms^{-1}$.

2.8 Summary of Literature Review

The studies presented in this literature review show that mountains can profoundly influence the atmosphere. A wide variety of mountain-induced flows on many different spacial scales occur. The flows are caused by heating or cooling of the elevated terrain and by air being forced to rise over or pass around a terrain obstacle.

The heating of the terrain produces upslope flow during the day and downslope flow during the night. In northeast Colorado the heating or cooling of the Front Range can greatly influence the flow on the eastern plains, and the Cheyenne Ridge and Palmer Divide can also influence the flow fields on the eastern plains. Observational studies of the diurnal circulations on the eastern plains of Colorado have used a wide variety of observing tools. Surface observations and towers have studied the surface and near surface flows throughout the diurnal cycle. Aircraft data and deep airsonde observations have mainly examined the late morning and afternoon state of the atmosphere showing the presence of strong vertical wind shear and warming above the CBL on days with fairly strong surface heating. The top of the CBL in the afternoon can approach the height of the barrier top.

The many modeling studies of the daytime evolution east of large north-south mountain barriers have upslope flow on the east side of the barrier and on flatter terrain to the east of the barrier. Above the upslope flow return flow is present with general sinking motion to the east of the barrier. The daytime circulation influences the thermal, wind and moisture fields over the eastern plains causing features such as a suppressed CBL, vertical wind shear, and movement of moisture. The previous modeling studies, except Tripoli and Cotton (1989a,b), do not have a nighttime phase before the daytime phase. Tripoli and Cotton (1989a,b) have too coarse a vertical resolution to identify some of the features of the nocturnal state. The nocturnal state is not close to horizontally homogeneous, and it can influence the daytime evolution

This dissertation expands on the present knowledge of the daytime evolution of the atmosphere east of the Front Range of the Colorado Rockies in several ways. First, a nighttime phase is simulated before the daytime phase. The vertical grid spacing is significantly less than Tripoli and Cotton (1989a,b) to better identify the features in the nighttime state. Second, the simulations are run on a sophisticated mesoscale model (CSU

RAMS). This model has parameterizations for calculating radiational heating in the atmosphere, and it has a soil module for calculating a surface energy budget. A soil module and a radiation parameterization are lacking in many previous studies (Orville, 1964, 1965, 1968, Dirks, 1969, Banta, 1982, for example). The simulations have realistic topography which was lacking in many previous studies (Orville, 1964, 1965, 1968, Dirks, 1969, for example). Third, simulations are run for a variety of initial thermal structures, wind structures, and soil moisture (which affects surface sensible heat flux) to study how the evolution changes for the different conditions. Previous studies do not have a wide range of initial conditions for simulations using a sophisticated model and having a nighttime phase preceding the daytime phase. Finally, airsonde are launched starting at sunrise and are launched until late afternoon. Previous observational studies of the daytime evolution in northeast Colorado do not utilize frequent deep airsonde launches especially early in the day. The variety of simulations and the observations are used to describe the daytime evolution of the atmosphere east of the Front Range of the Colorado Rockies under conditions of clear skies, little change in time ans space of the synoptic-scale wind and thermal fields, and light winds with a westerly component.

CHAPTER 3.
BASELINE SIMULATION

3.1 Introduction

This dissertation examines the west-east nature of the daytime evolution of the atmosphere east of the Front Range of the Colorado Rockies under conditions of clear skies, little change in the ambient thermal and wind fields, and light ambient winds with a westerly component ($5ms^{-1}$). In chapter 3 a "baseline" simulation is discussed in detail. The "baseline" simulation is not necessarily a simulation of a particular day, but it is a simulation of the evolution on a typical day. It is initialized with a thermal and wind structure typically seen on the observational days, and it has a twelve hour nocturnal cycle before the twelve hour daytime cycle. The baseline simulation is used to discuss the daytime evolution in detail describing the physical processes important to the daytime evolution, showing how the thermal and winds fields vary vertically throughout the day, and discussing the horizontal variation of the evolution. In the next chapter this simulation acts as a baseline to which other simulations with different initial conditions are qualitatively and quantitatively compared. The baseline simulation can also be called a control simulation because of its use in examining the influence of the many different initial conditions on the evolution.

The model set up for the baseline simulation is given in section 3.2 and in section 3.3 the initial conditions for this simulation are presented. In section 3.4 the complicated sunrise state and the phases of the daytime evolution are discussed concentrating on the physical processes important to the evolution. In section 3.5 the evolution of vertical profiles of thermal and wind fields over several sites in the baseline simulation are examined showing

how the evolution vertically changes these fields and how the evolution differs over several locations. In section 3.6 some quantities derived from the thermal and wind fields are used to quantitatively show how the evolution changes horizontally east of the base of the barrier.

The next two chapters build upon this baseline evolution. In chapter 4 the changes in the daytime evolution for various initial conditions including different time of the year, different patterns of soil moisture, different ambient winds, different ambient thermal structures, and half barrier height are examined. These simulations demonstrate the universality of many features seen in the baseline run and are compared to the baseline run to quantitatively show how the evolution changes for the different initial conditions. In chapter 5 the observations are discussed in detail showing how well the simulations match the observed daytime evolution.

3.2 Model Setup

The simulations are run using version 2A of the CSU RAMS. The CSU RAMS is a versatile primitive equation model which can simulate the atmosphere on many different scales. As seen in chapter 2 the model has been used extensively to simulate thermally induced mesoscale circulations. The CSU RAMS uses a quasi-Bousinesq system of equations with the acoustic terms included. A time split scheme is used with the acoustic terms being integrated with a smaller time step. The model uses a sigma-z coordinate system. Sigma-z surfaces are along the topography at the surface of the model and become horizontal at the top of the model domain. The basic model equations, as applied in the version of the CSU RAMS used in this study, are described in more detail in Tripoli and Cotton (1982). A more up to date description of the entire CSU RAMS is given in Tremback et al (1986), Cotton et al (1988), Cram (1990), and Tremback (1990).

A two-dimensional, non-hydrostatic version of the model is used for the baseline simulation. Since the daytime evolution is examined for clear skies, condensation and precipitation are not allowed to occur in the simulation. Moisture is a passive tracer, and it can be evaporated from or diffused into the soil. The longwave and short wave radiation scheme of Chen and Cotton (1983) is used. This scheme calculates the diabatic heating caused by longwave and shortwave radiation at all grid points and at the surface. The shortwave radiation scheme accounts for the angle of the topography when calculating the intensity of the shortwave radiation at the ground. The soil module of Tremback and Kessler (1985) is used. It calculates changes in the soil temperature and moisture at the surface and at levels below the surface. The surface sensible heat flux and the moisture flux from the surface to the atmosphere are calculated using the surface soil temperature, surface soil moisture, air temperature, air moisture, and wind speed. The soil type is clay loam which is common on the eastern plains of Colorado.

The simulation has two grids. The inner grid has a horizontal grid spacing of 2.5km and 158 horizontal grid points, while the outer grid has a horizontal grid spacing of 10km and 90 grid points. Both grids have 44 grid points vertically. Table 3.1 gives the height of the grid points. Near the surface the vertical grid interval is about 100m, and below 4.0km the vertical grid interval is between 100m and 250m. Above 4.0km the vertical grid increment increases to 500m at approximately 8.0km. The topography on the inner grid is based on an east-west cross-section through Fort Collins, Colorado (Figure 3.1). The main barrier rises over 2.0km from the base of the barrier in a horizontal distance of over 60km. A second mountain range to the west is the Park Range and the valley between the two mountains is North Park. On the outer grid the topography west of the mountains slopes to a flat plain to the west, which is done to bring the western boundary to the same height as the eastern boundary. With the presence of terrain of significant vertical relief, a Rayleigh friction layer,

Table 3.1

Height of vertical velocity grid levels in the model in meters. The levels are divided into groups of vertical distances between grid points.

Distance between grid points less than 200m:
0m, 100.0m, 211.7m, 336.5m, 475.6m, 631.6m, 805.6m, 1000.0m

Distance between grid points equal to 200m:
1200m, 1400m, 1600m, 1800m, 2000m, 2200m, 2400m, 2600m, 2800m

Distance between grid points from 225m to 250m:
3025m, 3250m, 3500m, 3750m, 4000m, 4250m, 4500m

Distance between grid points from 300m to 450m:
4800m, 5150m, 5550m, 6000m

Distance between grid points equal to 500m:
6500m, 7000m, 7500m, 8000m, 8500m, 9000m, 9500m, 10000m, 10500m, 11000m, 11500m, 12000m, 12500m, 13000m, 13500m, 14000m

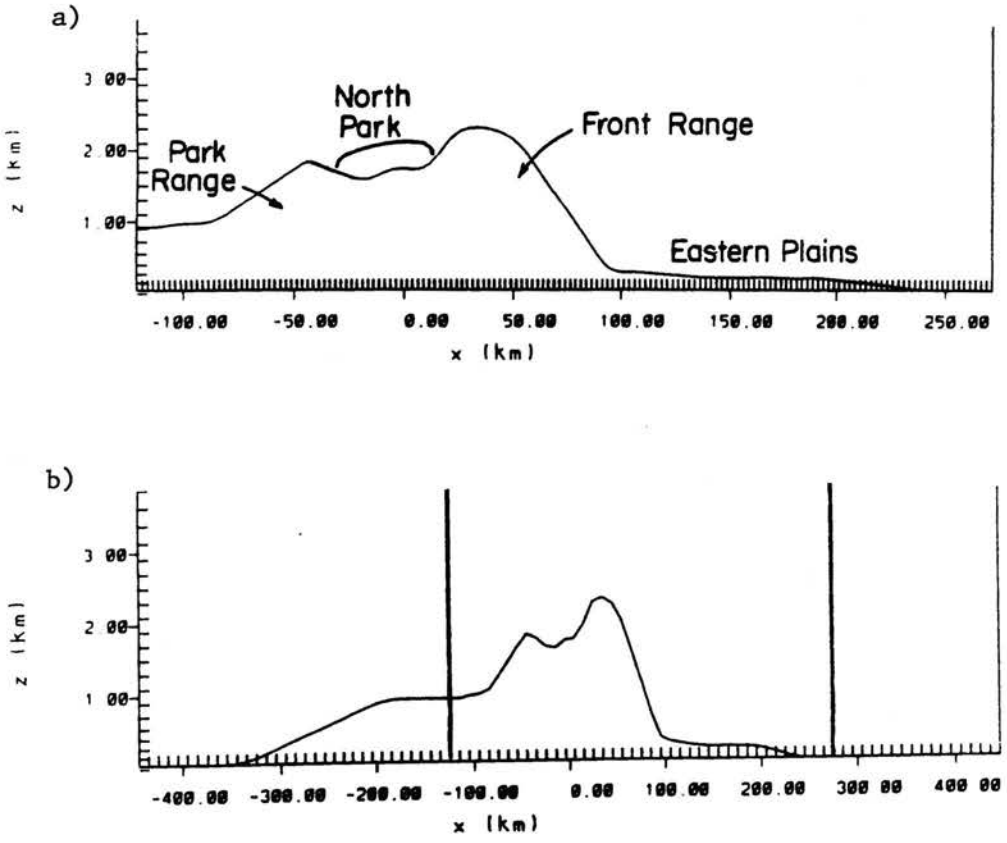

Figure 3.1. Topography in model: a) inner grid, b) outer grid. The vertical lines in the outer grid show the boundaries of the inner grid.

which covers the top seven vertical grid points, is added. This layer prevents the reflection of vertically propagating energy back into the domain. The horizontal boundaries are gradient inflow and radiative outflow. The grid nesting is similar to Clark and Farley (1984).

The horizontal subgrid scale closure (K closure) for wind and scalars is based on the deformation of the flow. The horizontal diffusion is sufficient to eliminate any significant 2 Δx noise that can make the simulations "blow up" as a result of aliasing; therefore, no additional horizontal smoothing is needed. A vertical diffusion scheme based on Helfand and Labraga (1988), which uses turbulent kinetic energy (TKE), is added to this version of the model. The equations for this scheme are given in Appendix A. This diffusion scheme uses the Mellor-Yamada level 2.5 scheme for decaying turbulence and uses level 2 closure for growing turbulence. This combination corrects some of the inconsistencies in the level 2.5 closure for growing turbulence, yet it allows for usage of the level 2.5 closure under other conditions. The level 2.5 closure scheme permits significant vertical mixing to occur with stable static stability if sufficient shear is present. Under stable conditions the level 2.5 closure scheme is superior to a deformation closure scheme. A constant gradient boundary condition is used for TKE at the boundary between the inner and outer grids since the magnitude of TKE has some dependence on the grid sizes. This boundary condition prevents exceptionally large or small values of TKE from being passed between the grids.

The model code is altered to extract changes to potential temperature resulting from horizontal advection, vertical advection, horizontal diffusion, vertical diffusion, and radiation calculated in cartesian coordinates over half hour periods. Coordinate-following and vertical values for advection and diffusion in sigma-z coordinates are not the same as in cartesian coordinates. During the simulation the vertical components of advection and diffusion in cartesian coordinates are calculated. The vertical advection in cartesian coordinates is subtracted from the total advection (calculated in sigma-z coordinates) to obtain the

horizontal advection in cartesian coordinates. A similar procedure is used to obtain the horizontal and vertical diffusion in cartesian coordinates. Sums of the cartesian components of advection and diffusion over a half-hour period are saved in analysis files. In the calculation of the tendency of potential temperature in the model, the components of advection and diffusion in sigma-z coordinates, and not cartesian coordinates, are used to ensure there is no change to the model results. Unless stated otherwise, horizontal and vertical advection and diffusion refer to the values in cartesian coordinates.

3.3 Initial Conditions

The baseline simulation is not designed to be a simulation of a particular day, but it shows the evolution on a "typical" day. This simulation is used to discuss the evolution in detail including the important physical processes, and it is used as a baseline to discuss how different initial conditions influence the daytime evolution. The model is initialized horizontally homogeneously at 6:00 P.M. LST, and a nighttime phase evolves before the daytime phase is simulated. Chapter 5 discusses airsonde observations taken in the vicinity of Fort Collins in detail. These observations are used to determine the thermal and wind structure on a "typical" day. Some of the main features of the atmosphere above barrier top at sunrise are listed in Table 3.2. Common features on many of these days are: a near neutral layer from 500 to 1000m above barrier top, winds above the neutral layer having a westerly component of 3 to 5ms^{-1}, and the mean potential temperature lapse rate ($d\theta/dz$) in the layer from 3 to 5km being 2.5 to 3.7 Kkm^{-1}. Table 3.3 gives the initial sounding for the model. The thermal profile has a neutral layer extending to 1.0km above barrier top with $d\theta/dz$ of 3.5Kkm^{-1} from 1.0km above barrier top to the tropopause. The moisture is a constant 7gkg^{-1} to 500m above the barrier top decreasing linearly to 1gkg^{-1} at 2.0km above the barrier top. The near neutral layer and nearly constant mixing ratio in the initial conditions approximate

Table 3.2

Mean 3-5km stability, mean 3-5km winds, and height of the near neutral layer above barrier top on the six observations days with westerly winds.

	Mean 3.0-5.0km stability $(\theta_{5km}-\theta_{3km})/2.0km$	Mean 3-5km winds.	Height of the near neutral layer above barrier top.
Oct. 29, 1987	2.5 Kkm^{-1}	3ms^{-1}	500m
Nov. 3, 1987	3.3 Kkm^{-1}	12ms^{-1}	---
Nov. 10, 1987	2.5 Kkm^{-1}	4ms^{-1}	200m
Jul. 5, 1988	3.7 Kkm^{-1}	5ms^{-1}	1000m
Oct. 25, 1990	5.0 Kkm^{-1}	5ms^{-1}	---
Nov. 12, 1990	3.5 Kkm^{-1}	4ms^{-1}	800m

Table 3.3

Initial sounding for the baseline run. Barrier crest is at 2274m.
The pressure at z=0 is 870mb.

Height (m)	Theta (K)	Mixing ratio (gkg^{-1})	u-component (ms^{-1})	v-component (ms^{-1})
0.0	319.00	7.0	2.0	0.0
200.	319.00	7.0	2.0	0.0
700.	319.00	7.0	2.0	0.0
1200.	319.00	7.0	2.0	0.0
1700.	319.00	7.0	2.0	0.0
2200.	319.00	7.0	2.0	0.0
2700.	319.00	7.0	3.0	0.0
3200.	319.00	5.0	4.0	0.0
3700.	320.75	3.0	5.0	0.0
4200.	322.50	1.0	5.0	0.0
5200.	326.00	1.0	5.0	0.0
6200.	329.50	0.78	5.0	0.0
7200.	333.00	0.55	5.0	0.0
8200.	336.05	0.33	5.0	0.0
9200.	345.50	0.1	5.0	0.0
10200.	354.50	0.1	5.0	0.0
11200.	363.50	0.05	5.0	0.0
12200.	372.50	0.05	5.0	0.0
13200.	381.50	0.05	5.0	0.0
14200.	390.50	0.05	5.0	0.0

a CBL from the surface to a height of 1.0km above barrier crest. On many of the observational days a weak west to east pressure gradient is present at the surface, so the winds below barrier top have a westerly component of $2ms^{-1}$. The westerly component of the wind linearly increases from $2ms^{-1}$ at the barrier top to $5ms^{-1}$ at 1.5km above barrier top. From 1.5km above the barrier top to the top of the model the westerly component is $5ms^{-1}$. The initial winds do not have a north-south component.

The solar heating in the baseline simulation uses data for September 21, which is the Autumnal Equinox. In the radiation scheme of the CSU RAMS the solar elevation angle and solar azimuth angles are calculated as a function of time for September 21. This solar data is used in the calculation of radiational heating of the air and to calculate the surface sensible heat flux at each surface grid point. Sunrise is very close to 6:00 A.M., and sunset is very close to 6:00 P.M..

The soil moisture can profoundly influence the surface sensible heat flux. During the nighttime phase strong flows can locally evaporate moisture from the surface leading to significant horizontal gradients of soil moisture by sunrise. Because the influence of horizontally varying soil moisture on the surface sensible heat flux is to be eliminated from this simulation, the soil is initialized with soil near the wilting point. During the night little moisture evaporates from the soil at all locations in the model resulting in nearly the same soil moisture at sunrise throughout the model. During the day the maximum surface sensible heat flux on the eastern plains reaches around $300Wm^{-2}$. Horizontal variability of soil moisture influences the daytime evolution, and simulations with varying soil moisture are be discussed in detail in the next chapter.

3.4 Simulated Evolution

The baseline simulation produces a complicated sunrise state and daytime evolution which influences the thermal and wind fields over the mountain and to the east of the mountain. This section discusses the sunrise state of the model and three phases of the daytime evolution mainly concentrating on model fields. A site at the base of the barrier is used to demonstrate how this evolution influences the development of the atmosphere on the eastern plains. In sections 3.5 and 3.6 vertical profiles of different model fields at several locations in the model domain are examined to show how the daytime evolution varies spatially.

3.4.1 Sunrise state: Interaction between Nocturnal Thermal and Ambient Flows

Figure 3.2 shows the potential temperature, u-component wind, vertical velocity, perturbation Exner function (which is a measure of pressure), and x-z streamline plot for the baseline simulation at sunrise. Twelve hours of nocturnal cooling has occurred since the simulation was begun. The atmosphere is much more complicated than a shallow nocturnal inversion along the terrain. In the potential temperature field (Figure 3.2a) the 318K isentrope is nearly horizontal except near barrier crest where it bulges downward above and to the east of the barrier crest. East of the barrier crest this isentrope dives below the height of the barrier top. The 319K isentrope has a similar behavior with less of a downward bulge. The region of a significantly downward bulging of the isentropes is referred to as the **bulging isentropes.**

The potential temperature field also shows an interesting thermal structure on the eastern plains below the height of the barrier. The 317K isentrope is nearly at the height of the barrier (around 2.0km) over the base of the barrier site, and it slopes downward to the east becoming about 1.0km high at the eastern edge of the diagram. The 317K isentrope is

a) Potential Temperature. Contour interval 1 K.

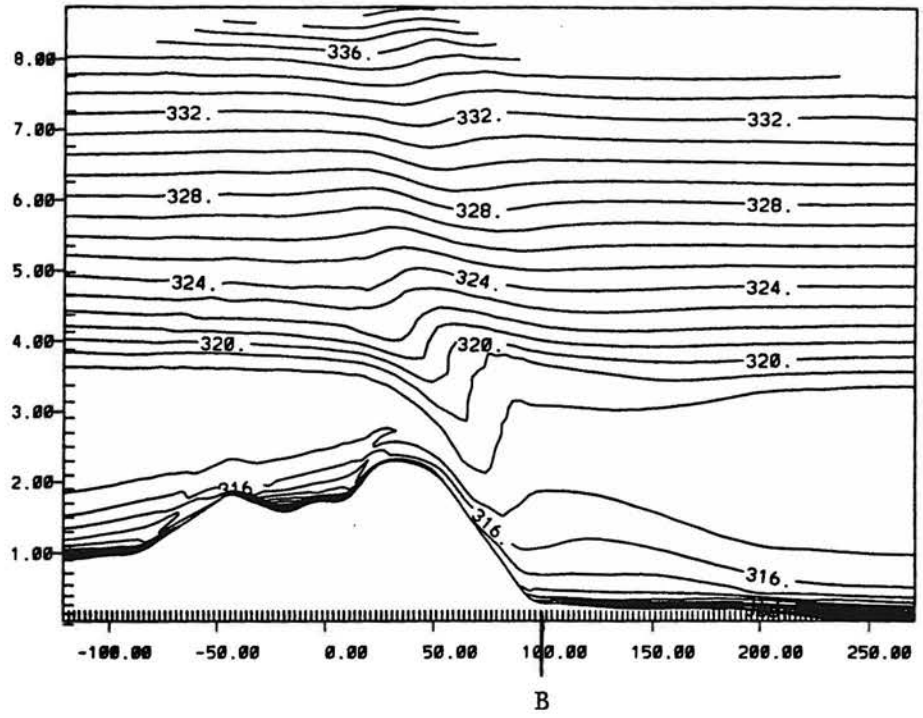

b) U-component. Contour interval 0.7 ms^{-1}. (Maximum: 9.1 ms^{-1}; minimum: -1.4 ms^{-1}).

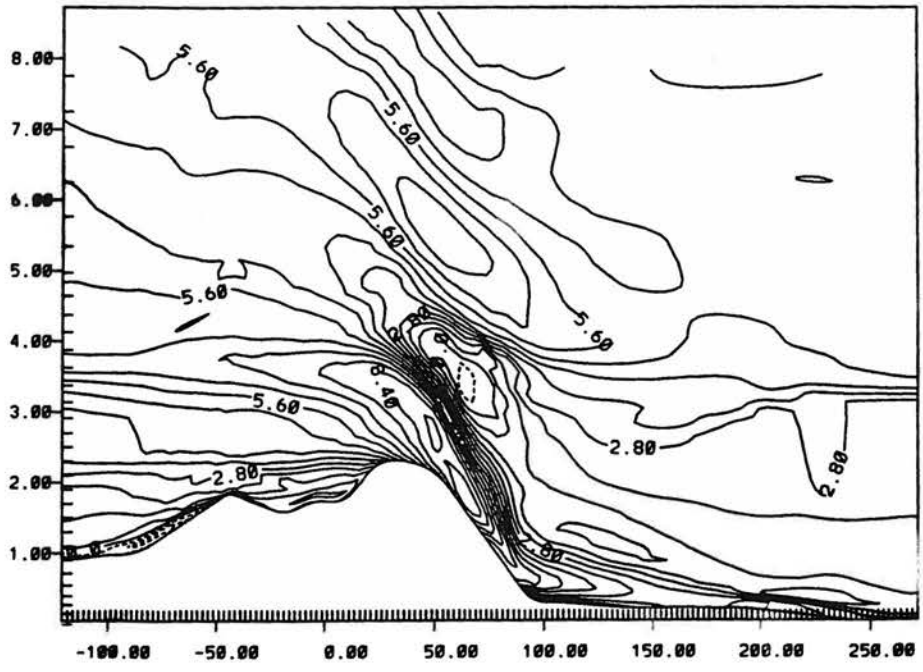

Figure 3.2. Baseline simulation at sunrise in the inner grid. a) potential temperature. Point "**B**" is the base of the barrier site. b) u-component. Horizontal and vertical distances are in kilometers.

c) Vertical velocity. Contour interval 4 cms^{-1}. (Maximum: 16 cms^{-1}; minimum: -44 cms^{-1}).

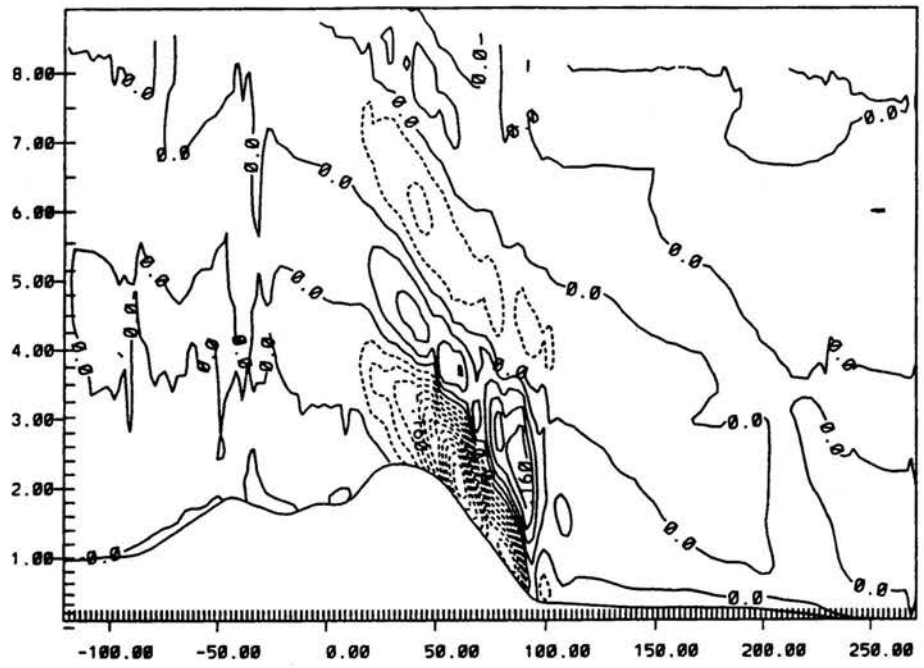

d) Perturbation Exner function. Contour interval 0.07 $Jkg^{-1}K^{-1}$. (0.026 mb at 700 mb).

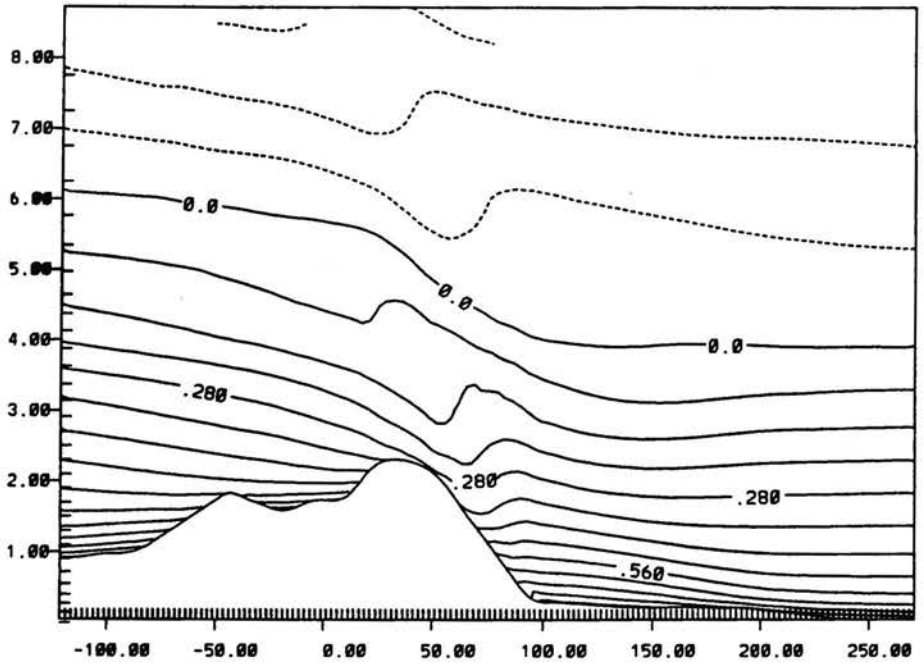

Figure 3.2. Baseline simulation at sunrise in the inner grid. c) vertical motion, d) perturbation Exner function.

e) Streamlines.

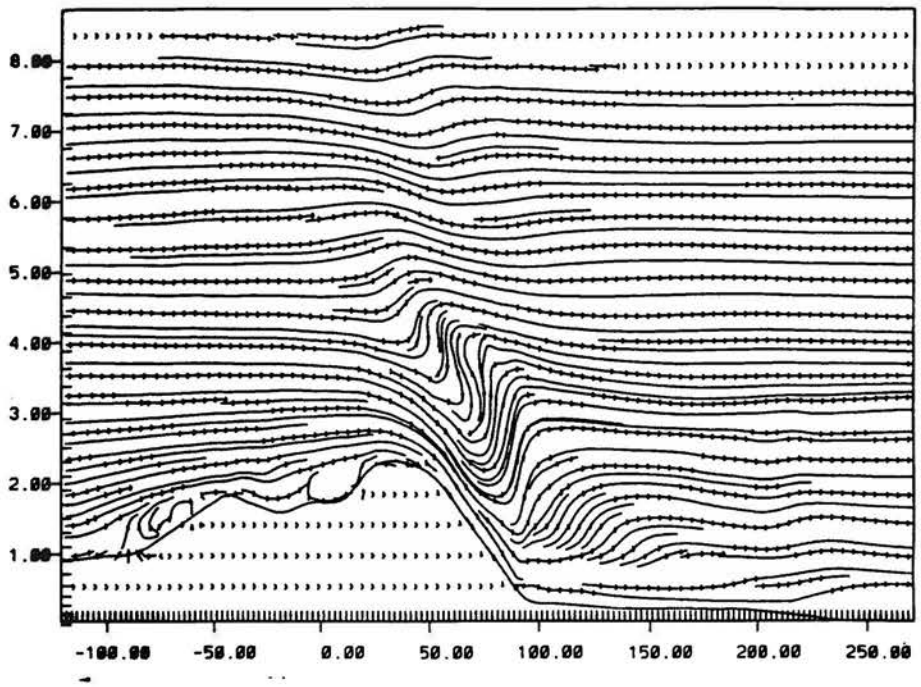

Figure 3.2. Baseline simulation at sunrise in the inner grid. e) streamlines.

almost at the top of a deep layer of cold, stable air which is referred to as the **stable core.** The depth of the stable core is nearly the height of the barrier at the base of the barrier site, and its depth decreases towards the east becoming 1.0km deep at 75km east of the base of the barrier.

The most pronounced feature of the wind field is the strong jet down the east side of the barrier. This jet flows beneath the bulging isentropes. The maximum u-component of the jet is over $9ms^{-1}$, and it occurs near the surface along the upper half of the eastern slope of the barrier. All the air flowing down the east side of the barrier does not remain in the jet as it reaches the base of the barrier. The streamline plot shows that over the lower half of the east slope of the barrier air flows eastward above the jet, as well as in it. The wind speeds in the jet decrease towards the east. At the base of the barrier the maximum u-component is about $5.5ms^{-1}$ at a height around 250m AGL, and further east the maximum is about $4ms^{-1}$ near the surface. Convergence associated with the slowing of the jet lifts the cold air creating the stable core.

The perturbation Exner function field shows that lowest perturbation pressure is east of the crest of the barrier, and it extends downward and eastward to about 20km west of the base of the barrier. The strongest u-component flow of the jet is located in this trough. The bulging isentropes are involved in the formation of this trough. The lowered layer of warmer air in the bulging isentropes tends to lower the pressure east of the barrier, and this lower pressure accelerates the flow in the jet. This region of lowest pressure angles to the west with height and is just east of the crest of the barrier at a height of 3.5km.

The west side of the bulging isentropes has strong u-component winds with sinking motion. On the east side of the bulging isentropes weakly positive and negative u-component flow occurs with ascending motion. The change from subsidence to ascent in the bulging isentropes moves westward with height. The circulations in the bulging isentropes resemble

a return flow for the movement of air down the east side of the barrier with the rising motion on the eastward side of the bulging isentropes being a return flow for the downward motion on the west side of the bulging isentropes. The weakening westward motion and eastward motion in the bulging isentropes is compensation for the accelerating westerly flow near the barrier slope. In fact the weak easterly flow indicates that some mass from the eastern side of the barrier is needed to replace the mass flowing in the jet.

Above 4.0km the atmosphere resembles a hydrostatic mountain wave (Smith, 1979). The vertical distance between the wind maximum and minimum is about 1.5km which closely matches the vertical wavelength for a wind of $5ms^{-1}$ and $d\theta/dz$ of $3.5Kkm^{-1}$. A simulation with the same initial conditions as the baseline simulation but without any diabatic heating (radiation or surface sensible heat flux) is run to examine how diabatic heating influences the atmosphere. Figure 3.3 shows the simulation after eight hours. After this time no significant changes in the model fields are evident. The downward bulging isentropes on the east side of the barrier and the strong jet down the east side of the barrier are not present. An oval shaped area of stronger u-component results from the vertical motion fields transporting momentum downward. Above 4.0km the maximum and minimum of the u-component, pressure ridges and troughs, and the rises and falls in the isentropes are about 20km further east than in the baseline simulation. The nighttime evolution in the baseline simulation causes the hydrostatic mountain wave to develop further west than if diabatic heating is absent. Thermally driven nighttime circulations and changes in the thermal and wind structure during the night can substantially influence the position of the mountain wave. The thermal and u-component fields above 4.0km also show that the amplitude of the wave is larger for the baseline simulation.

Tripoli and Cotton (1989a) is one of the few studies that simulate a nighttime phase before the daytime phase. They have a horizontally homogeneous initial state with a

a) Potential Temperature. Contour interval 1 K.

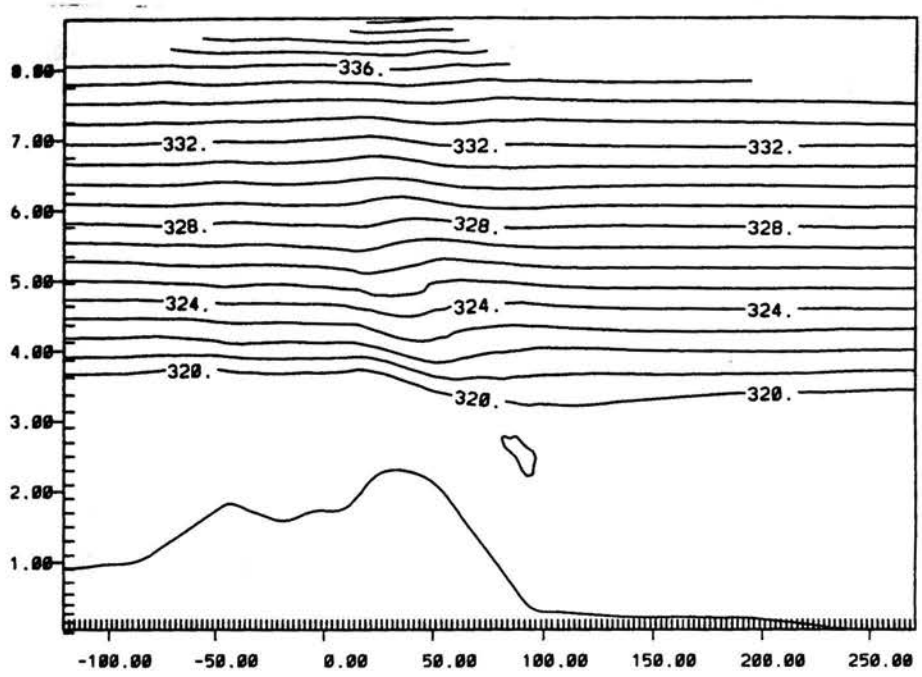

b) U-component. Contour interval 0.4 ms^{-1}. (Maximum: 8.0 ms^{-1}; minimum: 0.8 ms^{-1}).

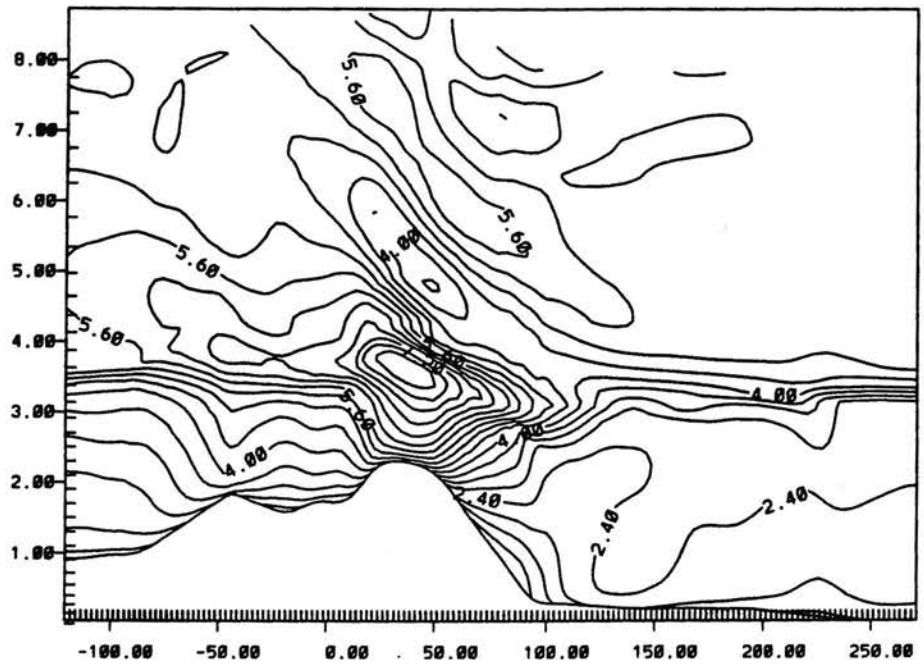

Figure 3.3. The no diabatic heating simulation at 8 hours after sunrise in the inner grid. a) potential temperature, b) u-component flow.

c) Vertical velocity. Contour interval 1 cms^{-1}. (Maximum: 12 cms^{-1}; minimum: -11 cms^{-1}).

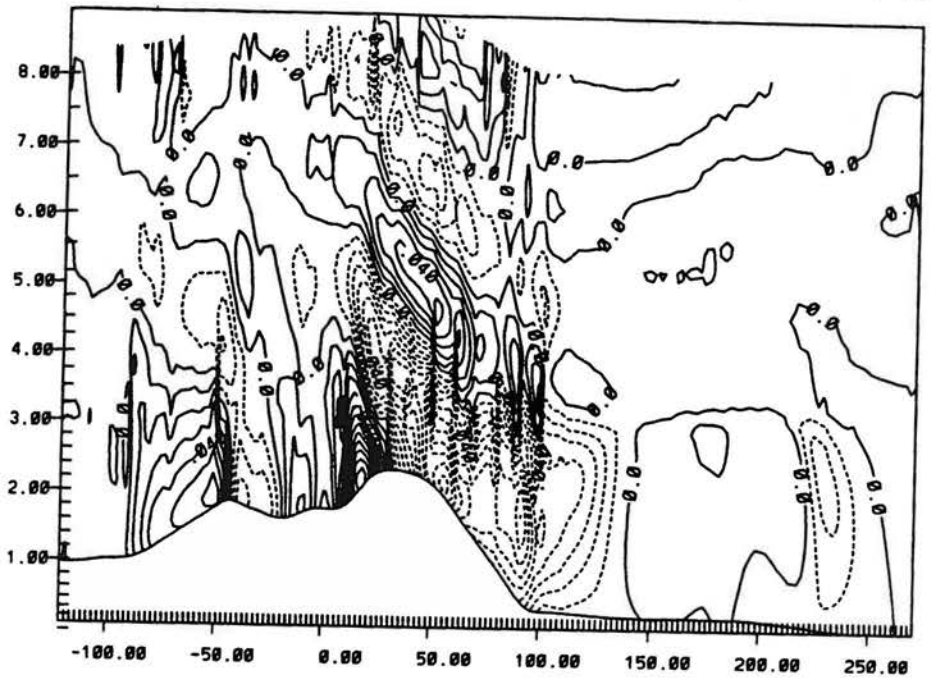

d) Perturbation Exner function. Contour interval 0.009 $Jkg^{-1}K^{-1}$. (0.003 mb at 700 mb).

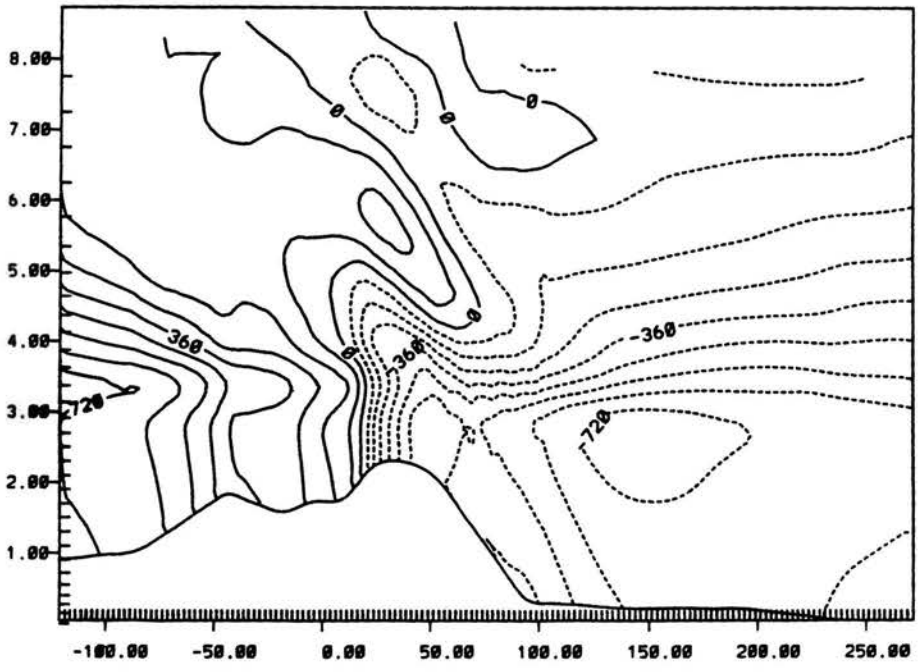

Figure 3.3. The no diabatic heating simulation at 8 hours after sunrise in the inner grid. c) vertical velocity, d) perturbation Exner function.

nighttime phase of nine hours and barrier height and width similar to the baseline run. Since they are mainly interested in the daytime phase of the evolution of a MCC, the sunrise state is only briefly discussed. In their simulation at sunrise a mountain wave is present with strong flow down the east side of the barrier. They suggest that the mountain wave and the thermally driven flow interact to create the strong flow down the east side of the barrier.

3.4.2 Phase 1: Weakening Nocturnal Flows Interacting with Heating

During the night the thermally driven flows interact in a complex fashion with the ambient flow, drastically changing the pressure, thermal, and wind fields by sunrise. Once the nighttime cooling ends these flows do not quickly dissipate. The main features of this phase are best seen in model generated soundings at the base of the barrier. Figure 3.4 shows vertical profiles of potential temperature and wind at sunrise and for the first three hours after sunrise at the site marked as the base of the barrier in figure 3.2. The horizontal component of the wind arrows show the u-component of the flow. The vertical component illustrated in this figure is magnified by ten times the actual model-simulated the vertical velocity. Between 2 and 3 hours after sunrise significant warming occurs from about 200m to 800m. This warming is associated with the weakening nocturnal westerly jet. By three hours after sunrise the jet has dissipated and the winds are nearly calm. This warming is evident as far as 20km to the east of the base of the barrier.

An obvious explanation for this warming occurring with the westerly flow off of the barrier is the eastward advection of air heated on the east slope of the barrier by a positive surface sensible heat flux. The simulation suggests that the reason for this warming is not that simple. Examination of the soundings at 10 and 20km west of the base of the barrier site shows that the lowest 500 to 1000m of the atmosphere warms beginning 1 hour after sunrise. This warming occurs despite negative surface sensible heat fluxes at this time! The surface

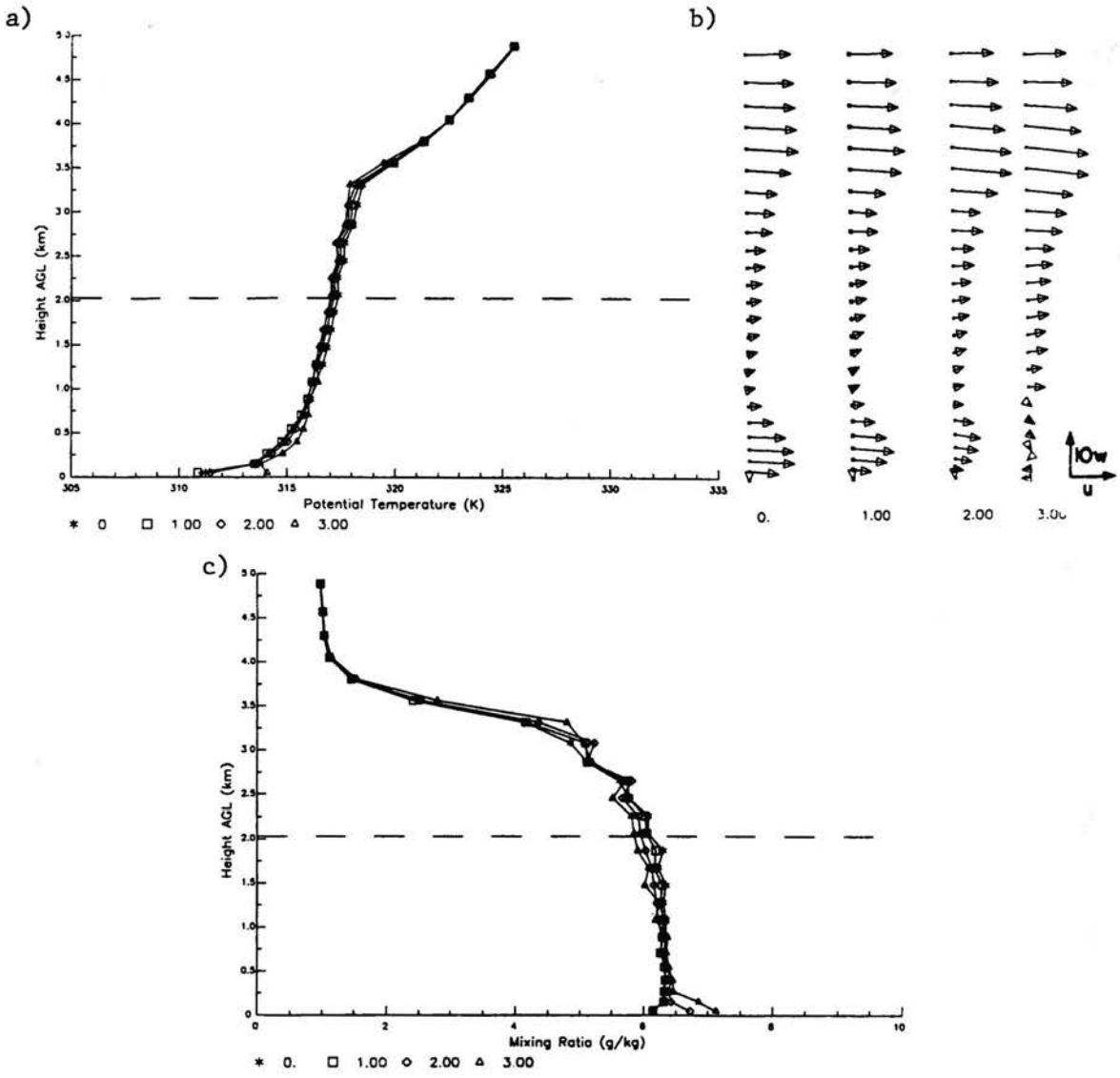

Figure 3.4. Vertical profiles of potential temperature and winds at the base of the barrier site in the baseline simulation for sunrise (0) and 1, 2 and 3 hours after sunrise (1, 2 and 3, respectively). The horizontal component of the winds are the u-component and the illustrated vertical component is magnified, for illustration purposes, to 10 times the model-simulated vertical velocity. The dashed horizontal line is the height of the barrier top.

sensible heat flux is still negative at this time because the solar heating is not sufficiently strong to increase the temperature of the upper layer of the soil above the temperature of the overlying air. One possible explanation for this warming shortly after sunrise is less cooling of the air in the jet as it descends the east slope of the barrier resulting from a less negative surface sensible heat flux. Since the jet does not slow much during this time, the less negative surface sensible heat flux results in the air in the jet being warmer than it is at sunrise. Other possible explanations for the warming include entrainment of warmer air into the jet or other changes to the dynamics of the jet. Much more examination is needed to better understand the exact cause for this warming. By 2 hours after sunrise the surface sensible heat flux on the east slope of the barrier becomes positive, and this heating naturally plays an important role in heating the air near the surface on the east slope of the barrier.

The wind fields at the base of the barrier show another interesting feature. At the base of the barrier the u-component of the flow weakens in this phase, becoming nearly calm up to 800m at 3 hours after sunrise. While the weakening nighttime circulation slows the u-component substantially, it only slightly weakens the vertical velocity. The persistence of the sinking motion near the base of the barrier is influential in producing the phase 1 warming. The source terms for potential temperature at the base of the barrier between 200m and 800m AGL show that the magnitude of vertical advection does not change much during the first three hours after sunrise. At sunrise heating from vertical advection is counteracted by net cooling from horizontal advection, horizontal diffusion, and radiational cooling. During phase 1 the heating due to horizontal advection and horizontal diffusion increase becoming less negative and eventually positive. With the magnitude of vertical advection (subsidence warming) remaining nearly constant, the warming between 200m and 800m results from horizontal advection and horizontal diffusion not counteracting the

subsidence warming. Horizontal advection and diffusion become positive contributing to the warming, but their magnitudes are not as large as the vertical advection.

The changes in the surface sensible heat flux throughout the domain cause changes in the pressure, thermal, and wind fields of the atmosphere. As the speed of the jet down the east side of the barrier continues to decrease, the u-component in the bulging isentropes increases, the downward extent of the bulge decreases, and the strength of the trough associated with the jet decreases. Throughout this phase the total mass flux over a given point on the eastern slope of the barrier below 4.0km remains about the same, but as the jet weakens more mass flows eastward at upper levels while less flows eastward at lower levels.

The atmosphere above 4.0km also undergoes some changes during this phase. The u-component maximum at about 6.0km increases and the u-component minimum at about 7.5km decreases. Even at 100km west of the barrier crest the u-component increases up to a height of 8.0km. This shows that the nighttime circulations can influence the atmosphere well into the troposphere and for large distances west of the barrier crest.

Tripoli and Cotton (1989a) have westerly flow down the east side of the barrier persisting for several hours after sunrise. They recognize that the persistence of the mountain wave after sunrise can possibly help maintain a westerly flow down the east side of the barrier and onto the eastern plains. In their simulation the vertical grid spacing at the surface is 250m to 333m in the lowest 1km, compared to 100m to 200m in the baseline simulation in this dissertation. With their more course grid spacing they cannot resolve many features of the flow near the surface.

3.4.3 Phase 2: Developing Solenoid

With continued heating the daytime circulation continues to evolve. The basic theory of the daytime circulation east of the crest a mountain barrier has upslope along at least part

of the eastern slope of the barrier, rising motion over the barrier, westerly return flow above, and sinking motion over the plains. Figure 3.5 shows the baseline simulation at 6 hours after sunrise. While this simulation has these elemental features of the daytime circulation, the structure and evolution of the solenoid is more complex. The solenoid evolution and structure is not as simple as an approximately horizontally symmetric circulation developing uniformly. The simulation shows that the solenoid is asymmetric horizontally and vertically, it does not develop uniformly with time, and it interacts with the ambient atmosphere which in turn affects the solenoid.

The easterly upslope flow in the solenoid meets the ambient westerly flow over the mountain in a region of strong rising motion and convergence. This zone is called the **lee side convergence zone** (adapted from Banta, 1984, and Tripoli and Cotton, 1989a). The air rising in this convergence zone lifts air into the more stable atmosphere above about 1.0km above the top of the barrier. The protrusion of the colder air into the more stable ambient atmosphere above creates an upward bulging region of neutral air that is colder than the ambient air at the same height. This region of colder air is called the **cold core**. The cold core is similar to the phenomenon observed by Brahm and Draginis (1960) near Tuscon when air rising up a mountain has enough upward momentum after leaving the heated mountain slopes to rise into the more stable air above the mountain.

The development of the cold core influences the vertical motion fields in the region. On the eastward leading edge of the cold core is a region of strong sinking motion. This strong sinking motion causes warmer air to descend, creating a pressure trough that extends downward to the surface. The center of the solenoid is located in this pressure trough. In the cold core higher pressure is present. The high pressure in the cold core and the low pressure in the trough immediately to the east of the cold core create a strong horizontal pressure gradient which accelerates the westerly return flow. A region of maximum

a) Potential Temperature. Contour interval 1 K.

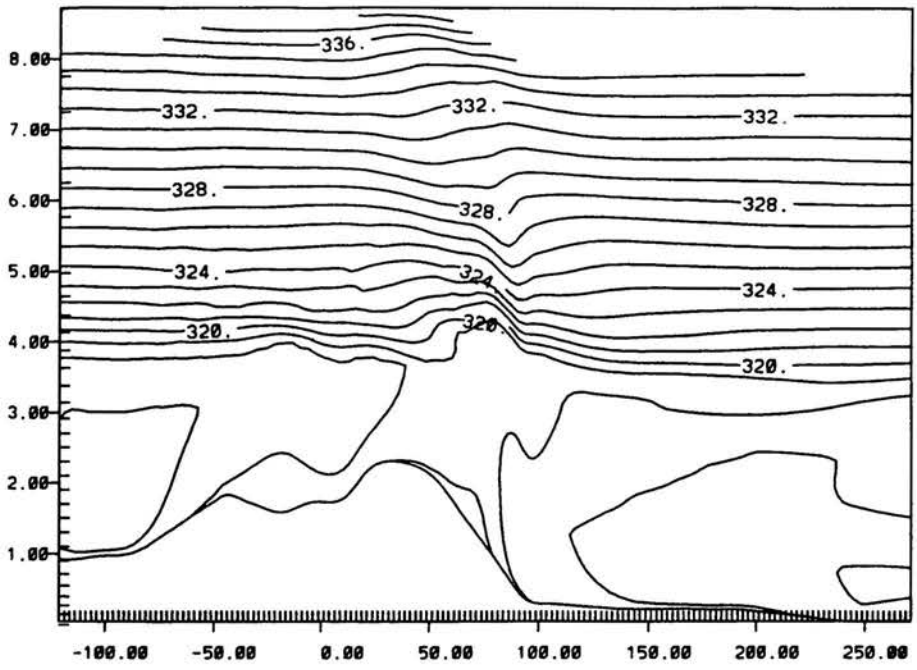

b) U-component. Contour interval 1.0 ms^{-1}. (Maximum: 12 ms^{-1}; minimum: -6 ms^{-1}).

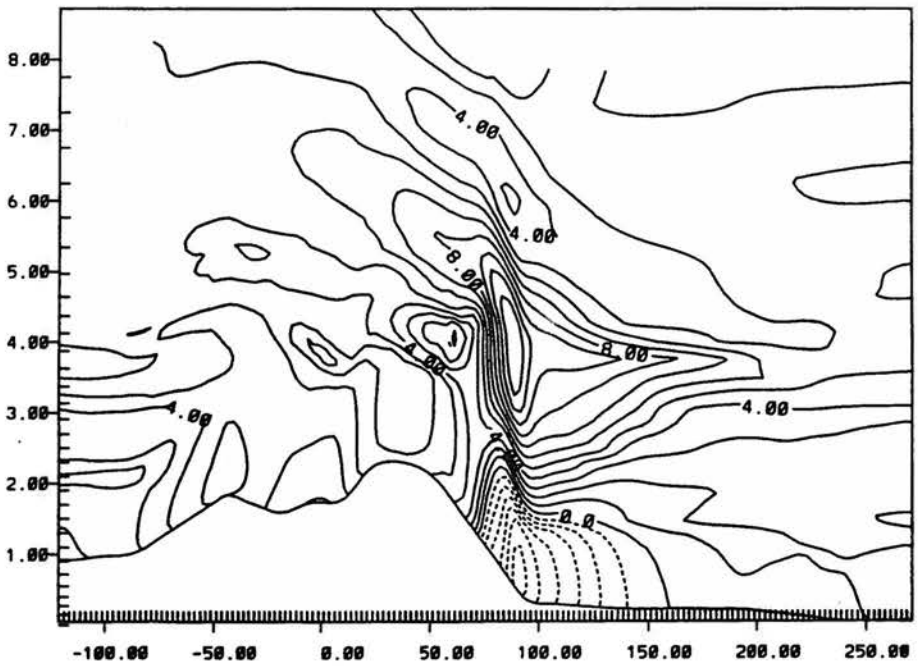

Figure 3.5. The baseline simulation at 6 hours after sunrise in the inner grid. a) potential temperature, b) u-component. Horizontal and vertical distances are in kilometers.

c) Vertical velocity. Contour interval 8 cms^{-1}. (Maximum: 80 cms^{-1}; minimum: -48 cms^{-1}).

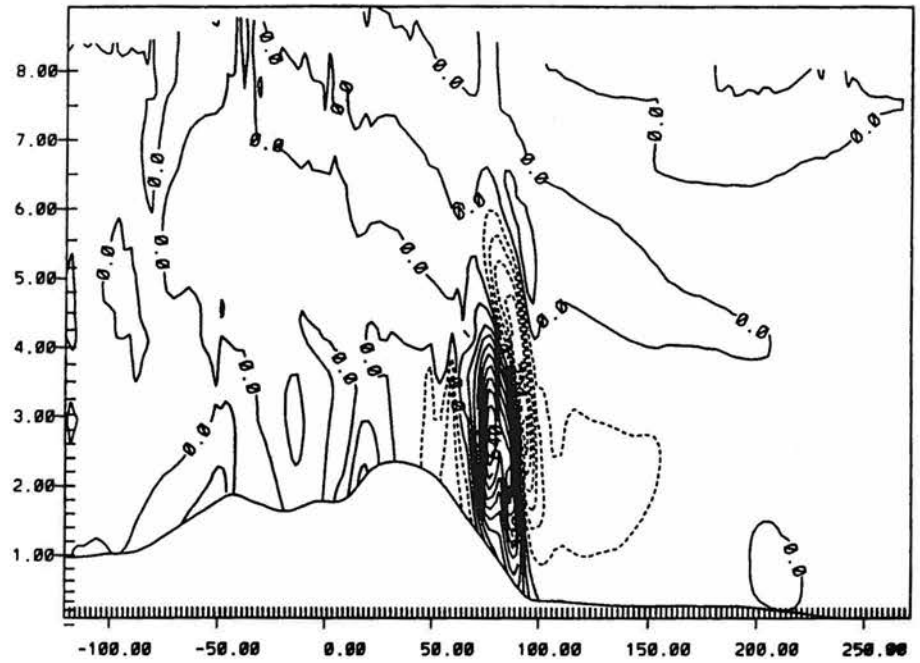

d) Perturbation Exner function. Contour interval 0.07 $Jkg^{-1}K^{-1}$. (0.026 mb at 700 mb).

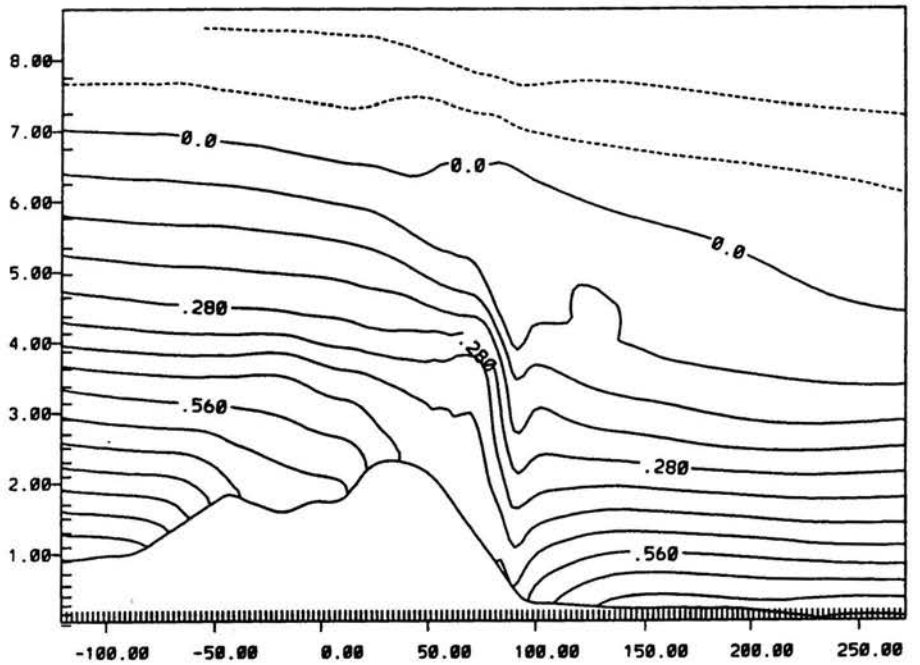

Figure 3.5. The baseline simulation at 6 hours after sunrise in the inner grid. c) vertical velocity, d) perturbation Exner function.

e) Streamlines.

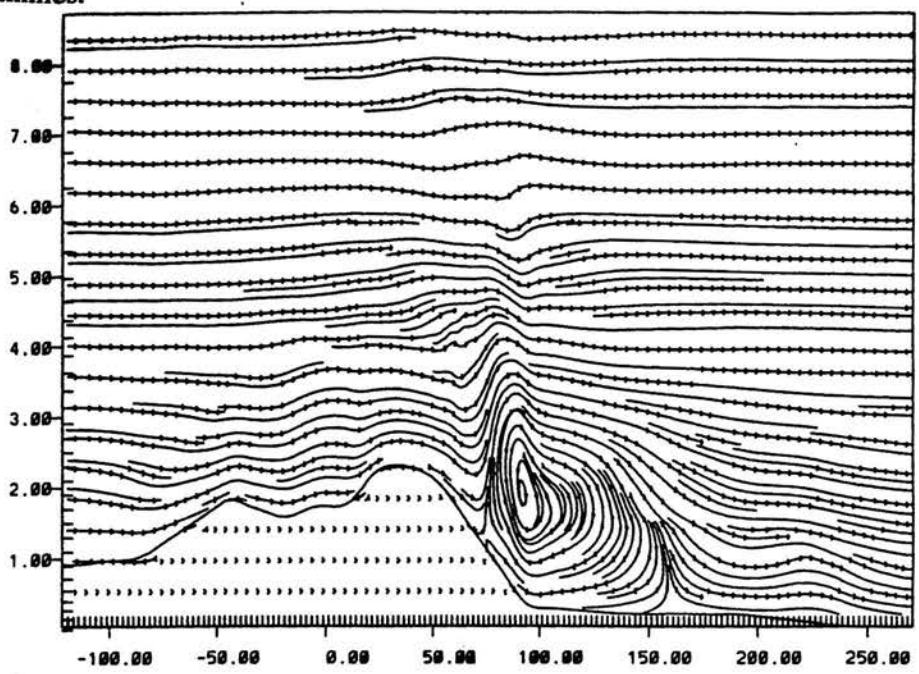

Figure 3.5. The baseline simulation at 6 hours after sunrise in the inner grid. e) streamlines.

u-component results from this strong horizontal pressure gradient, and the u-component maximum occurs above the center of the solenoid circulation. In the stable core above the convective boundary layer (CBL) sinking motion and horizontal advection produces warming. The strongest sinking motion is immediately east of the center of the solenoid.

The solenoid does not develop uniformly with time, and it has two stages in its evolution. In the first stage the pressure gradient is positive (higher to the west) in the stable core above the CBL, and the easterly upslope winds are confined to the CBL. Between the easterly upslope flow and westerly return flow is a region of weak westerly winds. This layer of weaker winds shrinks as the CBL and the upslope flow expand upward and the westerly return flow expands downward.

As the daytime heating continues warming occurs east of the solenoid above the CBL, and this warming lowers the pressure in the stable core above the CBL. If sufficient warming occurs, the pressure gradient in the stable core above the CBL becomes negative (lower pressure to the west), and the second stage of phase 2 occurs. The region of the negative pressure gradient expands eastward with time, and the boundary between the regions of negative and positive horizontal pressure gradients in the stable core is seen as a high pressure ridge. In Figure 3.5d a ridge in the stable core, separating the negative and positive pressure gradients, is located about 50km east of the base of the barrier. The change in the horizontal pressure gradient in the stable core influences the u-component of the flow. With the negative pressure gradient upslope flow appears above the CBL, and the easterly upslope flow and westerly return flow meet forming a region of strong vertical wind shear. The upslope circulation, as measured by mass flux towards the barrier in the upslope flow, intensifies more rapidly when the negative horizontal pressure gradient in the stable core is present.

Associated with the developing solenoid and the changes in the horizontal pressure gradient below barrier top are secondary circulations which can alter the vertical motion fields east of the solenoid. Immediately to the east of the solenoid is the main region of sinking motion, and further to the east a secondary maximum of sinking motion occurs. This secondary maximum is evident in Figure 3.5c centered at 40km east of the base of the barrier, and it is located at and to the west of the pressure ridge where the horizontal pressure gradient in the stable core changes from positive to negative. The sharp increase in the rate of intensification of the upslope flow, which occurs near the pressure ridge, creates stronger divergence in the easterly flow, and stronger convergence occurs in the westerly return flow. The stronger convergence and divergence create the secondary circulations inducing the secondary maximum in sinking motion.

The complexly developing circulation in phase 2 has profound influences on the wind and thermal structure of the atmosphere on the eastern plains. Figure 3.6 shows model derived soundings for 4, 5, and 6 hours after sunrise at the base of the barrier site. The soundings show the easterly flow deepening and strengthening throughout this period as well as the westerly return flow strengthening. The thermal profiles show a deepening CBL with significant warming above the CBL. The warming above the CBL results from the eastward advection of air heated by the barrier and from subsidence on the east side of the solenoid. Horizontal cold air advection occurs in the CBL due to cooler air moving westward in the upslope flow on the eastern plains. The warming above the CBL and the cold air advection in the CBL suppresses the growth of the CBL on the eastern plains.

The earlier simulations of the daytime evolution such as Orville (1964, 1965, 1968) and Dirks (1969) identify some of the features seen in the baseline simulation. These earlier simulations have the upslope flow near the surface, rising motion over the barrier, westerly return flow, and sinking over the eastern plains. The rising motion on the west side of the

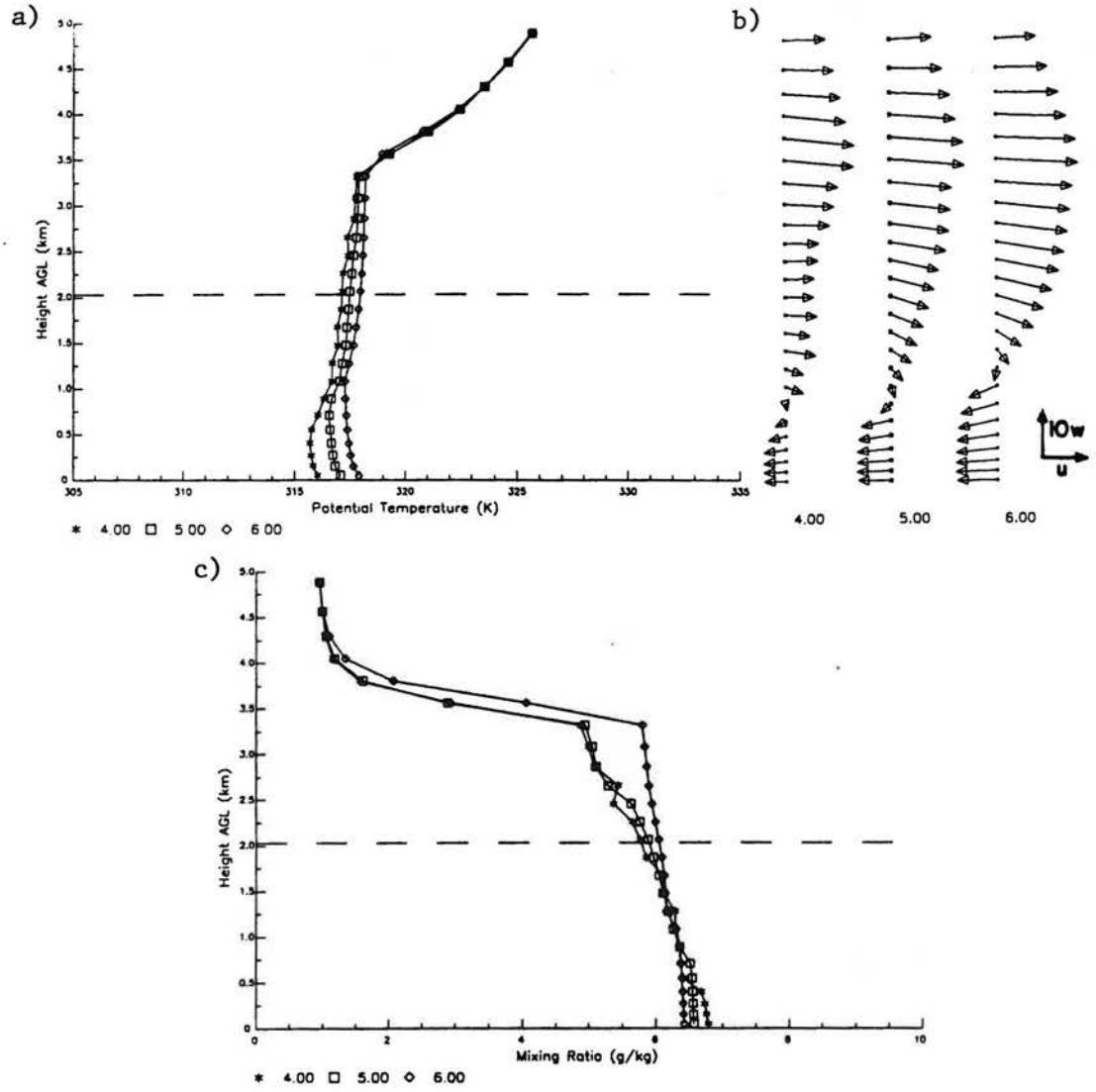

Figure 3.6. Vertical profiles of a) potential temperature, b) winds, and c) mixing ratio at the base of the barrier site for 4, 5, and 6 hours after sunrise. The components of the wind are the same as in Figure 3.4.

solenoid center is concentrated in a fairly narrow region, and a cold core is frequently associated with this rising motion when ambient stable stratification is present. The sinking motion on the east side of the solenoid occurs over a broad area. While these studies have the basic features associated with the solenoid, they do not identify many of the horizontal and vertical asymmetries in the solenoid. Some of features not seen in the earlier studies include the two stages to this phase, the interaction with the ambient flow above barrier top, and the strong sinking motion immediately east of the center of the solenoid.

More recently, Tripoli (1986), and Tripoli and Cotton (1989b) report on a simulation which is the same as in Tripoli and Cotton (1989a) except that no condensation or precipitation is allowed to occur. With the numerous advances in numerical modeling and computers in the past 15 years, their simulation has many improvements from the earlier studies including much more realistic topography, larger vertical domain, a soil module, and better model dynamics. Tripoli and Cotton have a solenoid with the westerly return flow developing to a height of about 7km MSL (about 3.5km above barrier top). A cold core, which has higher pressure than the surroundings, accelerates the westerly return flow. The warming above the CBL on the eastern plains suppressed the CBL. While recognizing that the atmosphere above the barrier top influences the structure of the solenoid and that the solenoid has many horizontal and vertical asymmetries, they do not discuss these aspects of the solenoid in much detail.

3.4.4 Phase 3: Migrating Solenoid

Starting around 7 hours after sunrise the solenoid begins to move eastward. The solenoid initially begins to migrate eastward slowly with its speed of migration increasing as it moves east. Near the base of the barrier, its migrating speed increases to about $5ms^{-1}$. Afterwards, it continues to migrate eastward at this speed. Figure 3.7 shows the baseline

a) Potential Temperature. Contour interval 1 K.

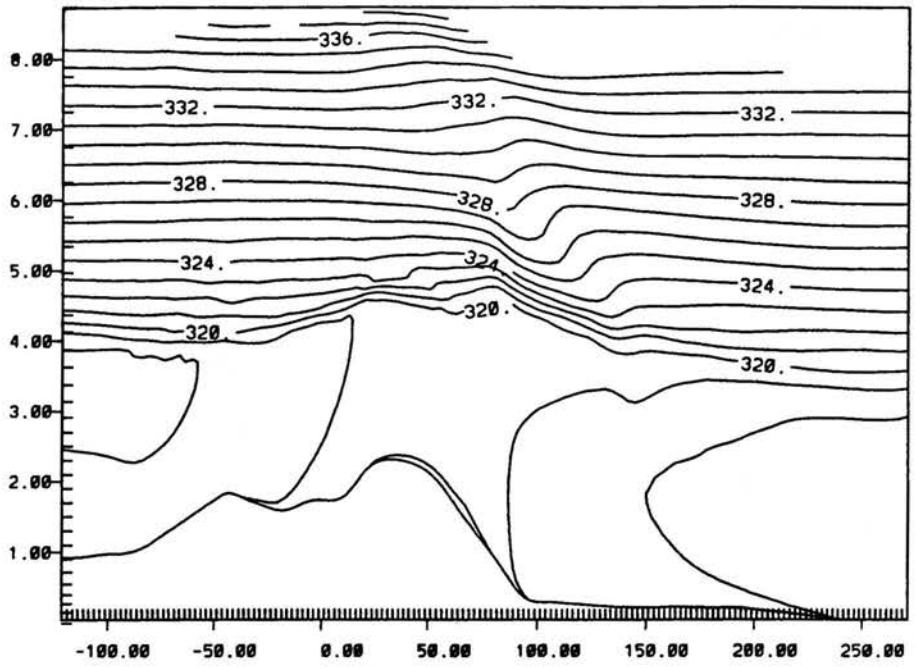

b) U-component. Contour interval 1.0 ms^{-1}. (Maximum: 12 ms^{-1}; minimum: -3 ms^{-1}).

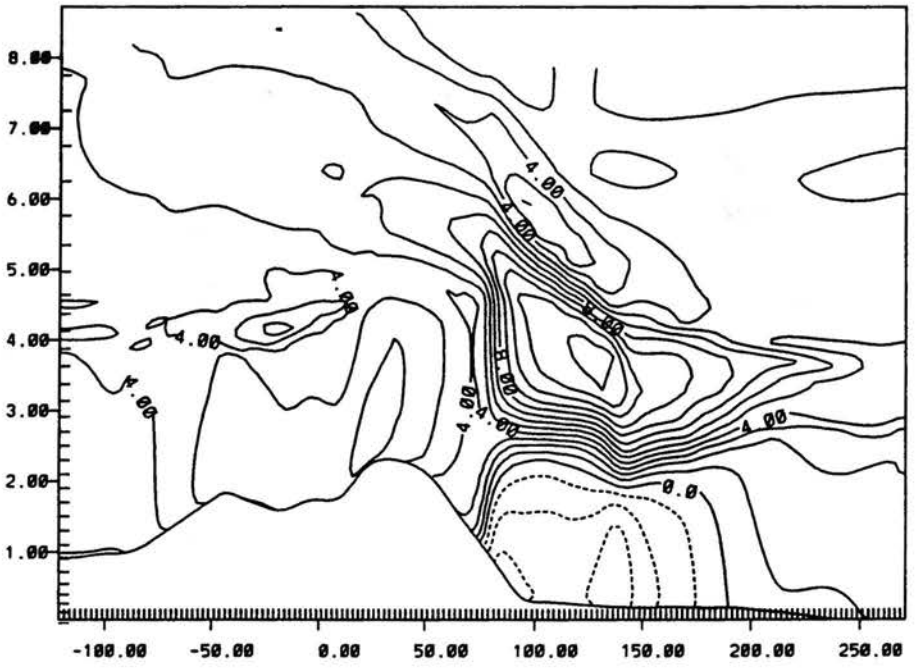

Figure 3.7. The baseline simulation at 10 hours after sunrise in the inner grid. a) potential temperature, b) u-component.

c) Vertical velocity. Contour interval 6 cms^{-1}. (Maximum: 78 cms^{-1}; minimum: -24 cms^{-1}).

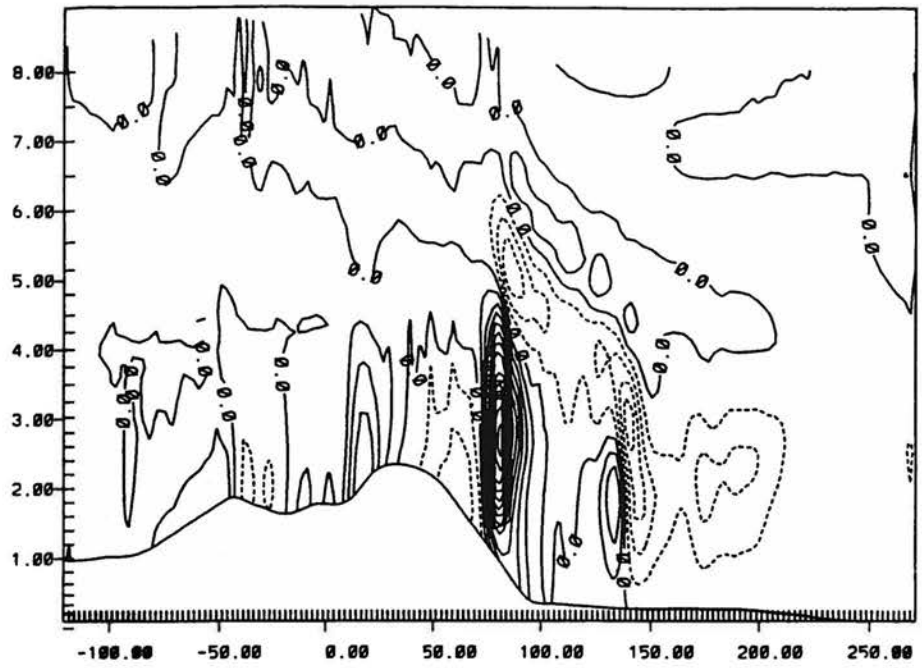

d) Perturbation Exner function. Contour interval 0.06 $Jkg^{-1}K^{-1}$. (0.022 mb at 700 mb).

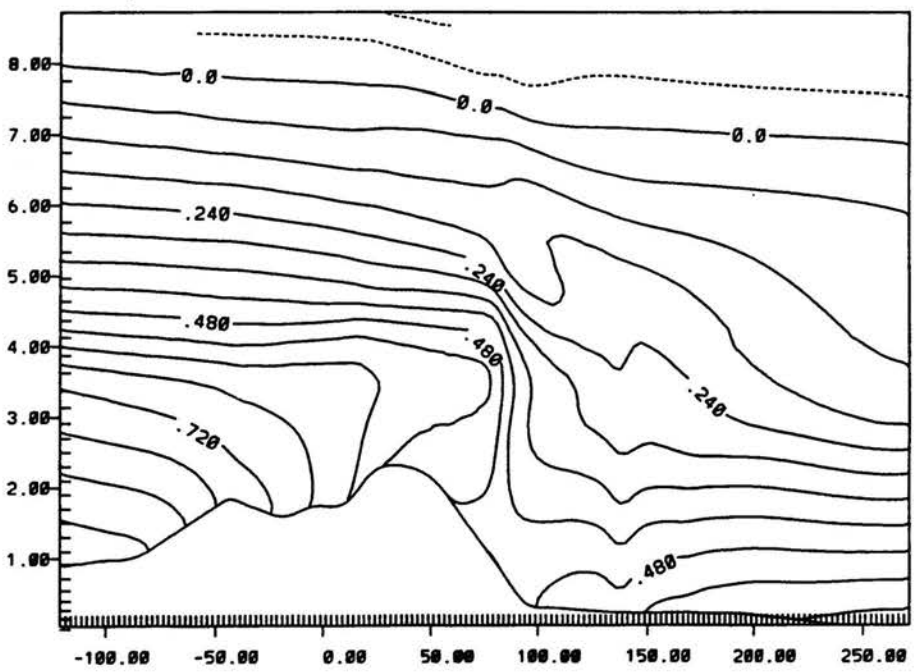

Figure 3.7. The baseline simulation at 10 hours after sunrise in the inner grid. c) vertical velocity, d) perturbation Exner function.

e) Streamlines.

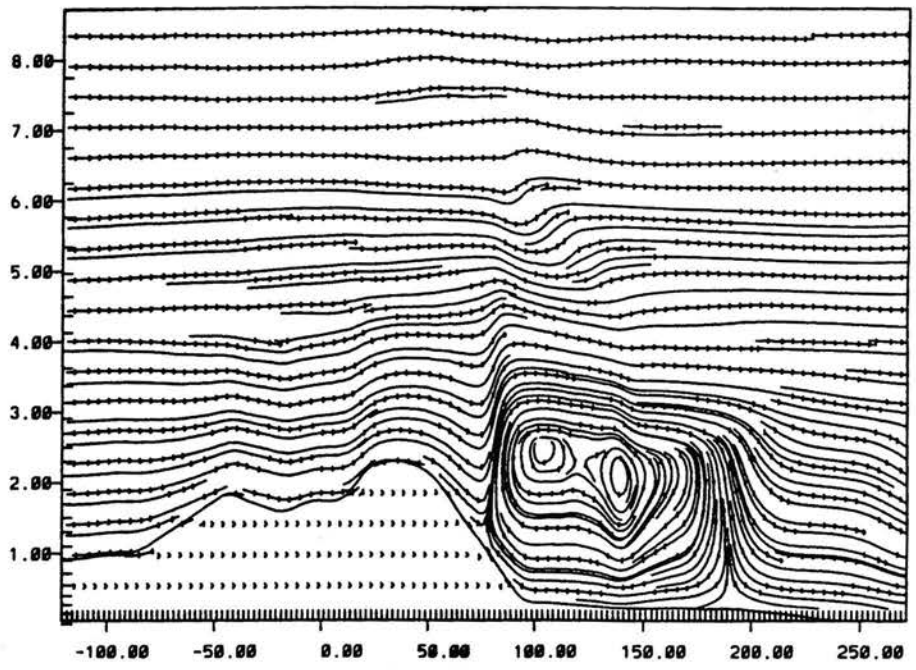

Figure 3.7. The baseline simulation at 10 hours after sunrise in the inner grid. e) streamlines.

simulation at 10 hours after sunrise. As discussed in the last section the solenoid is located in a pressure trough beneath the leading edge of the cold core. The solenoid migrates eastward in a pressure trough beneath the eastward advancing leading edge of the cold core. The entire cold core does not advance eastward along with its leading edge. Comparison of the potential temperature and vertical motion fields in Figures 3.5 and 3.7 show that the deepest portion of the cold core remains anchored over the nearly stationary lee side convergence zone. The model generated source of potential temperature terms show strong cold air advection on the at the leading edge of the cold core indicating that its eastward movement is an advective phenomenon.

The eastward movement of the leading edge of the cold core affects the advancing pressure trough in which the migrating solenoid is located. In phase 2 (Figure 3.5) the leading edge of the cold core is nearly vertical. The region of strong sinking motion immediately ahead of the leading edge of the cold core is nearly vertical, and correspondingly the pressure trough in which the solenoid is located is nearly vertical and extends from the surface to 5.0km. In phase 3 (Figure 3.7) the pressure trough and strong sinking motion at a height of 5.0km are nearly at the same location as in phase 2. However, the pressure trough and region of strong sinking motion between 3.5km and 5.0km rotate eastward like a spoke of a wheel with the center of the "wheel" being the stationary region of sinking motion (and lower pressure) at a height of 5.0km. Because the sinking motion between 3.5 and 5.0km becomes less vertical, the pressure trough below 3.5km, which contains the center of the migrating solenoid, weakens. The weakening of the pressure trough and the decreasing surface sensible heat flux cause the solenoid to weaken as it migrates eastward. By 1 hour before sunset the migrating solenoid dissipates, and a new solenoid redevelops near the base of the barrier with the main upward motion being the lee side convergence zone. The

disturbance which supported the migrating solenoid is still present as a wind maximum at 4.0km, and it continues to move eastward.

Figure 3.8 shows model generated soundings at the base of the barrier for 7, 8, 9, and 10 hours after sunrise. The solenoid passes over this site between 7 and 8 hours after sunrise. The CBL is suppressed before the solenoid reaches this site, and the CBL explosively grows from 1.2 to 2.2km deep in one hour (7 to 8 hours after sunrise) when the solenoid passes over the site. The vertical profile of potential temperature shows a neutral or slightly unstable profile below 1.2km and a slightly stable layer above 1.2km. The vertical diffusion of potential temperature is positive from the surface to 1.2km, and the vertical profiles of potential temperature and the vertical diffusion indicate that the CBL is 1.2km deep. At 8 hours after sunrise the vertical diffusion is positive up to 2.2km, and the vertical profile of potential temperature shows neutral or a slightly unstable profile below 2.2km and a stable lapse rate above 2.2km. The vertical diffusion and potential temperature profiles both show a 2.2km deep CBL at 8 hours after sunrise. Other substantial changes in the soundings accompany the passage over the solenoid over the site. The depth of the easterly upslope flow increases, the u-component of the return flow is faster, and the depth of the near neutral layer above barrier top increases.

As seen in the soundings at 8, 9, and 10 hours after sunrise, the near neutral layer above barrier top continues to deepen after the passage of the solenoid, because the depth of cold core over this location increases. During this time, the depth of the easterly flow remains the same, and the CBL becomes slightly shallower. The top of the CBL is not the top of the cold core, but its top is near the height of the barrier crest. A weak layer of stability with strong vertical wind shear is present immediately above the CBL. This vertical thermal and wind structure is very similar to the observations reported by Schneider (1991) in her examination of Phoenix II data taken east of Boulder, CO during the summer of 1984.

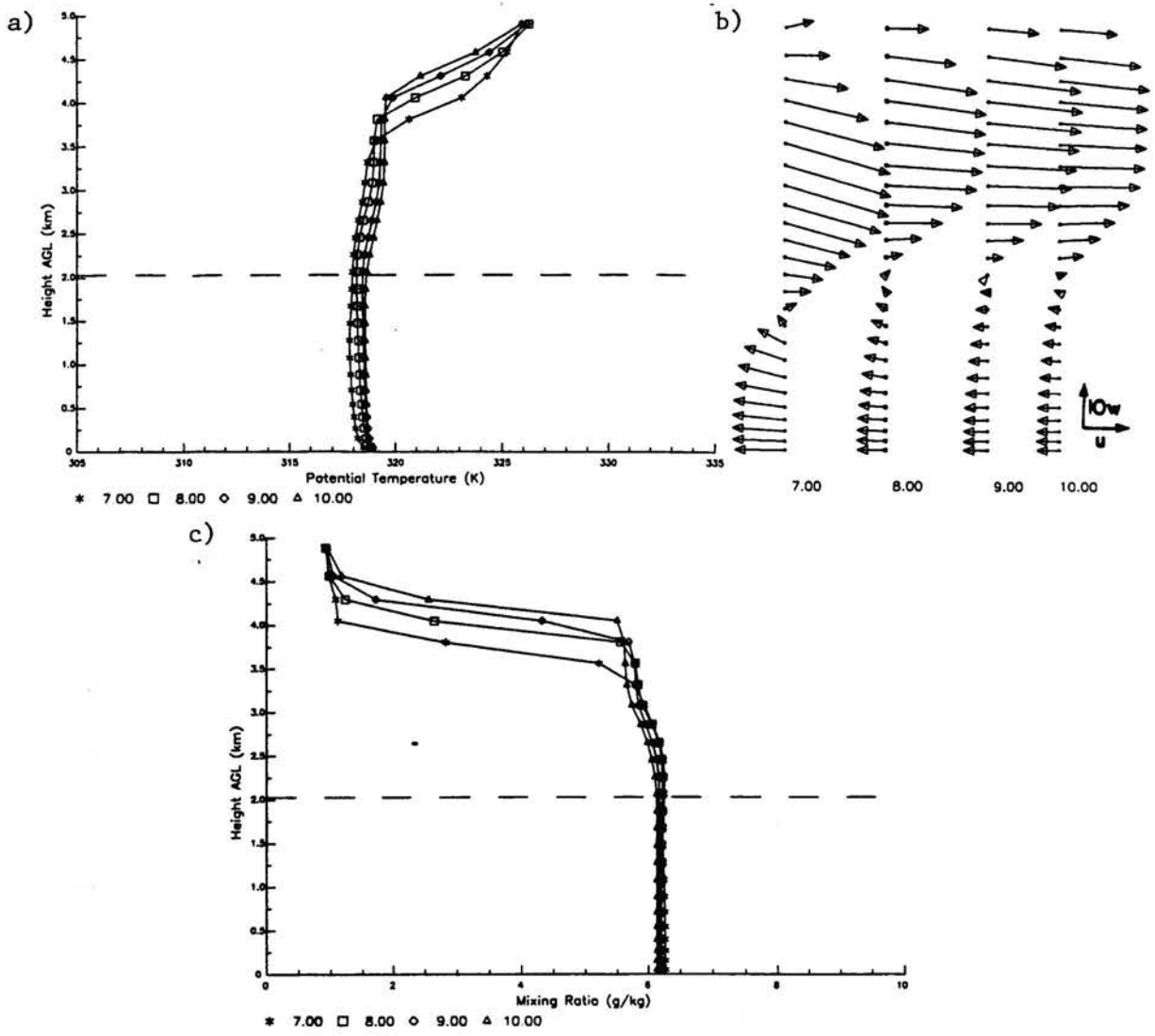

Figure 3.8. Same as "sounding" plots as in Figure 3.6 but for 7, 8, 9, and 10 hours after sunrise.

The eastward expanding cold core also influences the atmosphere above the cold core. The westerly flow in the cold core is stronger than in the region above and below it. To conserve mass flux the increased westerly flow in the cold core has to be accompanied by decreased westerly flow or increased easterly flow at other levels. The easterly upslope flow below the cold core does not increase sufficiently to counteract the increased westerly flow in the cold core. Instead, the wind speed above the cold core decreases to conserve mass flux. Flow west of the cold core is channelled into the cold core, and this channeling results in weaker westerly flow above the cold core. The weakening of the flow as well as a negative horizontal pressure gradient above the cold core looks similar to a return flow superimposed on the ambient westerly flow.

Tripoli (1986), and Tripoli and Cotton (1989b) in their no condensation simulation have the lee side convergence zone remaining stationary throughout the afternoon. Although not discussed in their papers, plots of this simulation at sunset (about 15 hours after sunrise) have an eastward expanding cold core and stronger sinking motion present immediately ahead of the leading edge of the cold core at the height of the barrier crest.

3.5 Model Generated Soundings and Vertical Integrals

The previous sections discuss the sunrise state and three phases of the daytime evolution as seen in the baseline simulation. These sections utilize plots of model fields on the inner grid and model generated soundings from the base of the barrier site. In sections 3.5.1 through 3.5.3 the vertical changes in the atmosphere for sites at the base of the barrier, on the eastern slope of the barrier, and 50km east of the base of the barrier are examined. In each section model generated soundings are presented to show what the simulated evolution would look like if it is observed by airsonde launches. Then, vertical integrals of eastward mass flux and heating are discussed. The shapes of these integrals provide further

insight into some features of the evolution, and quantities derived from these integrals are later used for further analysis of the simulations and observations. Finally, the simulated total heating in layers at differing heights are compared to the surface sensible heat flux to demonstrate how the simulated evolution moves energy.

3.5.1 Base of Barrier

Figure 3.9 shows soundings for sunrise and 3, 6, and 10 hours after sunrise for the base of the barrier site. This plot is a summary of the soundings shown previously and has a sunrise sounding plus one sounding from each phase. The soundings show the deep layer of stability at sunrise with the strong near surface jet (0 hours), the phase 1 warming (3 hours), development of the solenoid with the upslope and return flow (6 hours), and the atmosphere after the solenoid has passed (10 hours).

A better understanding of the circulation can be obtained by examining the u-component of the flow. The u-component measures the flow towards and away from the barrier. Figure 3.10 shows the u-component of the flow and the vertical integral of eastward mass flux at the base of the barrier site at two hours increments from sunrise to 10 hours after sunrise. The vertical integral of the eastward mass flux is given by:

$$M(z) = \int_0^z \rho u \, dz \tag{3.1}$$

where M(z) is the vertical integral of eastward mass flux at height z, ρ is density, u is the west-east component of the wind for a grid box, and z is height. From the model output this integral is calculated by:

$$M(z_n) = \sum_{i-1}^{i-n} \rho_i u_i (z_i - z_{i-1}) \tag{3.2}$$

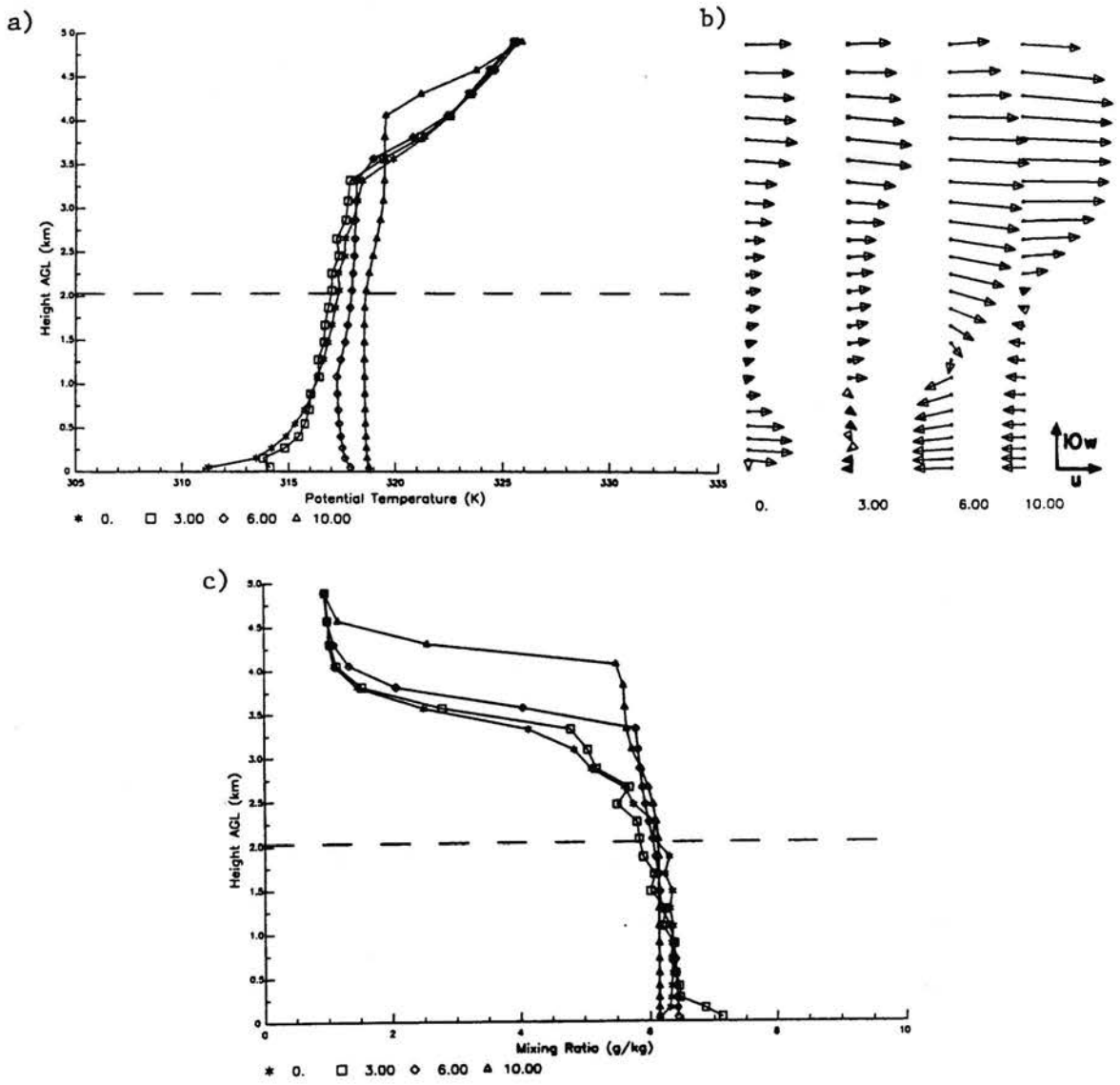

Figure 3.9. Same as "sounding" plots as in Figure 3.6 but for sunrise and 3, 6, and 10 hours after sunrise.

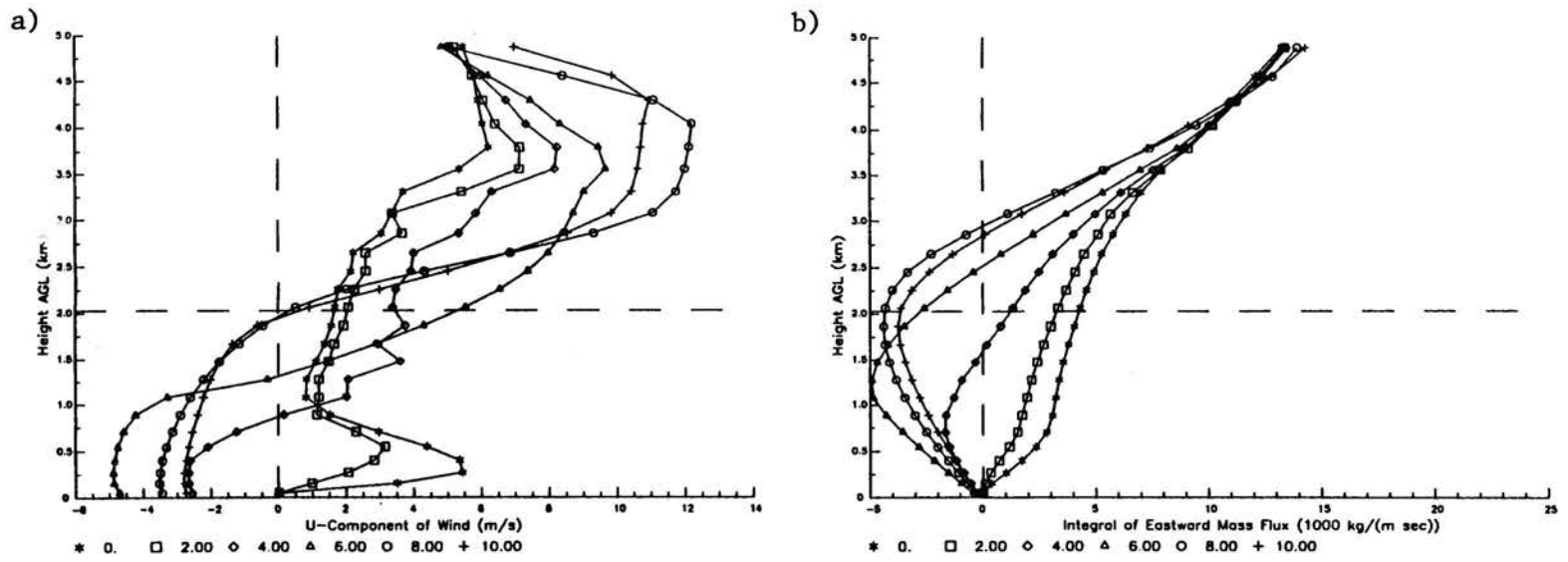

Figure 3.10. The vertical profile of the u-component of the flow and the vertical integral of eastward mass at the base of the barrier site in the baseline simulation for sunrise and 2, 4, 6, 8 and 10 hours after sunrise. The dashed horizontal line is at the height of the barrier top.

where ρ_i is the density of the grid box i, u_i is the west-east component of the wind in grid box i, and z_i is the height of the top of grid box i. The level z_0 is the surface, and z_0 equals zero. This integral examines the mass flux towards and away from the barrier. If the line slopes upward and to the right, there is net mass flux from the west toward the east (positive eastward mass flux). The opposite is true for a line sloping upward and to the left (positive westward mass flux). As the lines become closer to vertical, the magnitude of the mass flux decreases.

The u-component winds show the jet near the surface at sunrise with the flow slowing to a minimum at about 1.0km. Upslope flow develops by 4 hours after sunrise, and it continues to intensify until at least 6 hours after sunrise. During this time, the westerly return flow increases. The vertical integrals show increasing westward mass flux in the upslope flow between 4 and 6 hours after sunrise which is seen by the increasing magnitude of the integral minimum during this time. The integrals also show increasing depth of the upslope flow between 4 and 6 hours after sunrise which is seen by the increasing height of the minimum value during this time. Above the upslope flow the slope of the integral increases, and the integrals for all the times meet at 4.25km. The meeting of the integrals indicates that throughout the day the westerly return flow below 4.25km strengthens proportionally to the increasing mass flux towards the barrier in the easterly flow. Between 6 and 8 hours after sunrise the solenoid passes over this site with the depth of the upslope flow increasing but the speed of the upslope flow decreasing. The smaller magnitude of the minimum of the vertical integral of shows that the total westward mass flux in the upslope flow decreases during this time, and continued weakening of the westward mass flux in the upslope flow occurs between 8 and 10 hours after sunrise.

The point where the vertical integral of eastward mass flux equals zero is defined as the "top of the solenoid". This parameter gauges the depth of the circulation by defining the

height where the mass flux away form the barrier equals the mass flux towards the barrier in the upslope flow. The top of the solenoid does not define a height at which the influence of the thermally driven flow ceases, and it does not imply that all the air in the westerly return flow below this height was once in the upslope flow. The vertical integrals of eastward mass flux are almost identical throughout the day near the top of the model. The daytime evolution does not influence the total eastward mass flux throughout the entire depth of the model, but the evolution does greatly influence the mass flux at a particular heights.

The top of the solenoid increases from 4 to 8 hours after sunrise, while from 8 to 10 hours after sunrise the top of the solenoid lowers. At 4 and 6 hours after sunrise the top of the easterly upslope flow is about one-half the height of the top of the solenoid, and at 8 and 10 hours after sunrise the depth of the easterly flow is about two-thirds the height of the top of the solenoid. Before the solenoid passes, there is s vertical symmetry in the depth of the easterly upslope flow and the depth of the compensating westerly flow, but once the solenoid passes this vertical symmetry ceases.

Above 4.25km an increase in westward mass flux occurs after the solenoid passes. As discussed in section 3.4.4, the cold core channels ambient flow from west of the barrier crest into this region. Above this region of increased eastward mass flux, slowing of the wind conserves the mass flux over this site between the surface and the top of the model domain.

An approach similar to the vertical integral of eastward mass flux in the analysis of winds is used to quantify the thermal structure. Figure 3.11 shows plots of potential temperature and the vertical integral of heating, calculated from the sunrise sounding, for the base of the barrier site. The vertical integral of heating is given by:

$$I_H(z) = \int_{t_1}^{t_2} \int_{z}^{H} \rho C_p \frac{T}{\theta} \frac{\partial \theta}{\partial t} dz dt \qquad (3.3)$$

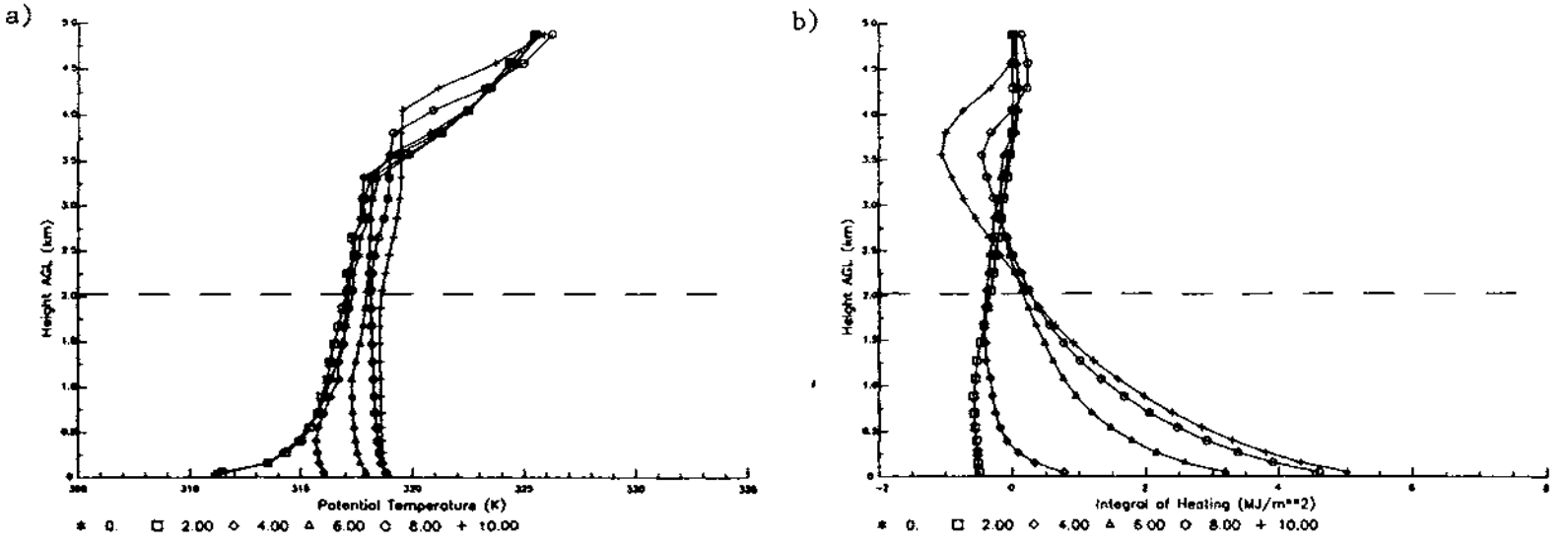

Figure 3.11. Vertical profiles of potential temperature and the vertical integral of heating calculated from sunrise for the base of the barrier site in the baseline simulation for sunrise and 2, 4, 6, 8, and 10 hours after sunrise. The dashed horizontal line is at the height of the barrier top.

where $I_H(z)$ is the vertical integral of heating from height H to height z, t_1 and t_2 border the time period over which the integral is calculated, H is a height from which the integral is calculated, ρ is the density of the air, C_p is the specific heat of the air, and θ is potential temperature. From the model output the vertical integral is calculated by:

$$I_H(z_{n-1}) - \sum_{i=n}^{m} \rho_i \pi_i C_p \left(\theta_i(t_2) - \theta_i(t_1)\right)(z_i - z_{i-1}) \tag{3.4}$$

where the π_i is the Exner function for grid level i, $\theta_i(t_2)$ is the potential temperature for grid level i at time t_2 ($\theta_i(t_1)$ is for time t_1), and z_m equals height H. In this Figure height H is the first model grid point below 5.0km AGL and t_1 is sunrise. Integrals which slope downward and to the right show warming with the opposite being true for lines sloping downward and to the left. The closer the line is to vertical; the smaller is the magnitude of heating or cooling.

This Figure shows warming throughout the day below barrier top, which is about 2.0km, and significant warming above the CBL throughout the day. After the leading edge of the cold core passes over the site, cooling is evident above 3.5km. The amount of warming above the CBL is a significant percentage of the heating in the CBL. From sunrise to 6 hours after sunrise the amount of warming above the CBL is about 25% the amount of heating in the CBL. From sunrise to 8 hours after sunrise it is about 17%, excluding the cooling from 3.5 to 4.5km. In the CBL the major source of heating is vertical diffusion which results from the positive surface sensible heat flux. Horizontal advection is the only significant term in the CBL providing cooling.

The circulations move energy laterally and vertically during the day causing heating at some heights and cooling at other heights. The combined effect of the circulations can cause a net import or export of energy over a site. Figure 3.12 shows the total amount of heating from the surface to 2.0km, 3.0km, 4.0km, 5.0km, and 6.0km along with the surface

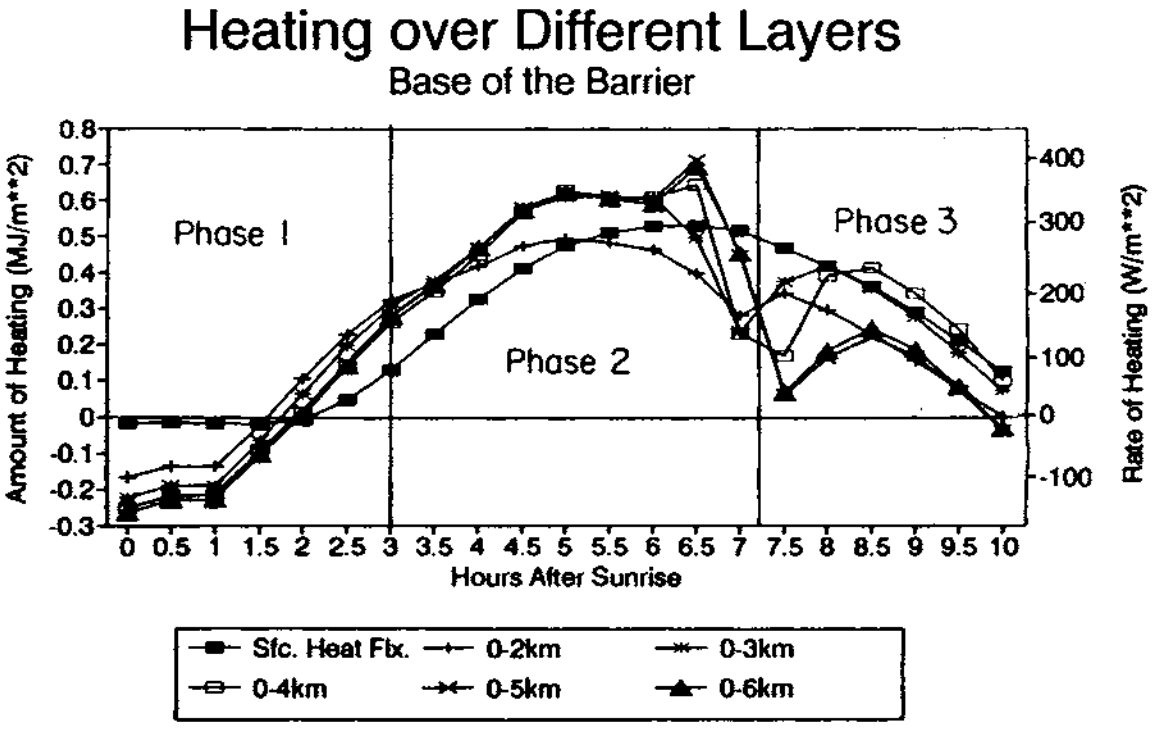

Figure 3.12. The surface sensible heat flux and amount of heating over different layers at the base of the barrier site in the baseline simulation. The values are for half hour periods and are plotted at the end of the half hour period.

sensible heat flux. The values plotted are the amount of heating over half hour periods. These values are calculated from equation 3.3 with H being the height of the top of the layer, z being the surface, t_1 being the beginning of the half hour period and t_2 being the end of the half hour period. For example, the amount of heating from the surface to 2.0km from 2.5 to 3 hours after sunrise is given by:

$$\int_{2.5Hr}^{3.0Hr} \int_{0}^{2.0km} \rho C_p \frac{T}{\theta} \frac{\partial \theta}{\partial t} \, dz dt \tag{3.5}$$

The difference between two integrals gives the amount of heating between the tops of the layers. For example, the difference between the 0-2.0km and 0-3.0km values gives the net heating between 2.0 and 3.0km. The data is plotted for the time at the end of the half hour period.

The phase 1 heating is clearly evident in the 0-2.0km amount of heating at 1.5 to 3 hours after sunrise (the data plotted at 2 hours covers the period from 1.5 to 2.0 hours). Warming up to $0.3MJm^{-2}$ ($167Wm^{-2}$) over a half hour period occurs despite negative or slightly positive surface sensible heat flux. At this time the circulations tend to import energy into the region. As phase 2 begins the net heating continues to be greater than the surface sensible heat flux. Until 6.5 hours after sunrise the net heating is greater than the surface sensible heat flux, but the difference between these two quantities decreases with time. During this time the daytime simulation is a net importer of energy into the region. Beginning at 4 hours after sunrise, a noticeable difference between the 0-2.0m and 0-3.0km values develops showing substantial warming between 2.0 and 3.0km.

The dip in the vertical integrals at 7.5 hours (7.0 to 7.5 hour period) after sunrise is associated with the passage of the solenoid. After the solenoid passes the amount of heating is generally less than the surface sensible heat flux indicating that the circulations tend to

export energy from over this site. The integrals show net heating up to 4.0km with substantial cooling from 4.0km to 5.0km (the 0-5km amount of heating is much less than for 0-4km). The vertical integral of heating (Figure 3.11) for times after the solenoid passed shows strong cooling above 3.5km associated with the top of the cold core becoming higher over this site. Throughout the day there is very little difference between the 0-5 and 0-6km amounts of heating, indicating little change to the thermal structure occurs above 5.0km.

3.5.2 East Slope of Barrier

Figure 3.13 shows soundings at a location 30km west of the base of the barrier. This site is near the middle of the eastern slope of the barrier, and its elevation is 1001m higher than the base of the barrier site. At sunrise a layer of stability exists from the surface to about 1500m AGL, and stronger u-component winds occur near the surface. Above the near surface jet the winds are nearly calm from about 1.2km to 3.0km. During the day the CBL deepens with cooling near the top of the CBL, and the u-component winds increase between about 1.0km and 2.7km with weakening u-component winds below 1.0km. The presence of westerly winds at the surface throughout the day shows that this site is west of the lee side convergence zone.

Figure 3.14 shows the same three plots as figure 3.10-3.12 for this site 30km to the west of the base of the barrier. The u-component shows a strong near surface jet at sunrise with a maximum u-component of $9.1 ms^{-1}$ at 275m AGL. As the day progresses the jet weakens. Between 1.0km and 2.7km the u-component increases, and above 2.7 the u-component weakens. The vertical integral of the mass flux shows that the daytime evolution makes a more uniform vertical distribution of mass flux throughout the lowest 2.75km. Above 2.75km the integrals show that the total mass flux decreases until 6 hours after sunrise and increases afterwards.

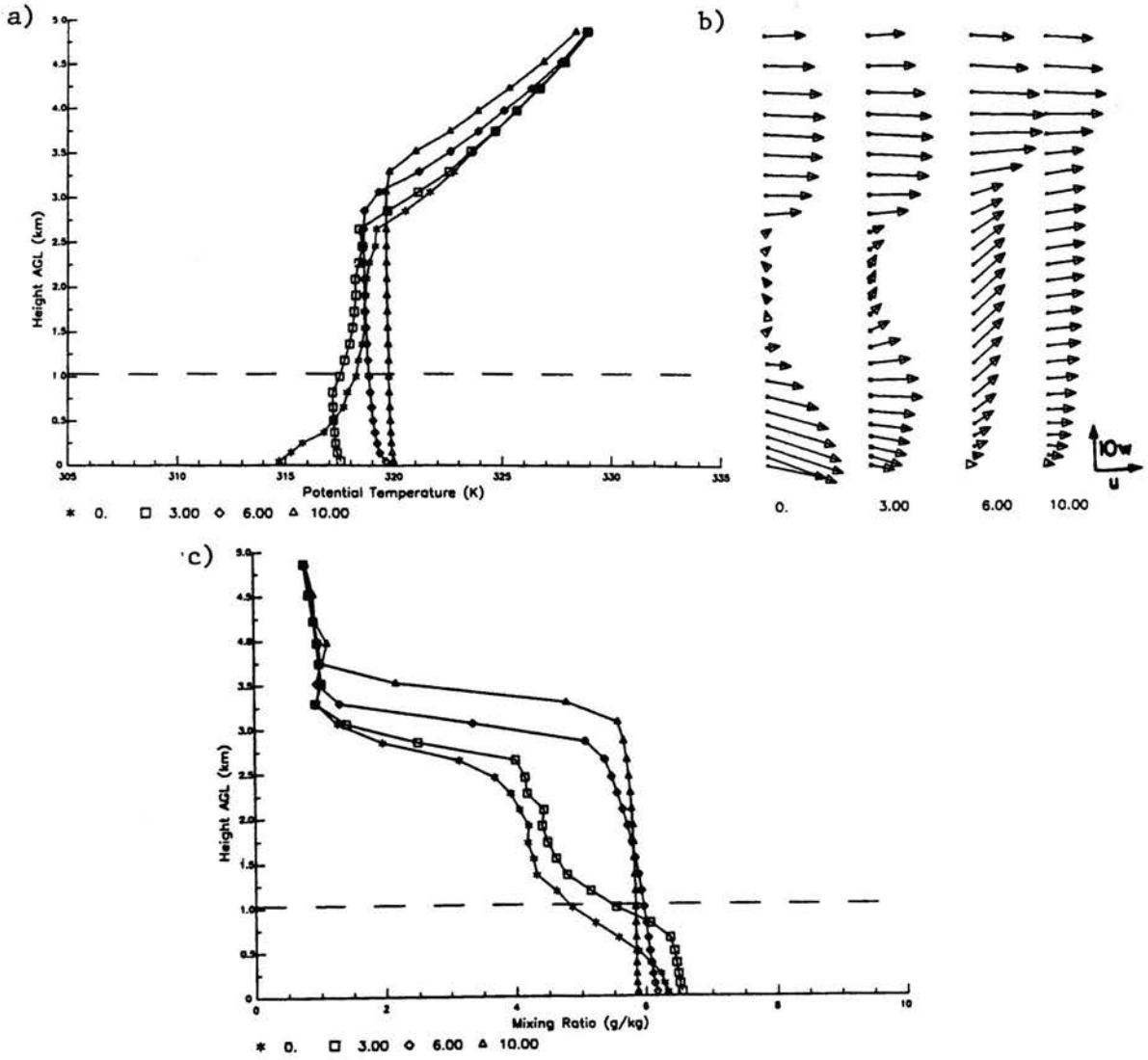

Figure 3.13. The same "sounding" plots as Figure 3.6 for a site 30km to the west of the base of the barrier in the baseline simulation.

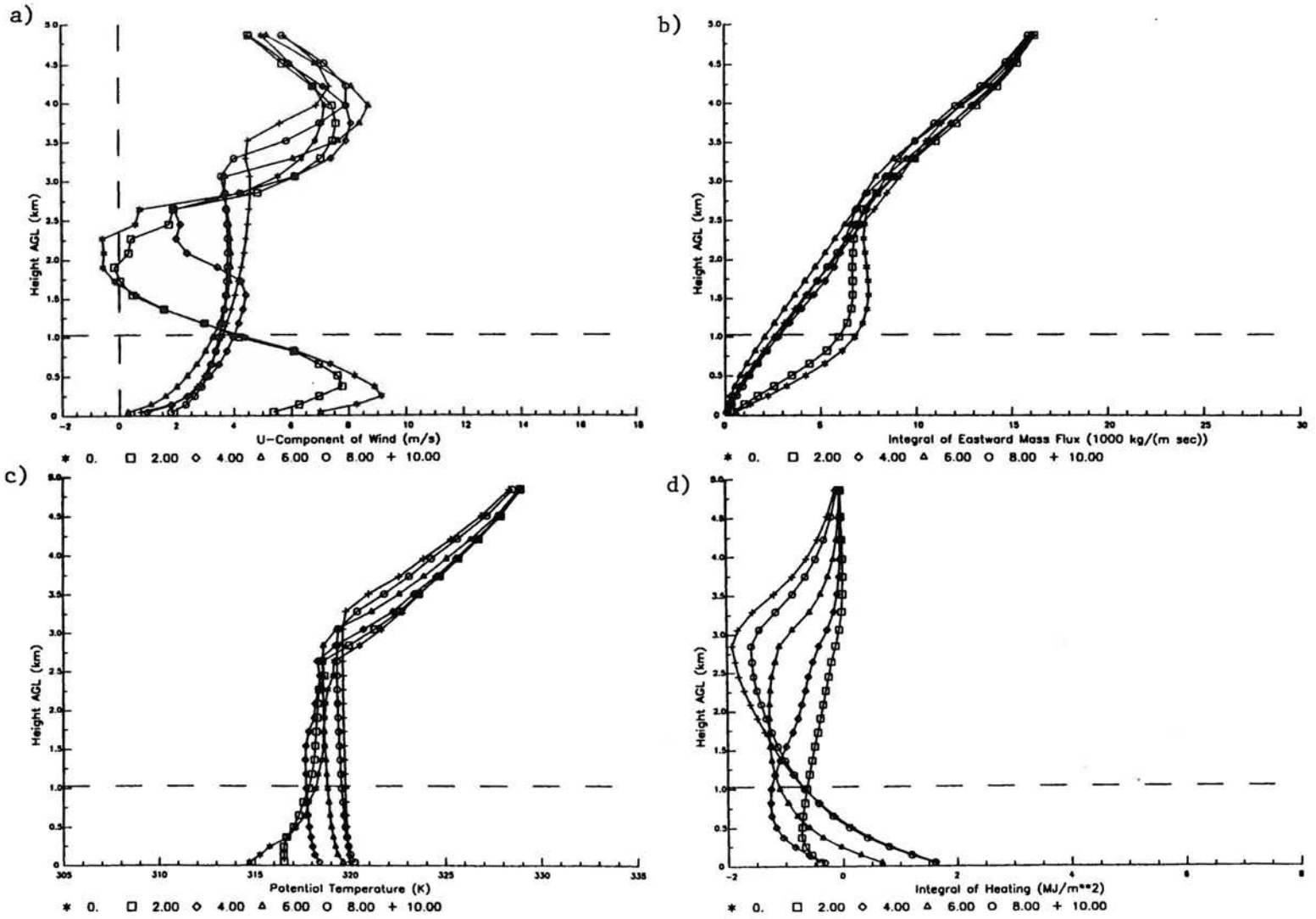

Figure 3.14. Plots for a site 30km west of the base of the barrier site in the baseline simulation. a) and b) are plots similar to Figure 3.10. c) and d) are plots similar to Figure 3.11.

e)

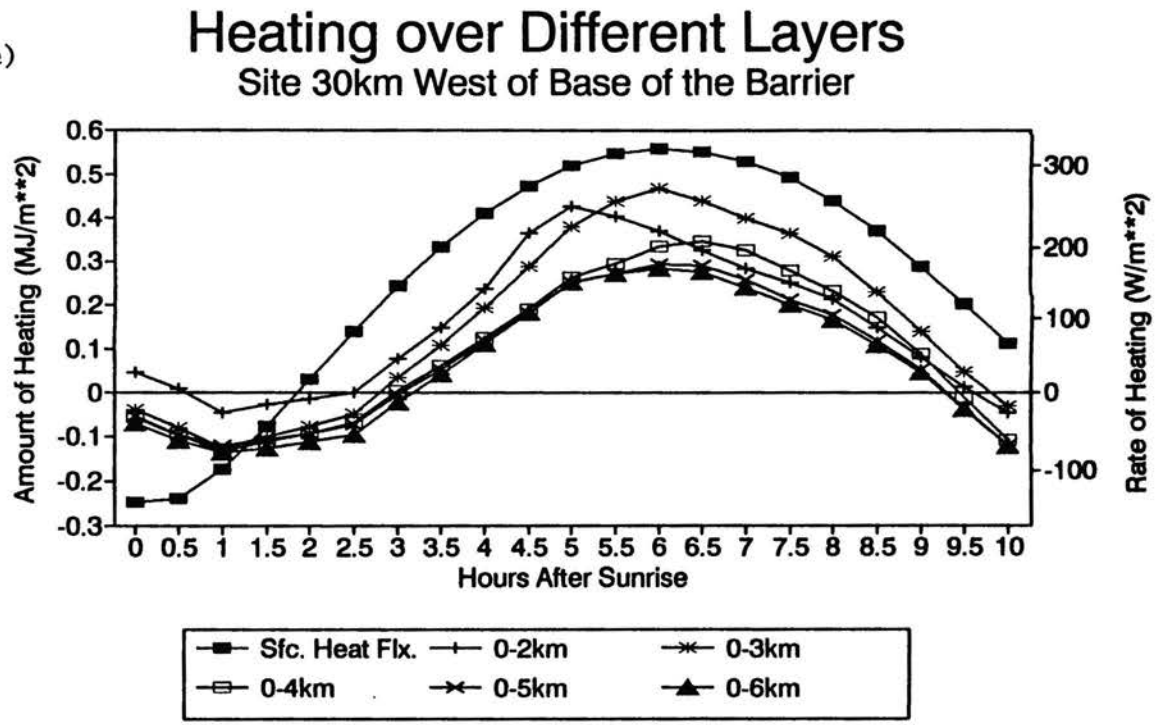

Figure 3.14. Plots for a site 30 km west of the base of the barrier site in the baseline simulation. This plot (e) is of the same format as in Figure 3.12.

The vertical integral of heating for sunrise to 2 hours after sunrise show strong warming in the lowest 500m of the sounding with cooling above. As the daytime evolution progresses strong cooling occurs in the upper portion of the CBL and above the CBL. From sunrise to six hours after sunrise the total amount of cooling from the lowest height where cooling occurs (1.75km) to 5.0km is about 65% of the total heating below 1.75km. The transition from net heating to net cooling is used to define the dividing height between lower and upper portion of the CBL. In the simulation the cold core builds into the warmer air, and the thermal profile shows the development of the cold core as cooling in the upper portion of the CBL and above the CBL.

The plot with total heating for different layers shows only slight cooling in the 0-2.0km layer during the early part of the day, and the warming in the lowest 500m of the sounding is masked by some cooling above 500m. The warming near the surface during the first 2 hours after sunrise occurs despite a negative or weakly positive surface sensible heat flux. As the daytime evolution continues, the total heating is generally largest in the 0-3km layer after 5.5 hours, and strong cooling occurs above 3km resulting from the deepening of the cold core. The total heating in the various layers, compared to the surface sensible heat flux, clearly shows that the circulations export energy away from over this site during the day. The similarity of the 0-5 and 0-6km total heating shows that little heating occurs above 5.0km AGL.

Figure 3.15 shows the same plots for a site which is 10km to the east of and about 220m lower than the previous site. During the day, the winds near the surface become easterly indicating that the site is east of the lee side convergence zone. The westerly return flow is stronger and deeper than the site 10km to the west. The vertical integral of eastward mass flux shows the easterly upslope flow in the lower layers, and the shape of the integral resembles the base of the barrier site more closely than the site 10km to the west. The

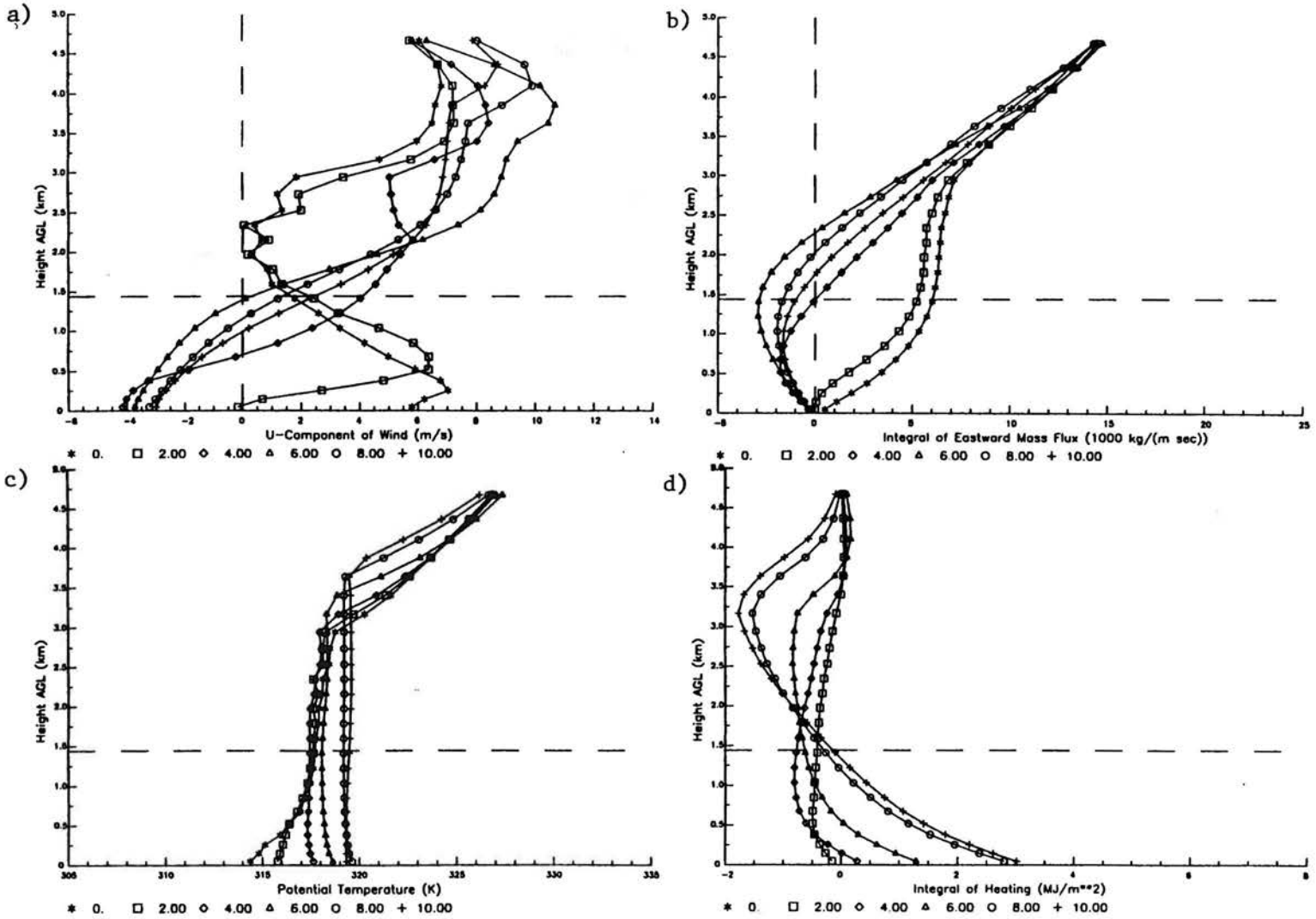

Figure 3.15. Same as Figure 3.14 but for a site 20km west of the base of the barrier in the baseline simulation. a) and b) are plots similar to Figure 3.10 and c) and d) are plots similar to Figure 3.11.

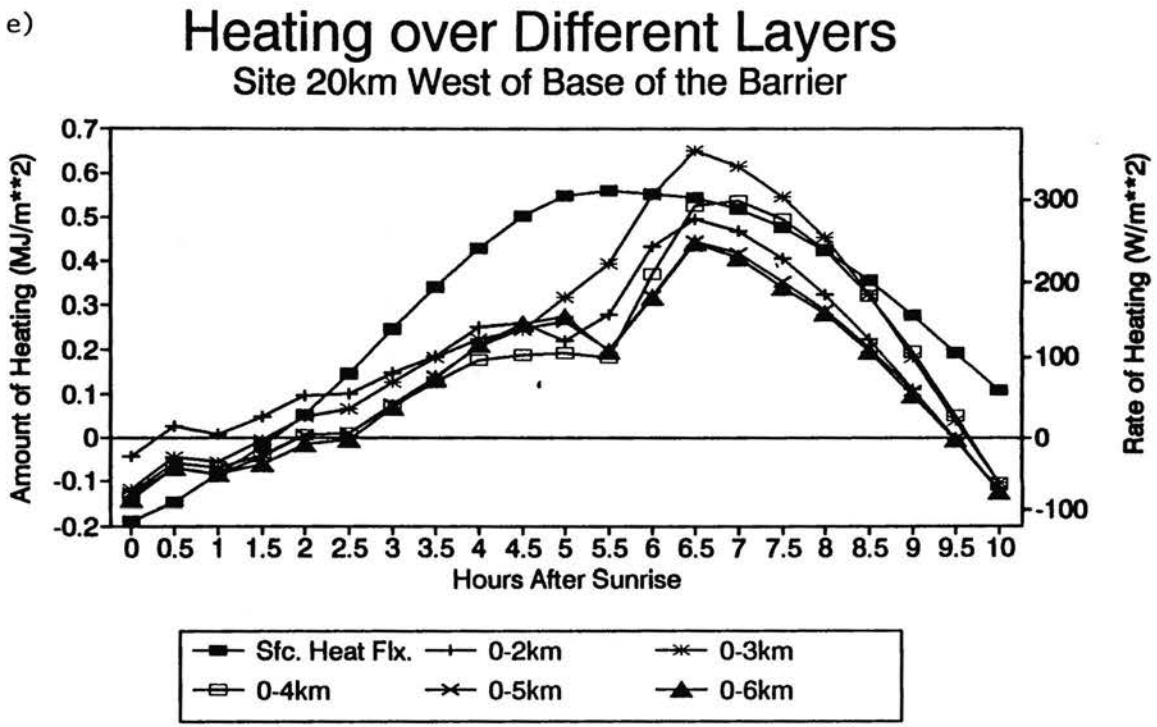

Figure 3.15. Same as Figure 3.14 but for a site 20km west of the base of the barrier in the baseline simulation. This plot (e) is of the same format as in Figure 3.12.

vertical integral of heating shows warming in the lowest 500m for the first two hours after sunrise. During the day strong cooling occurs in the upper portion of the CBL. From sunrise to 6 hours after sunrise the cooling in and above the CBL is about 35% of the total warming in the lower portion of the CBL. This percentage is less than the site 10km to the west. The total heating plots show the warming near the surface for the first two hours after sunrise despite the negative or weakly positive surface sensible heat flux. Afterwards, the circulations export energy from this site, but less energy is exported than the site 10km to the west especially after about 6 hours after sunrise. The differences in the surface sensible heat flux and amount of heating 0-5.0km is about 0.13MJm^{-2} (72Wm^{-2}) for this site versus about 0.26MJm^{-2} (144Wm^{-2}) for the site 10km to the west.

3.5.3 Site 50km East of Base of Barrier

Figure 3.16 shows model generated soundings for a site 50km to the east of and about 70m lower than the base of the barrier site. At sunrise westerly winds occur near the surface, and a layer of stability about 1.5km deep is present. During the day the westerly flow at the surface is replaced by weak easterly upslope flow. Warming appears above the growing CBL, and this warming is weaker than at the base of the barrier site. By 10 hours after sunrise significant warming is seen below 3.3km and above the CBL with some cooling above indicative of the leading edge of the cold core passing over the site.

Figure 3.17 shows the integral and total heating plots for this location. These plots are qualitatively similar to the base of the barrier site. At sunrise the maximum u-component is 3.2ms^{-1} at 150m AGL. The easterly upslope flow develops by 6 hours after sunrise, and it deepens throughout the day. Between 6 and 8 hours after sunrise the depth of the upslope flow and the westward mass flux in the upslope flow greatly increase. The mass flux in the upslope flow is less than at the base of the barrier site, suggesting a weaker thermally driven

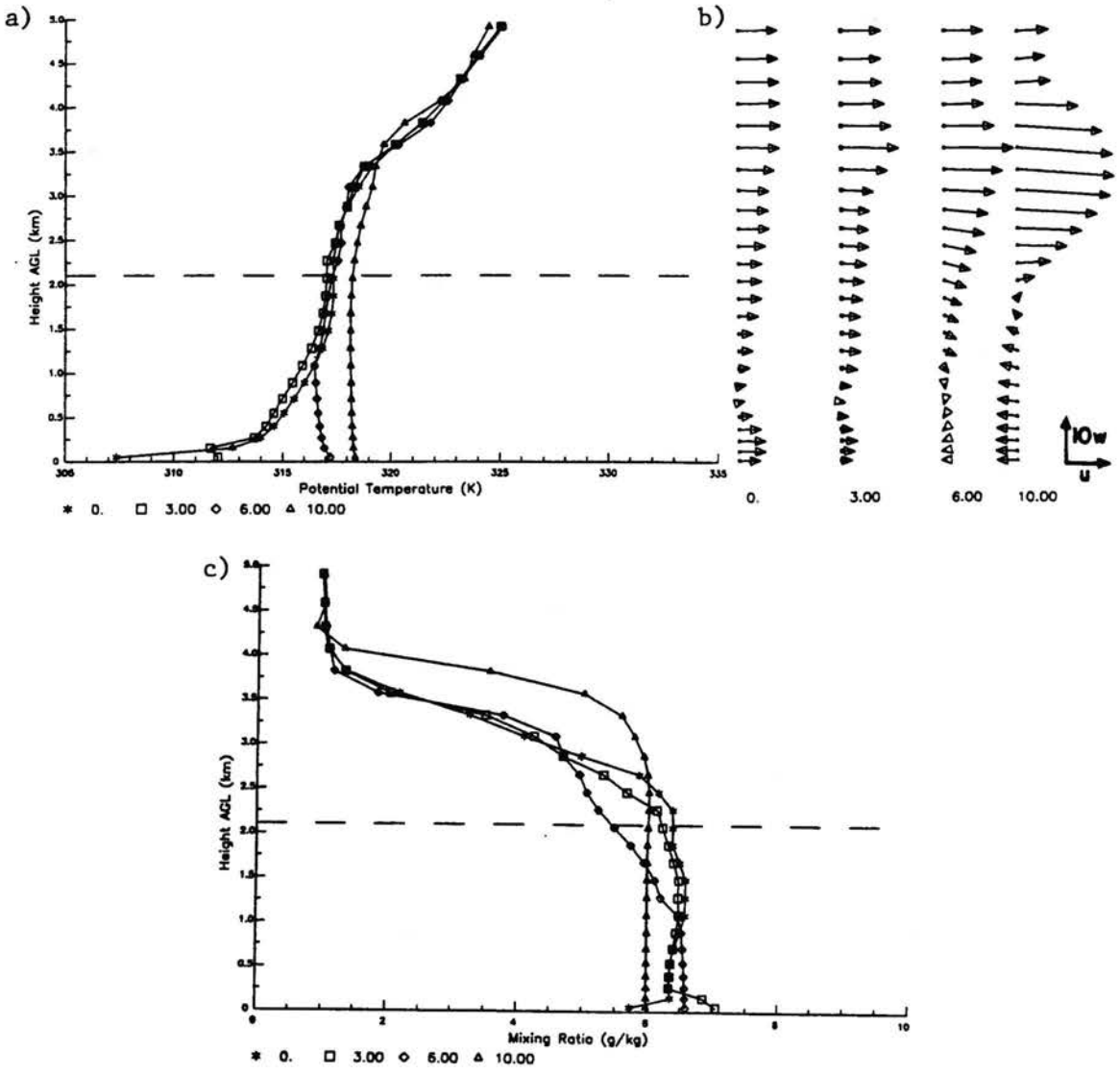

Figure 3.16. The same "sounding" plots as Figure 3.6 but for a site 50 km east of the base of the barrier in the baseline simulation.

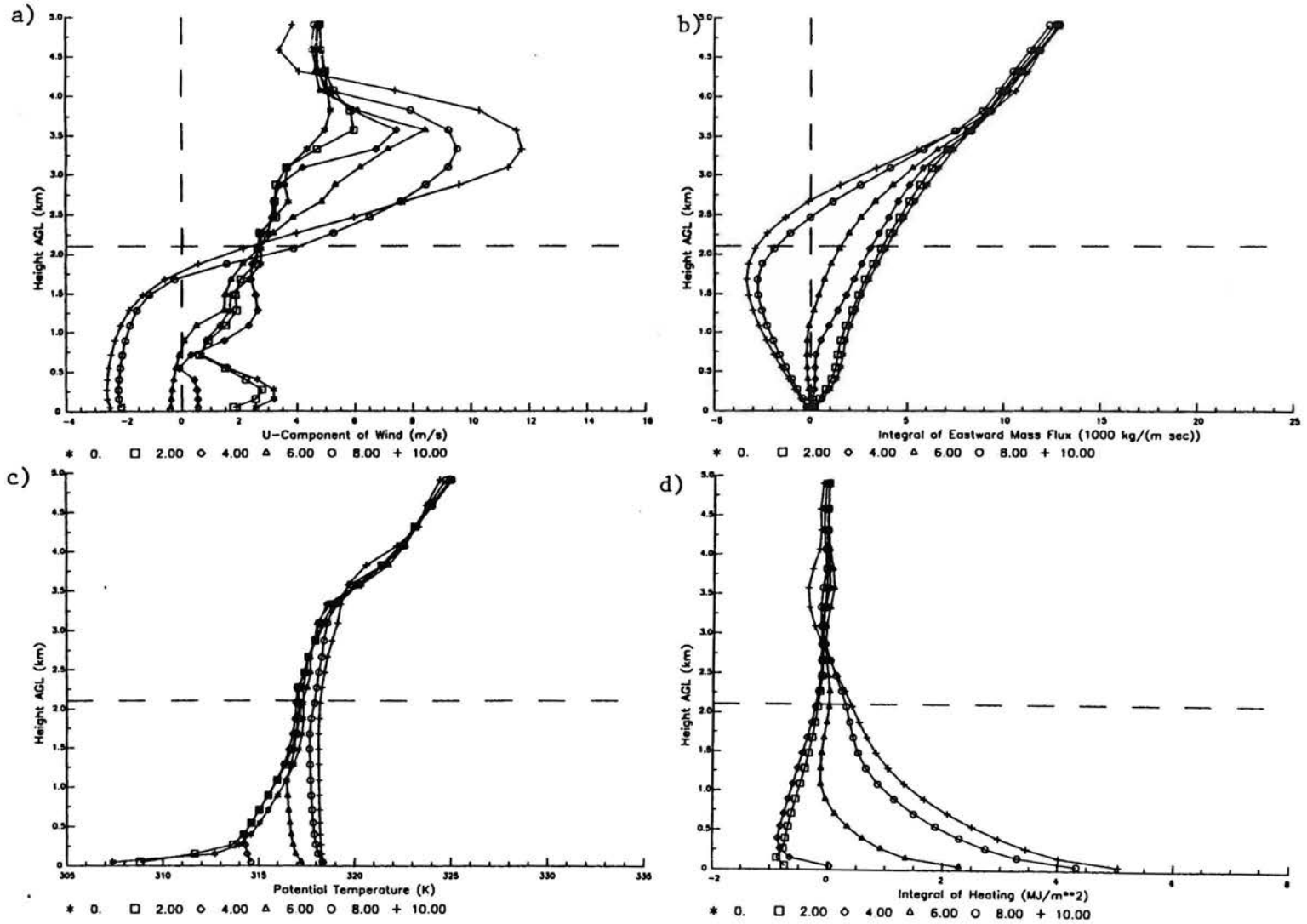

Figure 3.17. Same as Figure 3.14 but for a site 50km east of the base of the barrier site in the baseline simulation. a) and b) are plots similar to Figure 3.10 and c) and d) are plots similar to Figure 3.11.

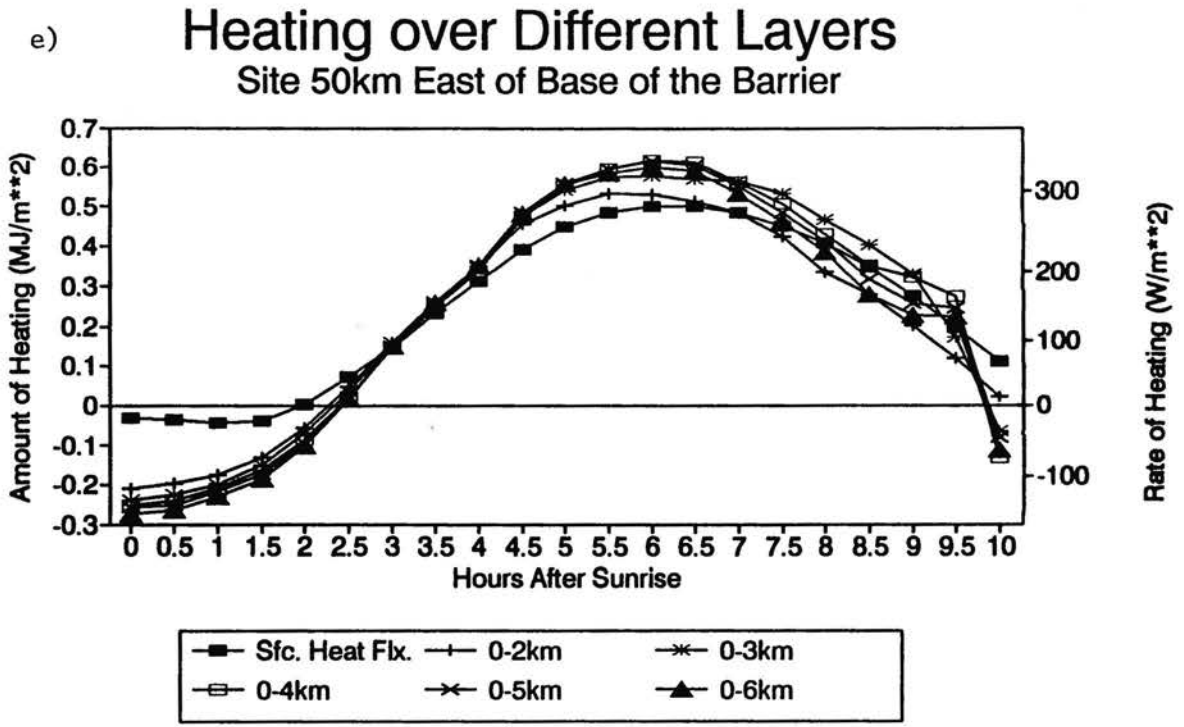

Figure 3.17. Same as Figure 3.14 but for a site 50 km to the east of the base of the barrier site in the baseline simulation. This plot (e) is of the same format as in Figure 3.12.

circulation at this site. The integrals of the eastward mass flux for all the times meet at about 3.8km which is lower than the base of the barrier site. The vertical integrals of heating have the same general shape as at the base of the barrier with less heating occurring above the CBL during the daytime than at the base of the barrier. At 6 hours after sunrise weak heating occurs above the CBL, and the CBL does not appear to be suppressed by this warming.

The total heating from the surface to different heights compared to the surface sensible heat flux (Figure 3.17e) does not show any phase 1 warming, which is expected since this warming is only seen to about 20km east of the base of the barrier. Beginning at 4.5 hours after sunrise the amount of heating above the site is significantly larger than the surface sensible heat flux. The increased heating is associated with the warming aloft resulting from the developing return flow. Compared to the base of the barrier site, much less of the heating occurs above barrier top, and the amount of warming in the layer from 2.0 to 3.0km is less. After 7 hours after sunrise some cooling occurs above 3.0km resulting in the total heating from the surface to 6km being about 0.07MJm^{-2} (39Wm^{-2}) less than the surface sensible heat flux at 8 hours after sunrise. At 9.5 hours after sunrise the leading edge of the cold core passes this location producing the cooling above 2km at 10 hours after sunrise.

3.6 Quantification of Model Generated Soundings

The vertical integrals of heating and eastward mass flux show that the evolution on the eastern slope of the barrier and on the eastern plains are different, with the east slope of the barrier being a net exporter of energy to the eastern plains. The shapes of the integrals for the two sites on the eastern plains are the same, but there are large differences in their magnitudes. In this section, quantities, some of which are derived from the vertical integrals, are compared for different sites on the eastern plains to examine how the evolution

varies laterally. Many of these quantities are used in the next chapter to compare the simulations with different initial conditions.

Figure 3.18 shows the total westward mass flux in the upslope flow and the maximum speed of the westerly return flow for the base of the barrier and sites up to 50km to its east. These quantities are used to examine the intensity of the upslope and return flows. As the distance from the base of the barrier increases, the upslope flow is weaker and develops later. Beginning at 20km east of the base of the barrier at 5 hours after sunrise, the slope of the westerly mass flux becomes steeper. This change in slope accompanies the passage of a high pressure ridge in the stable core over a site, and the development of this ridge is one of the main features associated with the second stage in phase 2 of the evolution. The rate of increase of the upslope mass flux is larger, seen as a steeper slope, after the ridge passes over a site. By 6.5 hours after sunrise the change in the rate of increase of mass flux in the upslope flow, associated with the ridge in the stable core, progresses eastward to the site 50km east of the base of the barrier. For at least the first 50km east of the base of the barrier the rate of intensification of the upslope mass flux west of the high pressure ridge is nearly the same, with a slightly less rate of intensification further east.

The peak in the mass flux at each site is associated with the passage of the migrating solenoid overhead. The spike in mass flux occurs later and is weaker further east, showing the eastward progression and weakening of the solenoid. After the solenoid passes a location the magnitude of the westward mass flux decreases. The post solenoid westward mass flux is similar for all the locations, suggesting that the circulation to the west of the solenoid is fairly horizontally uniform.

Before the solenoid passes a site the maximum u-component in the return flow is less further east, which is a similar trend to the westward mass flux. The peak of the maximum westerly return flow occurs half an hour later than the peak in westerly mass flux associated

a)

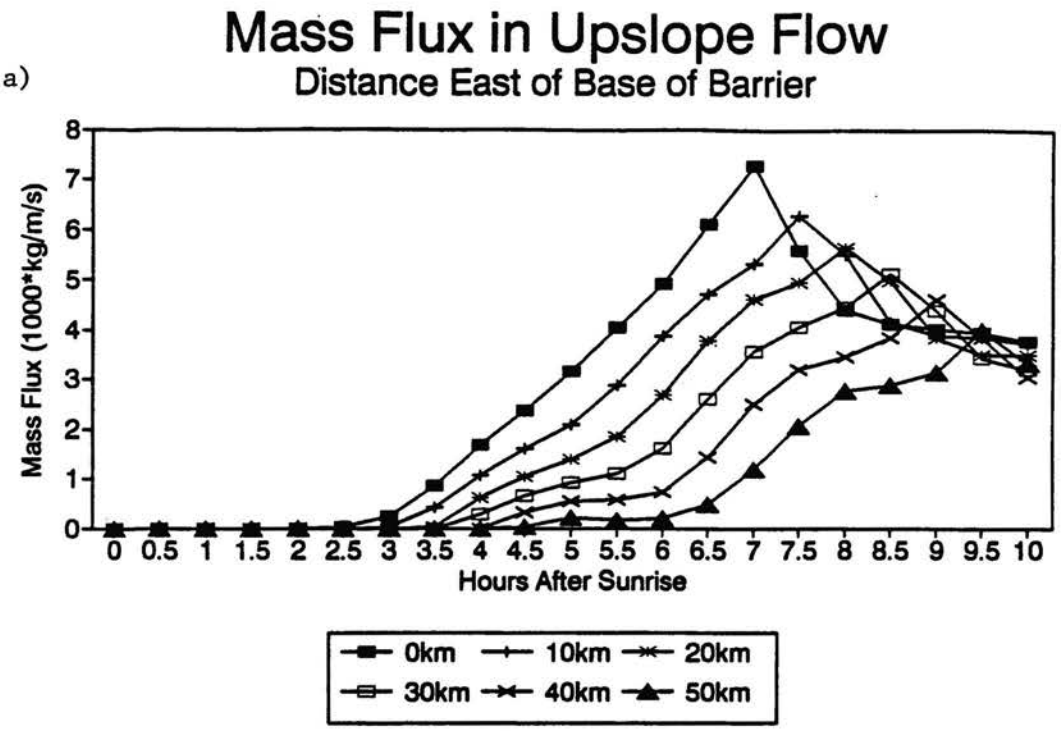

b)

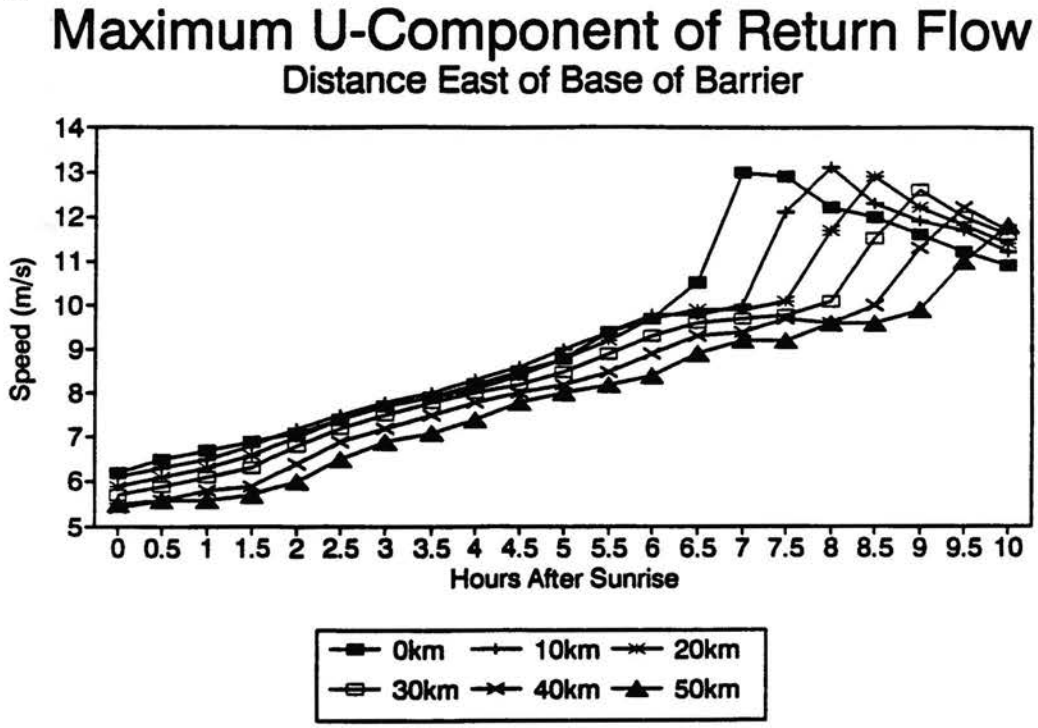

Figure 3.18. The westward mass flux in the upslope flow (a) and maximum u-component of the return flow (b) in the baseline simulation for the base of the barrier site and locations to the east.

with the passage of the solenoid. After the solenoid passes a site the speed of the maximum westerly flow continues to decrease because the region of strongest u-component flow, which is associated with the solenoid, continues to move eastward. At 10 hours after sunrise the sites further east have a larger maximum speed of the westerly flow, because the sites further east are closer to the u-component maximum associated with the migrating solenoid.

Figure 3.19 shows the depth of the easterly flow and the top of the solenoid, which is defined as the height below which the easterly mass flux equals the westerly mass flux in the upslope flow. These quantities define the depth of the different wind flows. The top of the solenoid is lower further east throughout the day, with the heights approaching the same value as the base of the barrier site after the solenoid passes the site. The top of the upslope flow generally has a similar behavior with lower heights further east. From about 7 hours after sunrise until the solenoid passes a site the depth of the upslope flow is nearly equal at all locations indicating that a steady state height of the upslope flow is achieved and that this height is changed by the passage of the solenoid. The upslope flow has approximately the same depths at all sites west of the migrating solenoid. The vertical integral of eastward mass flux shows the height where the integrals approximately meet. This height decreases moving eastward from the barrier being 4.2km, 4.1km, 4.0km, 3.9km, and 3.8km at 10, 20, 30, 40, and 50km east of the base of the barrier, respectively.

One important characteristic of the thermal field on the eastern plains is the height of the CBL. The height of the CBL is defined as the lowest grid box above the surface where the heating due to vertical diffusion is less than or equal to zero. Figure 3.20 shows plots of the CBL height. Many of the data points overlap showing that the CBL height has a generally horizontally uniform pattern. At 6 and 7 hours after sunrise the CBL height at 50km east of the base of the barrier is one grid box higher than the sites 0 to 30km east of the base of the barrier. The biggest differences in the depth of the CBL occur when the

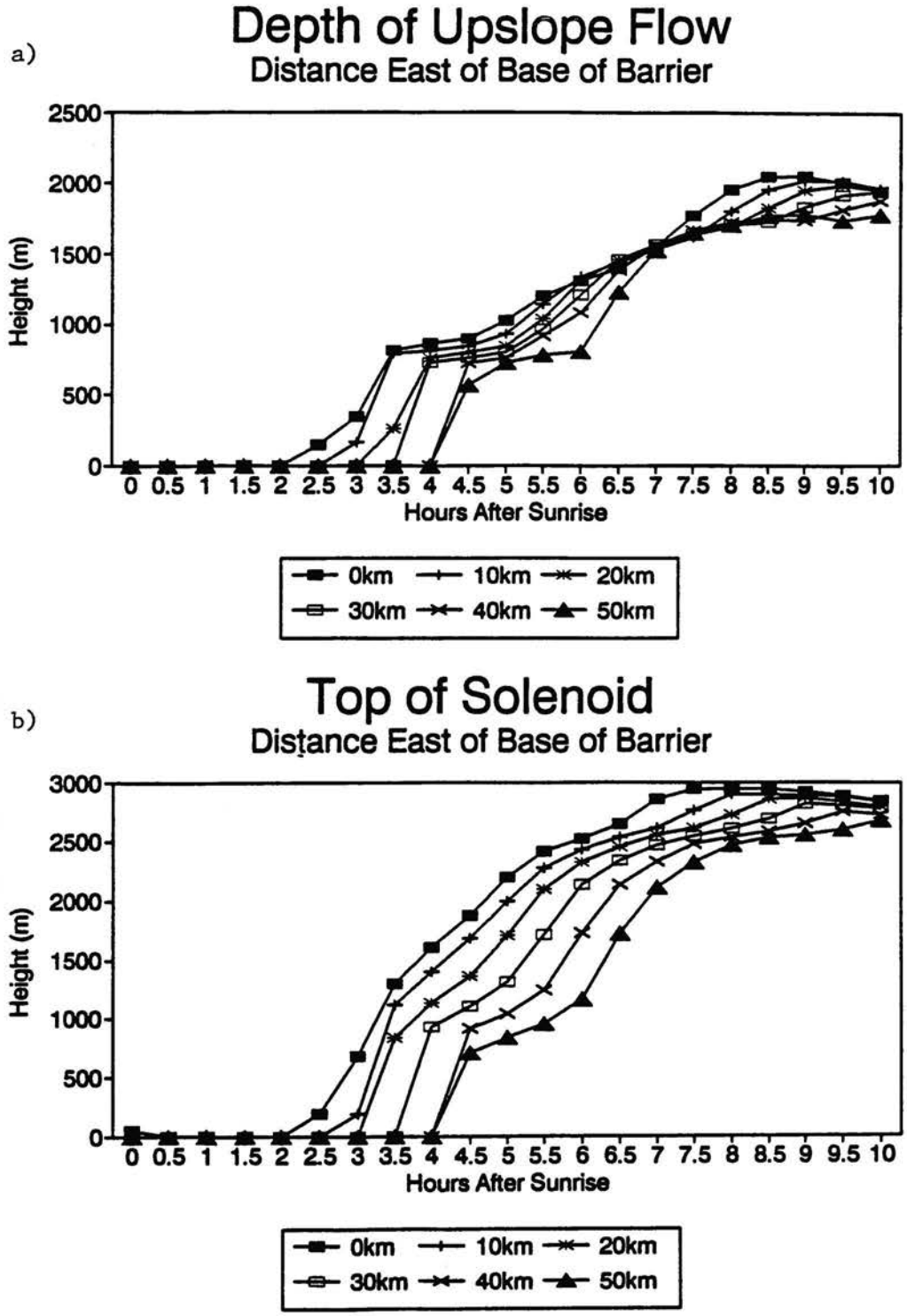

Figure 3.19. The depth of the upslope flow (a) and top of the solenoid (b) in the baseline simulation for the base of the barrier site and locations to the east.

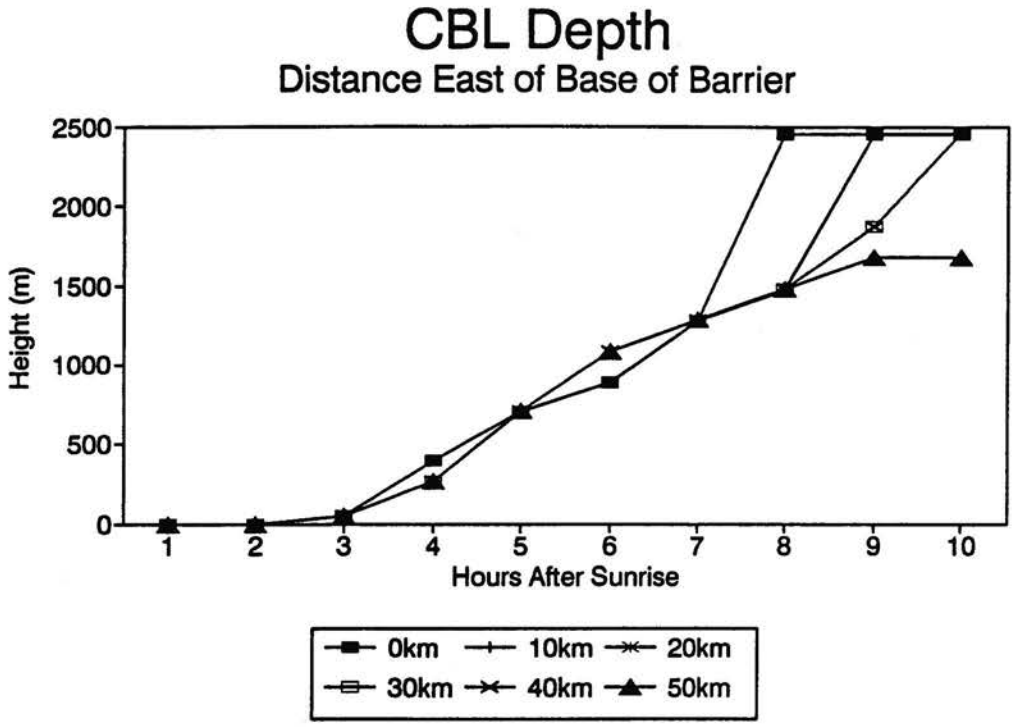

Figure 3.20. The CBL depth in the baseline simulation for the base of the barrier site and locations to the east.

migrating solenoid moves through the region. The CBL depths increase by 600 to 1200m in one hour when the solenoid passes, and the CBL depth is horizontally uniform to the west of the solenoid.

Figure 3.21 shows the amount of heating above the CBL and horizontal advection in the CBL during one hour periods for sites on the eastern plains. These parameters quantify how the circulations move energy, and these two ways the circulation moves energy suppress CBL depth. The amount of heating above the CBL is calculated by summing the total heating between the top of the CBL and the height above the CBL where heating ceases and significant cooling starts. The height of the upper level used in calculating this parameter is constrained to be at least the height of the barrier top; therefore, if significant cooling occurs above the CBL and below barrier top, the amount of heating above the CBL gives the heating from the top of the CBL to barrier top. Before the solenoid passes a site the amount of heating above the CBL increases during the day. To the east of the migrating solenoid, the amount of warming above the CBL is smaller further east. When the solenoid passes a site, the amount of warming above the CBL sharply decreases. At 10 hours after sunrise the amount of heating above the CBL is similar for the sites 0 to 30km east of the base of the barrier indicating that the circulation west of the migrating solenoid has a significant amount of horizontally uniformity.

The amount of heating above the CBL also shows the horizontal variability of phase 1 warming. The amount of warming above the CBL until 3 hours after sunrise is actually the amount of warming below barrier top, since the CBL depth is zero. The amount of warming from 1.5 to 3 hours decreases from 0 to 20km east of the base of the barrier showing the weaker phase 1 warming further east. At 20km east of the base of the barrier the phase 1 warming is weak, and east of this site there is no phase 1 warming which is seen by the significantly negative heating.

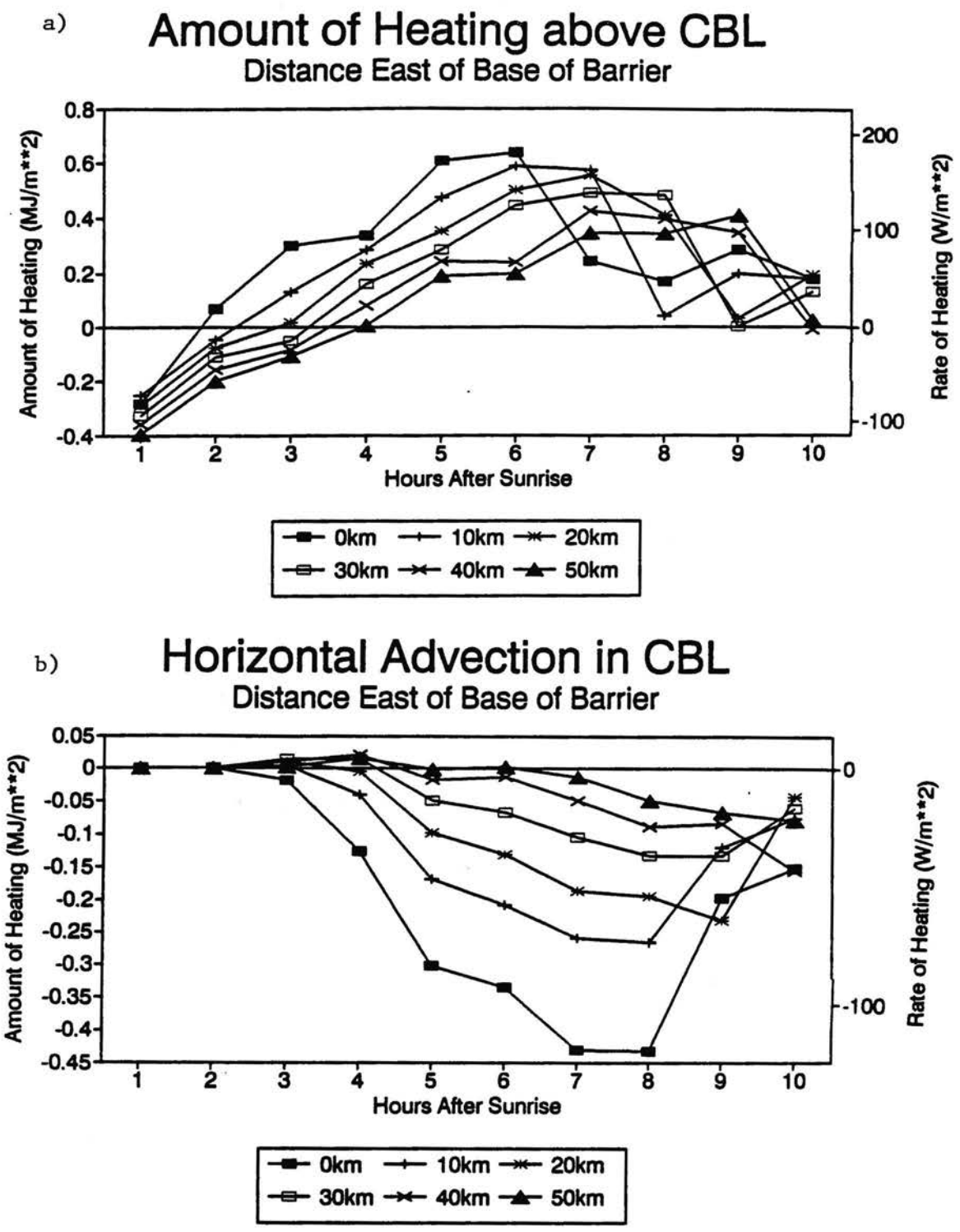

Figure 3.21. The amount of heating above the CBL (a) and horizontal advection of energy in the CBL (b) in the baseline simulation for the base of the barrier site and locations to the east. The values are for one hour periods and are plotted at the end of the period.

The horizontal advection in the CBL shows less cooling further east. This pattern of horizontal advection matches the eastward mass flux plots showing less horizontal cold air advection in the CBL for weaker upslope flow. With less cold air advection and less warming above the CBL, the CBL may be less suppressed by the solenoid further east. The CBL height diagram discussed previously shows that at 6 and 7 hours after sunrise the CBL is one grid point higher at 50km east of the base of the barrier than at the other locations; otherwise, no lowering of the CBL depth for sites closer to the base of the barrier is evident. The vertical grid point spacing at around 1.2km AGL is about 200m. If there is any west-east difference in CBL height and it is less than 200m, the model can not clearly identify such a difference using the definition of CBL height based on the heating due to vertical diffusion calculated by the model. The magnitude of horizontal advection in the CBL decreases after the passage of the solenoid. This decrease, along with the decrease in the amount of heating above the CBL, shows that west of the solenoid the daytime circulation moves less energy.

The comparison of the different quantities show that the wind and thermal changes associated with the daytime evolution further east develop later and are weaker. As seen in the mass flux plots and amount of heating above the CBL, the solenoid weakens as it moves further east. To the west of the solenoid the plots show that the atmosphere is rather similar horizontally. The horizontal changes in the warming above the CBL and in the cold air advection in the CBL do not appear to induce substantial horizontal variability in the CBL depth on the eastern plains.

CHAPTER 4.
SIMULATED DAYTIME EVOLUTION FOR DIFFERENT CONDITIONS

4.1 Introduction

The baseline simulation, which is discussed in the last chapter, shows a complex sunrise state in which the interactions between the thermally driven flows and ambient flows substantially change the atmosphere from its initial state. The daytime evolution has three phases in which the wind and thermal fields are constantly evolving. Part of the analysis of the baseline state includes the use of the vertical integral of eastward mass flux and the vertical integral of heating. The qualitative patterns of these integrals provide insight into the structure of the solenoid and the movement of energy. To study the horizontal variability of the evolution on the eastern plains, several quantities which characterize the daytime evolution are calculated for points on the eastern plains. Some of these quantities are derived from the vertical integrals, and they capture several important features of the daytime evolution.

In this chapter eleven other simulations with different initial winds, initial thermal structure, surface moisture patterns, time of year, and barrier height from the baseline run as well as a simulation without a nighttime phase are discussed. These simulations show how the differing initial conditions affect the evolution and how universal the three phase evolution is for various initial conditions. These additional simulations also provide greater insight into the physical processes associated with the evolution.

This chapter does not discuss each simulation with the same detail as in chapter 3. Showing plots of the thermal, wind, and pressure fields for several times in each simulation is very tedious. The comparison of the simulations concentrate on plots of the quantities

derived in the previous chapter. These quantities are mainly compared at the base of the barrier site, and they allow for a quantitative comparison of the simulations.

The eleven simulations are changed as little as possible from the baseline simulation, so the effect of changing one initial condition is not contaminated by other changes. Only the changes from the baseline run are mentioned; otherwise, the simulations have the same model set up, have the same initial conditions, and start at the same time as the baseline run.

4.2 Time of Year

For this group of simulations the time of the year is changed. The baseline simulation is run with heating for September 21, which is the autumnal equinox. The soil is uniformly dry at sunrise so the lateral variability of the surface sensible heat flux only results from changes in terrain slope and the wind and thermal fields in the first grid box above the surface. Three additional simulations are run. One simulation has June 21 heating, which is the summer solstice. Another run has December 21 heating, which is the winter solstice. The third run has November 1 heating, which is between the equinox and winter solstice. The comparison between the simulations uses hours after sunrise, not the time of day, as the temporal variable since sunrise occurs at different times on the different dates. Sunrise on June 21 occurs at about 4:30 A.M., at 6:00 A.M. on September 21, at about 6:30A.M. on November 1, and about 7:30 A.M. on December 21. To minimize the differences that longer or shorter nighttime phases have on the evolution, all the simulations use the 2:00 A.M. fields from the baseline simulation so the length of the nighttime cooling differs by no more than one and a half hours between the simulations.

Table 4.1 shows the maximum u-component of the near surface jet and the height of the jet maximum at sunrise for the base of the barrier site and for a site 30km to the west, which is on the eastern slope of the barrier. Both sites are discussed in detail in the previous

Table 4.1

Speed and height of the maximum u-component in the near surface jet and the height and speed of the minimum u-component at sunrise for the base of the barrier site and for the site 30km to the west for the different seasons runs.

BASE OF THE BARRIER

Run	Maximum U-component Speed (ms^{-1})	Height (m)	Minimum U-Component Speed (ms^{-1})	Height (km)
Baseline	5.5	250	0.8	1.0
June 21	5.6	250	1.1	1.1
Nov. 1	5.7	375	0.8	1.1
Dec. 21	4.8	375	0.8	1.3

30KM WEST OF THE BASE OF THE BARRIER

Baseline	9.1	275	-0.6	2.3
June 21	6.9	375	-0.2	2.3
Nov. 1	9.4	250	-0.7	1.9
Dec. 21	9.3	300	-0.5	1.9

chapter. At the base of the barrier site no substantial difference in the maximum speed between the simulations occurs, and the maximum u-component ranges from 4.8ms^{-1} to 5.7ms^{-1}. The height of the jet maximum ranges from 250m to 375m AGL with the maximum being one grid point higher for the November 1 heating and December 21 heating simulations. The speed and height of the minimum u-component and the u-component at 2.0km are similar in the simulations. At the site 30km to the west, the maximum u-component of the jet is 9.1 to 9.4ms^{-1} for the baseline, November 1 heating, and December 21 heating simulations at heights of 250 to 300m AGL. For the June 21 heating simulation the jet maximum is 6.9ms^{-1} at a height of 375m AGL.

Figure 4.1 shows the westward mass flux in the solenoid and the maximum speed of the westerly return flow at the base of the barrier site for the four simulations. These two quantities are used to compare the strength of the circulation. The values for the June 21 heating simulation are much more similar to the baseline run than the other two simulations are. After 5 hours the June 21 heating simulation has a greater westward mass flux than the baseline simulation, and the westerly return flow becomes larger by 6 hours after sunrise. By this time the cold core is deeper than in the baseline run, and the horizontal pressure gradient above barrier top which drives the westerly return flow is stronger in the June 21 heating simulation resulting in the stronger westerly winds. The peak in the westward mass flux, associated with the passage of the solenoid over the site, occurs about half an hour earlier for the June 21 heating simulation than the baseline simulation. The solenoid moves eastward at about 7ms^{-1} in the June 21 heating simulation which is about 2ms^{-1} faster than the baseline simulation.

After the solenoid passes, the westward mass flux and maximum speed of the westerly return flow are greater for the June 21 heating run than the baseline run due to the longer daylength and the greater heating. Sunrise is 1.5 hours earlier than the baseline simulation

a)

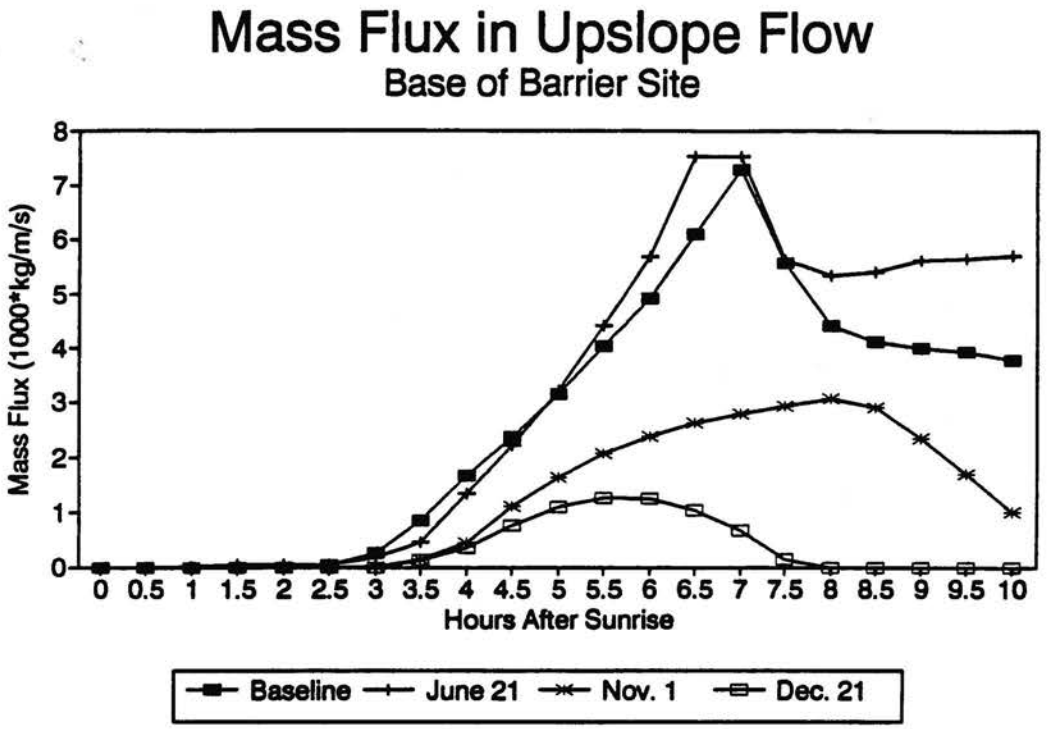

b)

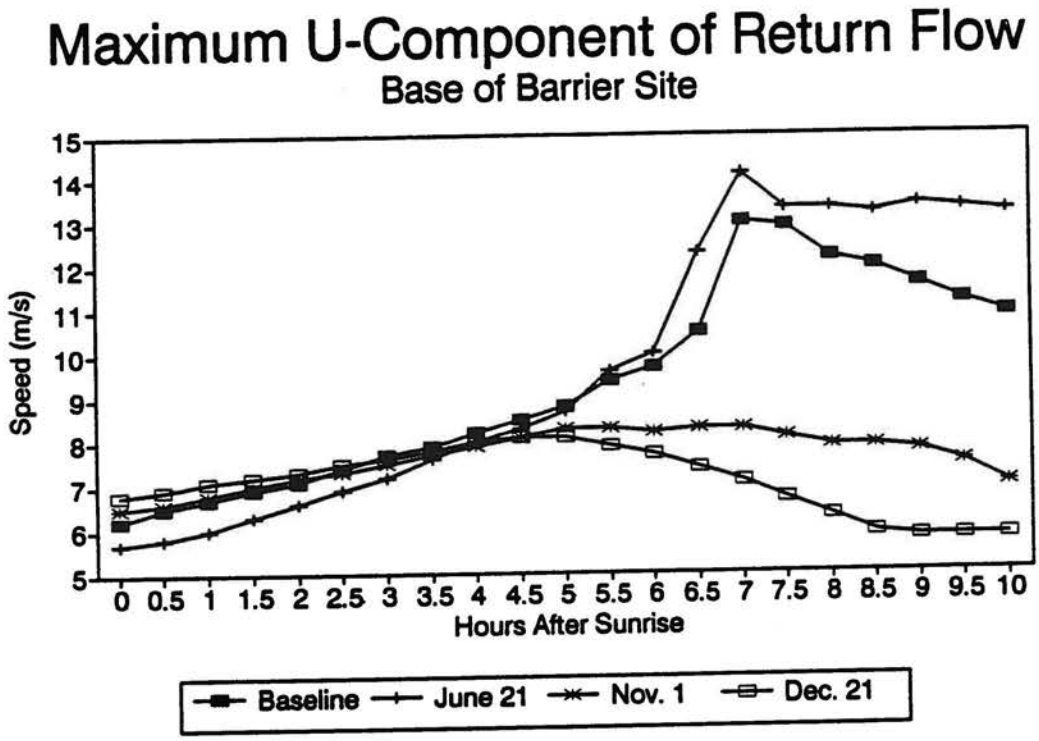

Figure 4.1. The westward mass flux in the upslope flow (a) and maximum u-component of the return flow (b) at the base of the barrier site for the time of year simulations.

and the solenoid passes over the site before noon. Plenty of strong heating occurs after the solenoid passes. In the baseline run the solenoid passes over the site at about 1:00 PM and sun sets at about 6:00 PM.

The December 21 heating and November 1 heating simulations have much different evolutions of these two quantities. The westward mass flux is weaker than the baseline run, and there is no evidence of the peak associated with the passage of the solenoid. The peak westward mass flux for the November 1 heating simulation is about 45% as large as the peak for the baseline simulation, and the peak for the December 21 heating simulation is only about 18% of the baseline's maximum. The maximum speed of the westerly return flow does not show the sharp increase seen in the baseline and June 21 heating simulations. For the November 1 heating simulation the maximum u-component of the return flow increases by only $2ms^{-1}$ throughout the day, and for the December 21 heating simulation the increase is about $1ms^{-1}$.

Figure 4.2 shows the height of the top of the solenoid and the depth of the easterly upslope flow. Like in the previous Figure, the June 21 heating and baseline simulations are similar with the two weaker heating simulations being substantially different. The depth of the upslope flow and top of the solenoid are higher for the June 21 heating run than the baseline run after 6 hours, and the differences increase later in the day. The longer daylength and stronger afternoon heating for the June 21 heating simulation causes deeper circulations after the solenoid passes compared to the baseline run. The June 21 heating simulation, like the baseline simulation, has the depth of the upslope flow half as high as the top of the solenoid until the solenoid passes.

The November 1 heating and the December 21 heating simulations show the influence of the reduced heating on the structure of the winds. The top of the solenoid reaches barrier top in the November 1 heating simulation while it is 500m below barrier top in the December

a)

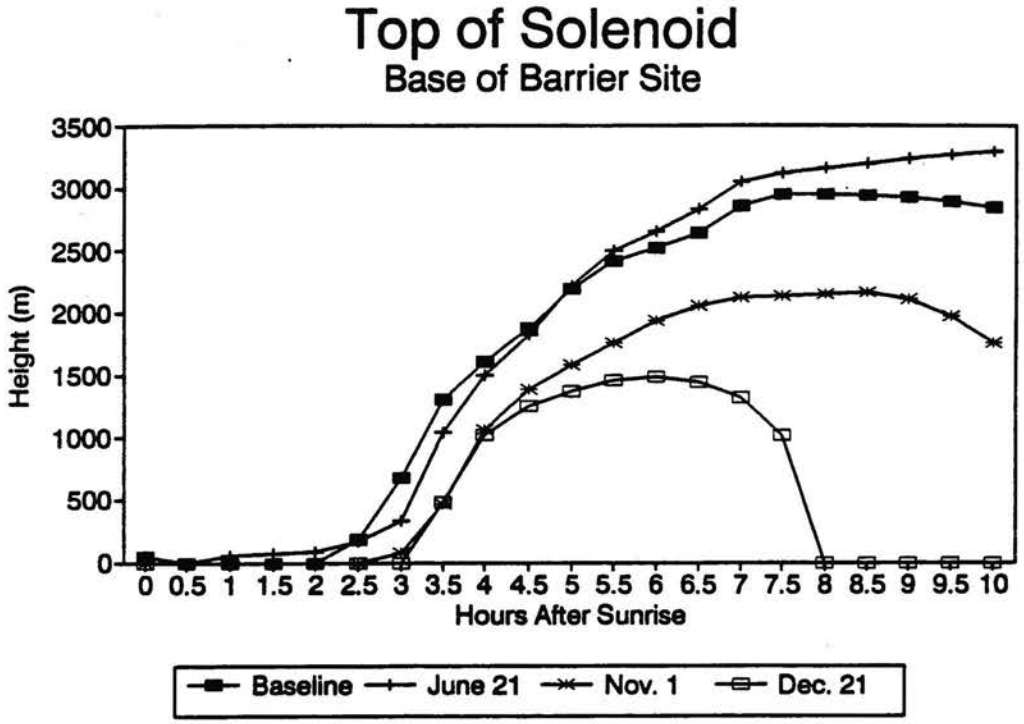

b)

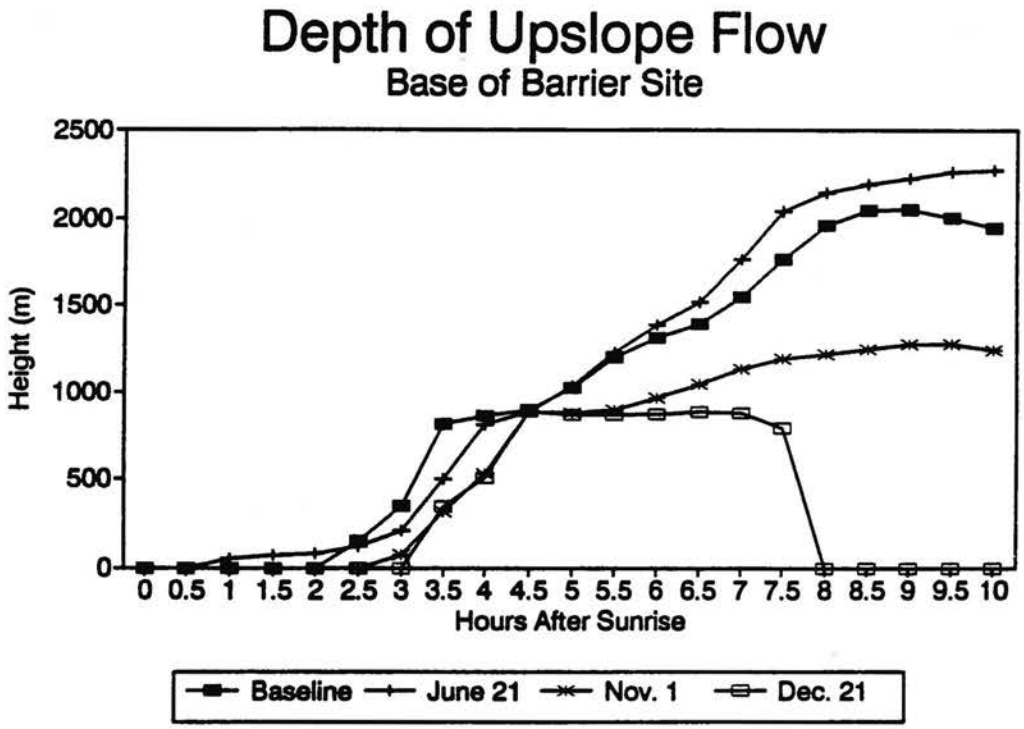

Figure 4.2. The top of the solenoid (a) and the depth of the upslope flow (b) at the base of the barrier site for the time of year simulations.

21 heating run. Both simulations have the depth of the upslope flow being about half as high as the top of the solenoid throughout the day.

Figure 4.3 shows the CBL height. Like the other quantities the baseline and June 21 heating simulations are similar with the height of the CBL being one grid point higher for in the June 21 heating run at 6 and 7 hours after sunrise. The November 1 heating and December 21 heating simulations have much lower CBL heights. The maximum height is about 800m in the November 1 heating simulation, and it is only about 350m for the December 21 heating simulation.

Figure 4.4 shows the horizontal advection in the CBL and the amount of warming above the CBL. These two quantities measure how the developing solenoid moves energy, and these quantities influence the CBL growth. The horizontal advection in the CBL shows cooling for all simulations with less cooling for the simulations with weaker solenoids. The amount of heating above the CBL is much greater in the June 21 heating and baseline simulations than the other two simulations, and this heating generally is larger the in June 21 heating run than in the baseline run. The similarity of the June 21 heating and baseline runs is not surprising given their similarity in the plots previous discussed. Once the solenoid passes the site stronger heating occurs above the CBL for June 21 heating run compared to the baseline run. For the November 1 heating simulation the peak heating above the CBL is about $0.35MJm^{-2}$ ($97Wm^{-2}$) over a one hour period, and for the December 21 heating run it is $0.07MJm^{-2}$ ($19Wm^{-2}$) compared to $0.65MJm^{-2}$ ($181Wm^{-2}$) for the baseline and $0.82MJm^{-2}$ ($228Wm^{-2}$) for June 21 heating runs.

These plots demonstrate that time of year can greatly influence the thermal and wind structures. The similarity of the June 21 heating and baseline simulations indicate that above a given amount of heating the evolution does not change significantly when the amount of heating is increased. In these two simulations the solenoid moves eastward and the depth of

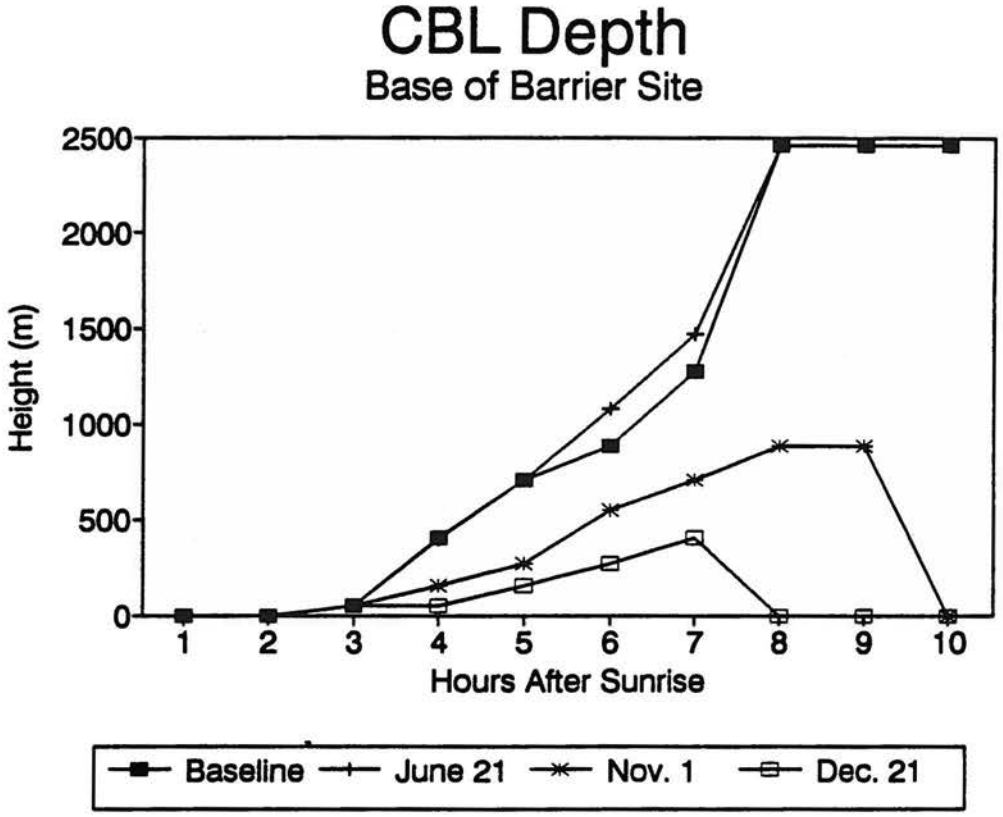

Figure 4.3. The depth of the CBL at the base of the barrier site for the time of year simulations.

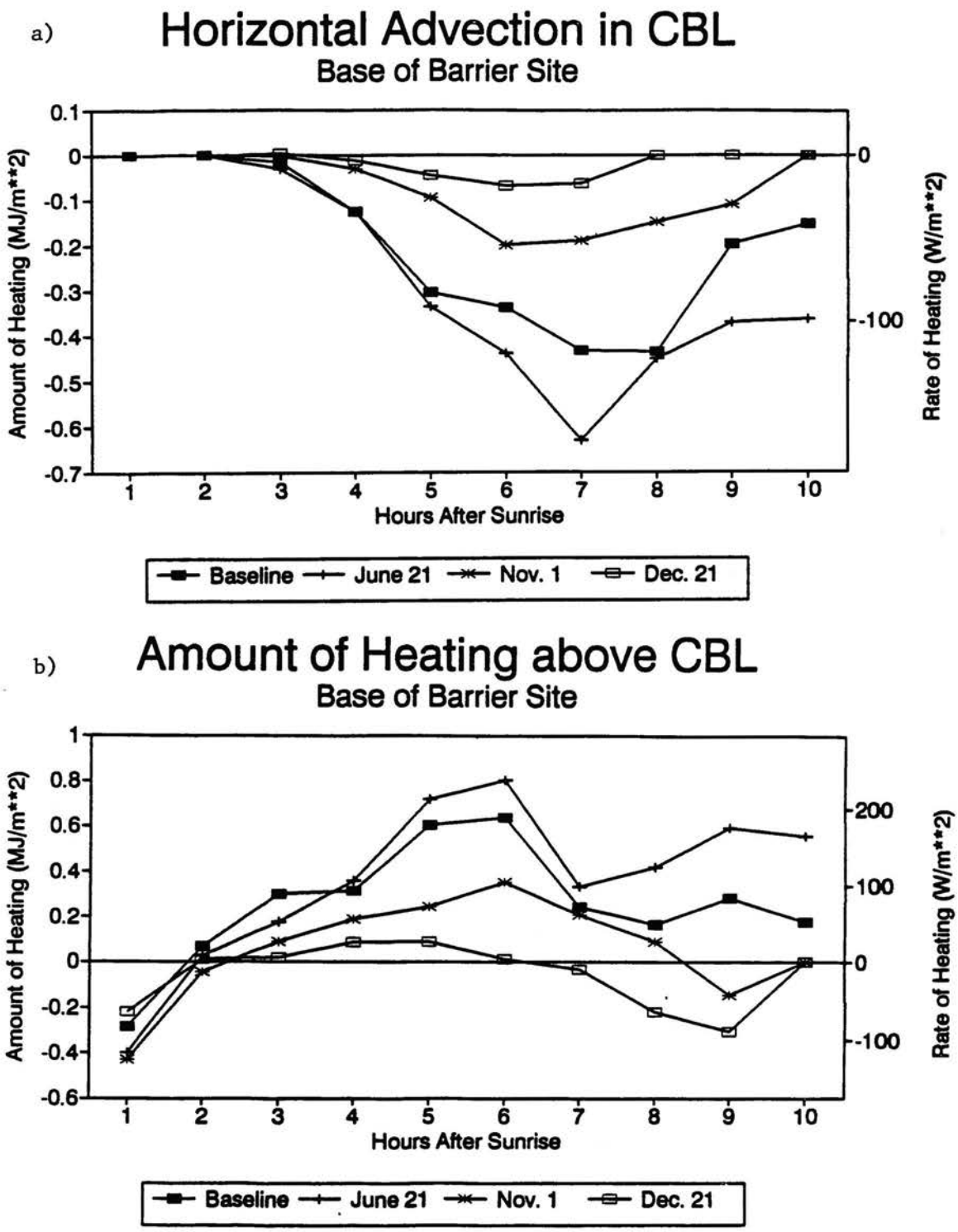

Figure 4.4. The horizontal advection of energy in the CBL (a) and the amount of heating above the CBL (b) at the base of the barrier site for the time of year simulations. The values are for one hour period and are plotted at the end of the period.

the upslope flow and CBL reaches barrier top. For less heating the solenoid is substantially weaker, and with less heating occurring over a shorter time period the leading edge of the cold core and the associated solenoid do not move eastward away from the barrier. Because of less heating and the solenoid not moving overhead, the depth of the upslope flow and CBL do not approach the height of the barrier crest.

4.3 Different Patterns of Surface Heating

In the soil module the soil moisture greatly influences the amount of surface sensible heat flux to the atmosphere (Lee and Pielke, 1992). In the CSU RAMS the atmosphere can evaporate water from the soil during the day and night, and sometimes water can condense into the soil. In this section the model is run with different patterns of soil moisture. Generally, a moister soil has a smaller surface sensible heat flux, while a drier soil has a larger surface sensible heat flux. The different patterns of soil moisture lead to different regions of stronger or weaker surface heating. The next group of simulations demonstrate how differing patterns of surface heating, caused by differing soil moisture, can influence the daytime evolution. Unless otherwise stated, the soil moisture does not change significantly during the nighttime.

In this section three simulations are discussed. One simulation is referred to as dry mountain-wet plains simulation (DMWP) in which the eastern plains has wet soil eastward from the base of the barrier and dry soil elsewhere. In this simulation much more heating occurs over the mountain than on the eastern plains, and it shows the possible influence on the daytime evolution of widespread irrigation on the eastern plains. Another simulation is the wet mountain-wet plain (WMWP) simulation. This simulation is initialized with a uniformly moist soil at 6:00 P.M. the previous evening. During the night the soil on the east side of the barrier dries substantially because of the strong nocturnal jet. The jet advects

drier air from higher levels down the east side of the barrier, and the dry air and strong winds cause significant evaporation on the eastern slope of the barrier. By sunrise the soil on the east side of the barrier is almost as dry as in the baseline simulation. The other simulation is the wet mountain - dry plains (WMDP) simulation. The purpose of this simulation is to examine the evolution with little or no heating over the mountains. In this simulation a sandy soil is used on the east slope of the barrier. While using a sandy soil may be "unrealistic", it prevents the strong nighttime drying of the soil on the east slope of the barrier induced by the strong jet, and little heating occurs over the east side of the barrier during the day. In WMWP and DMWP the nighttime circulations advect moisture eastward on the eastern plain resulting in less surface sensible heat flux further east during the day and in the surface sensible heat flux becoming positive later in the day further east.

Table 4.2 shows the maximum u-component and it height at sunrise at the base of the barrier site and the site 30km to the west. At both sites the maximum u-component of the jet is slightly stronger in the three new simulations than in the baseline run. Other parameters such as the minimum wind speed and height of the minimum are similar in the four runs.

Figure 4.5 shows plots of the westward mass flux and maximum return flow at the base of the barrier. Upslope flow does not develop in WMDP since there is very little surface heating over the barrier. For DMWP and WMWP the eastward mass flux is smaller and develops later compared to the baseline run with the mass flux in WMWP being smaller than DMWP. For example at 5 hours after sunrise the westward mass flux in WMWP is two-thirds of the baseline run, and DMWP's westward mass flux is three-quarters of the baseline run's value. These differences are larger at 4 and 6 hours after sunrise. The less mass flux in WMWP shows that reduced heating west of the crest of the barrier due to the moister soil can significantly influence the strength of the upslope flow. The eastward mass flux for

Table 4.2

Speed and height of the maximum u-component in the near surface jet and the height and speed of the minimum u-component at sunrise for the base of the barrier site and for the site to the west for the different patterns of soil moisture runs.

BASE OF THE BARRIER

Run	Maximum U-component Speed (ms^{-1})	Height (m)	Minimum U-Component Speed (ms^{-1})	Height (km)
Baseline	5.5	250	0.8	1.0
WMWP	6.5	250	0.5	1.0
DMWP	6.4	250	0.6	1.0
WMDP	6.2	250	0.5	1.1

30KM WEST OF THE BASE OF THE BARRIER

Baseline	9.1	275	-0.6	2.3
WMWP	10.0	175	-0.4	1.8
DMWP	9.5	175	-0.5	1.9
WMDP	9.9	125	-0.5	1.9

a)

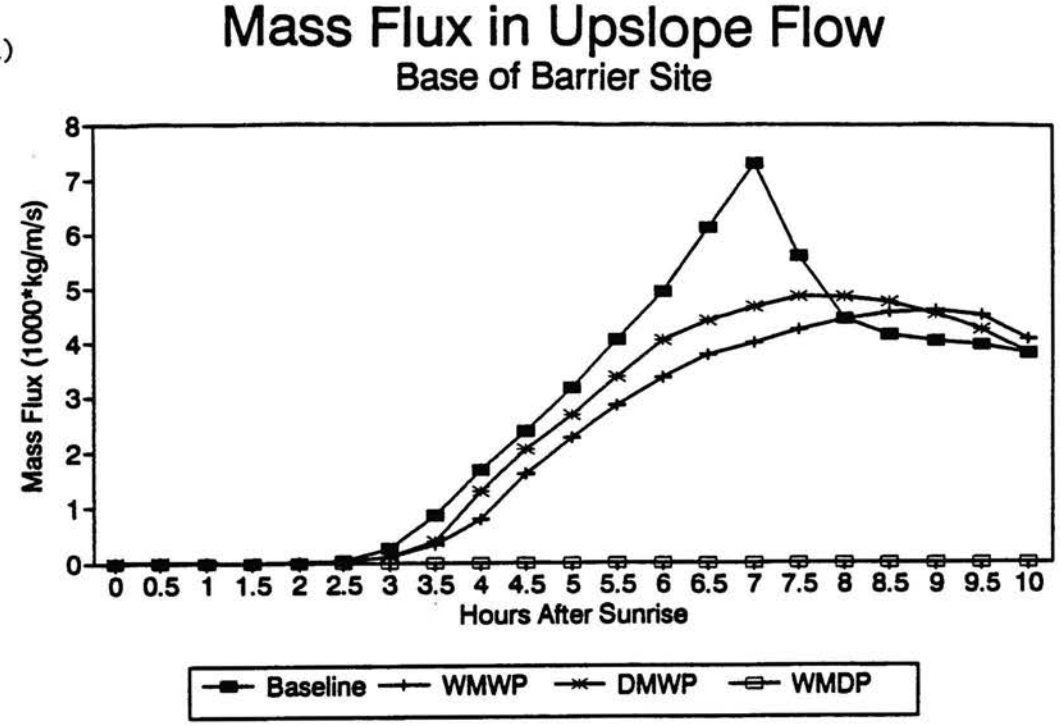

b)

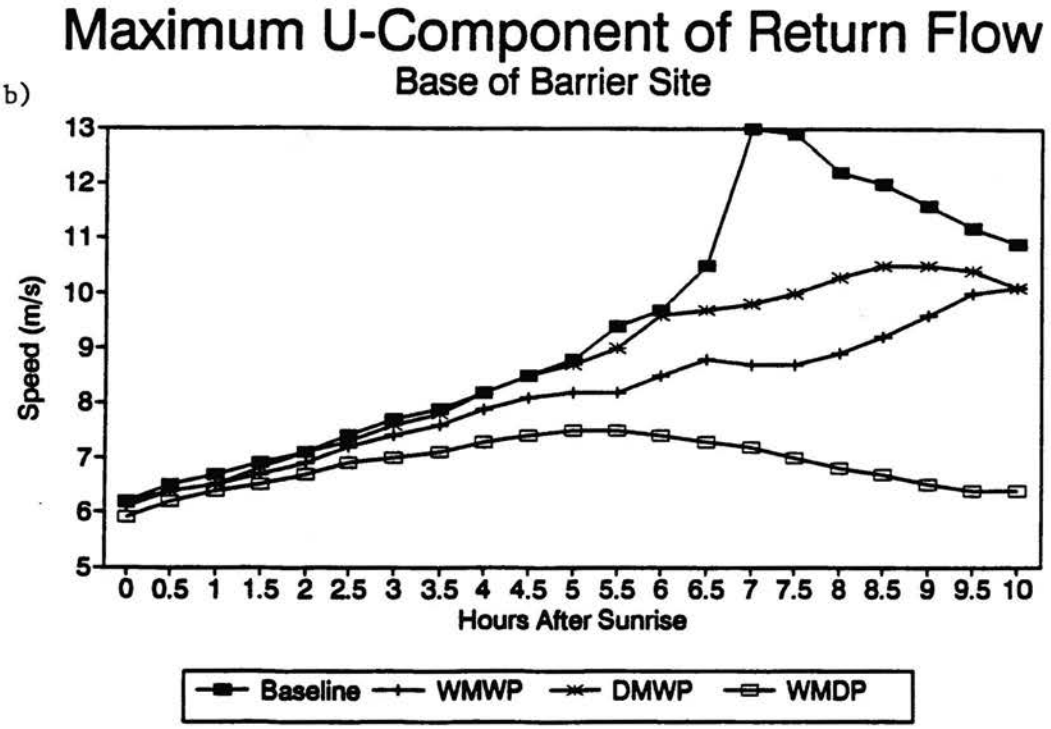

Figure 4.5. Same as Figure 4.1 but for the different patterns of surface heating simulations.

DMWP and WMWP are still much higher than the two less heating cases discussed in the last section. The jump associated with the passage of the solenoid does not occur for WMWP and DMWP, and the maximum value of the mass flux occurs later in WMWP than in WMDP with the maximum value in WMWP being less. The plots for the maximum u-component of the return flow show similar traits.

Figure 4.6 shows the depth of the upslope flow and top of the solenoid for the four simulations. Early in the day the depth of the upslope flow is more shallow in WMWP and DMWP, compared to the baseline run. Throughout the day the depth of the upslope flow is more shallow in WMWP than the baseline simulation. Until 6 hours after sunrise the depth of the upslope flow in DMWP is similar to the baseline run after which the depth of the upslope flow stops increasing in DMWP. The top of the solenoid is shallower in WMWP than in DMWP, and in both of these runs it less than the in baseline run. In general in both WMWP and DMWP the depth of the upslope flow is about one half the top of the solenoid.

The CBL height (Figure 4.7) shows large differences between the simulations. After 3 hours after sunrise the CBL height in WMWP and DMWP are similar and are much less than the baseline simulation. The less heating on the eastern plains reduces the intensity and depth of the circulations, and the less heating also greatly reduces the depth of the CBL. Throughout most of the day the depth of the CBL in WMWP and DMWP is one-half or less than one-half the value in the baseline run. Comparison of the top of the upslope flow plot with the CBL height shows that deep easterly flow is present above the top of the CBL.

Advective factors causing the suppression of the CBL height are horizontal advection in the CBL and the amount of warming above the CBL (Figure 4.8). More cold air advection occurs in the CBL in WMWP and DMWP than in the baseline simulation despite the presence of a more shallow CBL and a less intense upslope flow. The less surface sensible heat flux further to the east does not warm the air as much as much as in the baseline run,

a)

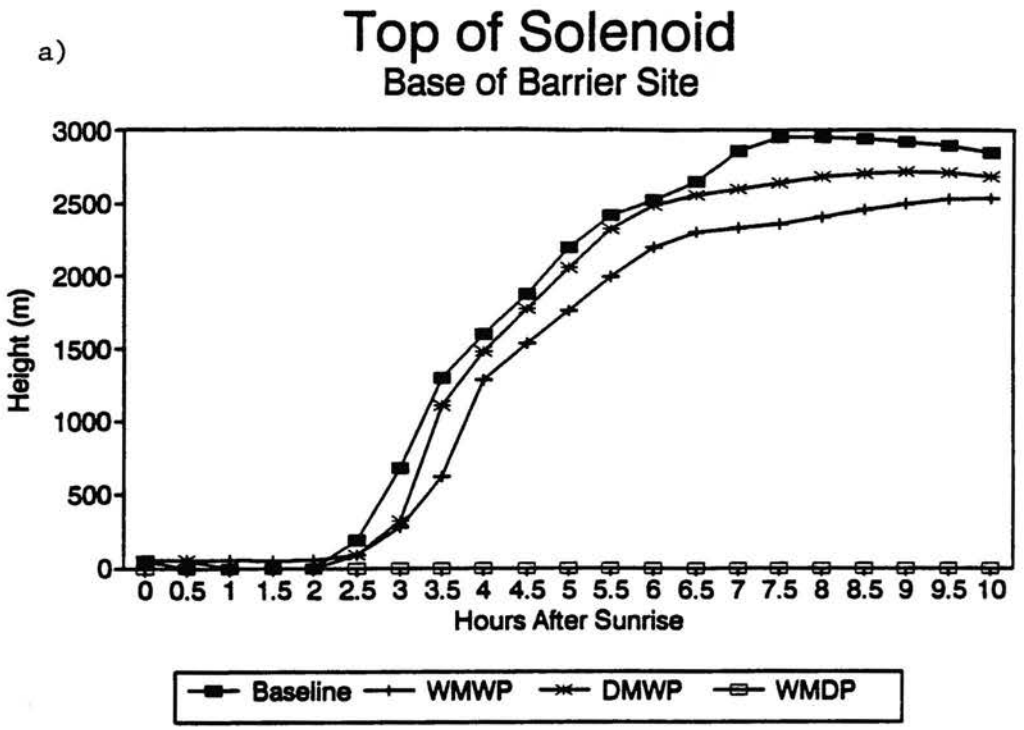

b)

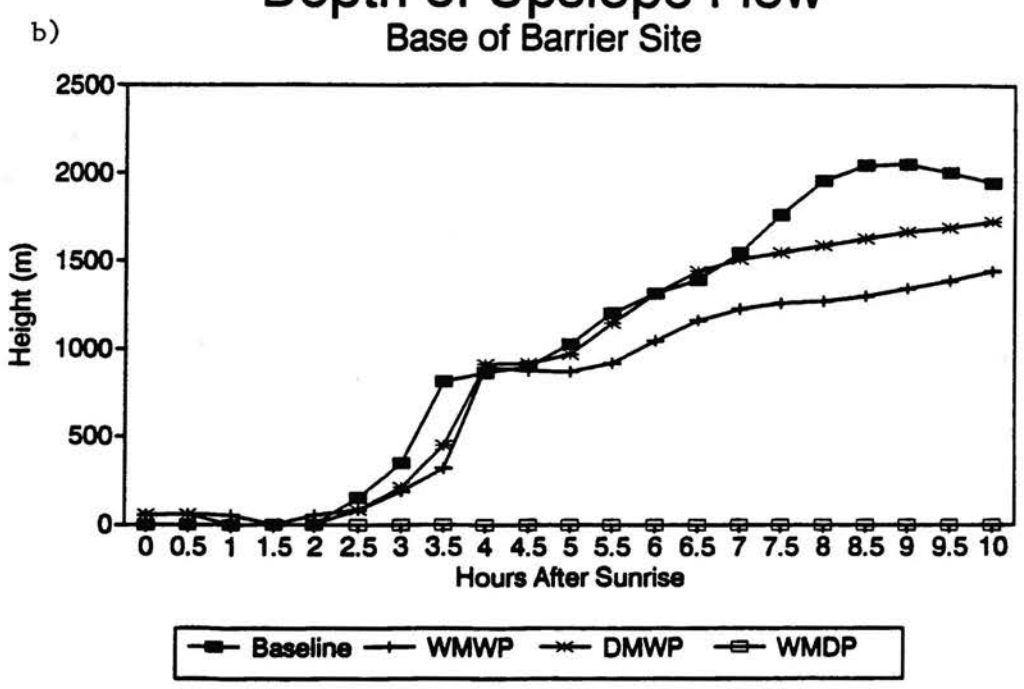

Figure 4.6. Same as Figure 4.2 but for the different patterns of surface heating simulations.

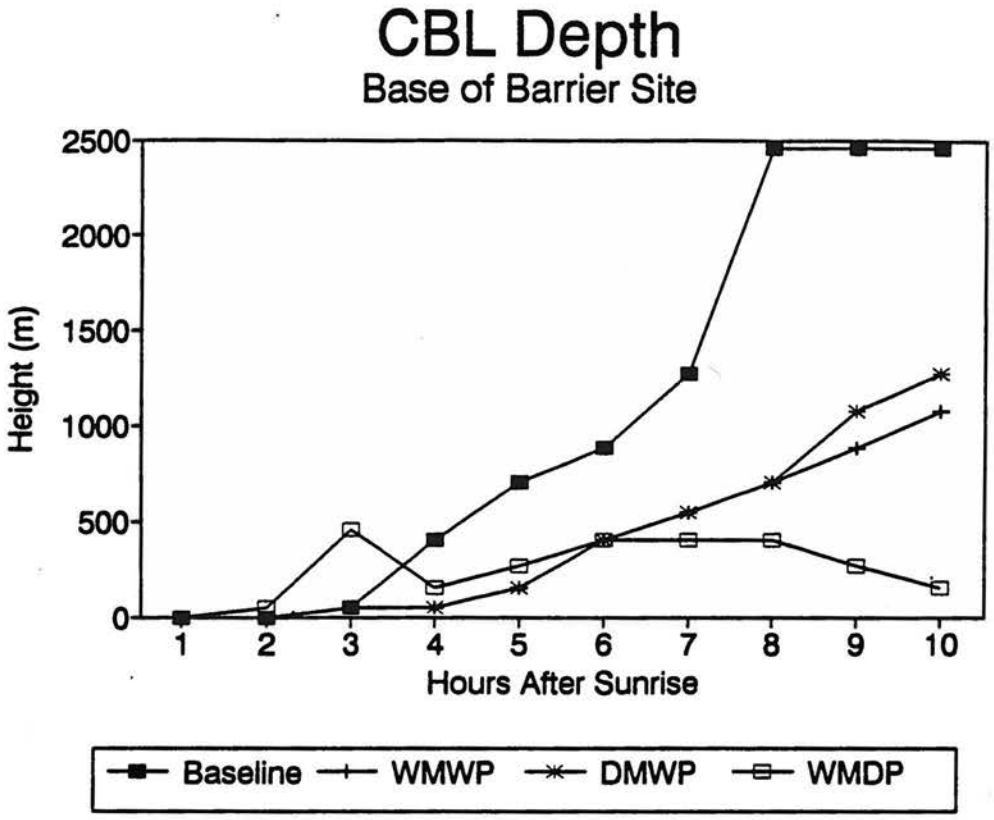

Figure 4.7. Same as Figure 4.3 but for the different patterns of surface heating simulations.

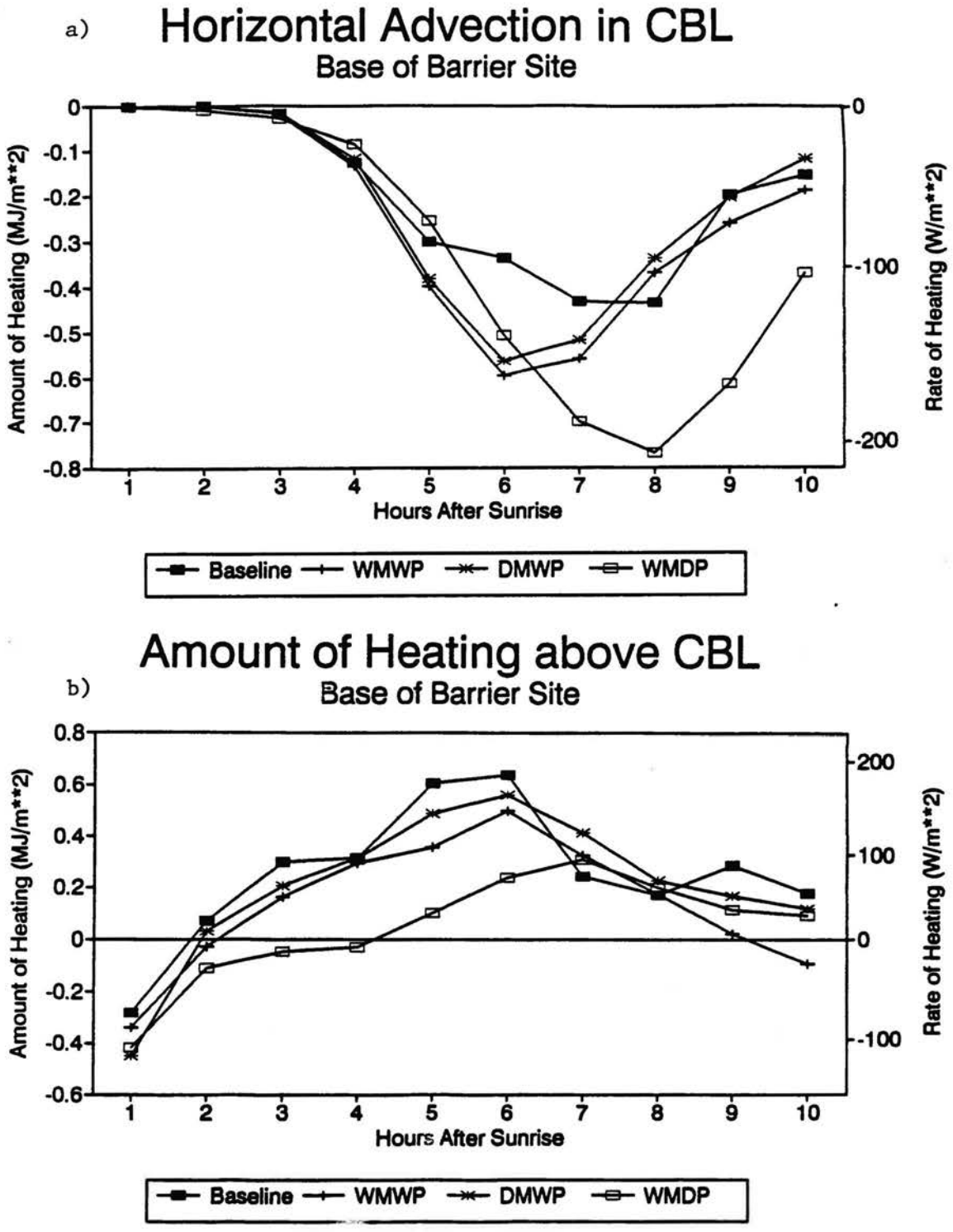

Figure 4.8. Same as Figure 4.4 but for the different patterns of surface heating simulations.

and the upslope flow created by the heating over the barrier is able to draw that cold air westward. The amount of heating above the CBL shows less heating in DMWP and even less in WMWP compared to the baseline run.

The greatest influence of the wet plains is a lower CBL height. The quantities describing the circulation demonstrate that the wet plains reduces the strength of the solenoid circulations. The wet soil west of the barrier crest can further weaken the circulation and noticeably reduce the depth of the solenoid. Except for the CBL depth the differences induced by moister soil on the eastern plains are significantly less than the differences due to changes in the time of year. In WMDP a solenoid does not develop making the daytime evolution vastly different from the other simulations.

The plots of the mass and thermal quantities indicate an absence of the migrating solenoid. This absence does not result from weak heating preventing the leading edge of the cold core from moving eastward, which occurs in the November 1 heating and December 21 heating simulations. Figure 4.9 shows the DMWP run at 9 hours after sunrise. A nose of stronger u-component winds, indicative of the leading edge of the cold core, is present at a height of 4.0km about 50km east of the base of the barrier. Other features associated with the leading edge of the cold core are also present including a strong horizontal pressure gradient and significant sinking motion ahead of the nose of strong winds. The leading edge of the cold core moves eastward at $7ms^{-1}$, and by 11 hours after sunrise a distinct wind maximum at a height of 3-4km is associated with this disturbance.

Net convergence occurs ahead of the leading edge of the cold core at a height of 2-3km, and net divergence occurs behind it at a height of 2-3km. The convergence tends to produce sinking motion beneath it, and the divergence tends to produce rising motion beneath it. In the DMWP simulation the stable core is sufficiently stable so the convergent and divergent areas do not produce sinking or rising motion down to the surface. In the

a) Potential Temperature. Contour interval 1 K.

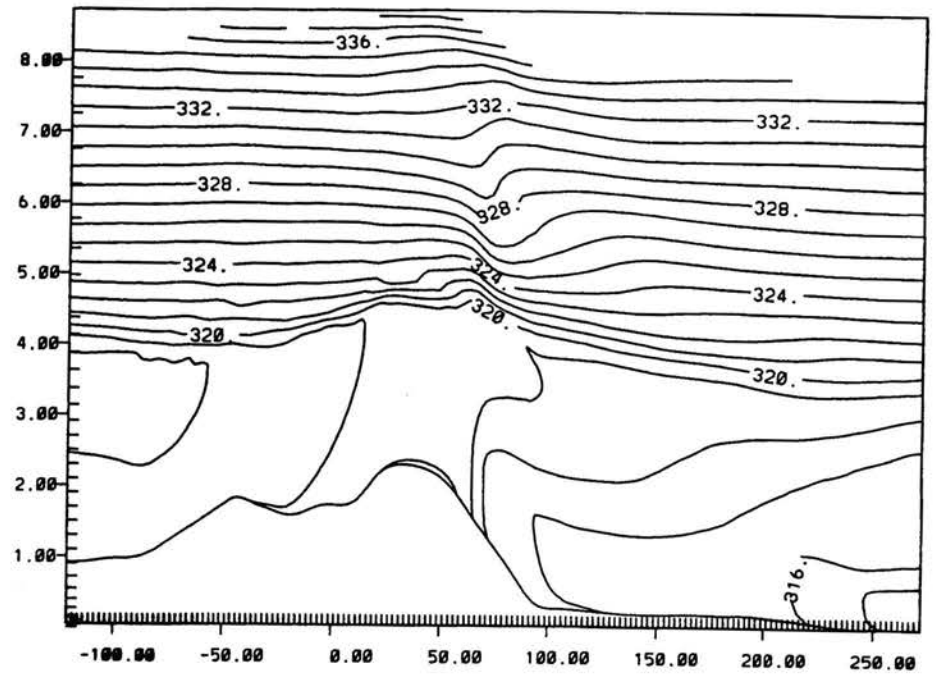

b) U-component. Contour interval 0.9 ms^{-1}. (Maximum: 10.8 ms^{-1}; minimum: -3.6 ms^{-1}).

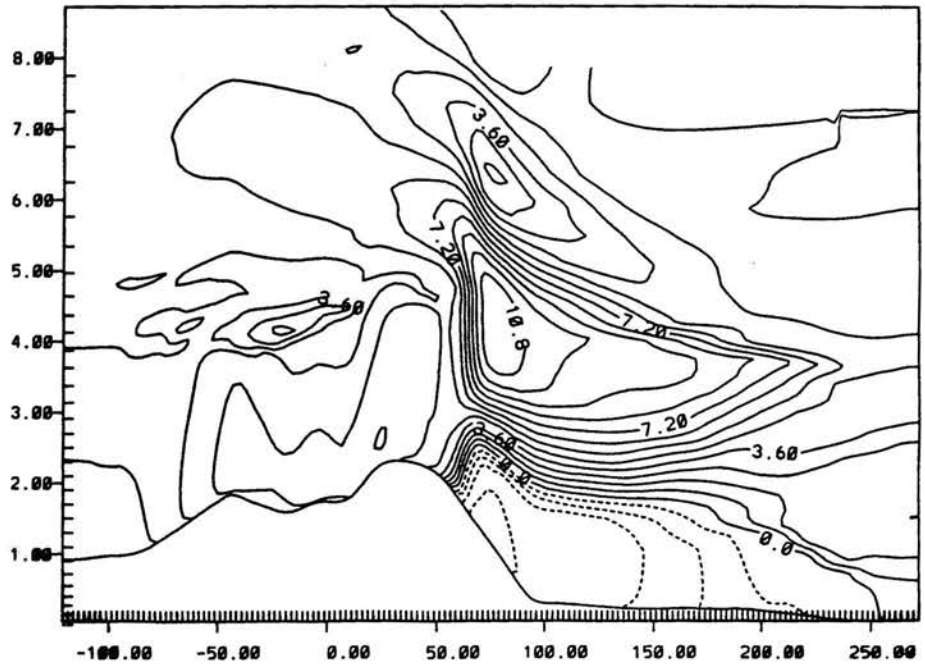

Figure 4.9. The wet plains–dry mountain simulation at 9 hours after sunrise in the inner grid. a) potential temperature and b) u-component.

c) Vertical velocity. Contour interval 6 cms^{-1}. (Maximum: 72 cms^{-1}; minimum: -30 cms^{-1}).

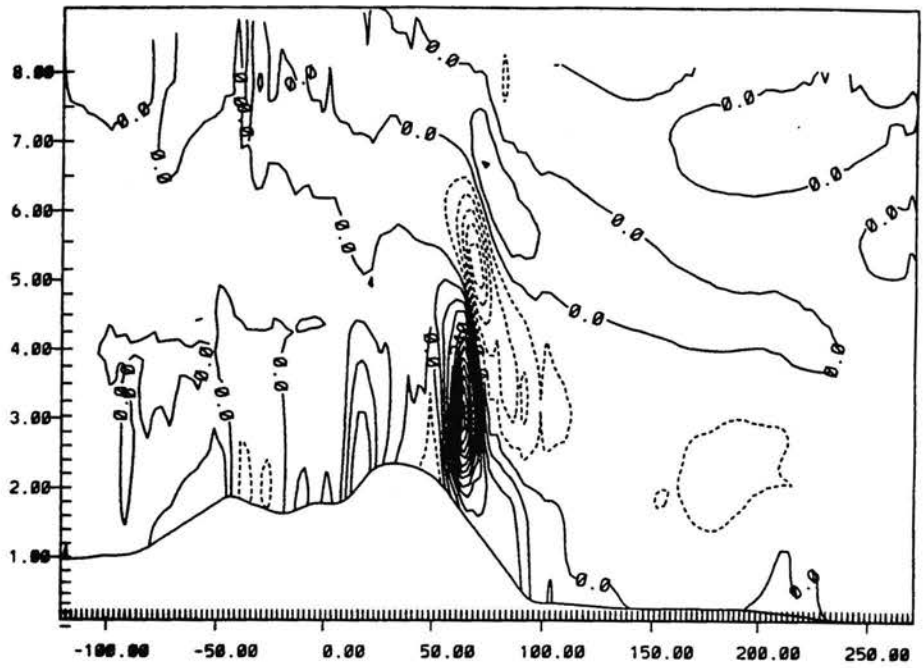

d) Perturbation Exner function. Contour interval 0.06 $Jkg^{-1}K^{-1}$. (0.022 mb at 700 mb).

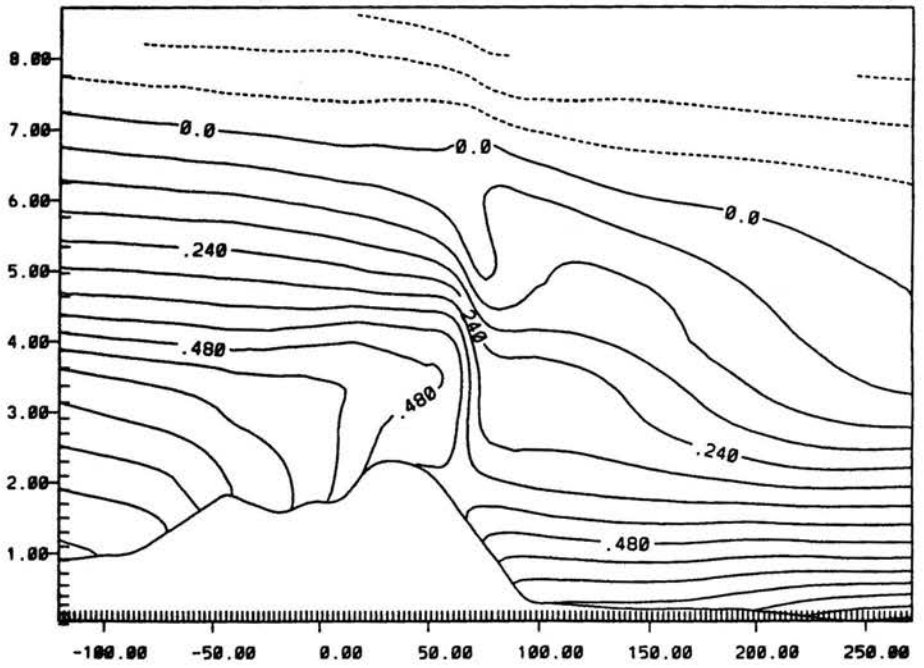

Figure 4.9. The wet plains–dry mountain simulation at 9 hours after sunrise in the inner grid. c) vertical velocity and d) perturbation Exner function.

e) Streamlines.

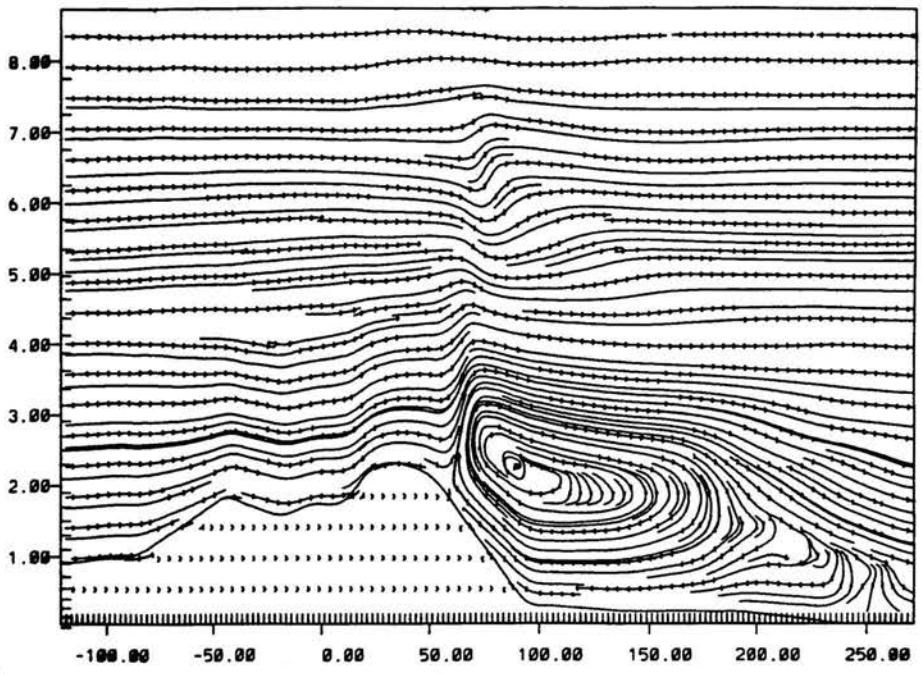

Figure 4.9. The wet plains–dry mountain simulation at 9 hours after sunrise in the inner grid. e) streamlines.

baseline simulation the stability below barrier top is sufficiently weak so the rising and sinking motion reaches the surface. This sinking motion ahead of and the rising motion behind the leading edge of the cold core produces the migrating solenoid in the baseline simulation (and many others).

As seen in many of the simulations the lee side convergence zone remains stationary over the eastern slope of the barrier while the solenoid migrates eastward. The main daytime circulation (the lee side convergence zone, upslope flow over the east side of the barrier and the eastern plains near the barrier, and westerly return flow above the upslope) does not move eastward. The migrating solenoid is a only a perturbation -- which can significantly influence the evolution -- in the main daytime circulation. In many of the simulations a new solenoid develops near the base of the barrier after the migrating solenoid moves sufficiently far eastward.

The timing of the eastward movement of the cold core can have profound influences on the atmosphere over the eastern plains. In the WMWP simulation the leading edge of the cold core does not begin moving eastward until 8-9 hours after sunrise which is about 1 hour later than the baseline simulation. The less surface heating west of the barrier does not allow the cold core to deepen or strengthen as fast as in the baseline run, and a weaker cold core is seen in the circulation and thermal quantities analyzed previously. The delay in the movement of the leading edge of the cold core could possibly lead to explosive CBL growth on the eastern plains because on the eastern plains more surface heating has occurred resulting in weaker stability in the stable core. However, in this simulation the leading edge of the cold core moves eastward late in the day when surface heating is weak, and this weaker heating later in the day is likely hampers the explosive CBL growth as the leading edge of the cold core moves over the eastern plains.

The WMDP simulation provides some insights into phase 1. Because of the lack of heating on the barrier, upslope flow does not develop (as seen in the plots of the circulation quantities). Throughout the day there is westerly flow down the east side of the barrier, and the bulging isentropes change little. Phase 1 warming does not appear in this simulation despite the prolonged presence of the flow down the east side of the barrier. The surface heat flux on the east side of the barrier does not increase rapidly during the day, and the surface sensible heat flux in this region never becomes positive. This supports the conclusion in the previous chapter that this rapid change in surface sensible heat flux is needed for phase 1 warming.

4.4 Different Ambient Winds

Two additional simulations are run with different ambient wind speeds. One simulation does not have any ambient winds (called the **no winds** simulation) showing the thermally induced evolution without any winds. The other simulation has stronger ambient winds and is called the **stronger winds** simulation. In the baseline simulation the winds below barrier top have a u-component of $2ms^{-1}$, and the u-component of the wind linearly increases from $2ms^{-1}$ at barrier top to $5ms^{-1}$ at 1.5km above barrier top. In the stronger wind simulation the u-component below barrier is the same as in the baseline run, but it linearly increases from $2ms^{-1}$ at the barrier top to $10ms^{-1}$ at 1.5km above barrier top. This change in winds increases the ambient shear in the layer from barrier top to 1.5km above barrier top from $2ms^{-1}km^{-1}$ to $5.33ms^{-1}km^{-1}$.

Table 4.3 shows the maximum u-component of the jet and it height of the maximum at sunrise at the base of the barrier and a site 30km to the west. At the base of the barrier the maximum u-component is the slowest for the case with no ambient winds, and the maximum occurs higher than the other two runs. At the site 30km to the west the maximum

u-component for the no winds and stronger wind simulations are less than half as strong as the baseline run. The height of the wind maximum occurs at the surface for these two runs while it is at 275m for the baseline run.

With the significant differences in the winds 30km west of the base of the barrier, the model fields for both simulations at sunrise are examined more closely. Figure 4.10 shows the sunrise state of the no winds simulation, and this Figure shows the nocturnal flows that develop without the influence of ambient winds. Weak bulging isentropes are present at barrier top. At barrier crest the u-component of the winds are near zero, and the wind speed increases in the jet as it descends the east slope of the barrier. To the east of the barrier crest a large region of easterly flow develops to replace the air which flows down the east side of the barrier in the nocturnal drainage flows.

Figure 4.11 shows the sunrise state of the atmosphere for the stronger wind simulation. The stronger wind simulation has weaker bulging isentropes than the baseline run, and east of the barrier crest most of the ambient flow remains above barrier crest with only a portion of the flow being channeled down the east side of the barrier. Similar to the baseline run the pressure perturbation field shows a low pressure trough immediately to the east of the barrier crest, but the pressure trough is closer to barrier crest than in the baseline run. Unlike the baseline run the trough does not appear to extend far down the barrier. Another pressure trough appears near the surface at 15km west of the base of the barrier. Associated with this pressure trough further down the slope is a maximum in the u-component flow. Unlike the baseline run this maximum appears to be separated from the stronger winds just east of barrier crest. The streamline plot for the stronger winds run shows sinking at the barrier top with a separate region of stronger sinking motion near the base of the barrier. In the baseline run the two regions of strong sinking motion appear to be near each other allowing for the strong channeling of the flow down the east side of the barrier.

Table 4.3

Speed and height of the maximum u-component in the near surface jet and the height and speed of the minimum u-component at sunrise for the base of the barrier site and for the site 30km to the west for the different ambient wind runs.

BASE OF THE BARRIER

Run	Maximum U-component Speed (ms^{-1})	Height (m)	Minimum U-Component Speed (ms^{-1})	Height (km)
Baseline	5.5	250	0.8	1.0
Stronger winds	5.0	250	0.7	1.3
No winds	3.0	500	-1.1	1.3

30KM WEST OF THE BASE OF THE BARRIER

Baseline	9.1	275	-0.6	2.3
Stronger winds	3.8	0	2.6	0.4
No winds	5.4	0	-1.3	1.8

a) Potential Temperature. Contour interval 1 K.

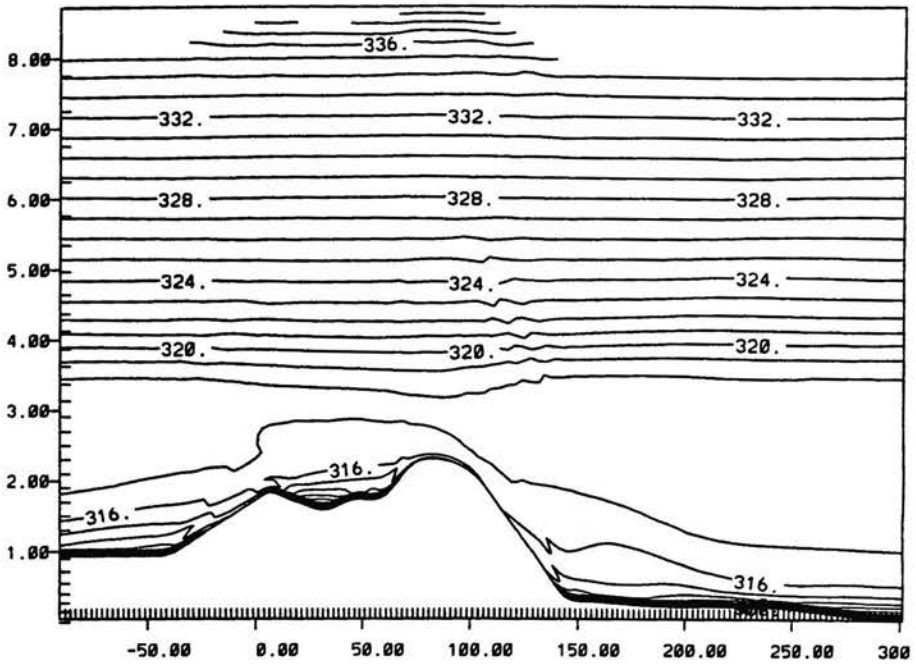

b) U-component. Contour interval 0.5 ms^{-1}. (Maximum: 5.0 ms^{-1}; minimum: -4.0 ms^{-1}).

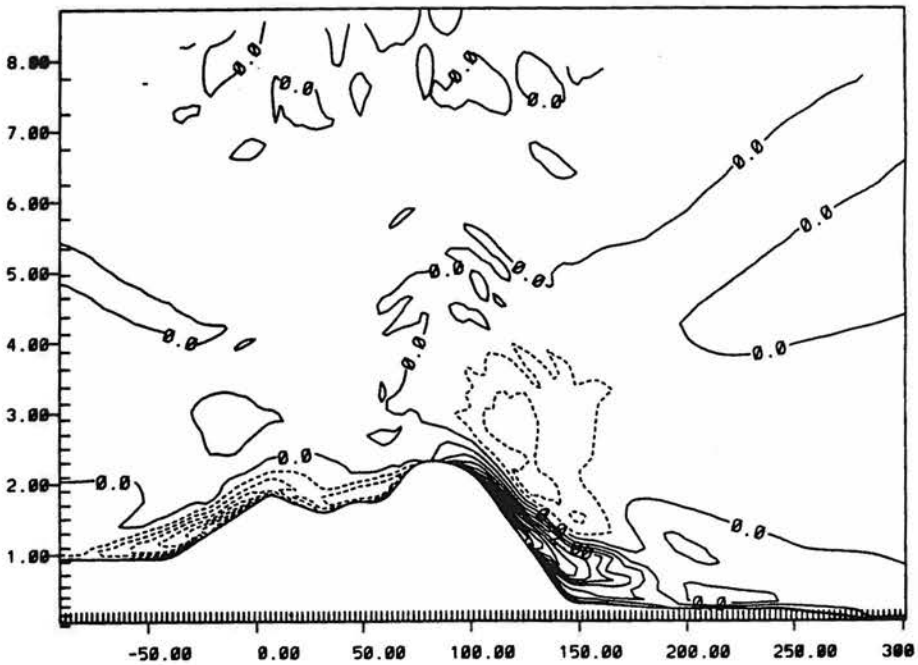

Figure 4.10. Figure 4.9 but for the no wind simulation at sunrise. a) potential temperature and b) u-component.

c) Vertical velocity. Contour interval 1 cms^{-1}. (Maximum: 4 cms^{-1}; minimum: -21 cms^{-1}).

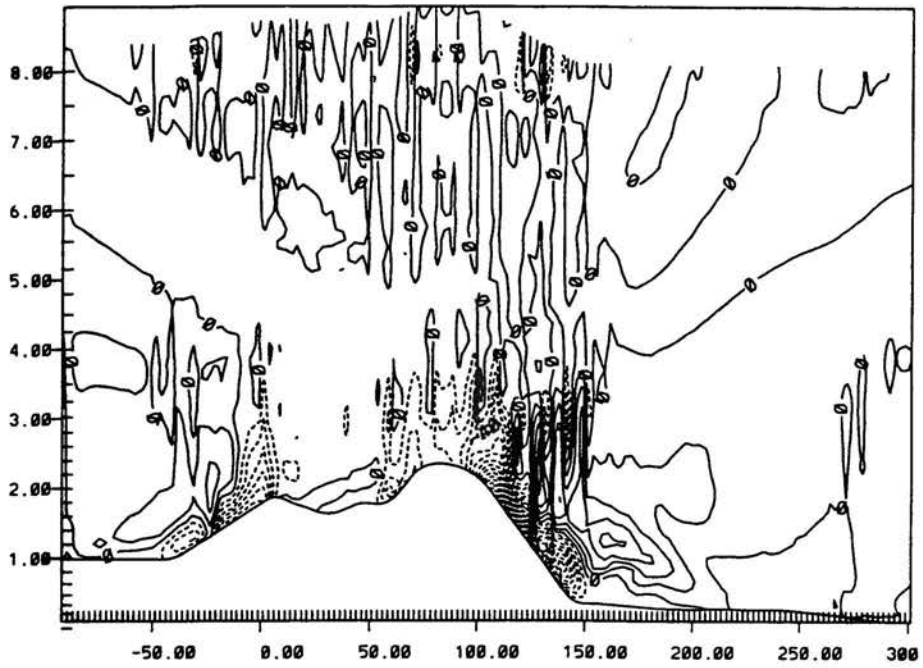

d) Perturbation Exner function. Contour interval 0.07 $Jkg^{-1}K^{-1}$. (0.026 mb at 700 mb).

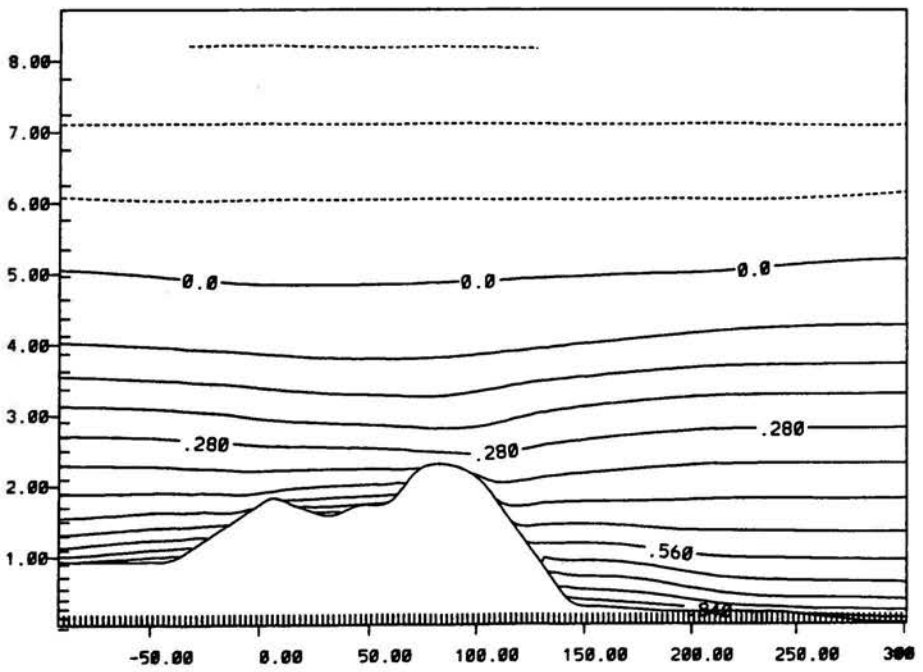

Figure 4.10. Figure 4.9 but for the no wind simulation at sunrise. c) vertical velocity and d) perturbation Exner function.

e) Streamlines.

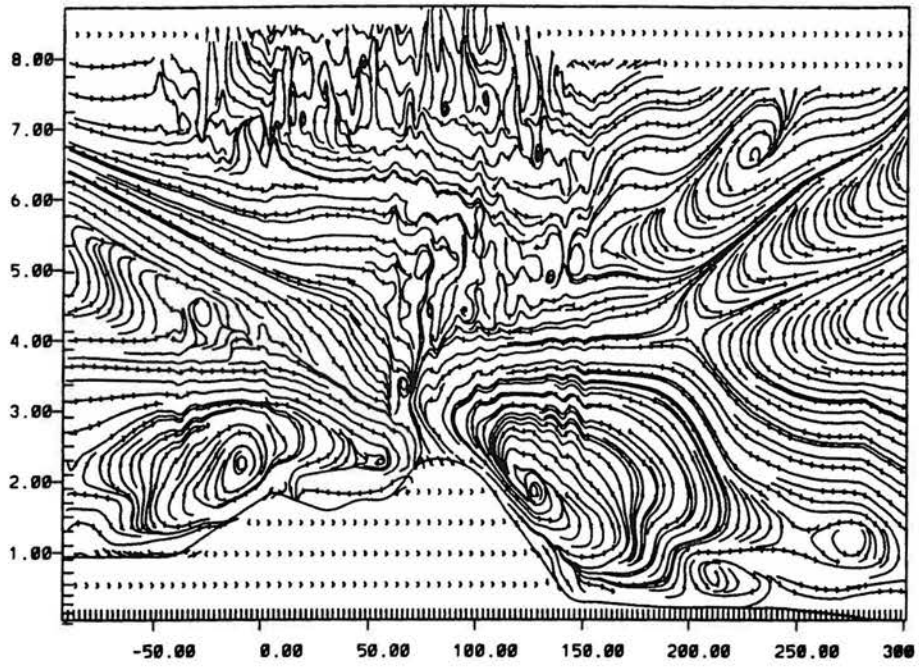

Figure 4.10. The same as Figure 4.9 but for the no wind simulation at sunrise. e) streamlines.

a) Potential Temperature. Contour interval 1 K.

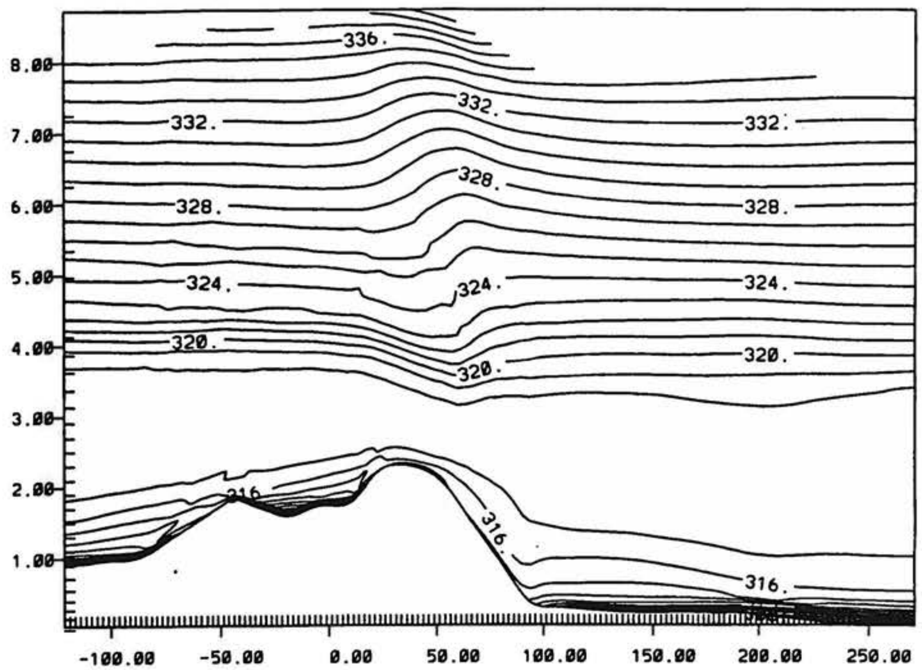

b) U-component. Contour interval 1.0 ms^{-1}. (Maximum: 14 ms^{-1}; minimum: -2 ms^{-1}).

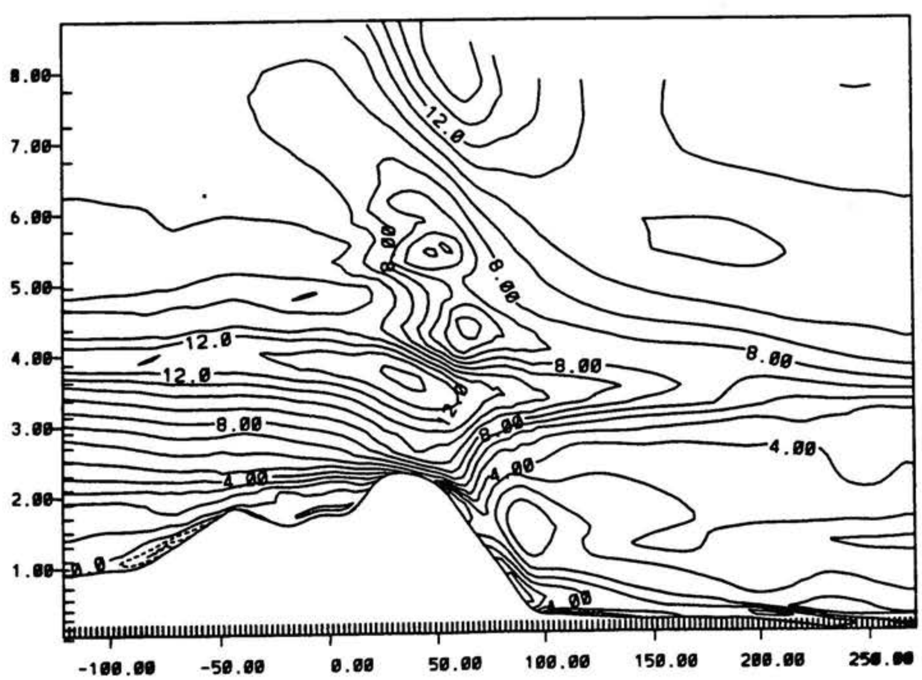

Figure 4.11. The same as Figure 4.9 but for the stronger wind simulation as sunrise. a) potential temperature and b) u-component.

c) Vertical velocity. Contour interval 3 cms^{-1}. (Maximum: 21 cms^{-1}; minimum: -27 cms^{-1}).

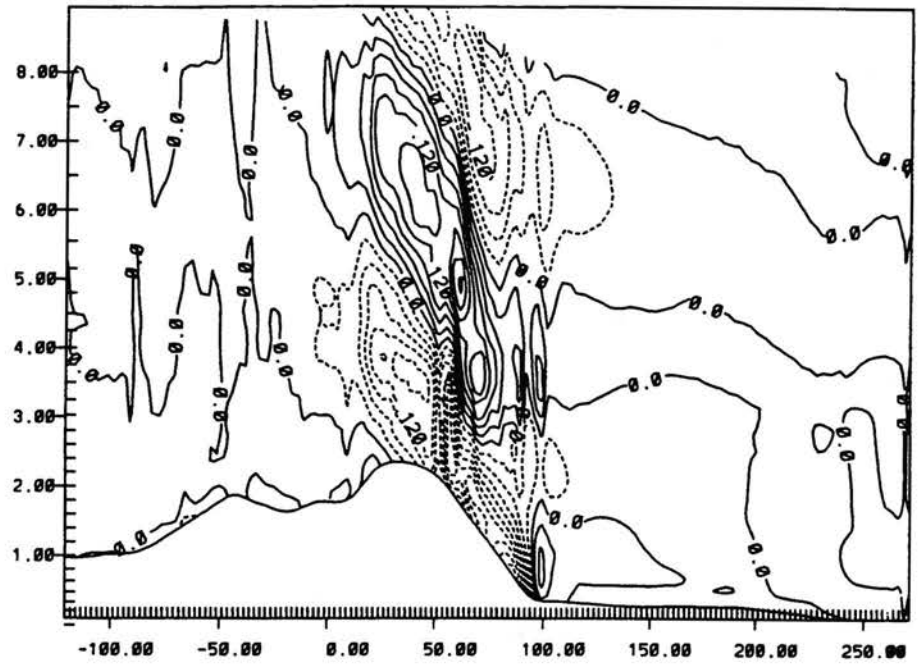

d) Perturbation Exner function. Contour interval 0.08 $Jkg^{-1}K^{-1}$. (0.030 mb at 700 mb).

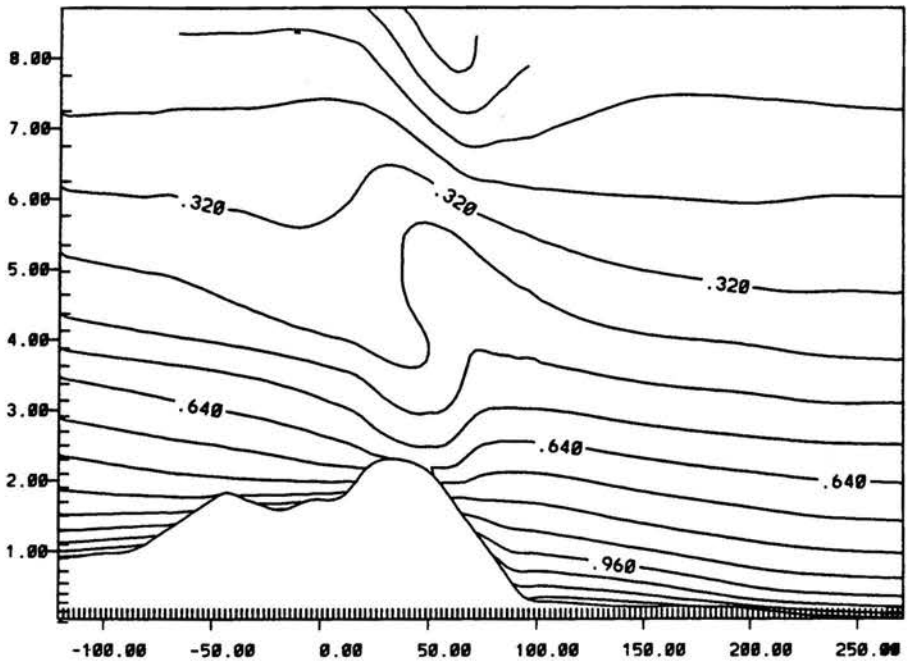

Figure 4.11. The same as Figure 4.9 but for the stronger wind simulation at sunrise. c) vertical velocity and perturbation Exner function.

e) Streamlines.

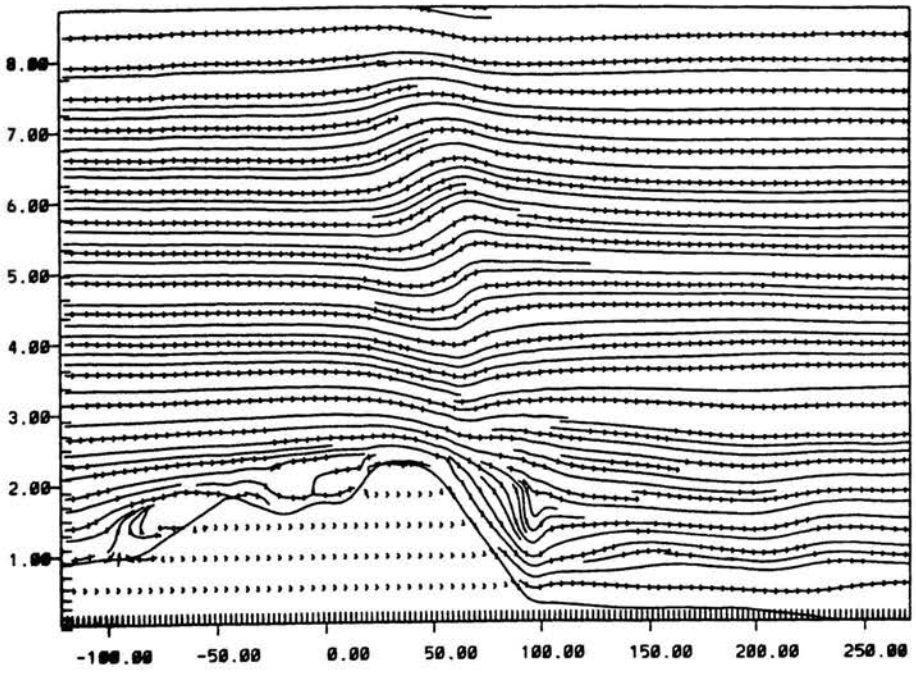

Figure 4.11. The same as Figure 4.9 but for the stronger wind simulation at sunrise. e) streamlines.

The depth of the stable core at the base of the barrier is 1.5km in the stronger winds run compared to 2km deep in the baseline run.

Doubling the wind speed affects the structure of internal buoyancy waves, which are called mountain waves when air flowing over mountains force these waves. As discussed in chapter 2 the Scorer parameter describes the character of internal buoyancy waves giving the vertical wavelength for hydrostatic mountain waves. The Scorer parameter, not including the effects of vertical wind shear, is N^2/U^2 where N is the Brunt-Vaisala frequency. The Brunt-Vaisala frequency is $(g/\theta * d\theta/dz)^{1/2}$ so doubling the wind speed produces the same Scorer parameter as if the Brunt-Vaisala frequency is reduced to one-half of its value. Assuming the same g and θ, the Brunt-Vaisala is reduced by one half when $d\theta/dz$ is one-fourth as large. In the baseline simulation $d\theta/dz$ from 1.0km above barrier top to the tropopause, which is at 8.2km, is $3.5 Kkm^{-1}$.

Figure 4.12 shows the sunrise state of a simulation where $d\theta/dz$ from 1.0km above barrier top to 8.2km is $0.875 Kkm^{-1}$ (one-quarter of $3.5 Kkm^{-1}$). The simulation with one quarter stability is much more similar to the stronger winds simulation than to the baseline simulation. In the stronger winds and one-quarter stability simulations the vertical distance between u-component maximum and minimums above 4.0km are about twice as large as in the baseline simulation, and only weakly bulging isentropes near barrier crest are present. The stronger winds and one-quarter stability runs have a trough near the surface at about 15km west of the base of the barrier separated from the trough near barrier crest. In both simulations the maximum u-component in the jet on the east side of the barrier is at about 15km west of the base of the barrier, and the maximum is separated from the stronger winds at the top of the barrier. Unlike the baseline simulation the strong channeling of the ambient flow down the east side of the barrier is not present. In the pressure field the horizontal location of the near-surface trough 15km west of the base of the barrier is immediately to the

a) Potential Temperature. Contour interval 1 K.

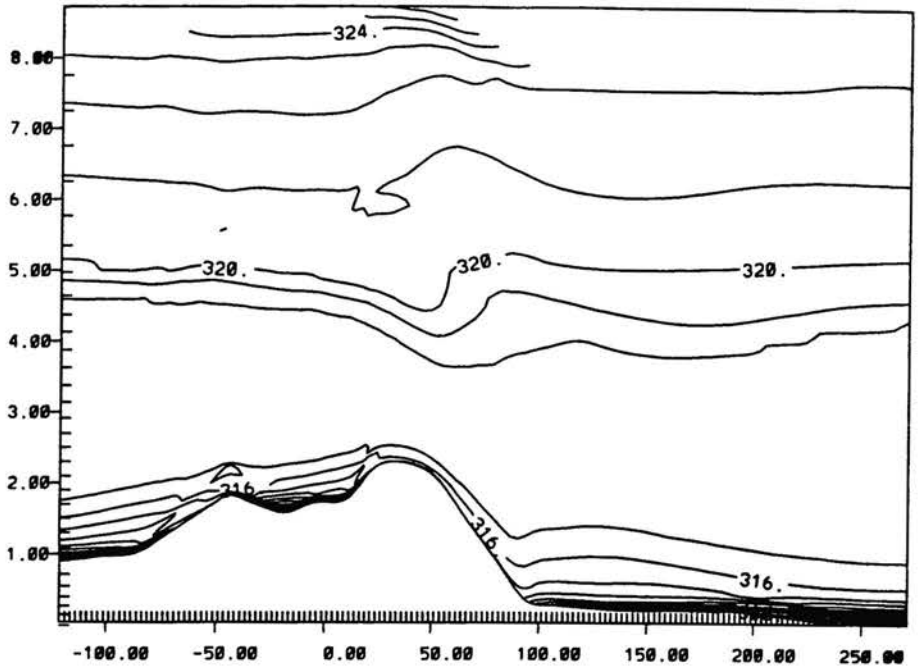

b) U-component. Contour interval 0.6 ms^{-1}. (Maximum: 8.4 ms^{-1}; minimum: -1.8 ms^{-1}).

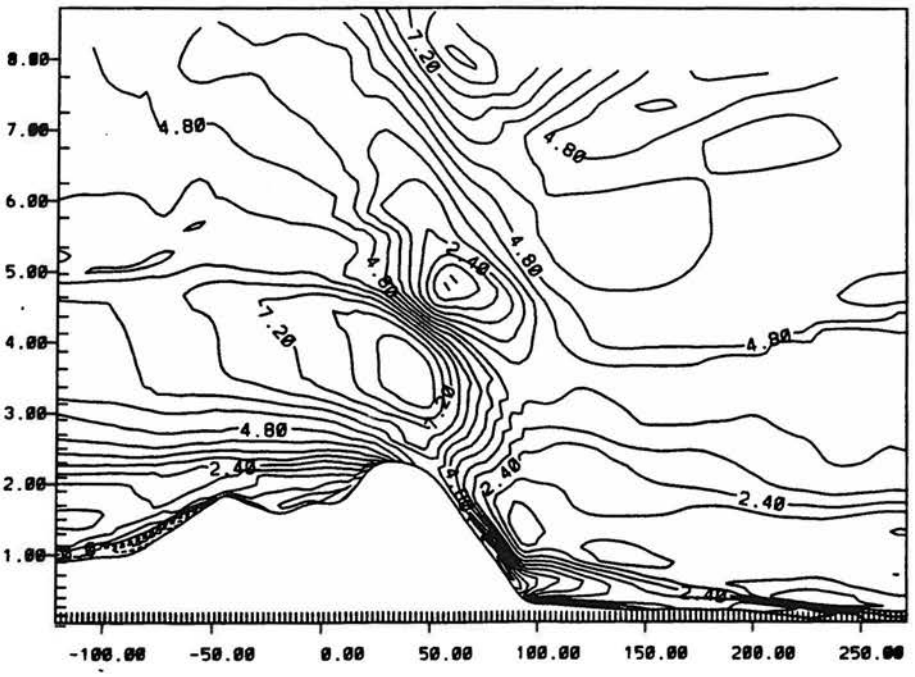

Figure 4.12. The same as Figure 4.9 but for the one-quarter stability simulation at sunrise. a) potential temperature and b) u-component.

c) Vertical velocity. Contour interval 3 cms^{-1}. (Maximum: 18 cms^{-1}; minimum: -33 cms^{-1}).

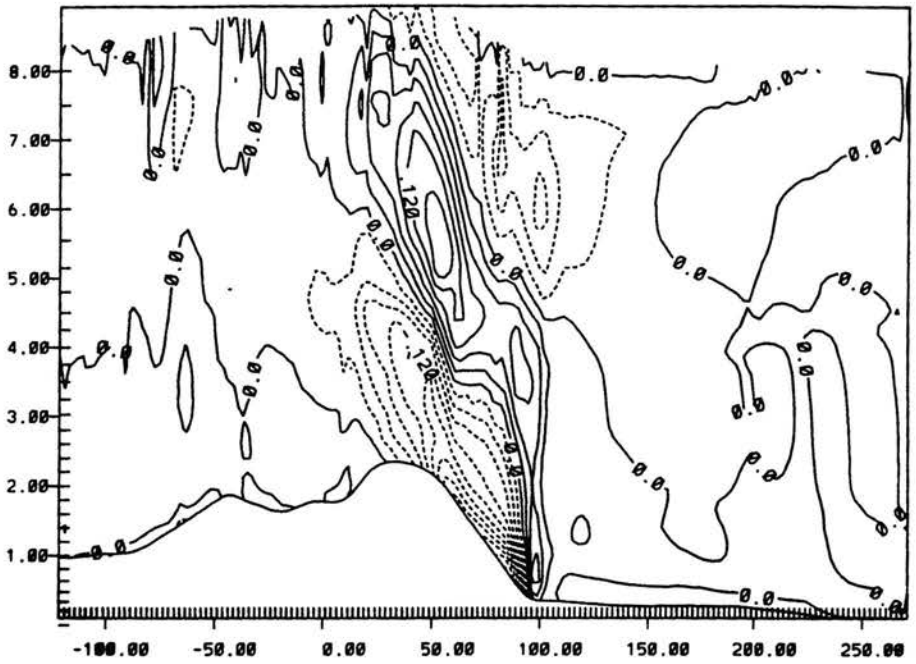

d) Perturbation Exner function. Contour interval 0.07 $Jkg^{-1}K^{-1}$. (0.026 mb at 700 mb).

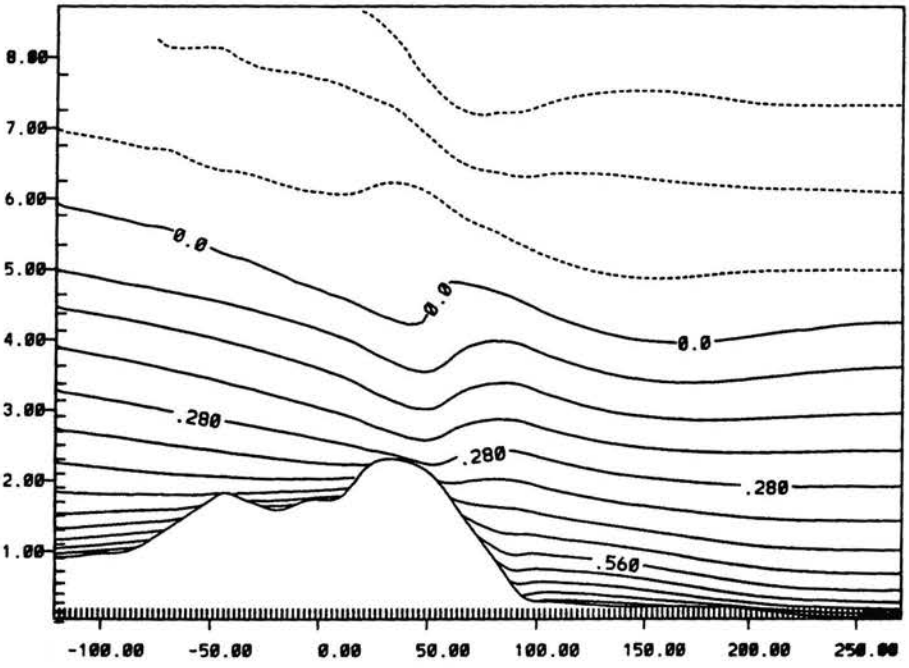

Figure 4.12. The same as Figure 4.9 but for the one-quarter stability simulation as sunrise. c) vertical velocity and d) perturbation Exner function.

e) Streamlines.

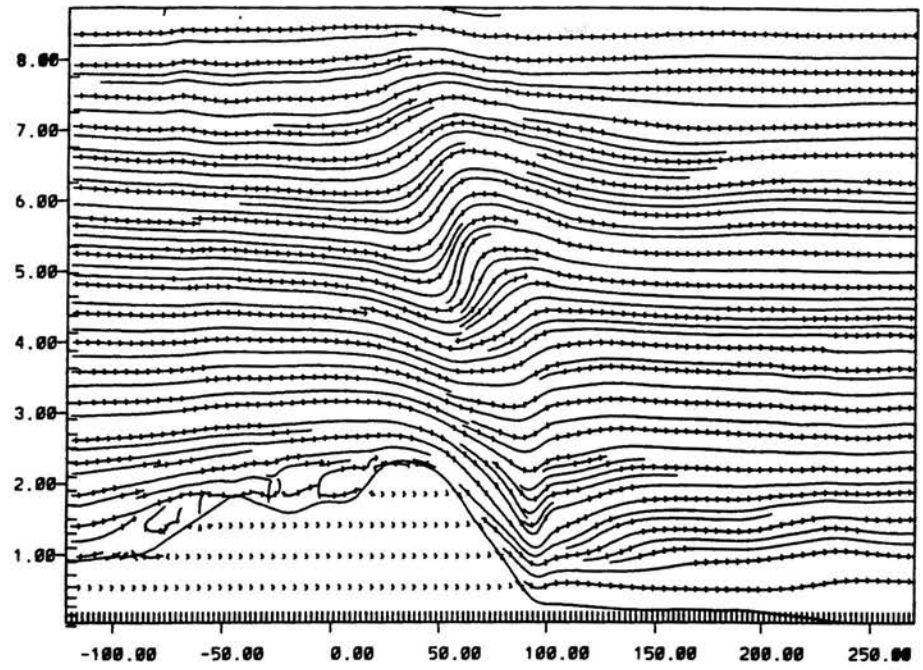

Figure 4.12. The same as Figure 4.9 but for the one-quarter stability simulation at sunrise. e) streamlines.

east of the horizontal location of a pressure ridge at 3.0km. The ridge at 3.0km is further east in the stronger wind and one quarter stability simulations than in the baseline run.

The wavelength of the mountain wave appears to be an important controlling factor for the structure of the atmosphere at sunrise east of the barrier crest. The use of the linear theory to further study the sunrise state of the atmosphere is very difficult because of the changing stabilities west of the barrier crest due to nocturnal surface cooling, the fairly complicated initial thermal and wind structure, the development of thermally driven nighttime flows producing regions of strong divergence and convergence, and the non-linear interactions between the thermally driven and ambient flows. The simulations show some features of the sunrise state which are related to mountain waves. With nocturnal cooling the mountain wave develops further to the west, and the magnitude of the perturbations in the mountain wave are greater. The wavelength of the mountain wave appears to influence the structure of the sunrise state of the atmosphere by changing the pressure fields on the east slope of the barrier and above 4.0km. The baseline simulation shows that given the proper conditions the atmosphere can be "tuned" to have strong channeling of the ambient flow down the east side of the barrier.

Figure 4.13 shows the westward mass flux in the upslope flow and the maximum u-component of the westerly return flow. The westward mass flux is weaker in the stronger winds and the no winds simulations than in the baseline simulation. Despite it having a weaker westward mass flux the stronger winds simulation shows the spikes characteristic of the passage of the solenoid occurring about 1.5 hours earlier than the baseline run. The earlier movement of the solenoid eastward is related to less of a downward bulge of the isentropes at sunrise. The lee side convergence zone does not have to build through the strongly bulging isentropes, so it is able to develop a cold core more quickly allowing for the earlier eastward movement of the solenoid. The speed at which the solenoid migrates

a)

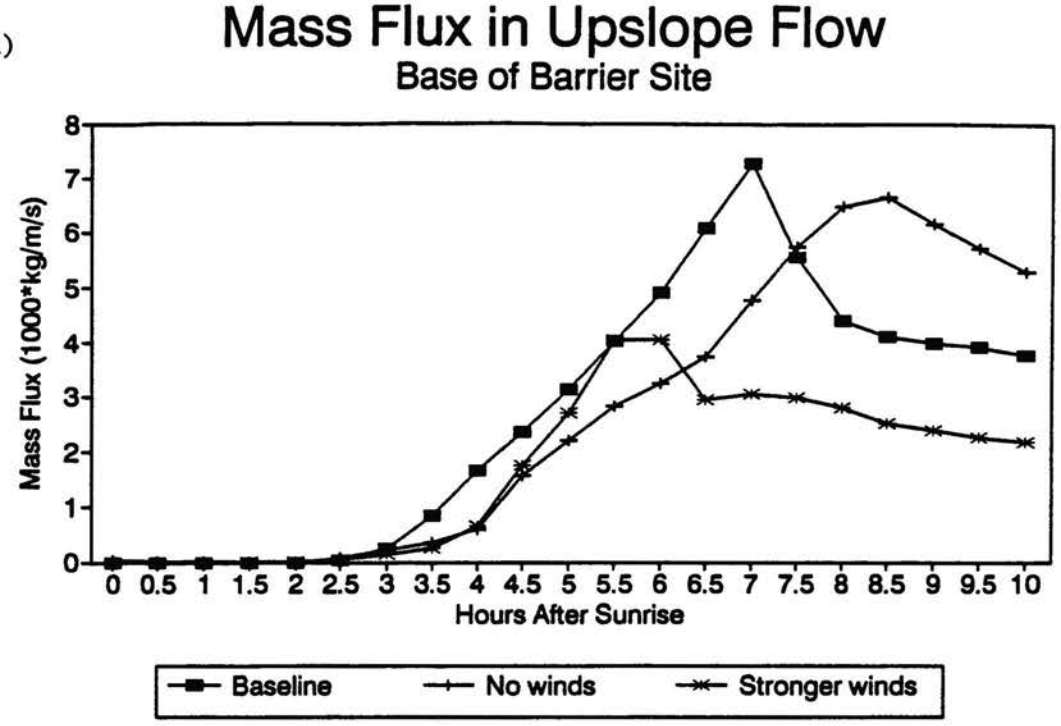

b)

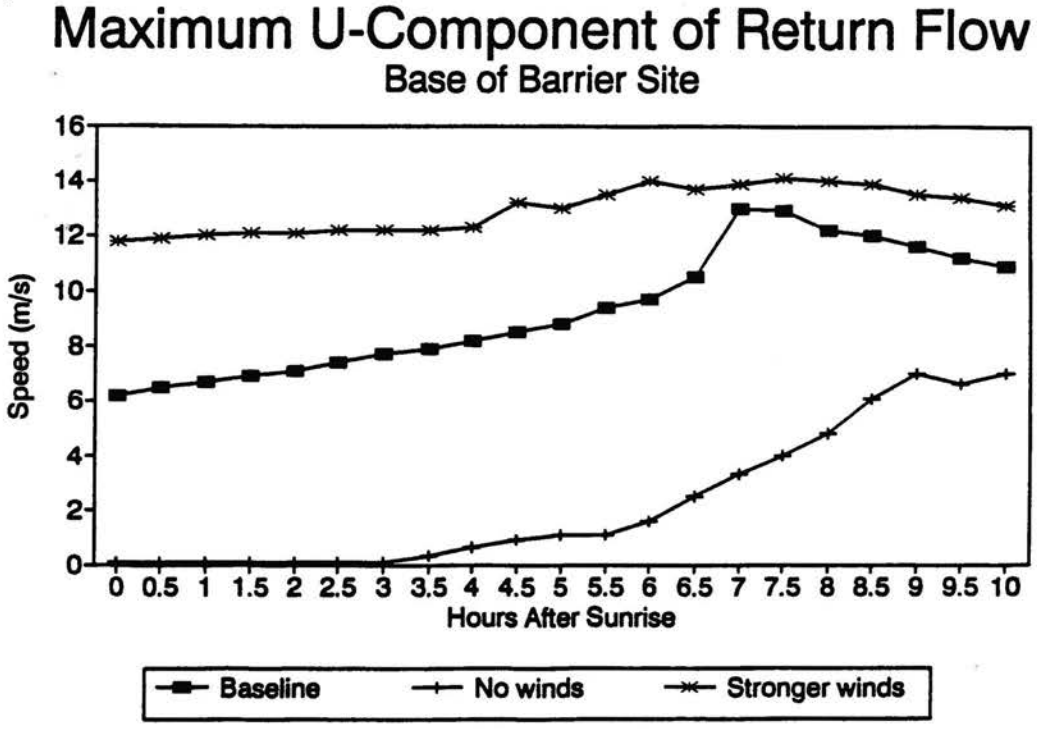

Figure 4.13. The same as Figure 4.1 but for the different wind simulations.

eastward is 5.5ms^{-1} at 7 hours after sunrise increasing to 8.5ms^{-1} by 11 hours after sunrise. The no wind simulation does not have the strong spikes, and its maximum westerly mass flux occurs at 8.5 hours after sunrise.

Figure 4.14 shows plots of the depth of flow quantities. The depth of the upslope flow is greatest in the stronger wind simulation between 5 and 7 hours after sunrise which results from the solenoid passing overhead sooner. The top of the solenoid is initially shallower in the stronger winds run than in the baseline run, but by 4 hours after sunrise it is nearly equal to the baseline run. After 7 hours after sunrise the top of the solenoid in the stronger wind simulation is shallower than in the baseline, and it is decreasing. The top of the solenoid is very deep for the no wind simulation, showing that the thermally driven circulation can influence the atmosphere to great depths.

Figure 4.15 shows the depth of the CBL. The CBL in the baseline simulation is the shallowest, and the CBL height in the stronger winds run is generally greater than the baseline run until 8 hours after sunrise. The strong jump in CBL height between 5 and 6 hours after sunrise in the stronger wind run is associated with the passage of the solenoid overhead. For the no wind simulation the CBL height is between the baseline and stronger wind simulation until 8 hours after sunrise, and the sharp jump in the CBL depth does not occur. Figure 4.16 shows the horizontal advection in the CBL and the amount of warming above the CBL. The horizontal cold air advection is smaller in the stronger wind simulation than in the baseline simulation. For the no winds simulation the horizontal cold air advection is much less than both simulations until 9 hours after sunrise.

The amount of warming above the CBL is nearly similar in the no winds and stronger winds simulations, and this quantity in both simulations is less than in the baseline simulation. The less heating above the CBL is one possible explanation for the deeper CBL in the stronger wind simulation early in the day. The slower return flow in the no wind simulation

a)

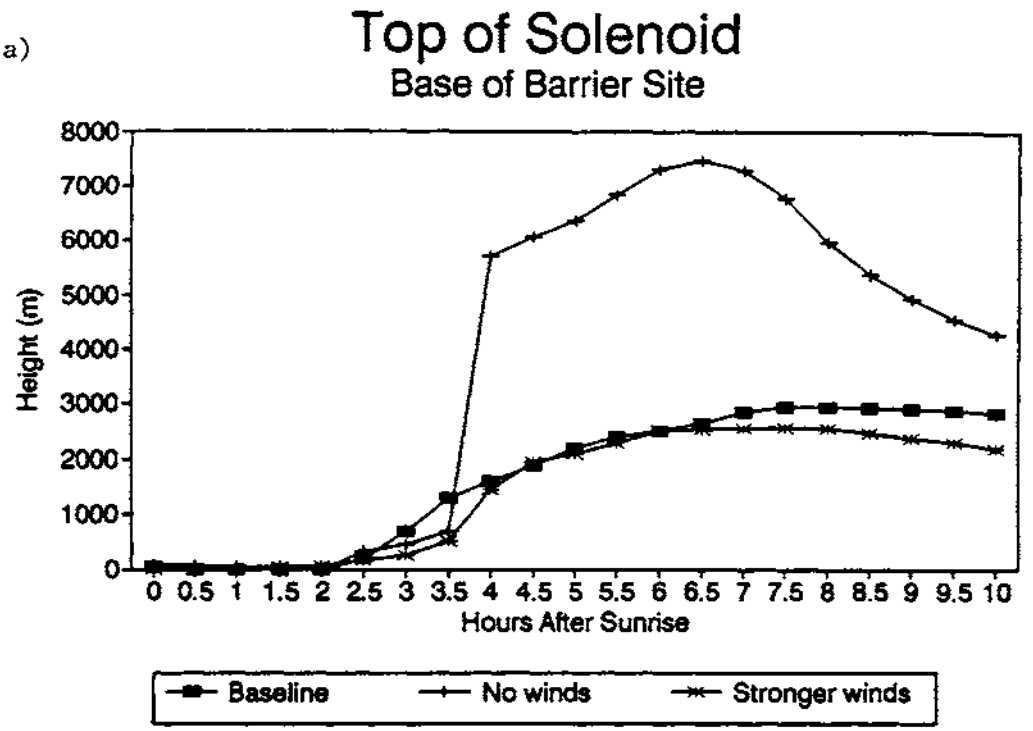

b)

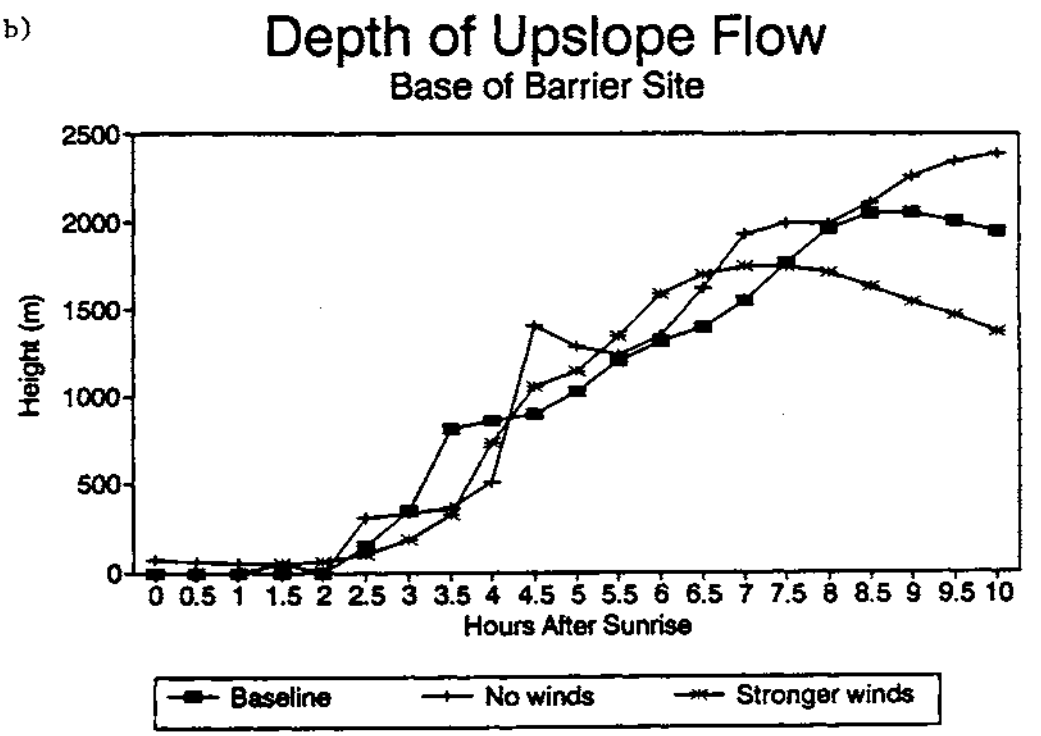

Figure 4.14. The same as Figure 4.2 but for the different wind simulations.

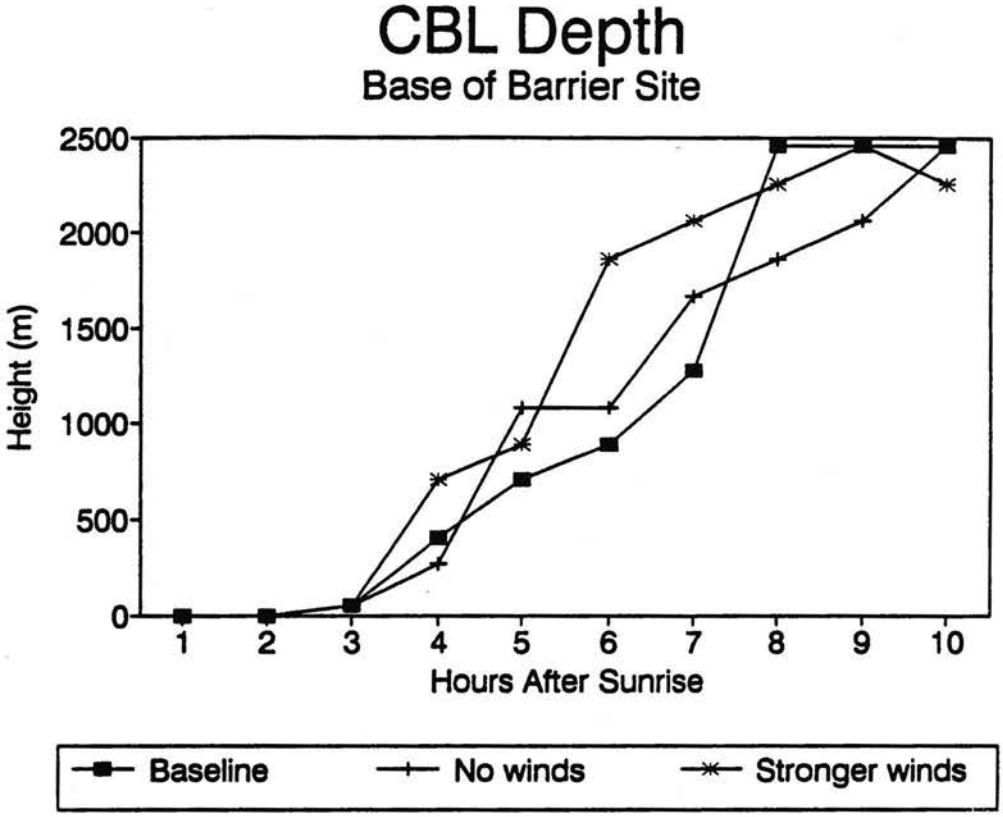

Figure 4.15. The same as Figure 4.3 but for the different wind simulations.

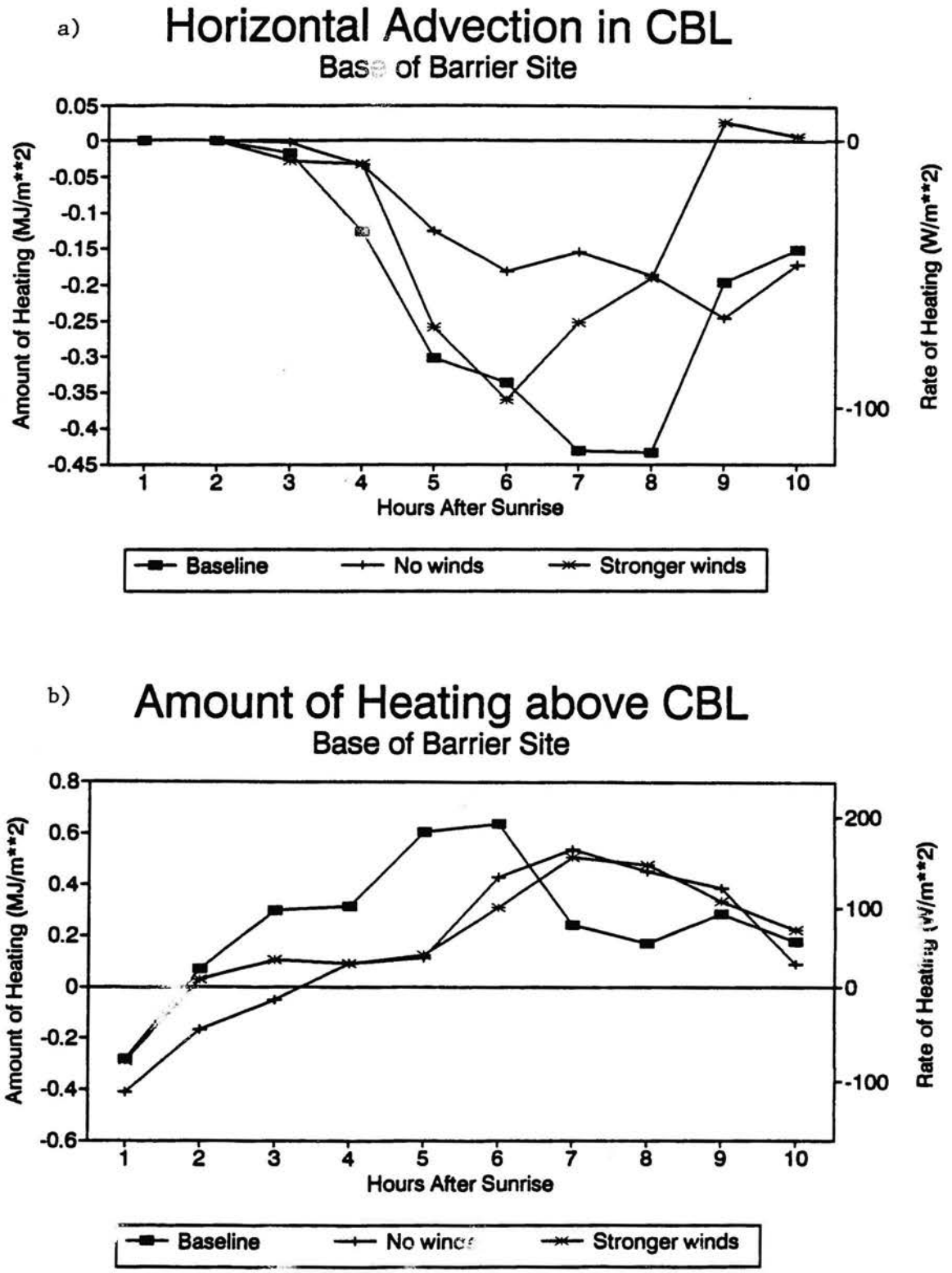

Figure 4.16. The same as Figure 4.4 but for the different wind simulations.

can reduce the heating above the CBL. Plots of the circulation and thermal quantities show that for the no winds and stronger winds runs the solenoid and the associated movement of energy are weaker than in the baseline run. The solenoid appears to have an optimum ambient wind speed for its development and its movement of energy, and this wind speed is near the ambient wind speed in the baseline simulation.

The no winds simulation differs from the baseline run in the absence of phase 1 warming, shown by the lack of warming up to 3 hours after sunrise in the heating above the CBL diagram (Figure 4.16). The changes in the pressure fields associated with the presence of the ambient flow and the channeling of part of the flow down the east side of the barrier is important for phase 1 warming. Examination of the model terms for the no wind simulation show slight advective warming between two and three hours after sunrise, but the magnitude of this warming is less than radiational cooling and is insignificant compared to other processes. A simulation with east winds is also run, and it only shows weak evidence of warming above the CBL near the base of the barrier.

4.5 Different Thermal Profiles

In this section two additional simulations are discussed. In one simulation the initial thermal profile has the top of the neutral layer at the height of the barrier top, instead of 1.0km above barrier top as in the baseline simulation. Since the initialized deep neutral layer is an approximation of the late afternoon CBL on from the previous day, this new simulation is referred to as the **lower CBL** simulation. The second simulation has weaker stability than the baseline run. The stability from 1.0km above barrier top to 8.2km (the tropopause) has a $d\theta/dz$ of $1.75 Kkm^{-1}$ compared to $3.5 Kkm^{-1}$ in the baseline run, and this simulation is referred to as the **less stability** run.

Table 4.4 lists the maximum u-component of the jet and the height of the maximum at sunrise for the base of the barrier site and a site 30km to the west. No significant differences in the speed or height of the jet between the three simulations are evident. Figure 4.17 shows the westward mass flux in the upslope flow and the maximum u-component of the westerly return flow for the three simulations. The lower CBL simulation has less westerly mass flux after 4 hours, and the speed of the return flow is less. The initialized lower CBL does not allow for a cold core to develop to as great a depth than in the baseline simulation, and this change to the cold core apparently weakens the intensity of the solenoid circulation. In the less stability simulation the cold core can build to a greater depth, and after 5 hours after sunrise the westward mass flux in the less stability simulation is greater than in the baseline simulation. The spikes in all the simulations appearing at 7 hours after sunrise show that the solenoid passes the base of the barrier site at the same time (between 7 and 7.5 hours after sunrise).

The solenoid begins to move eastward at about the same speed in the three simulations reaching the base of the barrier site almost the same time. As the solenoid continues to migrate eastward, the speed at which it moves eastward can change. After the solenoid passes the base of the barrier, in the lower CBL simulation the solenoid moves eastward at 2.5-3.0ms^{-1}, which is slower than the baseline simulation, and in the less stability simulation the solenoid moves eastward at about 5.0ms^{-1}, which is the same speed as the baseline simulation.

Figure 4.18 shows the depth of the upslope flow and the top of the solenoid. The lower CBL simulation has a shallower circulation than the baseline simulation while the less stability simulation has a deeper circulation. The depth of the cold core over the mountain influences the depth of the circulations. In the less stability simulation the deeper cold core produces a deeper circulation than in the baseline run, and the shallower cold core in the

Table 4.4

Speed and height of the maximum u-component in the near surface jet and the height and speed of the minimum u-component at sunrise for the base of the barrier site and for the site 30km to the west for the different thermal profiles runs.

BASE OF THE BARRIER

Run	Maximum U-component Speed (ms^{-1})	Height (m)	Minimum U-Component Speed (ms^{-1})	Height (km)
Baseline	5.5	250	0.8	1.0
Low CBL	4.8	500	0.8	1.3
Less Stability	5.4	500	1.2	1.1

30KM WEST OF THE BASE OF THE BARRIER

Baseline	9.1	275	-0.6	2.3
Low CBL	9.3	250	-0.1	1.4
Less Stability	6.5	250	-0.4	2.8

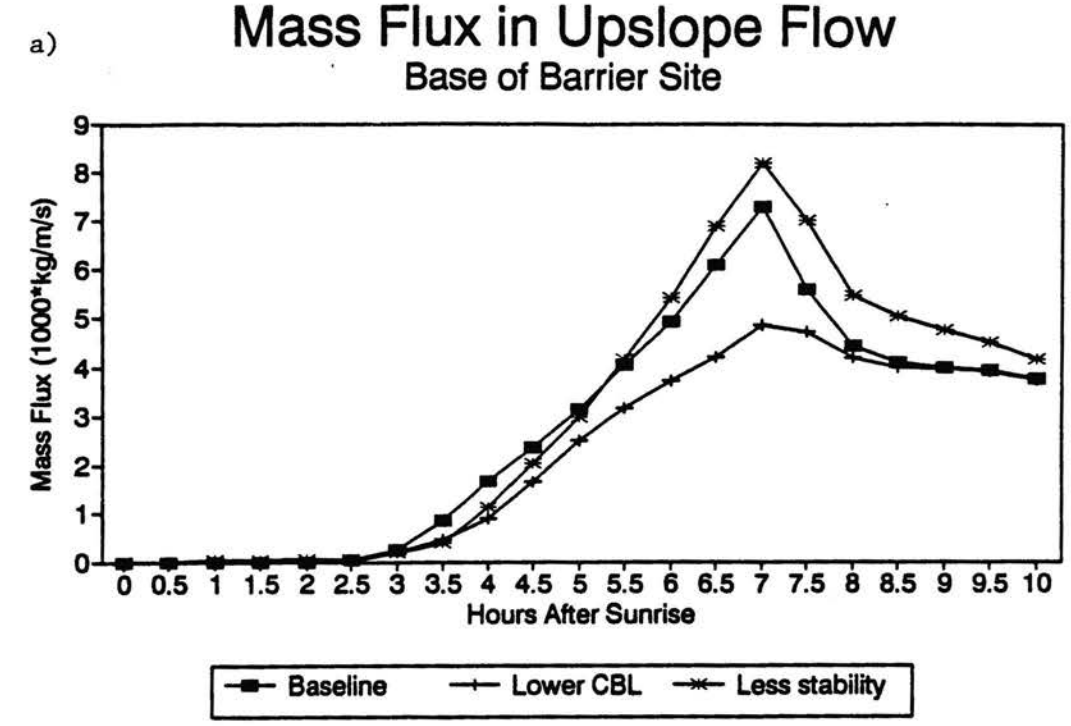

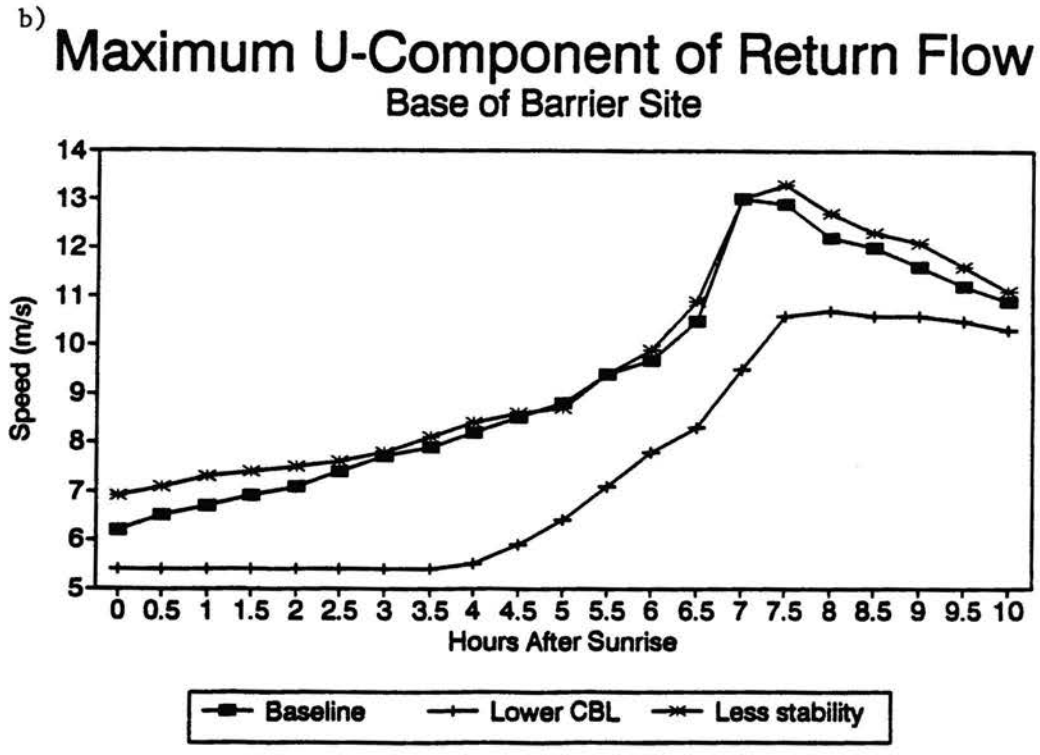

Figure 4.17. The same as Figure 4.1 but for the different thermal structure simulations.

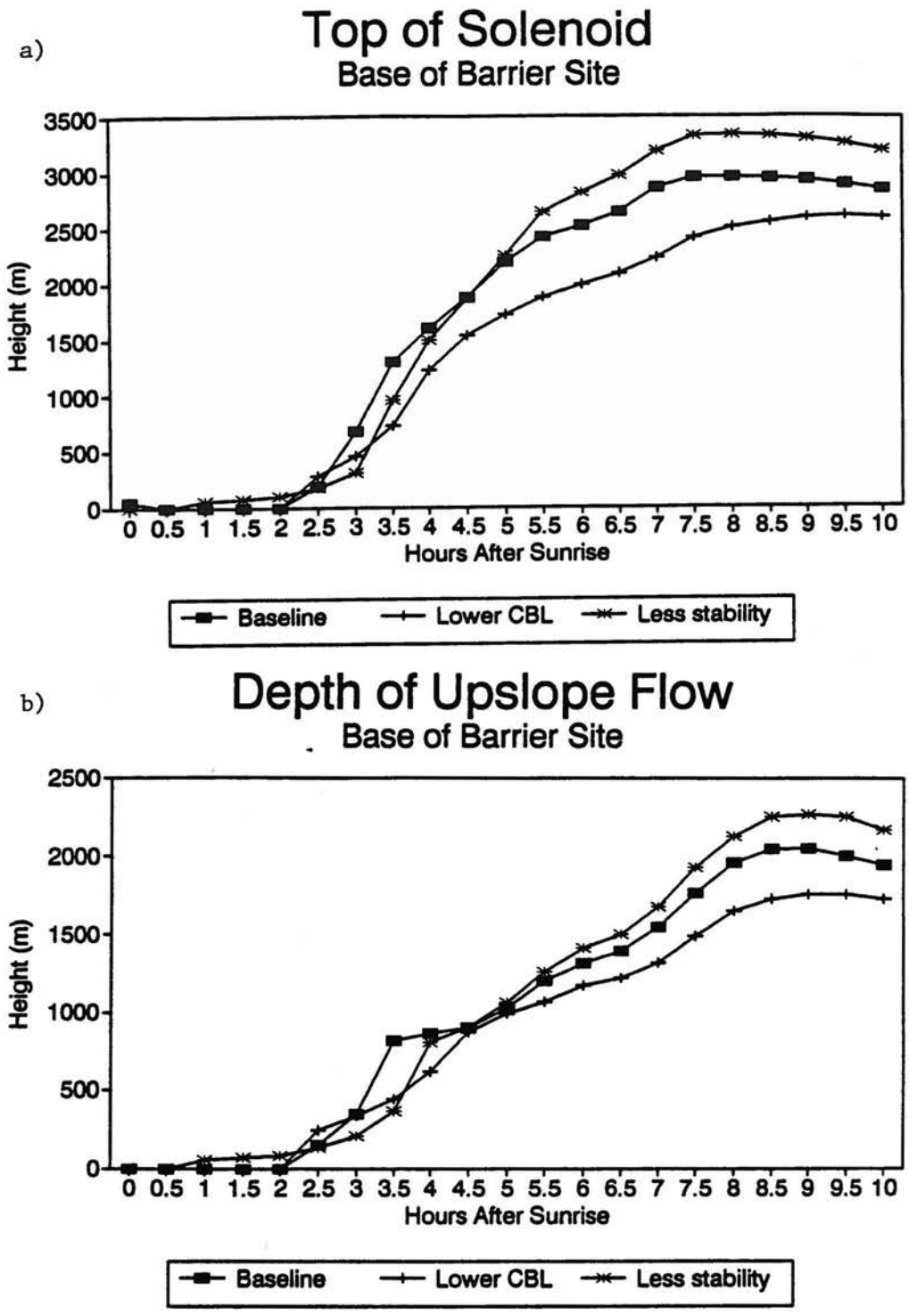

Figure 4.18. The same as Figure 4.2 but for the different thermal structure simulations.

lower CBL simulation produces shallower circulations. The CBL depth (Figure 4.19) shows that after 7 hours after sunrise (the solenoid passes over this site between 7 and 7.5 hours) the CBL is deeper for the less stability simulation. The deeper CBL is associated with the deeper circulation as seen in the four circulation quantities. In the lower CBL simulation the CBL is shallower than in the baseline run. A jump in the CBL depth does not occur with the passage of the solenoid, but the CBL continues to deepen after the passage of the solenoid. The lower CBL after the passage of the solenoid is consistent with the lower depths of the circulation in this simulation compared to the baseline run.

In the lower CBL simulation, after the solenoid passes the base of the barrier site the cold core to the west is still becoming deeper, and the depth of the upslope and return flow are increasing. With the initially lower stability the cold core builds to a shallower depth before the solenoid moves eastward. After the solenoid begins migrating eastward, the circulations do not move energy away from the barrier sufficiently quick to stop the deepening of the cold core. The cold core grows deeper in the afternoon, and the continued growth of the cold core in the afternoon builds a deeper near neutral layer above barrier top over the east slope of the barrier. For a given amount of heating and similar stability the cold core appears to build a neutral layer above barrier top to a particular depth.

The baseline and June 21 heating simulations further support this idea. In the baseline run the cold core builds to a greater height more quickly than in the lower CBL simulation, because of the presence of initial near neutral layer up to 1.0km above the barrier crest in the baseline run. The cold core stops deepening in the baseline run by the time the solenoid begins moving eastward. The quantities describing the intensity and depth of the circulation in the June 21 heating simulation (discussed previously in Figures 4.1 and 4.2) show continued deepening and intensification of the circulation after the solenoid passes the

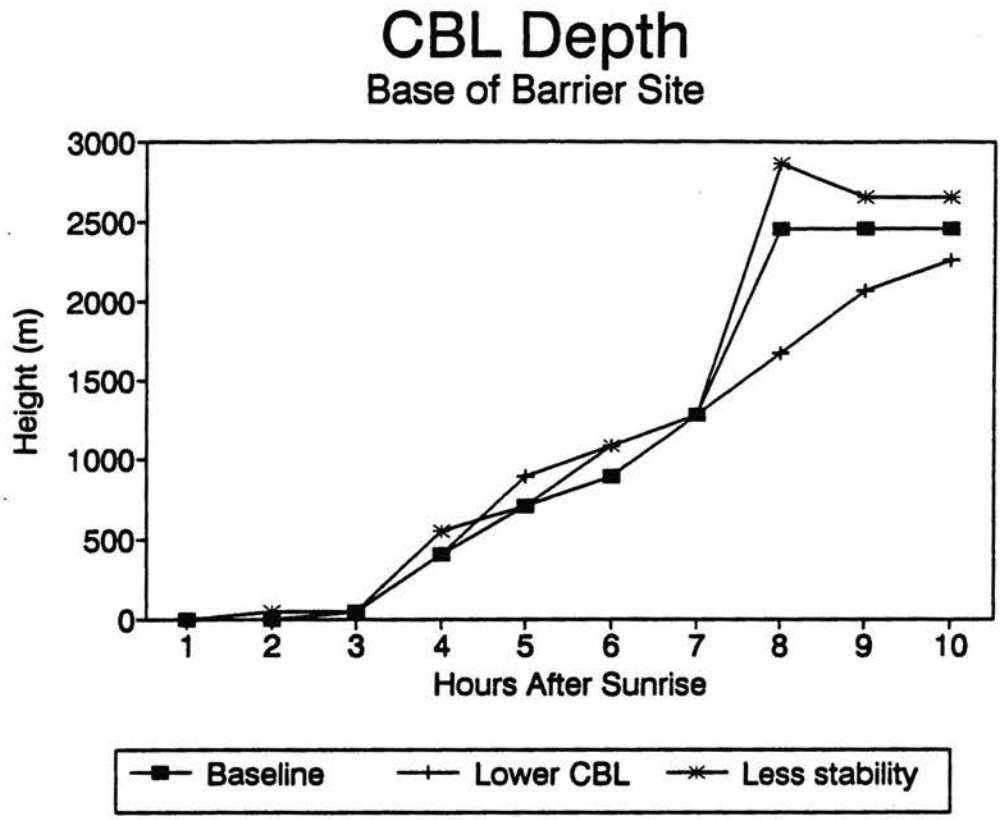

Figure 4.19. The same as Figure 4.3 but for the different thermal structure simulations.

base of the barrier site. The stronger heating than in the baseline run leads to continued deepening of the cold core at this time.

Figure 4.20 shows the horizontal advection and heating above the CBL for the three simulations. The horizontal cold air advection is less for the lower CBL simulation and higher for the less stability simulation, especially after 5 hours. The behavior of the advection is similar to the westward mass flux which has weaker flux for the lower CBL simulation and greater flux for the less stability simulation. The warming above the CBL is similar for the three simulations.

The quantities show that the circulations are deeper for the less stability simulation and shallower for the lower CBL simulation. The intensity of the circulations is less for the lower CBL simulation and generally is greater for the less stability simulation. The lower CBL simulation has a continued deepening of the cold core throughout the day suggesting that for a given amount of heating the atmosphere builds a cold core to at least some depth, and this depth is likely also dependent on the strength of the ambient stability.

4.6 Half Barrier Height

In the **half barrier height** simulation the elevation of the terrain is reduced by one half of the baseline run. The barrier rises 1.0km over a horizontal distance of 60km with a nearly flat plain to the east. The wind, thermal, and moisture fields are altered so the changes in the fields above barrier top match those in the baseline simulation. Similar to the baseline run, the height of the near neutral layer is 1.0km above barrier top resulting in the top of the near neutral layer having at a height of 2.0km. (In the baseline run the top neutral layer is at about 3.0km.) The winds are $2ms^{-1}$ below the barrier top and linearly increase to $5ms^{-1}$ at 1.5km above barrier top. The moisture is also adjusted to have similar changes above barrier top as in the baseline run. Figure 4.21 shows the sunrise state of the atmosphere.

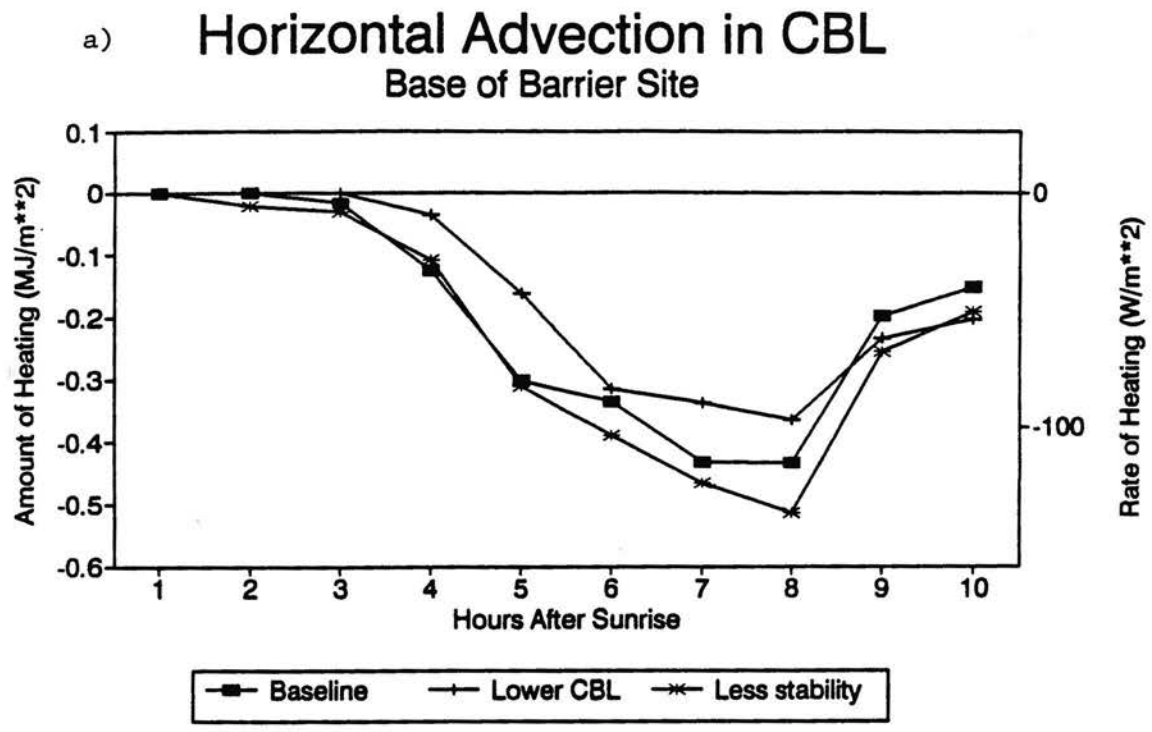

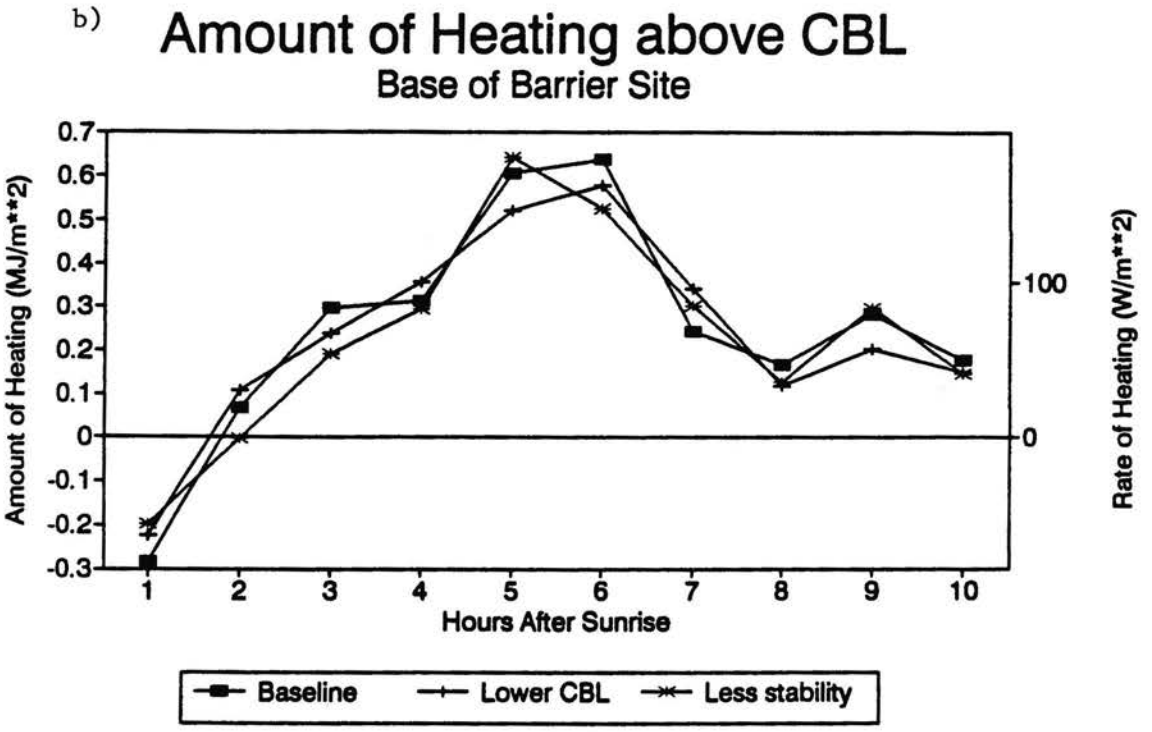

Figure 4.20. The same as Figure 4.4 but for the different thermal structure simulations.

a) Potential Temperature. Contour interval 1 K.

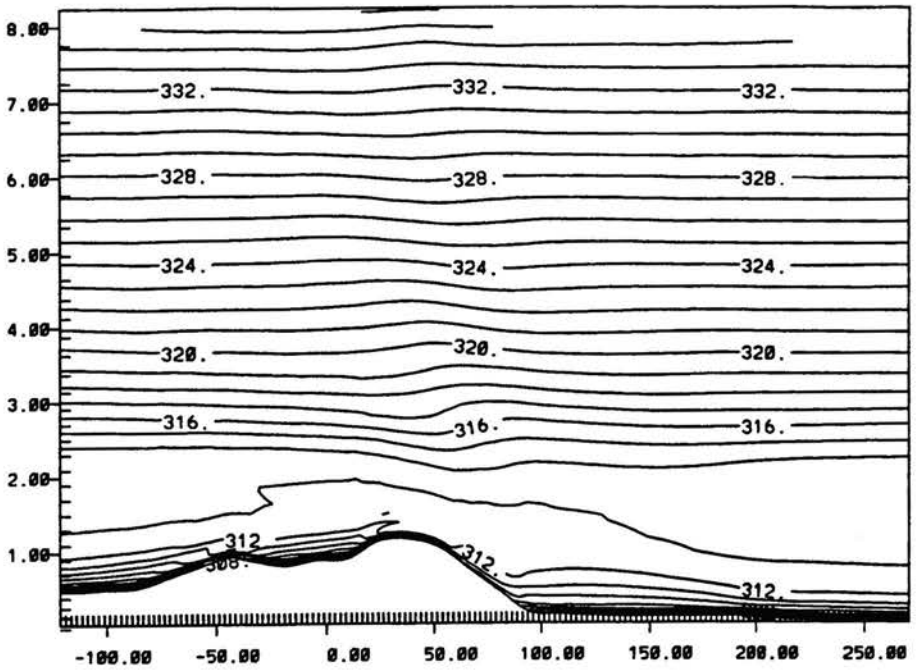

b) U-component. Contour interval 0.4 ms^{-1}. (Maximum: 6.4 ms^{-1}; minimum: 0 ms^{-1}).

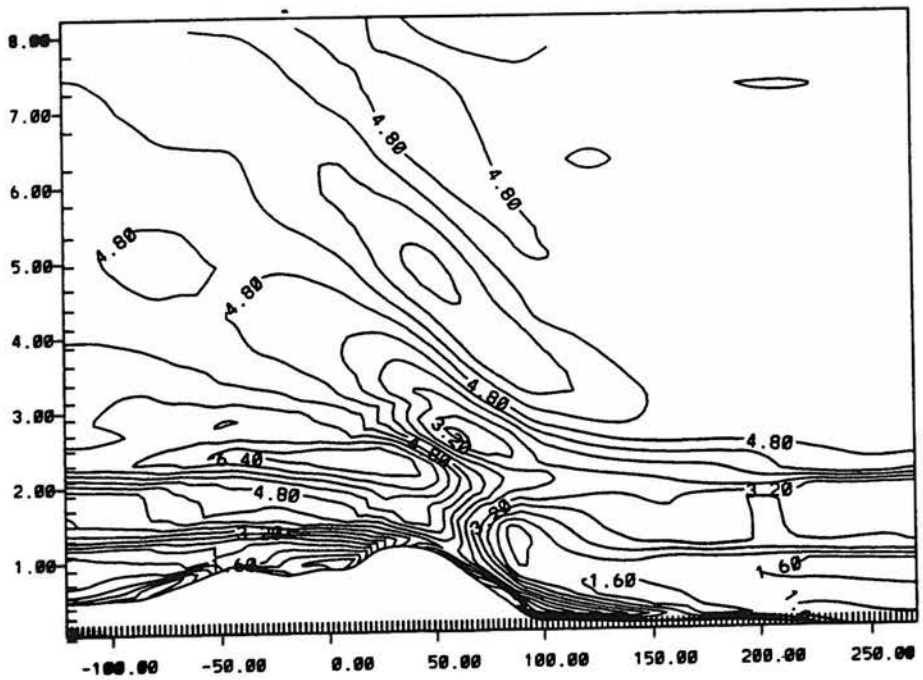

Figure 4.21. Figure 4.9 but for the half barrier height simulation at sunrise. a) potential temperature and b) u-component.

c) Vertical velocity. Contour interval 1 cms^{-1}. (Maximum: 4 cms^{-1}; minimum -13 cms^{-1}).

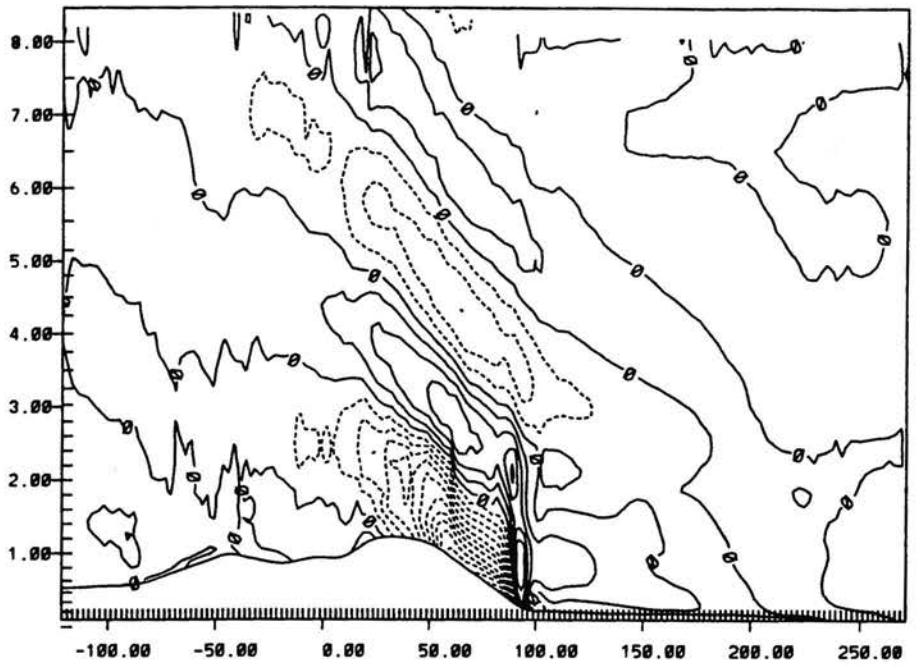

d) Perturbation Exner function. Contour interval 0.06 $Jkg^{-1}K^{-1}$. (0.022 mb at 700 mb).

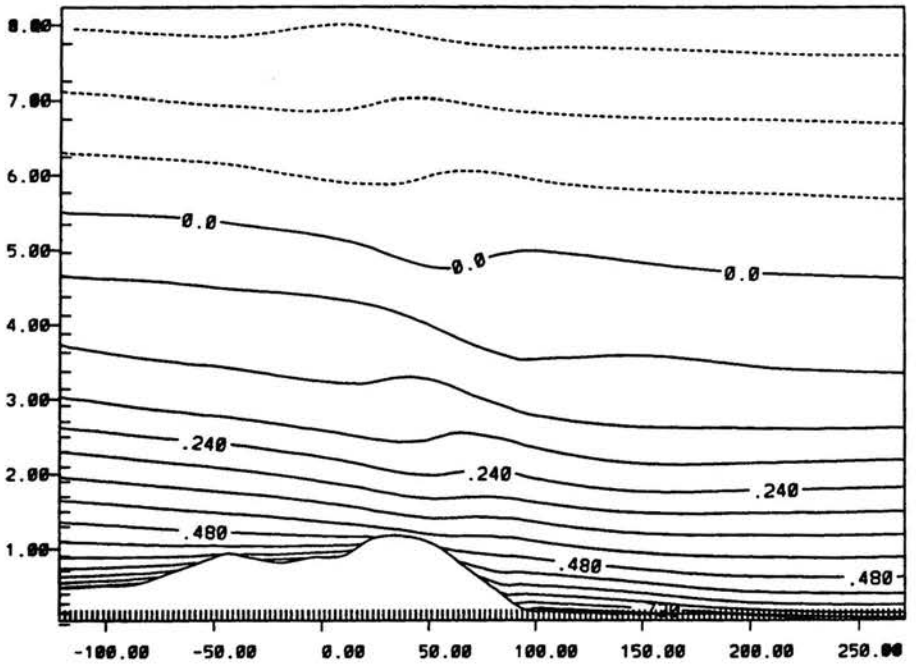

Figure 4.21. The same as Figure 4.9 but for the half barrier height simulation at sunrise. c) vertical velocity and d) perturbation Exner function.

e) Streamlines.

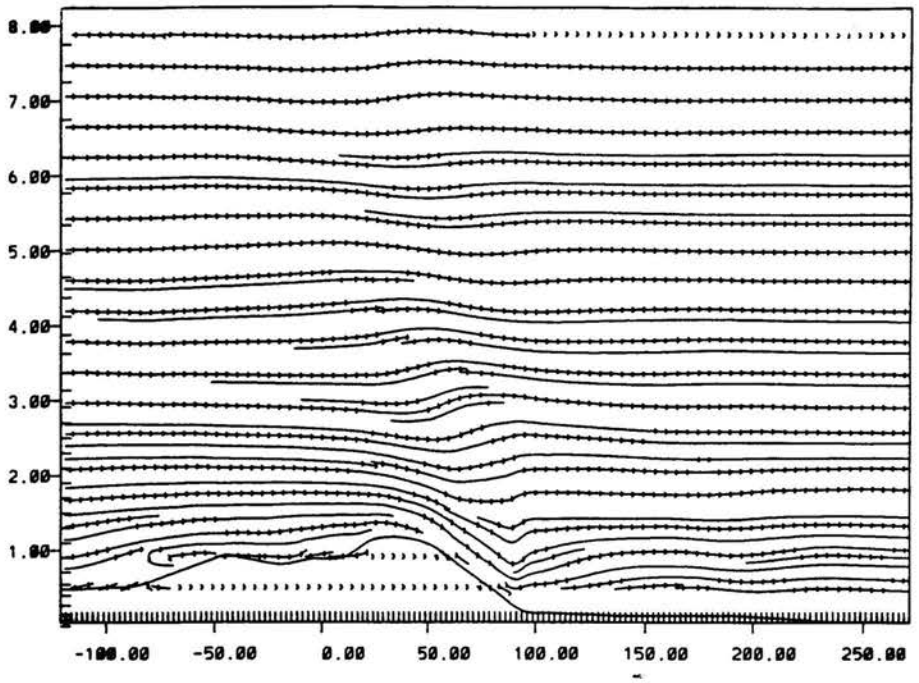

Figure 4.21. The same as Figure 4.9 but for the half barrier height simulation at sunrise. e) streamlines.

Similar to the stronger winds simulation, the sunrise state has the weakly bulging isentropes and lack of the strong channeling of the winds down the east side of the barrier. The lower barrier height creates a weaker thermally driven flow down the east barrier which causes weaker divergence along the barrier near barrier crest. Since less mass from the ambient flow is needed to replace the mass lost due to the thermally driven flows, only a portion of the ambient flow gets channeled down the east side of the barrier. This simulation shows that the intensity of the thermally induced cooling can be another influential factor in the sunrise state of the atmosphere.

Figure 4.22 shows the westward mass flux, depth of the upslope flow, CBL height, and amount of heating above the CBL for the baseline and lower barrier height simulations. The westward mass flux is much less in the half barrier height run, reaching a peak value at 5.5 hours after sunrise. The depth of the upslope flow shows a similar trait. The heating of the lower barrier height does not create as low a pressure over the barrier as in the baseline run resulting in weaker upslope flow. The CBL height in the half barrier height simulation is one grid point lower until 6 hours after sunrise, and after this time the CBL generally is deeper than in the baseline run. The CBL height does not reach a steady state value in the afternoon near barrier top, but it continues to grow. The amount of heating above the CBL is much weaker than in the baseline run, and the negative values for the first 3 hours after sunrise suggest that phase 1 warming is weak or absent. Closer examination of the model fields show that the phase 1 warming is much less than in the baseline run; it lasts for a shorter time; and it does not extend to 20km east of the base of the barrier as in the baseline run.

The quantities describing the daytime circulation are substantially different than the previous simulations. The half barrier height simulation has a weak phase 2. The lee side convergence zone forms near the base of the barrier and not at 20-40km to the west of the

a)

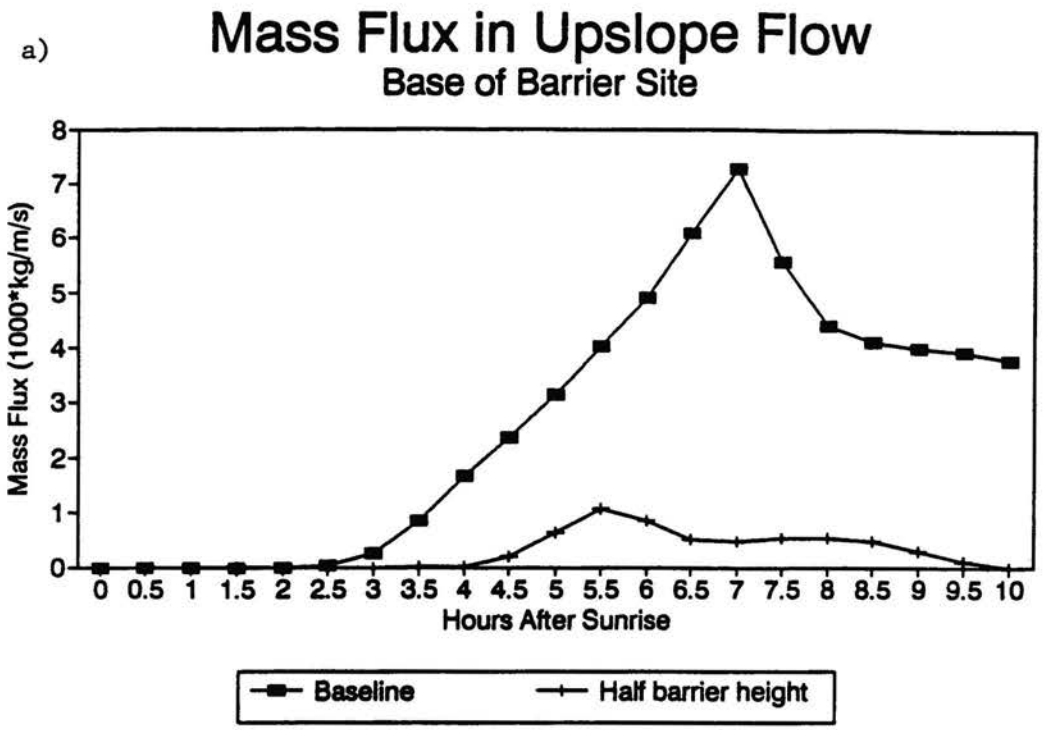

b)

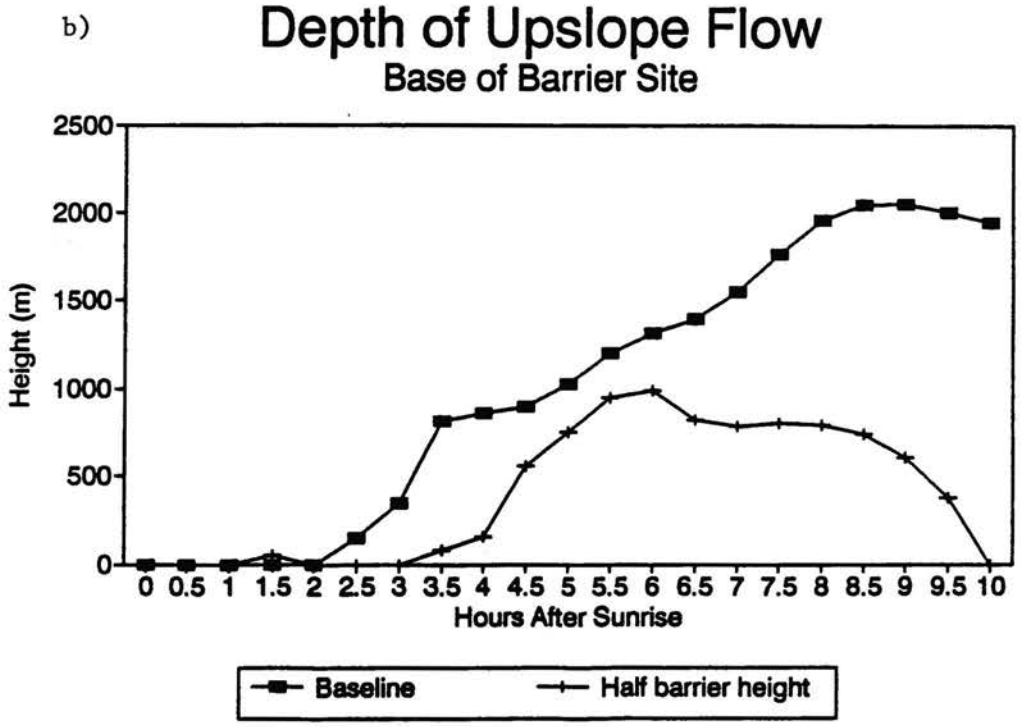

Figure 4.22. The westward mass flux in the upslope flow (a) and depth of the upslope flow (b) at the base of the barrier site for the baseline and half barrier height simulations.

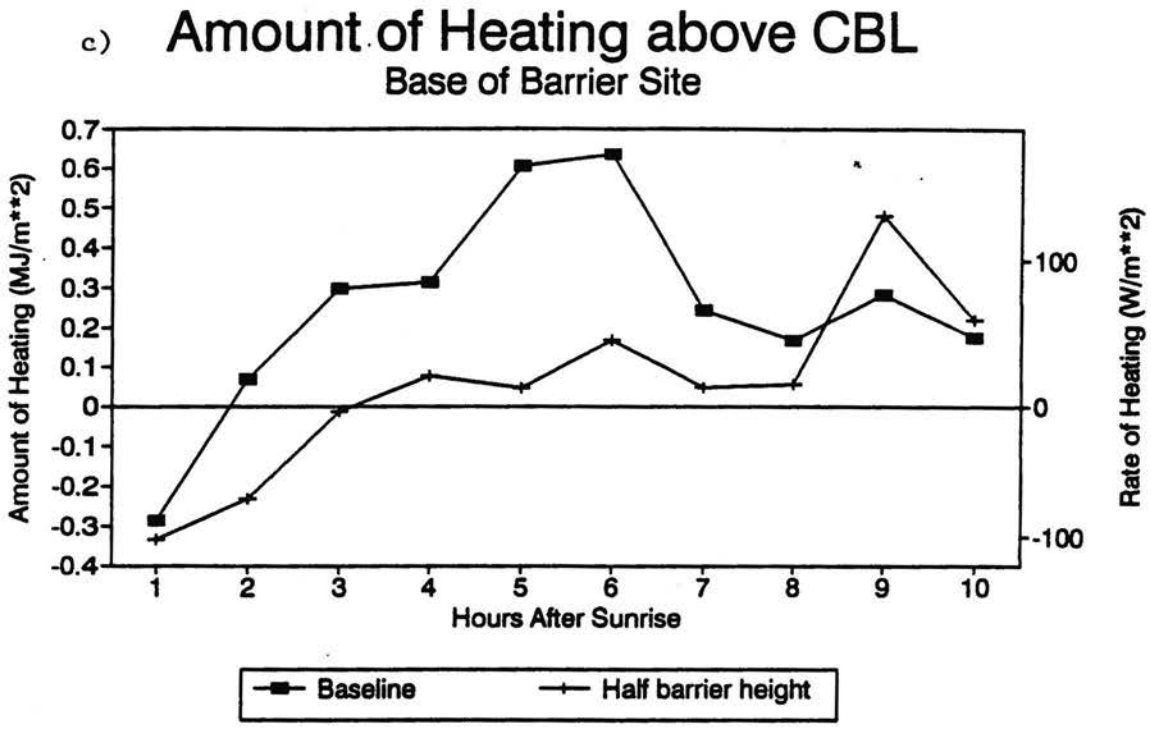

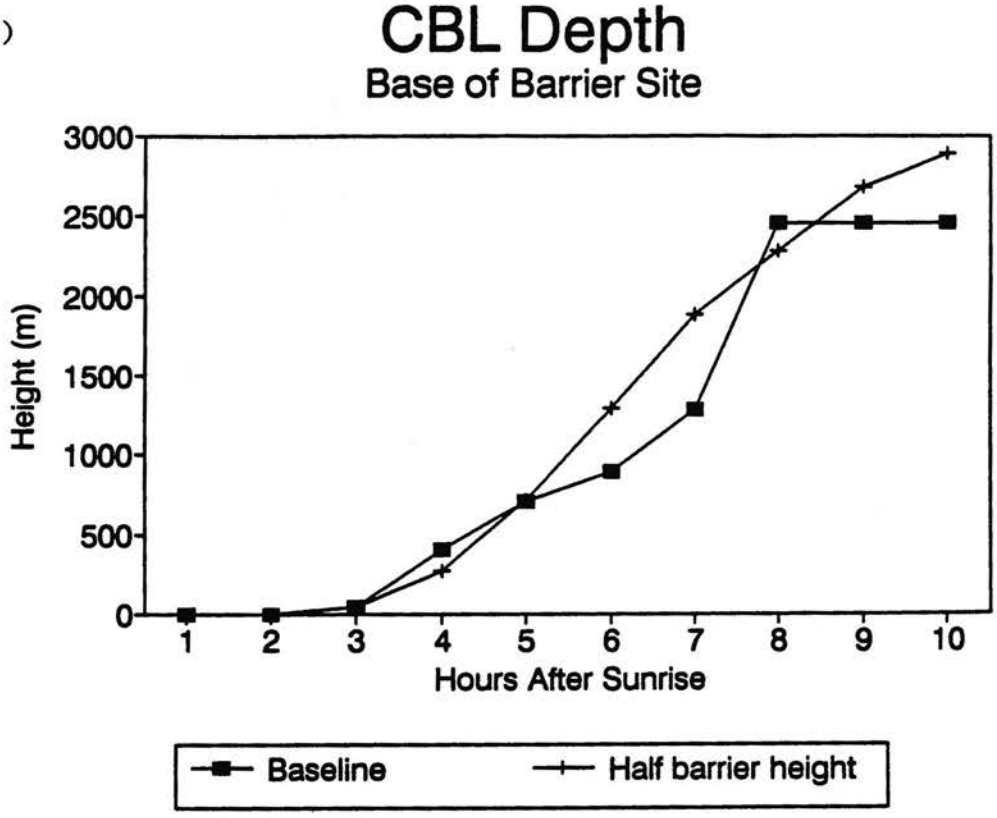

Figure 4.22. Amount of heating above the CBL (c) and the CBL depth (d) at the base of the barrier site for the baseline and half barrier height simulations.

base of the barrier as in the other simulations. By six hours after sunrise the solenoid begins moving eastward, which is about 2 hours earlier than the baseline simulation. Figure 4.23 shows the simulation at 9 hours after sunrise. Easterly flow only occurs near the base of the barrier and beneath the migrating solenoid. Like the other simulations, the center of the migrating solenoid is in a pressure trough, and a maximum in the u-component of wind occurs above it. The solenoid moves eastward at 4-5ms^{-1}, which is similar to the baseline run. Unlike the other simulations, lee side convergence zone moves eastward with the migrating solenoid. The plots of the westward mass flux and height of upslope flow show that the depth and intensity of the upslope flow decrease after the solenoid moves over the site. By 10 hours after sunrise the absence of westward mass flux shows that westerly winds are present at the surface.

Banta (1982) simulates the evolution of the atmosphere east of a 1km high and 9km wide barrier using a much earlier version of the CSU RAMS. While the horizontal dimensions, initial conditions, surface heating, and model set up are different for Banta's simulations, his simulations have many common features with the half barrier height simulation. In Banta (1982) the lee side convergence zone develops and moves eastward with the migrating solenoid. To the west of the lee side convergence zone westerly flows replace the easterly flow. Associated with the solenoid is a cold core with its center moving eastward as the lee side convergence zone moves eastward. These common features indicate that heating of the lower barrier does not create a sufficiently strong region of lower pressure below barrier top to maintain upslope flow on the eastern plains once the solenoid moves eastward. Later in the day the ambient westerly flow is able to over power the lower pressure over the barrier allowing for westerly flow to the surface.

a) Potential Temperature. Contour interval 1 K.

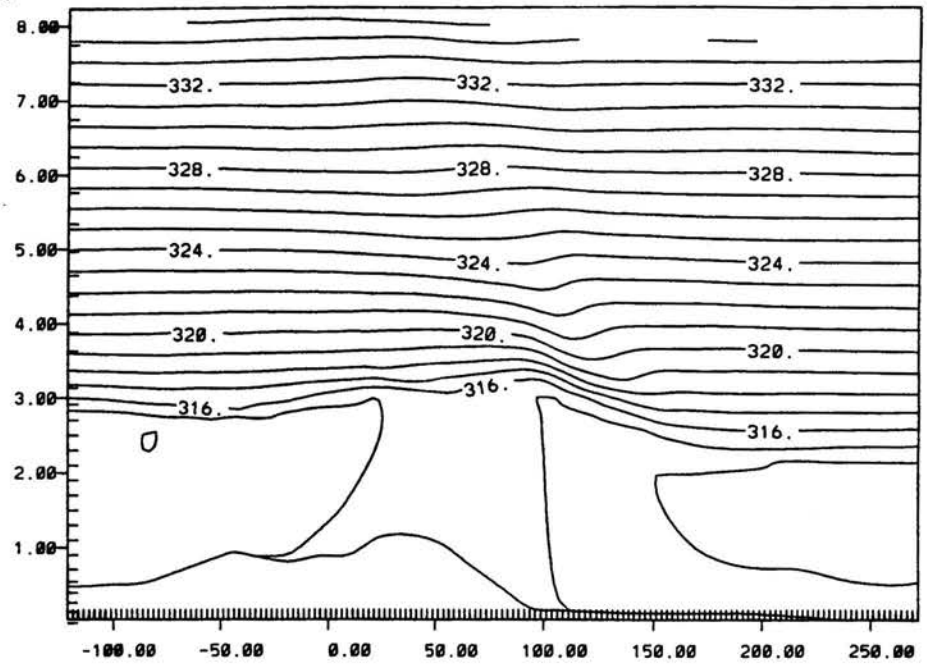

b) U-component. Contour interval 0.6 ms^{-1}. (Maximum: 9.6 ms^{-1}; minimum: -1.2 ms^{-1}).

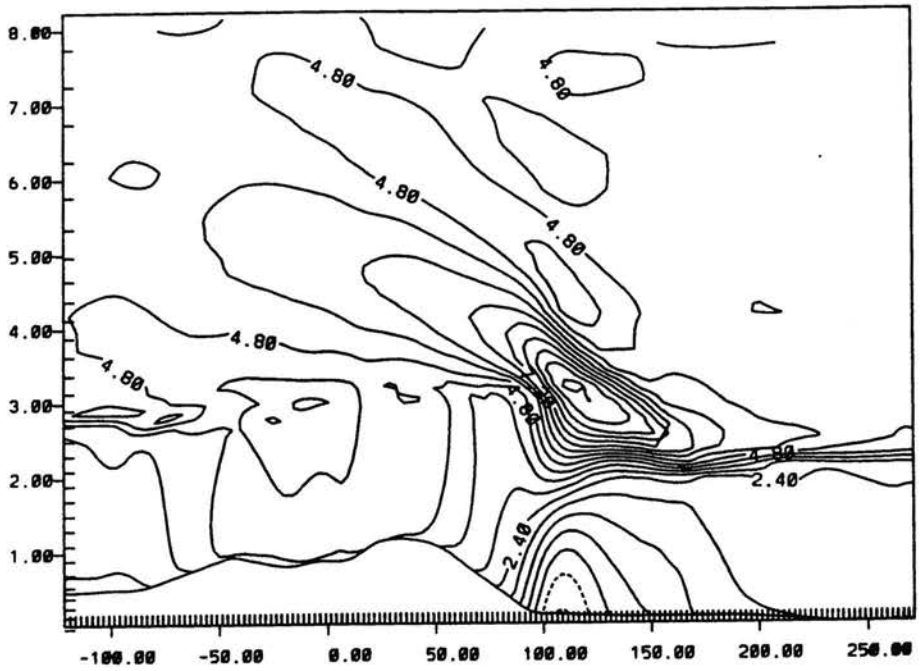

Figure 4.23. The same as Figure 4.9 but for the half barrier height simulation at 9 hours after sunrise. a) potential temperature and b) u-component.

c) Vertical velocity. Contour interval 2 cms^{-1}. (Maximum: 22 cms^{-1}; minimum: -10 cms^{-1}).

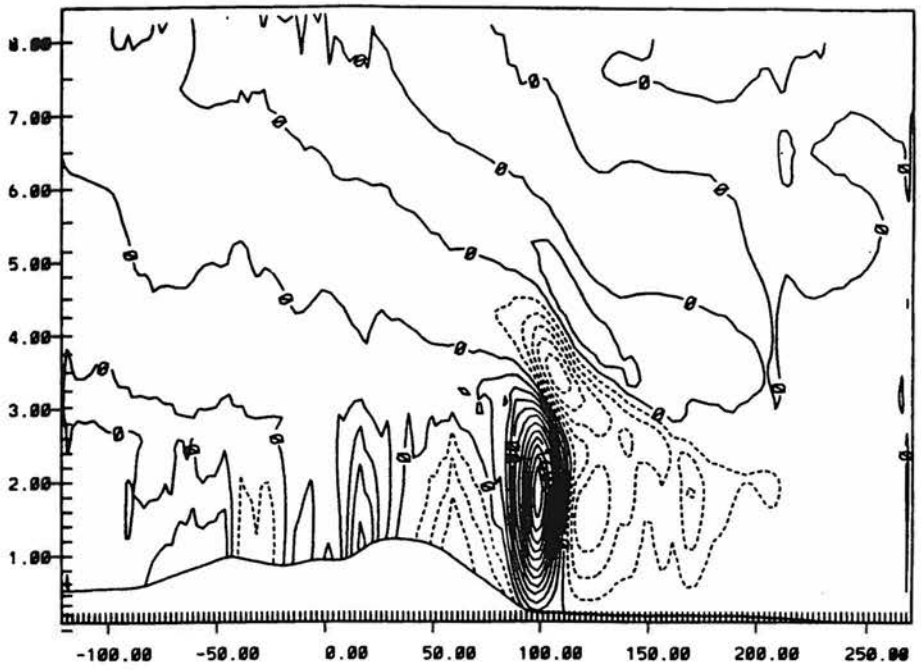

d) Perturbation Exner function. Contour interval 0.05 $Jkg^{-1}K^{-1}$. (0.019 mb at 700 mb).

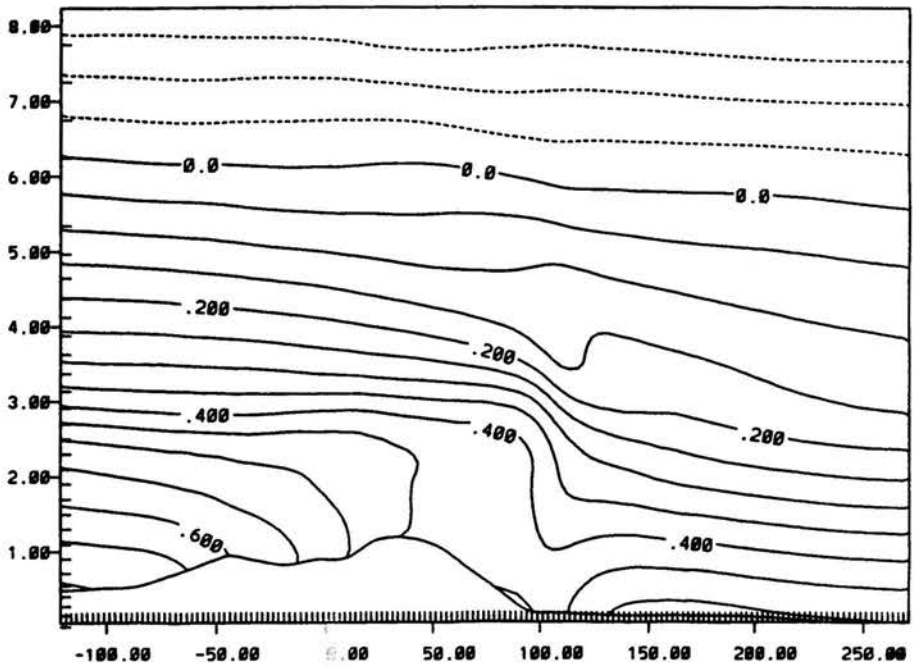

Figure 4.23. The same as Figure 4.9 but for the half barrier height simulation at 9 hours after sunrise c) vertical velocity and d) perturbation Exner function.

e) Streamlines.

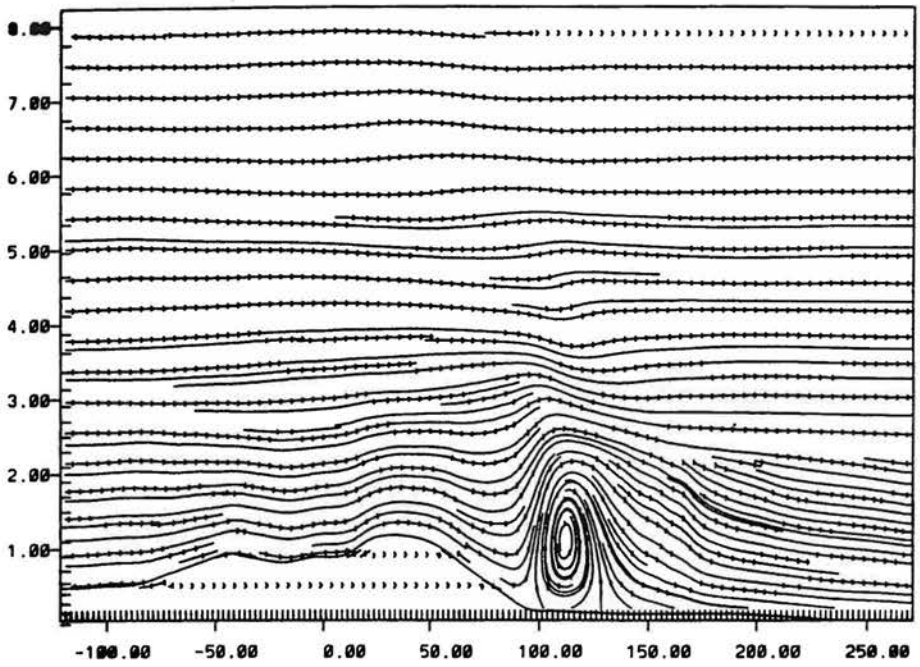

Figure 4.23. The same as Figure 4.9 but for the half barrier height simulation at 9 hours after sunrise. e) streamlines.

4.7 No Nighttime Phase

In the previous simulations a nighttime phase is allowed to evolve before the daytime phase is simulated. The **no nighttime phase** simulation starts at sunrise and has the same initial conditions as the baseline simulation with a deep layer of stability below barrier crest. The deep layer of stability below barrier top has a similar depth to the stable core at the base of the barrier in the baseline simulation. With the horizontally homogeneous initialization at sunrise, the substantial horizontal variability in the wind and thermal fields at sunrise, which is seen in the other simulations, does not occur.

With the lack of strong flow down the east side of the barrier phase 1 warming does not occur. Early in the simulation warming is seen throughout the depth of the stable core near the base of the barrier. To see if this warming results from the model adjusting to the initial conditions, an additional simulation is run with the same initial conditions as the no nighttime phase simulation but without any diabatic heating (no surface heating or radiational cooling). Figure 4.24 shows the thermal field of this simulation at 12 hours. A steady state is not achieved by this time. The depth of the stable core near the barrier is much shallower than its initial depth of 2.0km, and its depth is continuing to decrease. This lowering of the stable core and the associated warming results from the horizontally homogeneous initialization at sunrise.

By 3 hours after sunrise in the no nighttime phase simulation (with heating), upslope flow has begun along the east side of the barrier, and the lee side convergence zone develops 15 to 17.5km further west than in the baseline simulation. Weaker u-component flow, than in the baseline run, is present west of the lee side convergence zone. As the heating continues the upslope flow continues to develop. Figure 4.25 shows the westward mass flux and height of the top of the upslope flow. The upslope flow is deeper and stronger than in the baseline run until 8 hours after sunrise when the values are similar. The simulation has

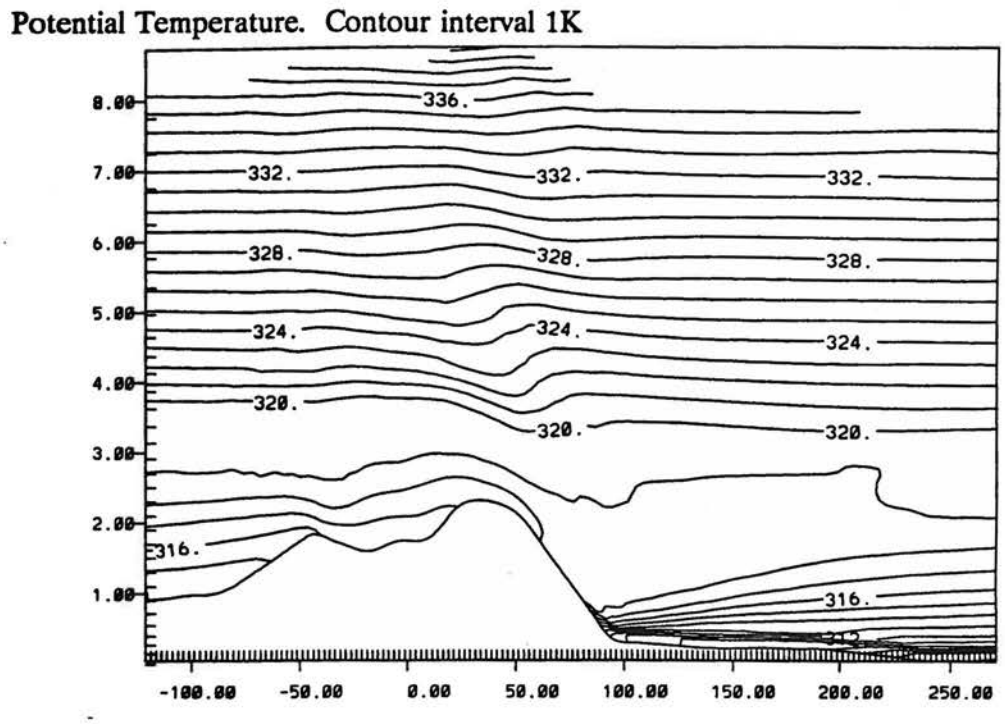

Figure 4.24. The potential temperature field in the inner grid for the no diabatic heating simulation with a stable atmosphere below barrier top at 12 hours.

a)

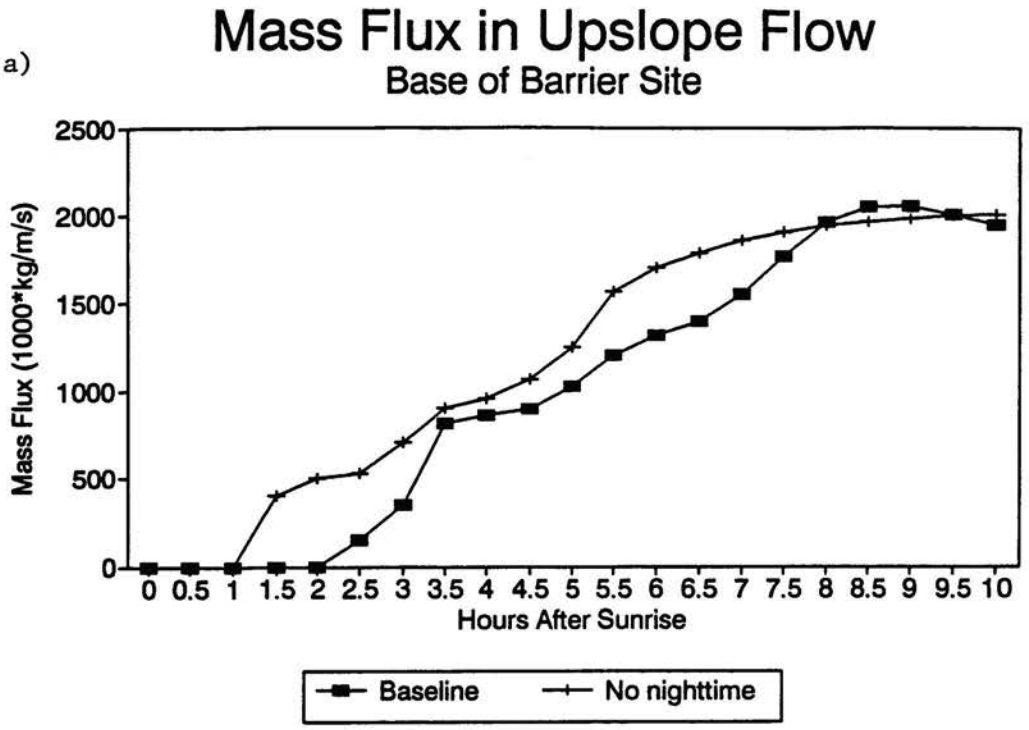

b)

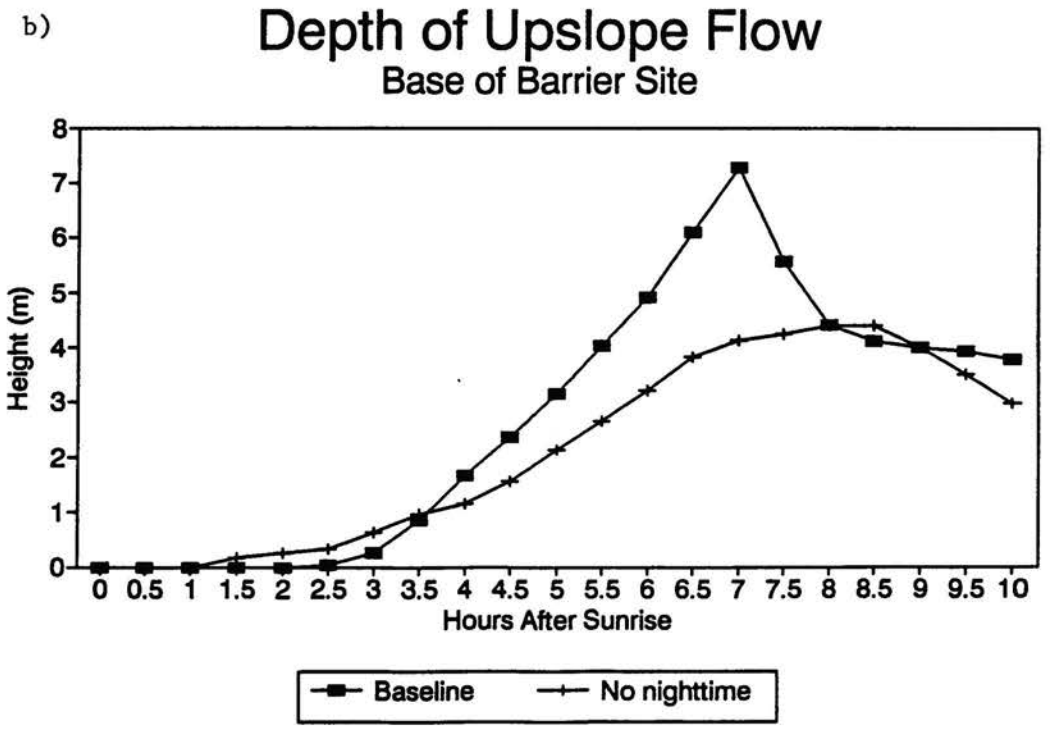

Figure 4.25. The westward mass flux in the upslope flow (a) and depth of the upslope flow (b) at the base of the barrier site for the baseline and no nighttime phase simulations.

a phase 2 with many similar characteristics to the baseline run including: the development of the cold core, strong sinking motion immediately to the east of the cold core, two stages in phase 2 of the evolution, easterly upslope flow in and above the CBL, and the appearance of a strong return flow in and above the cold core. As the daytime heating continues the leading edge of the cold core moves eastward similar to phase 3 in the other simulations.

4.8 Summary of Sensitivity Runs

This chapter has examined a number of simulations of the west-east evolution of the atmosphere east of the Front Range of the Colorado Rockies in the vicinity of Fort Collins, Colorado. Table 4.5 gives a summary of the sensitivity runs presented in this chapter. At sunrise the jet is weaker in the no wind and half barrier height simulations than in the baseline simulation. The jet maximum is further east on the slope of the barrier in the stronger wind case than in the baseline run. Phase 1 heating does not occur in the no wind and wet mountain - dry plains (WMDP) simulations, and very weak phase 1 heating is evident in the half barrier height simulation. For phases 2 and 3, circulations are generally weaker and shallower for moister soil on the eastern plains (DMWP and WMWP), moister soil west of barrier crest (WMWP), days closer to the winter solstice (November 1 and December 21), stronger winds, and lower CBL the previous day. The phase 2 and 3 circulations are generally deeper and stronger for less stability (after about 5 hours after sunrise) and for times closer to the summer solstice (June 21), especially by 5 hours after sunrise. The CBL on the eastern plains is shallower for moister soil on the eastern plains (DMWP and WMWP), days closer to the winter solstice (November 1 and December 21), stronger winds, and the lower CBL the previous day (after the solenoid passes).

Table 4.5

Summary of the different sensitivity runs compared to the baseline run. Percents and fractions are in comparison to the baseline run.

	Sunrise	Phase 1	Phase 2	Phase 3
June 21	Similar to Baseline	Similar to Baseline	Similar to Baseline	Solenoid moves about 2m/s faster
Nov. 1	Similar to Baseline	Similar to Baseline	CBL depth 1/2, Solenoid weaker	Does not appear
Dec. 21	Similar to Baseline	Similar to Baseline	CBL depth 1/3, Max. mass flux 18%	Does not appear
WMWP	Similar to Baseline	Similar to Baseline	CBL depth 1/2, mass flux 2/3 at SR+5hr.	No solenoid with leading edge cold core
DMWP	Similar to Baseline	Similar to Baseline	CBL depth 1/2, mass flux 3/4 at SR+5hr.	No solenoid with leading edge cold core
WMDP	Similar to Baseline	Does not appear	Does not appear	Does not appear
No wind	Much weaker jet	Does not appear	Mass flux 1/2 to 2/3; 1/3 amount heating above CBL	Does not appear
Stronger winds	Jet max. lower on slope	Similar to Baseline	Mass flux up to 60% less, CBL deeper, 1/3 amount heating above CBL	Solenoid moves 1.5 hours earlier and moves eastward faster
Lower CBL	Similar to Baseline	Similar to Baseline	Weaker and shallower solenoid	Solenoid moves 2m/s slower. CBL, upslope deepen after it passes.
Less Stability	Similar to Baseline	Similar to Baseline	Stronger and deeper solenoid	Upslope flow deeper and stronger.
Half Barrier	Much weaker jet	Very weak, only near base bar.	Mass flux 10-25% as large. Upslope 20-80% as deep.	Lee side Conv. zone moves east with solenoid.
No Night	No jet	Does not appear	Upslope develops 1 hour earlier	Present

CHAPTER 5.
OBSERVATIONS OF THE DAYTIME EVOLUTION

5.1 Introduction

The last two chapters discuss a variety of two-dimension simulations of the daytime evolution of the flow east of the Front Range of the Colorado Rockies showing how the time of year, pattern of surface heating, ambient winds, ambient thermal structure, barrier height, and absence of the nighttime phase affects the simulated evolution. Most of the simulations contain a three phase evolution with the first phase having surface heating on the eastern slope of the barrier interacting with the weakening nighttime flows; the second phase having a developing solenoid with a complex wind and thermal structure which does not develop uniformly with time; and the third phase having the leading edge of the cold core move eastward frequently with a solenoid beneath it.

Past observational studies of the daytime evolution in northeast Colorado and other regions with mountainous terrain have used several different strategies. One major strategy is to investigate the surface or near surface evolution. Smith and McKee (1983), and Toth and Johnson (1984) use PROFS mesonet stations to study the evolution of the surface flow in northeast Colorado. Hahn (1981) uses the 300m high BAO tower, located east of Boulder, CO, to study the daytime evolution. The BAO tower can give frequent observations of winds and temperatures, but its height is much less than the depth of the barrier. Another approach is to use aircraft data such as in Schneider (1991) in northeast Colorado, Hahn (1980) in South Park of Colorado, and Brahm and Draginis (1960) and Raymond and Wilkening (1980) for convection over mountain peaks. The aircraft data identifies horizontal gradients well and can give direct measurements of turbulence. The fairly long time of the

flight legs causes the measurements at different heights to occur at different times, and during the time of the flight legs the vertical structure of the atmosphere can change significantly. Another approach is to compile a climatology of soundings such as in Wetzel (1973). By averaging temperature, moisture, and winds from many soundings for different heights he derives a mean structure for the daytime atmosphere in eastern Colorado.

In this present study the main observational method for studying the daytime evolution is frequent launches (every 2 to 3 hours) of airsondes at several sites to measure temperature, humidity, and wind as a function of height. This observational approach is similar to Banta and Cotton (1981), and Banta (1984) which use frequent tethersondes launches in South Park of Colorado. The frequent launch of airsondes shows how the atmosphere is evolving over a given location to a height well above the height of the barrier to the west. The rapid rise rate (about $5ms^{-1}$) covers 6.0km vertically in about 20 minutes which provides an almost instantaneous vertical view of the atmosphere.

In the previous two chapters the major method for studying the computer simulations is to examine how the simulated atmosphere evolves vertically over several sites. Vertical integrals of heating and eastward mass flux are shown for the baseline simulation. To show the horizontal variability of the daytime atmosphere on the eastern plains and to compare simulations with different initial conditions, several quantities are derived which characterize the wind fields, the thermal field, and the movement of energy. In this present chapter these integrals and several of these quantities are shown for the observations and are used to compare the simulated evolution to the observations. From this analysis the utility of the use of frequent airsonde launches as an observing tool is discussed. New observing devices, such as RASS and wind profilers, measure the wind and thermal fields to heights of at least several kilometers over a location many times during the day. The results of the usefulness of frequent airsonde can be applied to these devices.

5.2 Choice of Observation Days and Locations

One of the main goals of this research is to study the west-east nature of the daytime evolution of the atmosphere east of the Front Range of the Colorado Rockies under conditions of clear skies, little change over time of the synoptic scale wind and thermal fields, and ambient winds around $5ms^{-1}$ from the westerly quadrant. Days with these characteristics are usually found on the east side of deep synoptic ridges and are not likely to have strong thunderstorms or significant downslope winds. All the observation days presented in this chapter were forecast to have synoptically undisturbed conditions with light westerly winds and were forecast to remain on the east side of a deep ridge throughout the day.

The observations are taken at several sites in the vicinity of Fort Collins, Colorado. One site is at the base of the barrier, another site is on the eastern slope of the barrier, and the remaining site is on the eastern plains, about 50km east of the base of the barrier. The simulations show that the daytime evolution at the three sites have some different characteristics. The observations are taken during two observing regimes. The Fall 1990 regime has observations at all three sites. The second regime has observations taken in Fall 1987 and Summer 1988 only at the base of the barrier. In this second regime the observations are supplemented by tethersonde launches and are collocated with a micrometeorological station which measures the components of the surface energy budget.

The next two sections show the soundings and vertical integrals of heating and eastward mass flux for each of the observing days in the two different regimes. These sections discuss the observed sounding and integrals, showing how they qualitatively compare to the model generated vertical integrals. After these two sections, some quantities from the observations are compared to the model derived quantities to examine how well the simulations quantitatively agree with the observations. From the observations and their

comparison with the simulations, the usefulness frequent airsonde launches as an observing method is discussed.

5.3 Fall 1990 Regime

Figure 5.1 shows the topography map presented in the introduction which shows the observing sites. During this regime observations are taken on October 25 and November 12 at Rustic, Fort Collins, and Carpenter, WY. The Fort Collins site is at Christman Field near the Colorado State University Department of Atmospheric Science. The site has an elevation of 1570m (5150 feet) MSL and is about 2km east of the base of the foothills. The first ridge of foothills crest about 600m above the site 5km to the west. The Rustic site is 30km west of the Fort Collins site and has an elevation of 2207m (7240 feet) which is about 640m higher than the Fort Collins site. It is located in a 450m deep, west-east river valley so the terrain surrounding the valley is about 1100m higher than the Fort Collins site. The Carpenter, Wyoming site is about 80km northeast of Fort Collins and about 50km east of the base of the barrier. This site is on the south side of the Cheyenne Ridge at an elevation of 1634m (5360 feet), and it is located in a slightly sloping field that does not have any distinct terrain features for several kilometers in all directions.

5.3.1 November 12, 1990

On November 12, 1990 sunrise is at 0700 MST. Airsondes are launched every two hours from sunrise until 8 hours after sunrise (1500 MST). General northwesterly flow aloft occurs on this day with an estimated speed of 5 ms^{-1} (10 knots) from 300 degrees at 500mb and light and variable winds at 700mb. The region is under the east side of a deep ridge. At the surface pattern a weak westerly pressure gradient is present across the region with a stationary front far to the east in central Nebraska and central Kansas.

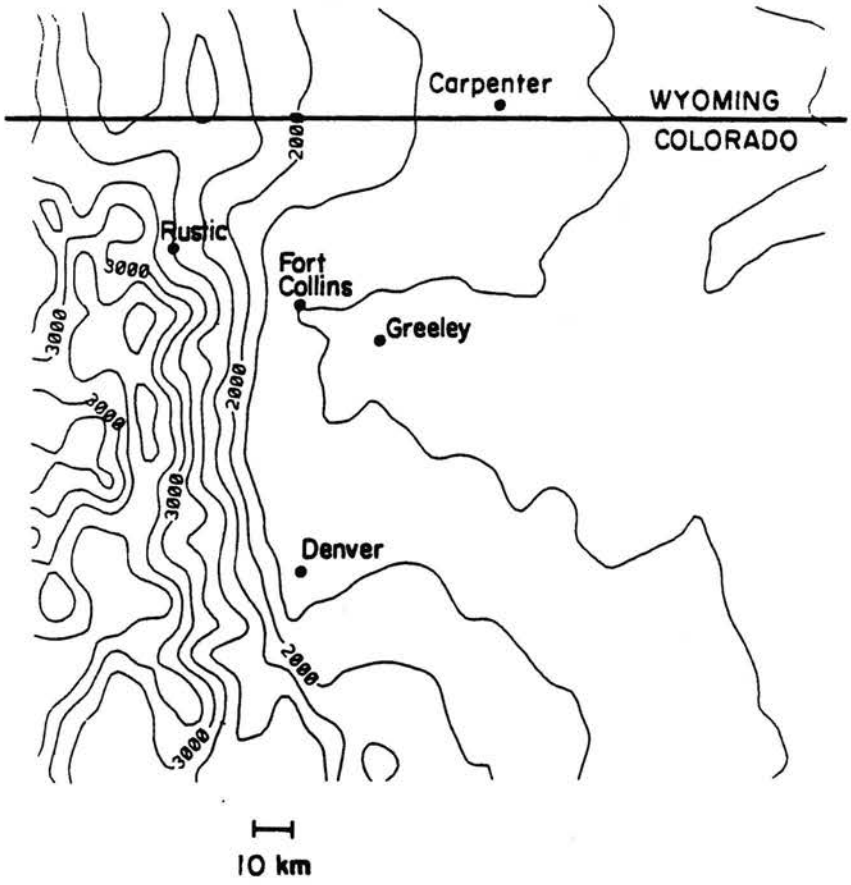

Figure 5.1. A topography map of northeast Colorado with the observation sites. Contour interval is 250m.

The thermistors on the airsondes are calibrated using a room temperature water and ice water bath. The thermistor portion of the airsondes are wrapped in a plastic bag and immersed one at a time in an agitated room temperature water bath and ice water bath. Other thermistors, which will be referred to as the baseline thermistors, are in the water baths, and the temperature of these thermistors are measured along with the airsonde thermistors. This procedure is done for all airsondes using the same baseline thermistors. The differences between the airsonde thermistor and baseline thermistors for the two baths are calculated. Using these two data points a correction as a function of temperature is used to adjust the airsonde thermistors to have the same temperature as the baseline thermistors. Since the same baseline thermistors are used for all the airsondes, the thermistors are calibrated to a common instrument. In this study the temperature in the lowest 3.0km of the atmosphere is mostly between room temperature and freezing.

Figure 5.2 shows the soundings of potential temperature, mixing ratio, and wind for the Fort Collins site. At sunrise a deep layer of stability is present to 1.3km AGL with a more weakly stable layer from 1.3 to 2.8km. Above 2.2km, which is about the height of the barrier crest to the west, the wind direction changes to more northwesterly. Below 600m the winds are light, and above 600m they rapidly increase to a maximum speed at 1000m. By 0904 MST significant warming between 500 and 1000m occurs with the strong westerly flow. As the daytime circulation evolves, easterly flow develops in and above the shallow CBL. From 1110 to 1305 MST significant warming is present between 2.3 and 3.0km, and the winds above 2.0km weakening somewhat. By 1503 MST, which is 8 hours after sunrise, the CBL is only 300m deep.

Figure 5.3 shows plots of the u-component of the wind, the vertical integral of eastward mass flux, and the vertical integral of heating for the Fort Collins site. The u-component of the flow is smoothed using a 3 point to 9 point center weighted filter on data

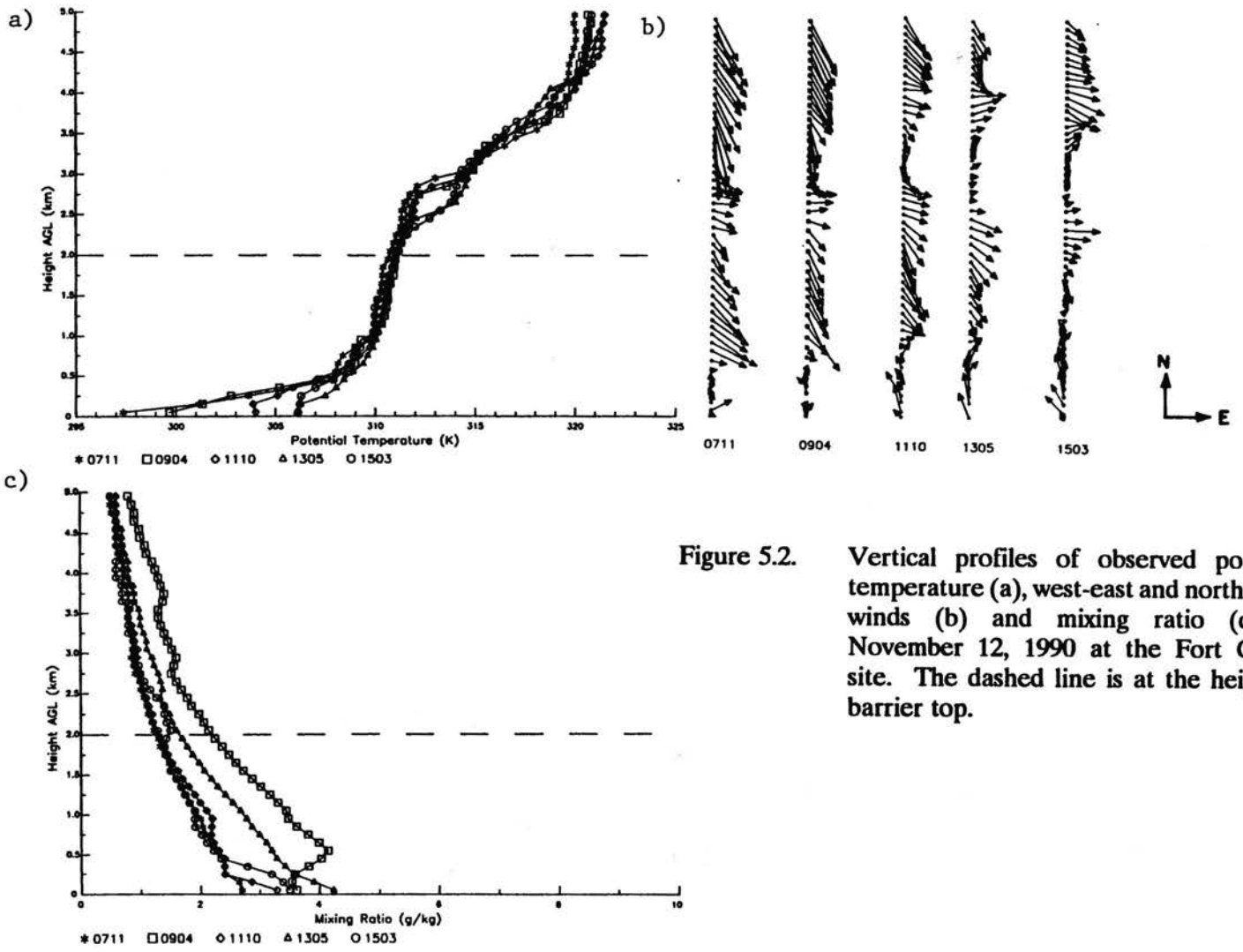

Figure 5.2. Vertical profiles of observed potential temperature (a), west-east and north-south winds (b) and mixing ratio (c) on November 12, 1990 at the Fort Collins site. The dashed line is at the height of barrier top.

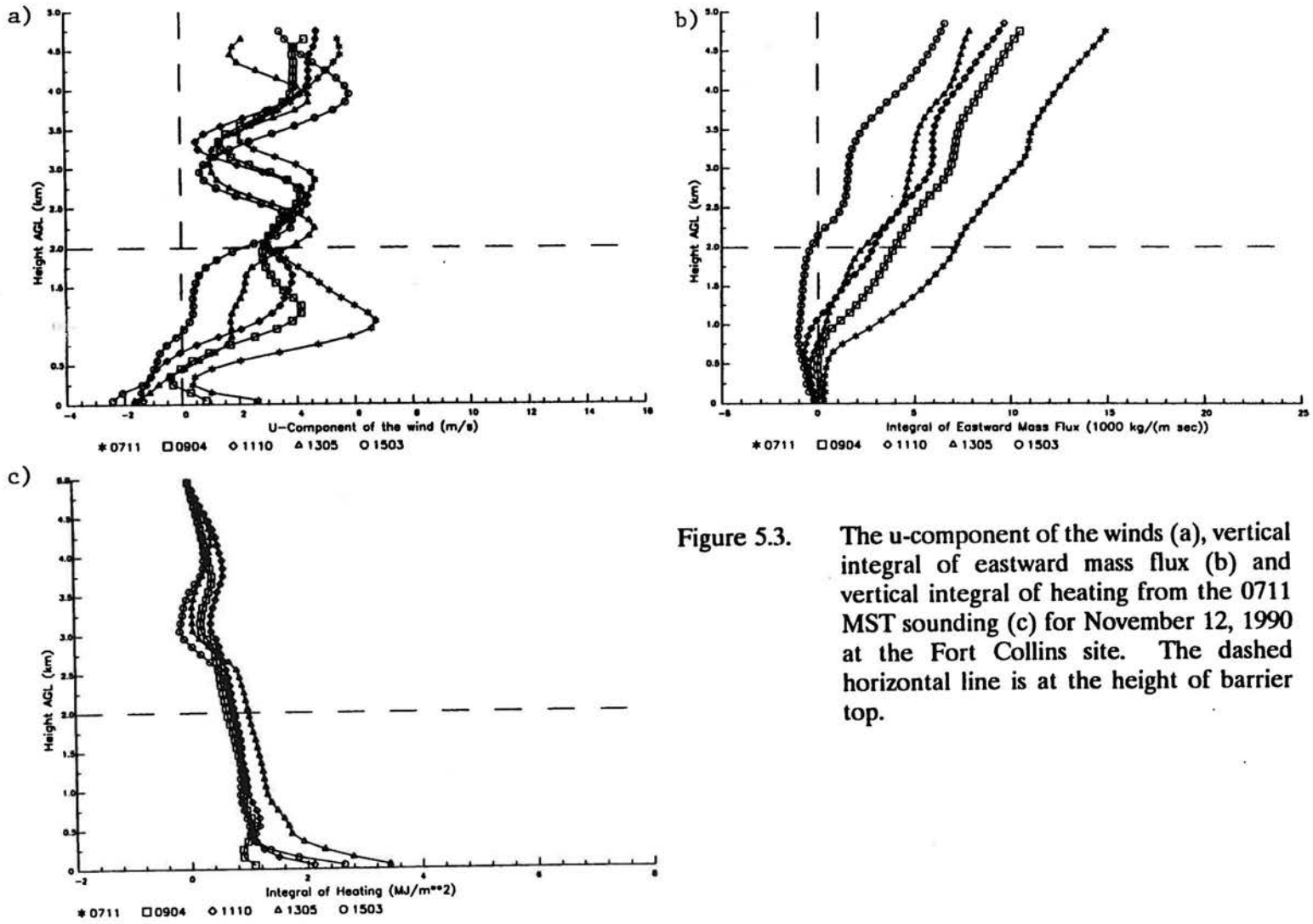

Figure 5.3. The u-component of the winds (a), vertical integral of eastward mass flux (b) and vertical integral of heating from the 0711 MST sounding (c) for November 12, 1990 at the Fort Collins site. The dashed horizontal line is at the height of barrier top.

averaged over a 100m depth. This filter does not influence the changes in the wind speed with vertical wavelengths greater than 300m, and the calculation of the vertical integral of mass flux does not use the smoothed winds. A low level jet with a maximum u-component of 6.5ms^{-1} at 1.0km AGL is present. The westerly jet weakens throughout the morning, and easterly upslope flow appears. Above the upslope flow the u-component of the flow does not show a significant increase in speed. In fact, the flow weakens from 1110 to 1305 MST between 2.5 and 3.0km. The vertical integral of eastward mass flux shows that the total eastward mass flux substantially weakens during the day as seen in the large difference in the integrals at heights of around 4 to 5km. This does not agree well with the simulated evolutions which have the integrals meet at heights between 3.5 and 4.5km. The vertical integral of heating shows significant warming below 1.0km until 1305 MST. Between 1110 and 1305 MST substantial warming occurs between 2.3 and 3.0km with cooling above 3.0km. By 1503 MST the atmosphere below 2.0km begins to cool.

Figure 5.4 shows the soundings and integral plots for Rustic which is on the east slope of the barrier. At sunrise strong westerly flow is present in the lowest 1.0km. This site is located in a 450m deep narrow, west-east mountain valley, and the nighttime downvalley flows typical in narrow mountain valleys likely influence the winds near the surface. The maximum u-component at sunrise is 9.5ms^{-1} at 650m. Many previous observational and modeling studies of flow in deep mountain valleys show that the maximum speed of the nocturnal flow is typically 100-200m above the valley bottom and that above the valley a return flow is sometimes present. In the Rustic observations the wind maximum is above valley top and significant westerly component exists up to 1.5km. The strong winds, especially above valley top, cannot be explained by the local valley drainage winds. The sunrise winds have a weak easterly component around 1.8km with the flow becoming westerly above 2.1km.

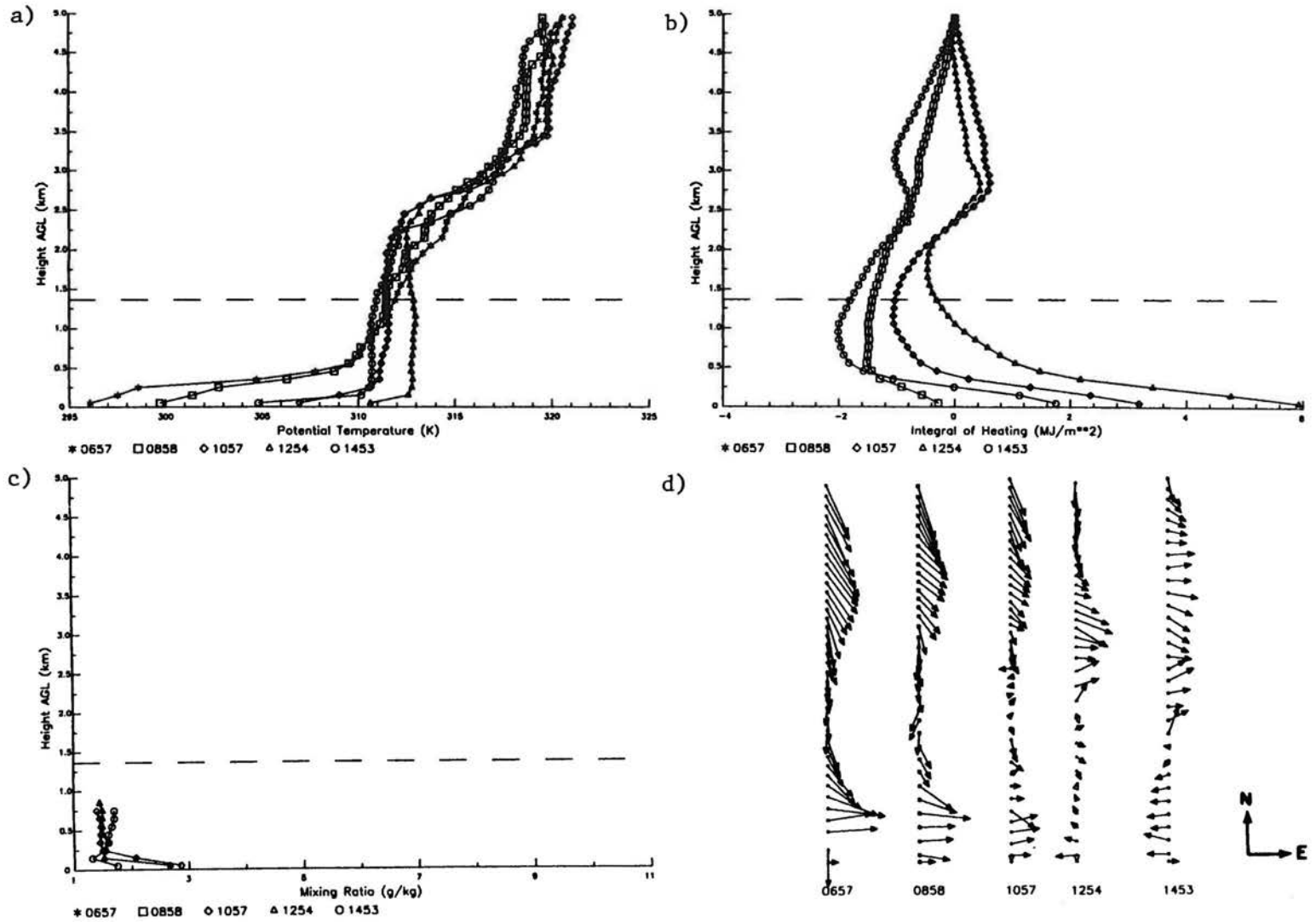

Figure 5.4. The vertical profile of potential temperature (a), vertical integral of heating from 0657 MST (b), mixing ratio (c), and winds (d) at the Rustic site on November 12, 1990. The dashed horizontal line is at the height of barrier top.

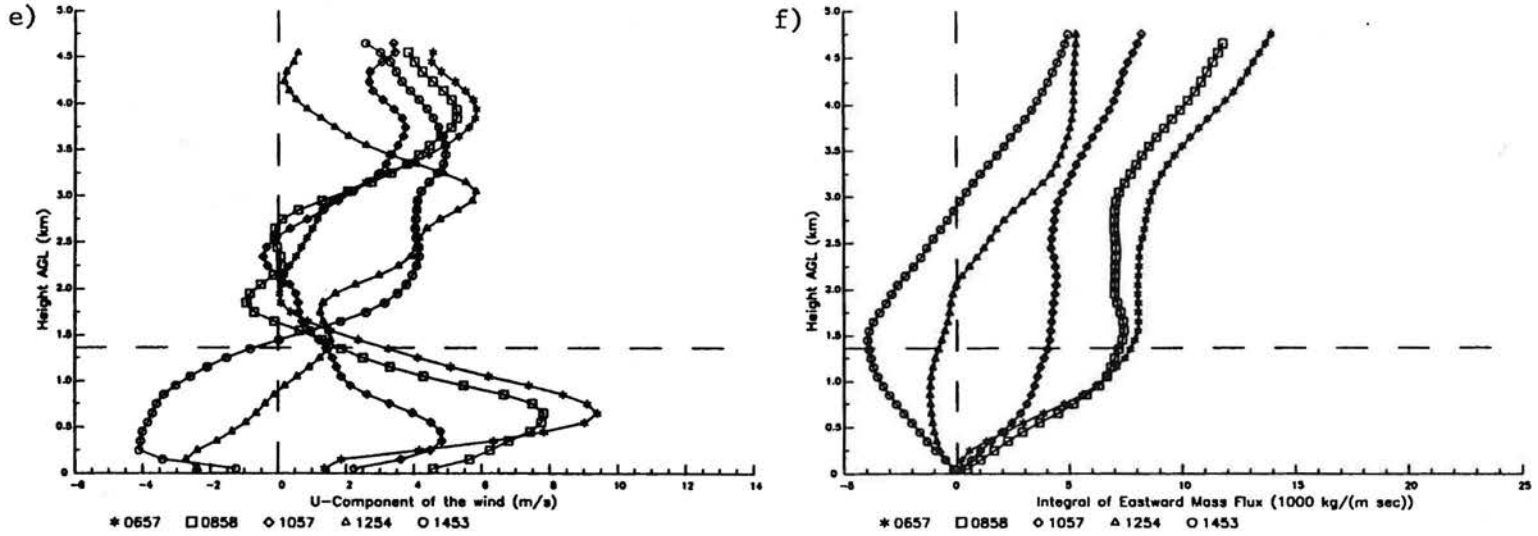

Figure 5.4. U-component of the winds (e) and vertical integral of eastward mass flux (f) at the Rustic site on November 12, 1990. The dashed horizontal line is at the height of barrier top.

As the daytime circulation evolves the magnitude of the westerly component of the flow decreases near the surface and above the valley. By the afternoon there is easterly flow in and above the valley. The u-component of the flow increases sharply from 1.5 to 3.5km while at similar heights on the eastern plains the u-component of the flow decreases during this time. Similar to the Fort Collins site, the vertical integral of momentum shows a net decrease in the total westward mass flux throughout the day, while in the simulations this integral has very similar values by 5.0km AGL.

The thermal structure at sunrise has a strong inversion in the valley with weaker stability from the valley top to about 3.0km. The thermal profile and the vertical integral of heating show that until 1057 MST the CBL deepens with substantial cooling in its upper portion. This cooling is also seen in the simulations. The vertical integral of heating shows that the magnitude of the cooling in the upper portion of the CBL is roughly equal to the total amount of heating in the lower portion of the CBL above valley top, indicating little net heating above the valley top. Between 1057 and 1254 MST the depth of the CBL changes little, and the cooling in the upper portion of the CBL ceases. By 1453 MST cooling below 2.2km occurs.

Figure 5.5 shows similar diagrams for Carpenter, Wyoming. The winds have a positive u-component in the lower 3.0km of the atmosphere with the u-component weakening throughout the day. The thermal profile shows some warming throughout the day above the CBL to about 2.2km AGL. From 1100 to 1259 MST warming generally occurs above the CBL to nearly 5.0km. Similar to the two other sites, the eastward mass flux decreases throughout the day which does not agree with the simulations. The simulations indicate that a site this far east should not be greatly influenced by the thermally induced flow and that the net effect of the thermally induced flow is to increase wind speed above barrier top. This site, along with the other two sites, indicate that the synoptic-scale atmosphere above barrier

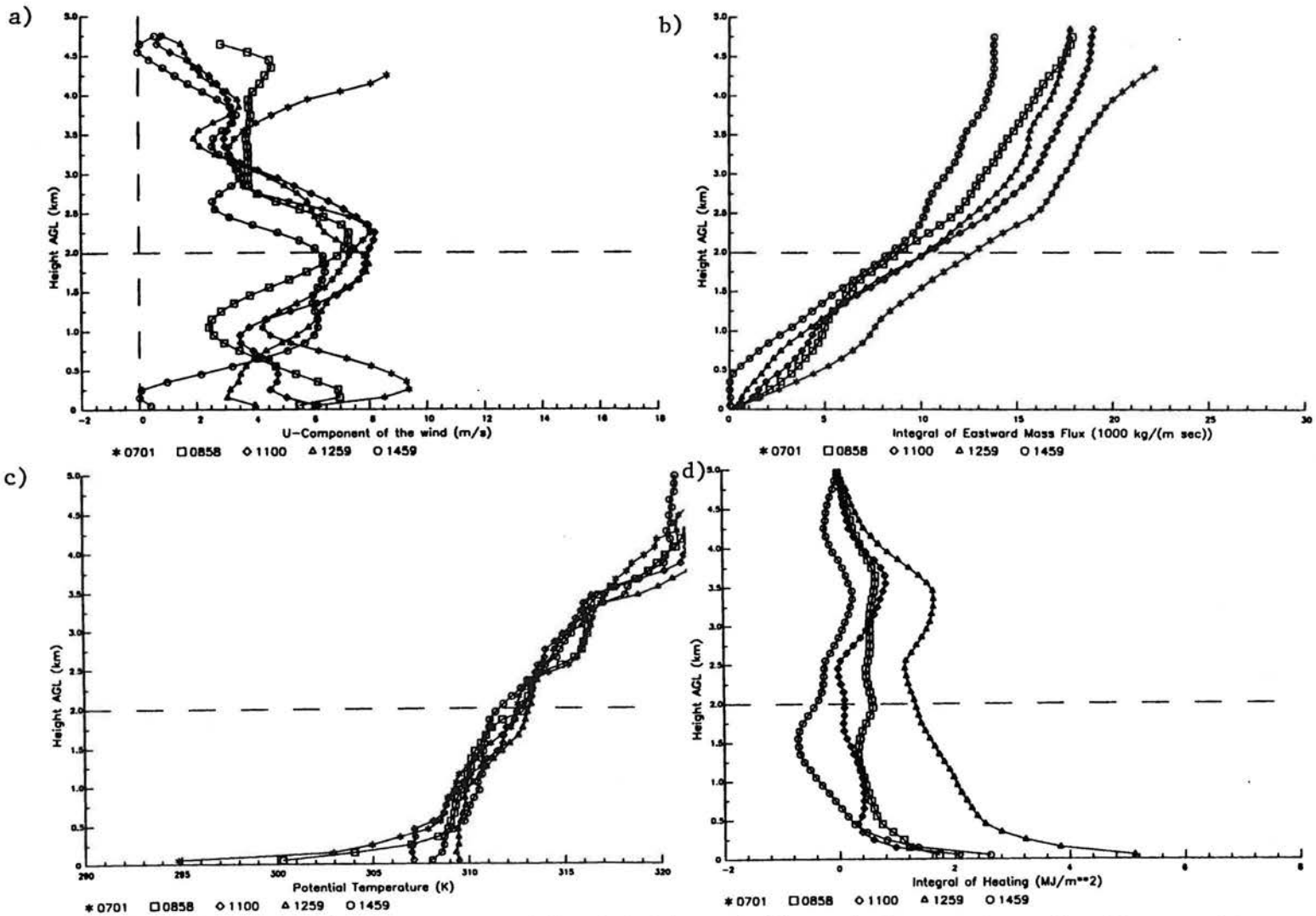

Figure 5.5. Vertical profiles of the u-component of the winds (a), vertical integral of eastward mass flux (b), potential temperature (c), and the vertical integral of heating from 0701 MST (d) on November 12, 1990 at the Carpenter, Wyoming site. The dashed horizontal line is at the height of the barrier top.

top is changing with the u-component of the winds weakening by about 4ms^{-1} and with general warming and subsidence occurring above barrier top especially in the afternoon.

5.3.2 October 25, 1990

On this day observations are taken at the same locations as November 12, 1990 using calibrated airsonde thermistors. Sunrise on this day is close to 0630MST, and observations are taken every two hours starting at 0630MST. This day is on the eastern side of a ridge and was forecast to have little change to the winds and pressure fields at the surface and aloft. Figure 5.6 shows the soundings and integrals for the Fort Collins site. At sunrise the jet is present at 1.0km AGL with the strongest u-component being 4ms^{-1}. A deep layer of significant stability is present to about 1.1km, with a layer of weaker stability up to 2.0km. By 0834MST the westerly jet has disappeared being replaced by weak easterly component flow. There is some warming from 2.0km to 2.5km associated with the lowering of the layer of strong stability. By 1035 MST upslope develops to 500m, and the warming from 2.0 to 2.5km increases and expands downward. Throughout the day this warming increases and expands downward dominating the thermal profile, and the u-component of the flow increases above 2.0km. The vertical integral of eastward mass flux shows a much greater eastward mass flux below 5.0km. This does not agree with the simulations and is opposite to the trend on November 12, 1990.

Figure 5.7 shows the same plots on this date for Rustic. At sunrise a strong jet is present with a maximum u-component of over 11ms^{-1} at 300m AGL, and the u-component decreases to about 1.0ms^{-1} at 1.0km. The thermal profile has strong stability in the valley with weaker stability up to 1.4km and a nearly neutral layer up to 2.0km. Throughout the day noticeable warming occurs above 1.75km. From 0828 to 1026 MST there is some cooling in the top of the CBL similar to November 12. For the rest of the day the strong warming

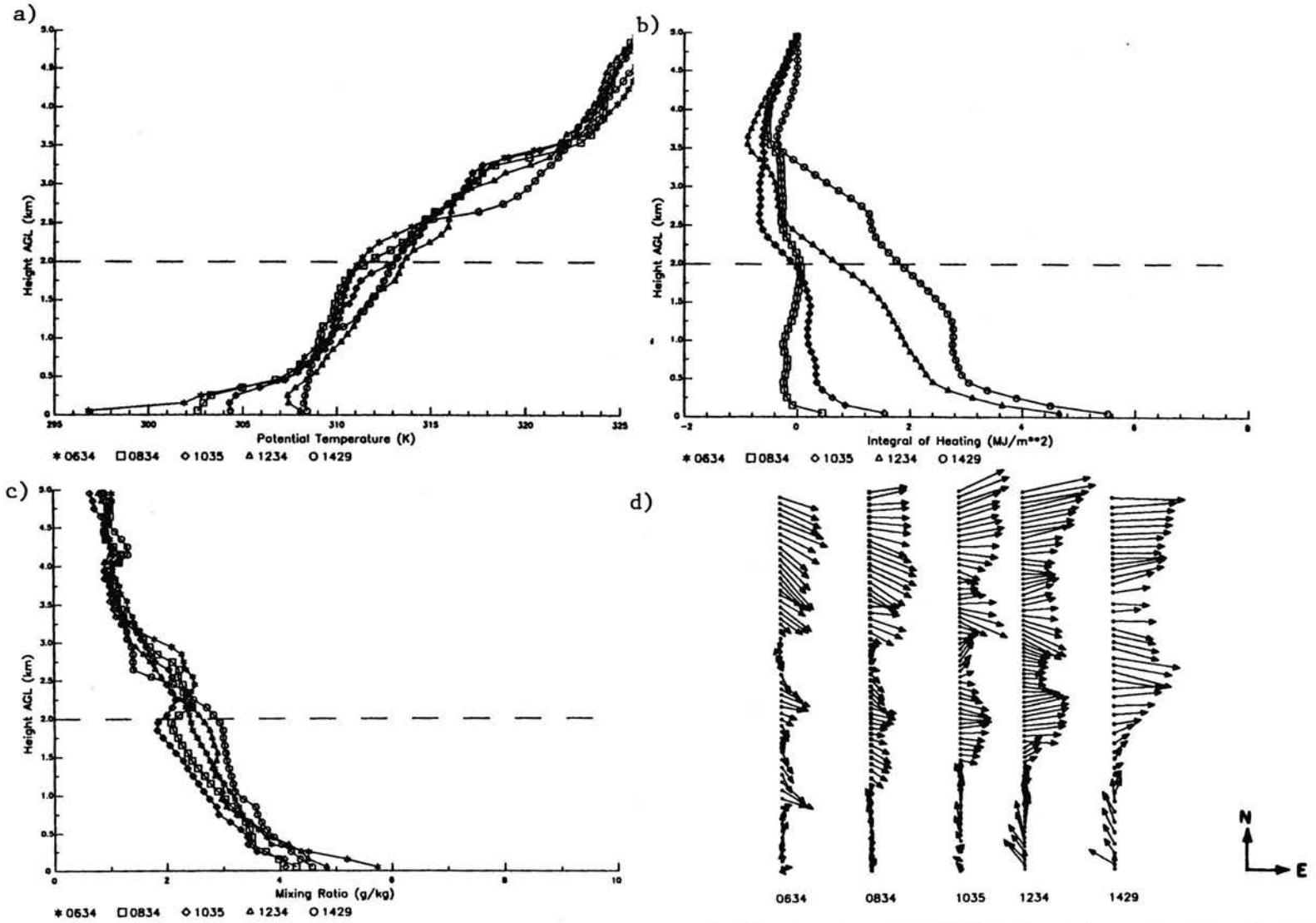

Figure 5.6. The vertical profile of potential temperature (a), vertical integral of heating from 0634 MST (b), mixing ratio (c), and winds (d) at the Fort Collins site on October 25, 1990. The dashed horizontal line is at the height of barrier top.

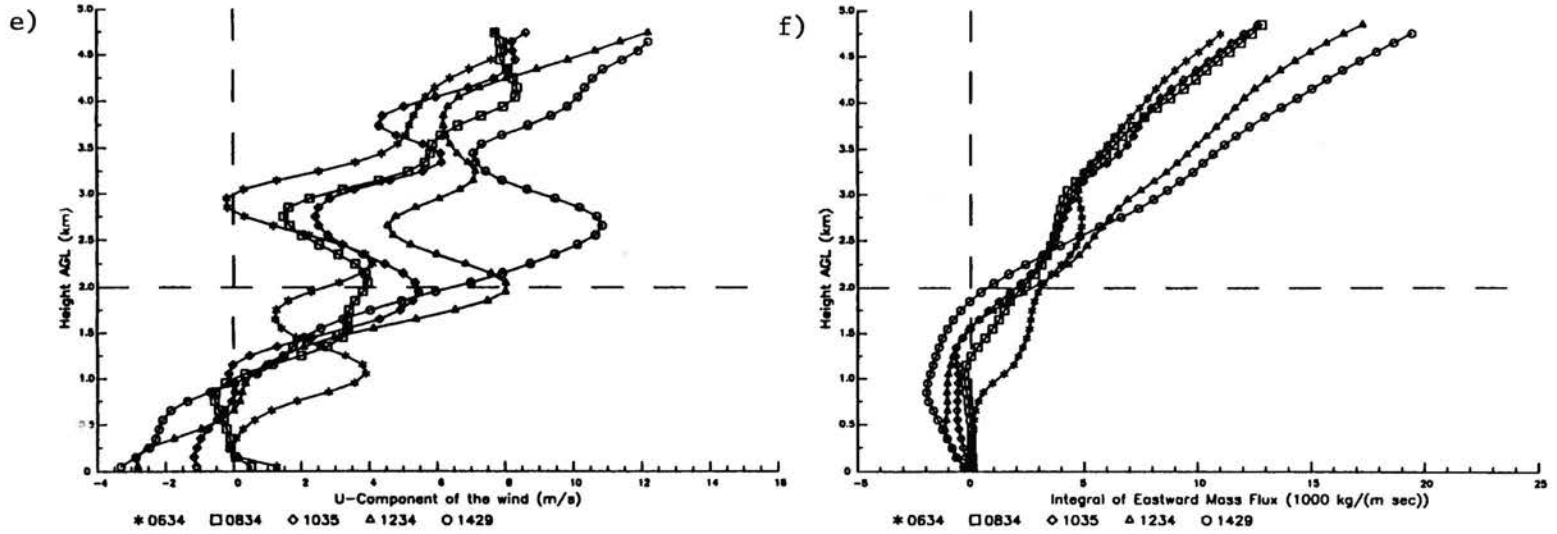

Figure 5.6. component of the winds (e) and vertical integral of eastward mass flux (f) at the Fort Collins site on October 25, 1990. The dashed horizontal line is at the height of barrier top.

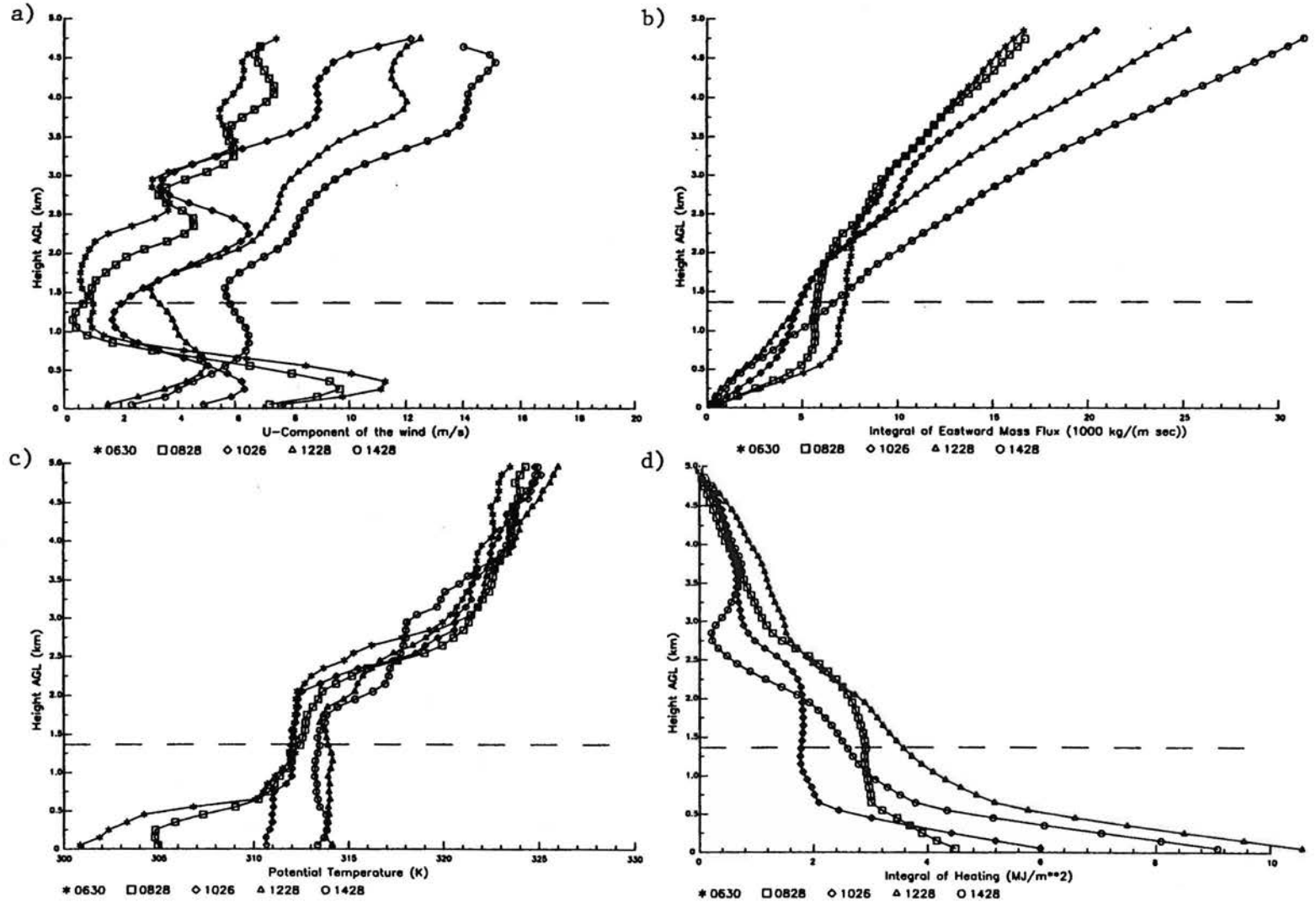

Figure 5.7. Vertical profiles of the u-component of the winds (a), vertical integral of eastward mass flux (b), potential temperature (c), and the vertical integral of heating from 0630 MST (d) on October 25, 1990 at the Rustic site. The dashed horizontal line is at the height of the barrier top.

above the CBL suppresses it growth. Throughout the day the u-component of the flow becomes more vertically uniform below 2.0km. Above 2.0km the u-component increases, especially starting at 1026 MST. The vertical integral of eastward mass flux shows substantially increasing total eastward mass flux below 5.0km throughout the day.

Figure 5.8 shows the same plots for Carpenter, Wyoming. These profiles show increasing u-component winds above about 2.0km throughout the day with a strong layer of sinking motion. This day also appears to be synoptically disturbed despite being on the east side of a deep ridge. The changes in the wind patterns above 2.0km are opposite to November 12, 1990.

5.4 Fall 1987 and Summer 1988 Regime

This regime is the first set of observations taken of the daytime evolution east of the Front Range of the Colorado Rockies. Observations are only taken at the Fort Collins site, and the thermistors on the airsondes are not calibrated using the two water baths. The observations are taken on October 29, 1987, November 3, 1987, November 10, 1987, and July 5, 1988. Like the Fall 1990, observations are taken on days that are forecast to have clear skies, to have light winds above barrier top, and to be synoptically undisturbed. A micrometeorological station is collocated with this observing site providing the net radiation, heat flux into the soil, latent heat flux into the atmosphere, and surface sensible heat flux into the atmosphere.

5.4.1 October 29, 1987

Figure 5.9 shows the soundings and the vertical integrals of eastward mass flux and heating for this day. Sunrise is at 0630MST. At one hour before sunrise a deep layer of stability exist to 2.0km with less stable air above 2.0km. Unfortunately, there are no winds

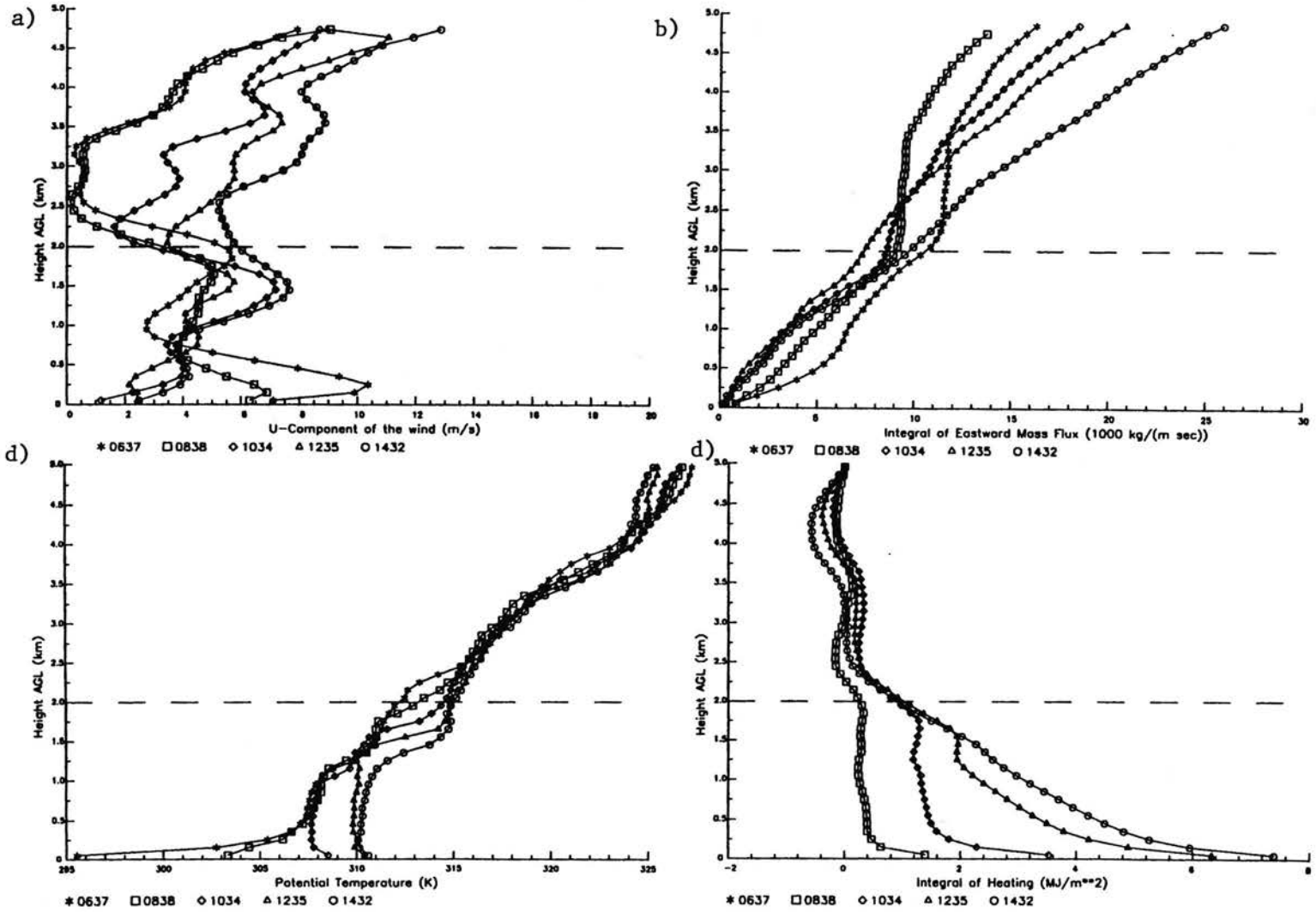

Figure 5.8. Vertical profiles of the u-component of the winds (a), vertical integral of eastward mass flux (b), potential temperature (c), and the vertical integral of heating from 0637 MST (d) on October 25, 1990 at the Carpenter, Wyoming site. The dashed horizontal line is at the height of the barrier top.

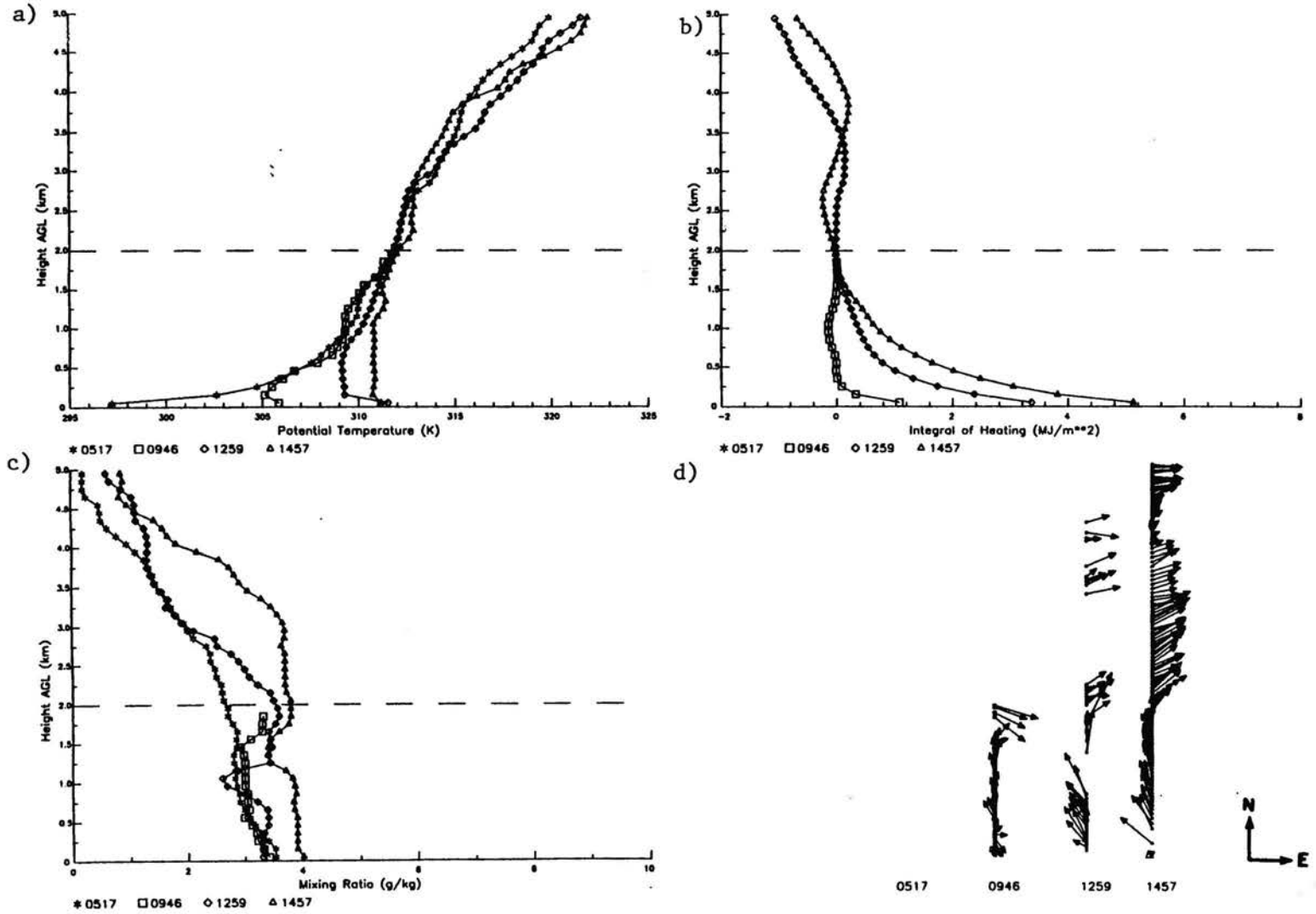

Figure 5.9. The vertical profile of potential temperature (a), vertical integral of heating from 0517 MST (b), mixing ratio (c), and winds (d) at the Fort Collins site on October 29, 1987. The dashed horizontal line is at the height of barrier top.

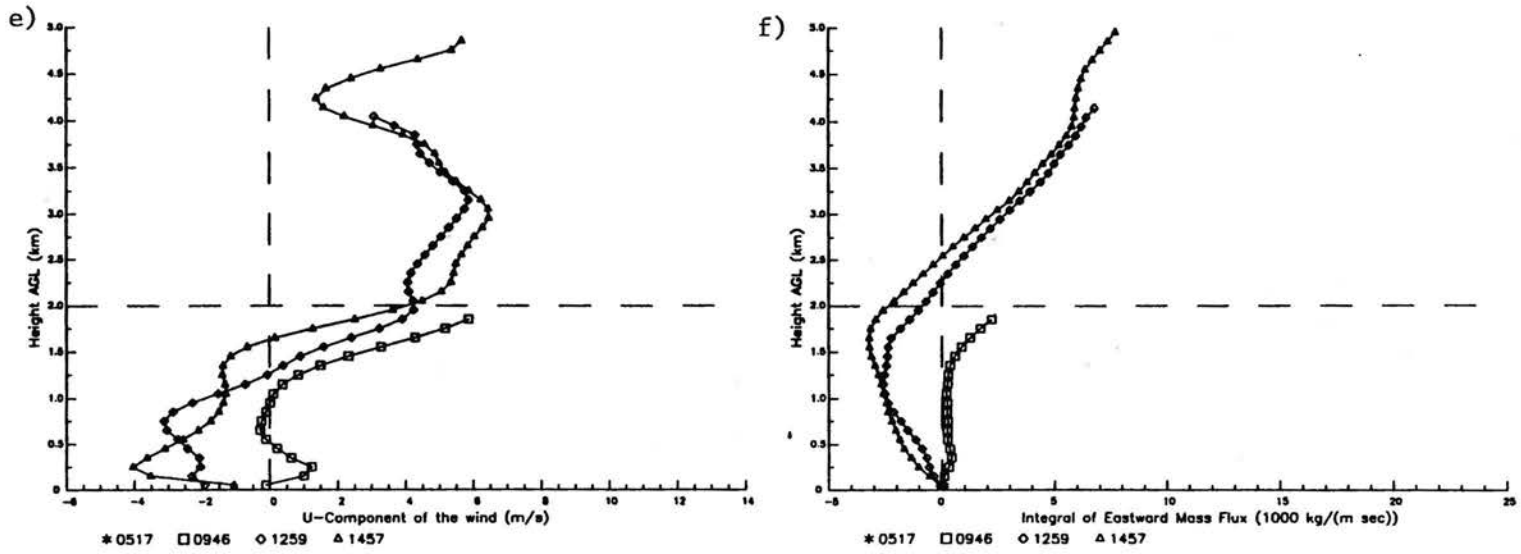

Figure 5.9. U-component of the winds (e) and vertical integral of eastward mass flux (f) at the Fort Collins site on October 29, 1987. The dashed horizontal line is at the height of barrier top.

for this sounding. Tethersondes are launched starting at sunrise and they reach about 800m. The tethersondes do not show any evidence of strong westerly winds for the first two hours after sunrise. The sounding at 0946MST stops at 2.0km. The winds below 1.5km generally have a weak westerly component with increasing westerly component above 1.5km. Some warming occurs below 1.0km during that time. As daytime evolution progresses a CBL develops with easterly flow in and above the CBL. Winds are missing from 2.3km to 3.2km because the Loran tracking signal is temporarily lost, and the u-component plots and integral of mass flux linearly interpolate winds between these heights. The CBL and the depth of the upslope flow deepen between 1259 and 1503 MST. At 1503 MST the easterly component flow near the surface rapidly changes to westerly component flow between 1500m and 2200m.

During the afternoon a moisture inversion appears. The moisture decreases in the easterly flow above the CBL with the moisture increasing in the westerly return flow. At 1503 MST the CBL has a nearly constant mixing ratio with less moisture for a 500m deep layer above the CBL and a nearly constant mixing ratio from 1.8 to 3.0km. The thermal profile also shows a neutral layer from 2.2 to 2.8km. This neutral layer is associated with the increased moisture and the westerly return flow off of the barrier to the west. In the baseline simulation a deep near neutral layer is evident above barrier top in the afternoon.

On this date a micrometeorological station is collocated with this observing site, and the surface sensible heat flux is calculated using the Bowen ratio. The energy budget for the surface at a given location is

$$R_n = H + LE + G \tag{5.1}$$

where R_n is the net radiation into the soil, H is the heat flux into the atmosphere, LE is the energy needed to evaporate moisture from the surface into the atmosphere, and G is the energy flux into the soil. The Bowen ratio is the ratio of the sensible heat flux to the latent heat flux. Rewriting the surface energy budget gives:

$$R_n - G = H + LE. \tag{5.2}$$

The Bowen ratio divides the net radiation minus the flux into the soil between sensible heat flux and latent heat flux. The surface sensible heat flux is given by:

$$H = (R_n - G)\left(\frac{B}{1+B}\right) \tag{5.3}$$

where

$$B = \frac{H}{LE}. \tag{5.4}$$

The Bowen ratio (B), assuming down gradient fluxes, only requires the measurement of a gradient in temperature and moisture between two levels in the surface layer. Thermal and humidity data measurements are taken at heights of 1m and 3m AGL. Soil measurements are taken at 1, 5, 10, and 20cm, and the soil type is clay loam. The net radiation is calculated by upward and downward pointing longwave and shortwave sensors. Soil moisture is not measured, and the thermal conductivity of the soil varies greatly with the soil moisture. A dry soil is assumed which is typical of non-irrigated surfaces in eastern Colorado. Using a dry soil generally maximizes the surface sensible heat flux, because a dry soil generally is the least conductive to heat minimizing the heat flux into the soil. In this first regime of observations the thermal sensors on the airsondes are not calibrated and systematic errors can appear.

Despite some impreciseness in the observing technique, the comparison of the total integral of energy to the local surface sensible heat flux provides insight into the daytime evolution. Table 5.1 list the amount of heating seen by the airsondes from the surface to 2.0km, net radiation minus the flux into the soil, and the surface sensible heat flux for the observing days. Much more warming appears in the lowest 2.0km than the surface sensible heat flux, and the warming in the lowest 2.0km is also greater than the net radiation minus the heat flux into soil which gives the sensible heat flux if the latent heat flux is zero. Throughout the day the amount of warming remains greater than the locally calculated

Table 5.1

The observed amount of heating between soundings from the surface to 2.0km AGL at the Fort Collins site on October 29, 1987 compared to the locally measured surface sensible heat flux, net radiation, and net radiation minus the flux into the soil. The values are normalized to 1 hour periods.

Values normalized to 1 hour period (MJm^{-2})

Time period (MST)	Observed heating 0 to 2.0km AGL	Sensible heat flux	Net Radiation	Net Radiation minus soil flux
0517-0946	0.25 ($69Wm^{-2}$)	0.05 ($14Wm^{-2}$)	0.15 ($42Wm^{-2}$)	0.10 ($28Wm^{-2}$)
0946-1259	0.85 ($236Wm^{-2}$)	0.48 ($133Wm^{-2}$)	0.92 ($256Wm^{-2}$)	0.80 ($222Wm^{-2}$)
1259-1457	0.73 ($203Wm^{-2}$)	0.29 ($81Wm^{-2}$)	0.51 ($142Wm^{-2}$)	0.48 ($133Wm^{-2}$)

surface sensible heat flux and the net radiation minus the heat flux into the soil.

5.4.2 November 3, 1987

Figure 5.10 shows the soundings and vertical integrals for November 3, 1987. A wave cloud shades the eastern plains in the vicinity of Fort Collins until about 1200 MST while throughout this period the mountains to the west are receiving unobstructed sunshine. At about one and one-half hours before sunrise (0515 MST) a deep layer of modest stability extends from the surface to about 1.8km. Westerly winds are present from 0.5 to 1.2km with the maximum speed being about 3.1ms^{-1} at 1.0km AGL. A layer of easterly component winds are observed below 2.0km, and the u-component rapidly increases above 2.0km. At 0946 MST substantial warming occurs below 2.0km associated with the near surface jet and the flow above it. The surface sensible heat flux is very weak at this time due to the shading produced by the lee wave cloud. As the day evolves shallow upslope flow develops near the surface with increasing westerly flow above the upslope flow. By 1502 MST the CBL is only 400m deep with weak upslope flow rapidly changing to westerly flow above 500m. Similar to October 29, 1987, throughout the day the amount of heating from the surface to 2.0km is larger than the surface sensible heat flux. For the first three hours after sunrise strong heating occurs from the surface to 2.0km despite a very small surface sensible heat flux.

5.4.3 November 10, 1987

Figure 5.11 shows the same diagrams for November 10, 1987. The most apparent feature on this day is the strong cooling above barrier top associated with a disturbance moving into the region from the west. By 0946 MST noticeable warming is observed from 300m to 1200m associated with weak winds which have a maximum u-component of 1.5ms^{-1} at 950m. On this day frequent tethersonde launches identify westerly winds above 600m, and

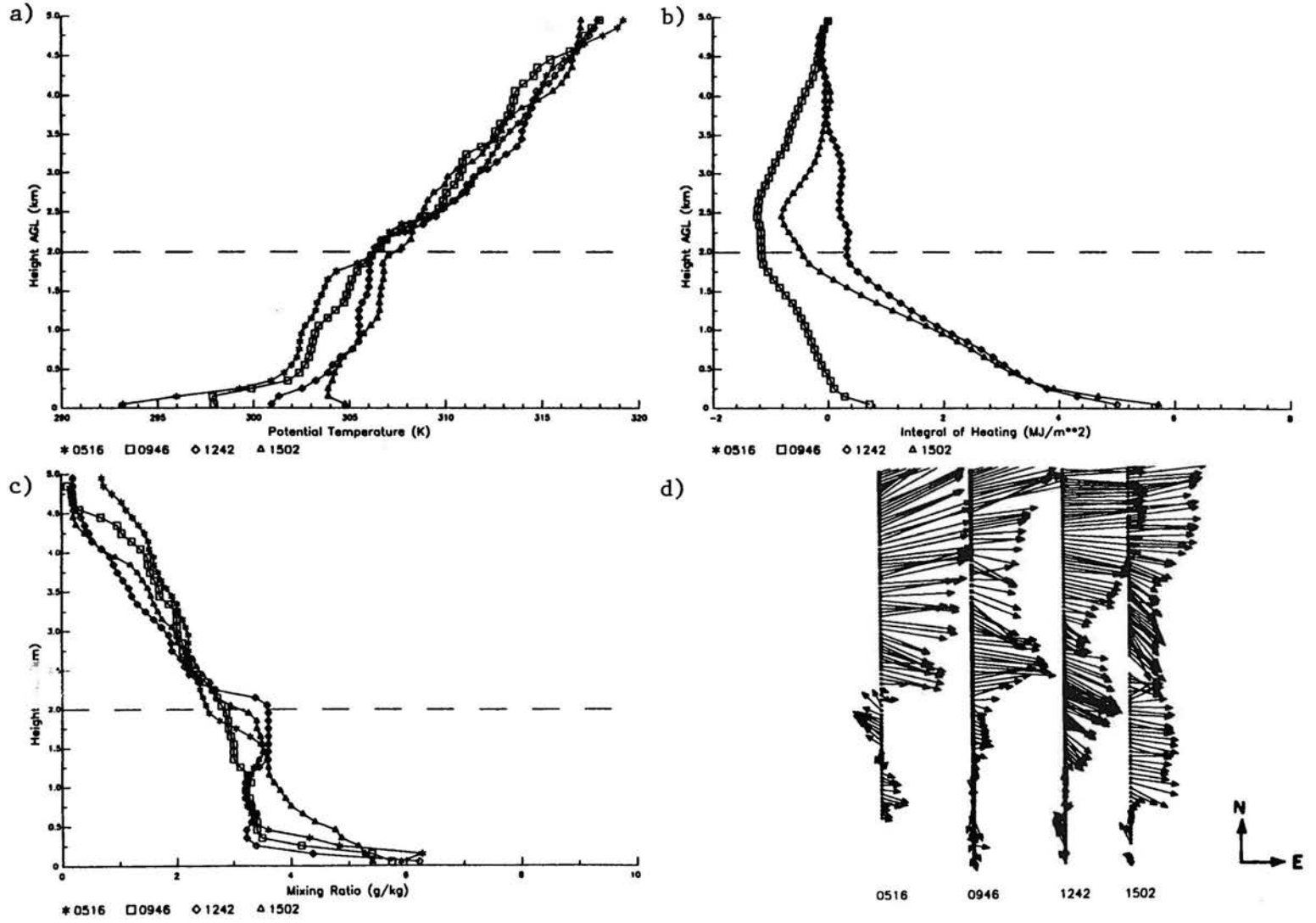

Figure 5.10. The vertical profile of potential temperature (a), vertical integral of heating from 0516 MST (b), mixing ratio (c), and winds (d) at the Fort Collins site on November 3, 1987. The dashed horizontal line is at the height of barrier top.

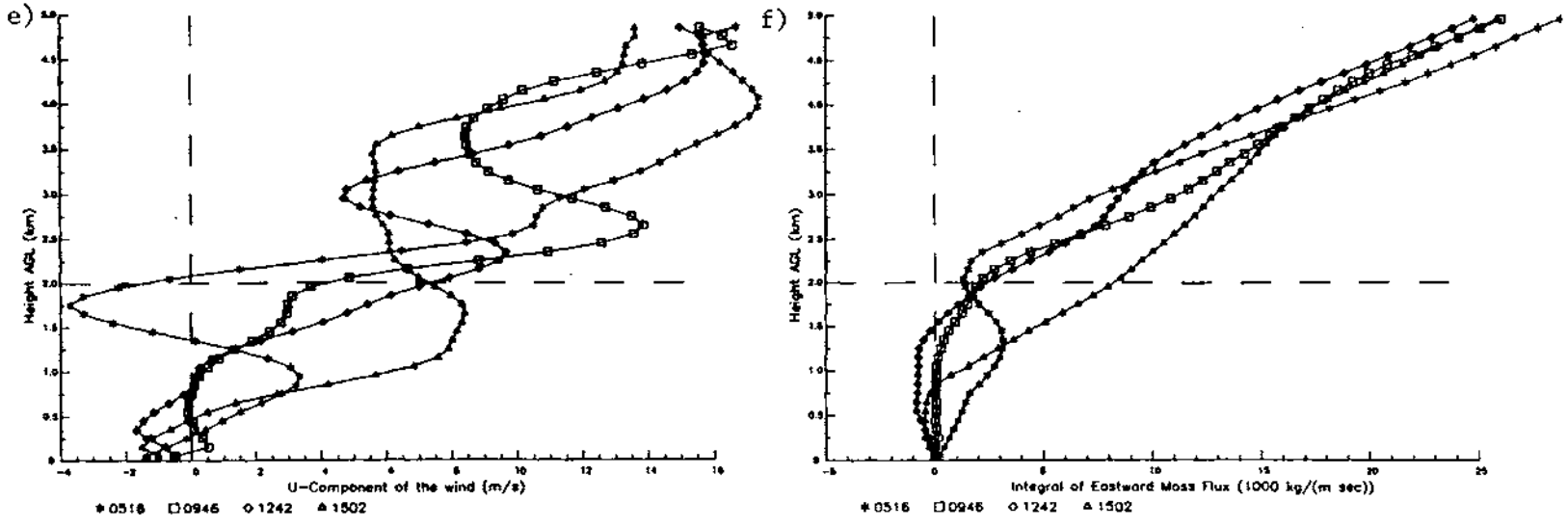

Figure 5.10. U-component of the winds (e) and vertical integral of eastward mass flux (f) at the Fort Collins site on November 3, 1987. The dashed horizontal line is at the height of barrier top.

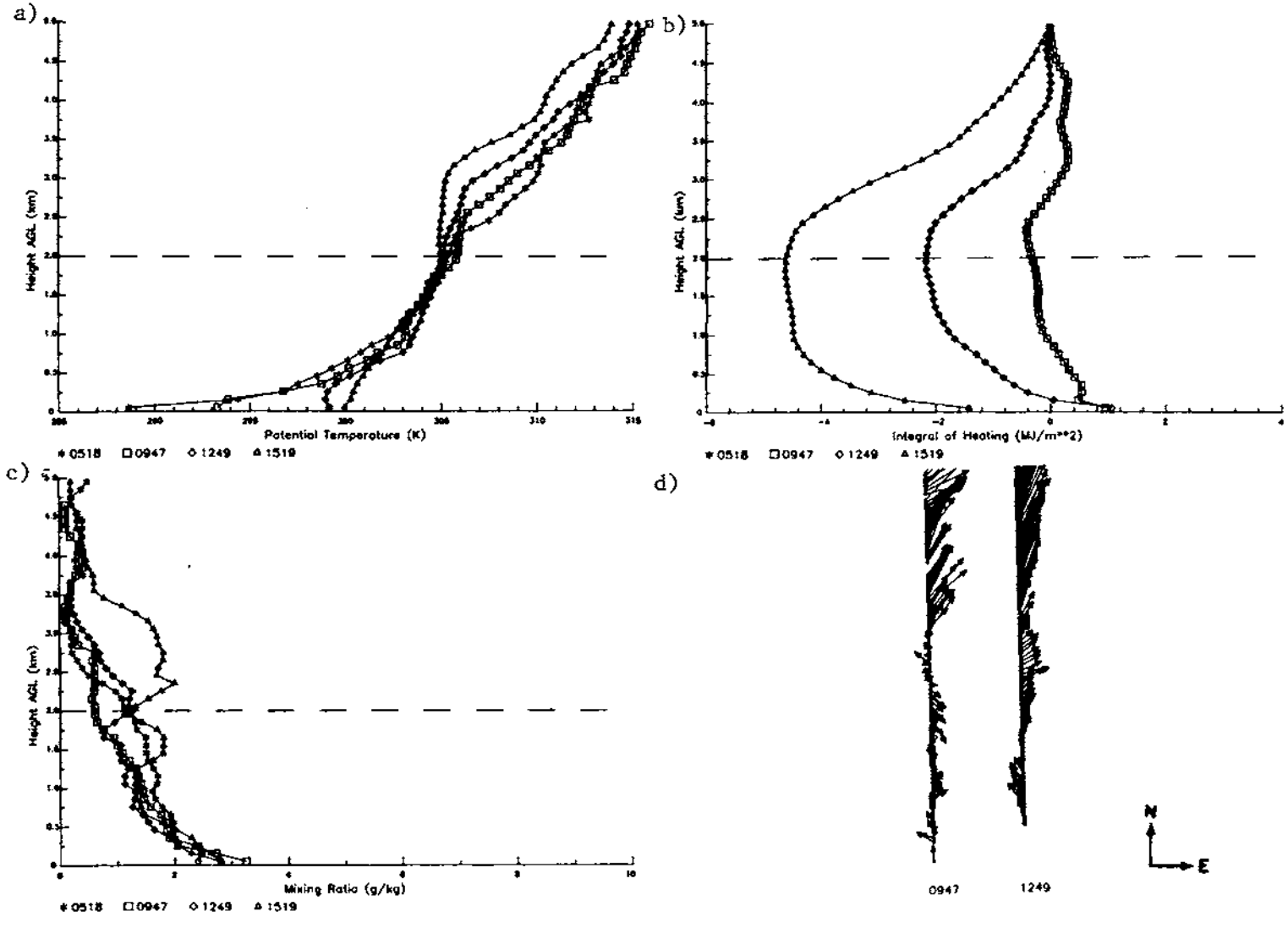

Figure 5.11. The vertical profile of potential temperature (a), vertical integral of heating from 0518 MST (b), mixing ratio (c), and winds (d) at the Fort Collins site on November 10, 1987. The dashed horizontal line is at the height of barrier top.

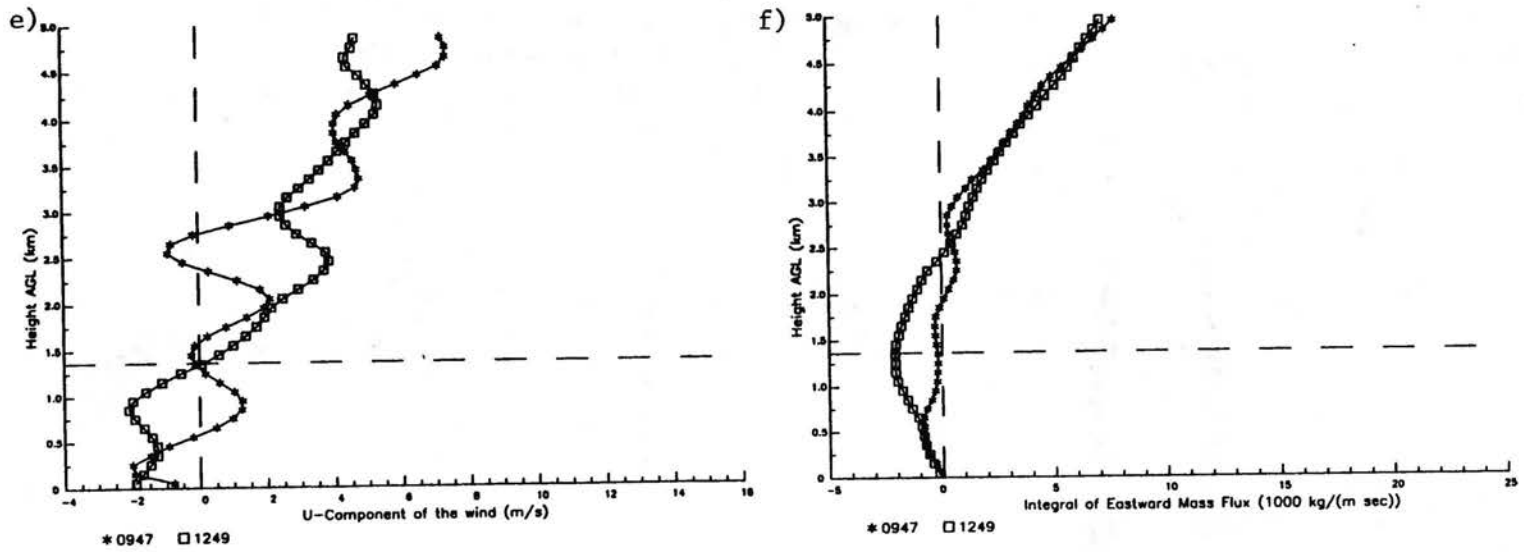

Figure 5.11. U-component of the winds (e) and vertical integral of eastward mass flux (f) at the Fort Collins site on November 10, 1987. The dashed horizontal line is at the height of barrier top.

warming occurs with these westerly winds and below these winds. The warming with the westerly winds agrees with the simulations which have warming associated with the weakening jet early in the day. The deep airsondes show the continued warming above the CBL throughout the day with the suppression of the CBL depth, and the winds suggest that a westerly return flow develops between 0947 and 1259 MST. The micrometeorological data has a small surface sensible heat flux at three hours after sunrise. Throughout the day the surface sensible heat flux is less than the observed heating to 2.0km.

5.4.4 July 5, 1988

Figure 5.12 shows the sounding and integrals for July 5, 1988. At sunrise (0430 MST) a deep layer of stability is present up to 2.0km with a near neutral layer up to 3.0km. The winds generally show an easterly component in the lowest 1.8km. This region of easterly flow descends to 1.0km by 0936 MST when it appears to become incorporated into the easterly upslope flow. The speed of the westerly return flow above increases by 0936 MST. The thermal profile shows that warming occurs throughout the morning with the easterly winds. By 0936 MST a moisture inversion is present with drying in the easterly upslope flow and moistening in the westerly return flow, and the moisture inversion is seen to some extent on the last three dates discussed. The micrometeorological data shows that the surface sensible heat flux is less than the observed heating to 2.0km throughout this period.

5.5 Comparison of Observations and Simulations

The previous section has discussed the observed evolution on six days. These observation days are chosen because they are forecast to have little change to the synoptic wind and thermal fields, have light winds above barrier top, and have clear skies. Some of the days are fairly disturbed. November 3, 1987 has a lee wave cloud shading the eastern

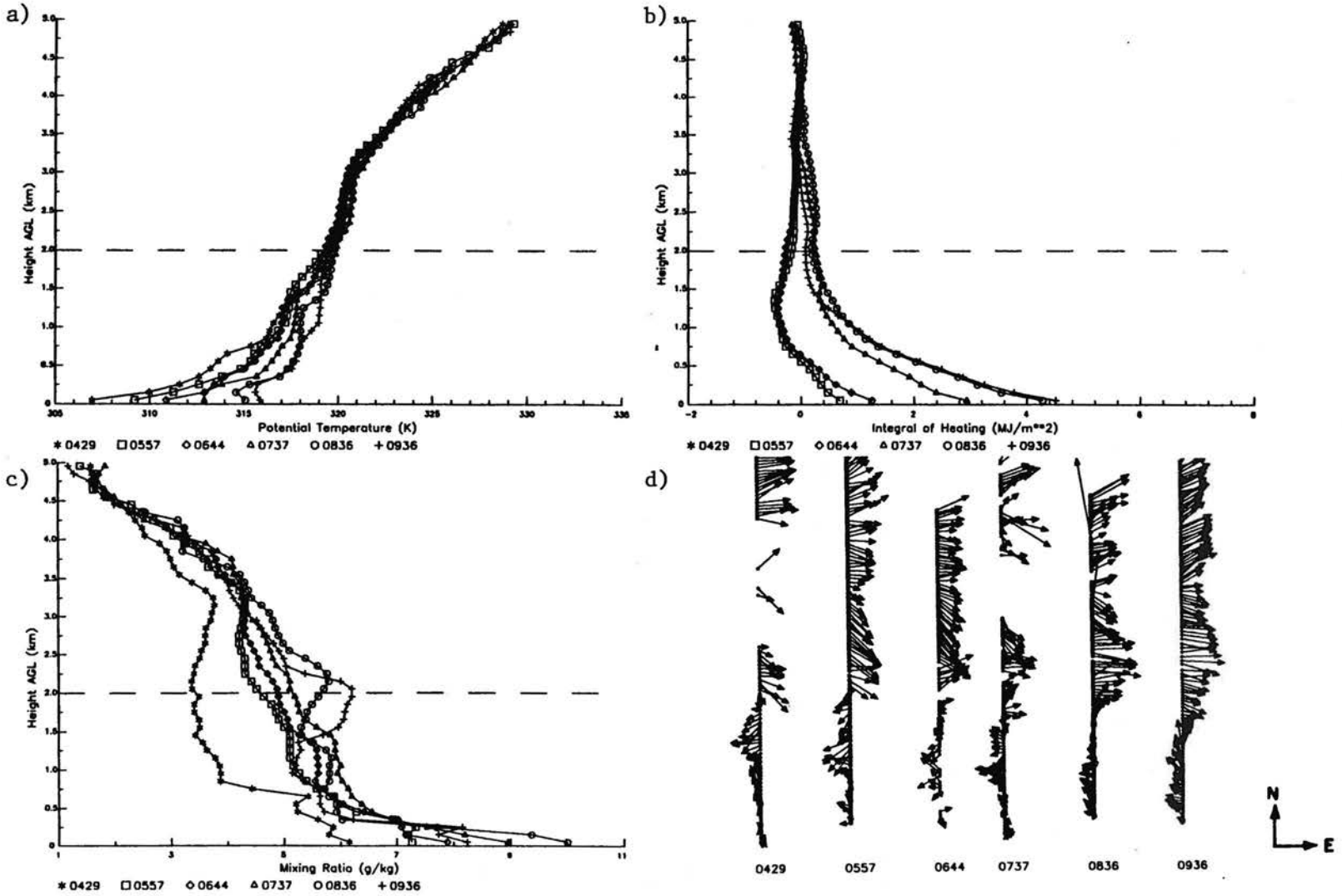

Figure 5.12. The vertical profile of potential temperature (a), vertical integral of heating from 0429 MST (b), mixing ratio (c), and winds (d) at the Fort Collins site on July 5, 1988. The dashed horizontal line is at the height of barrier top.

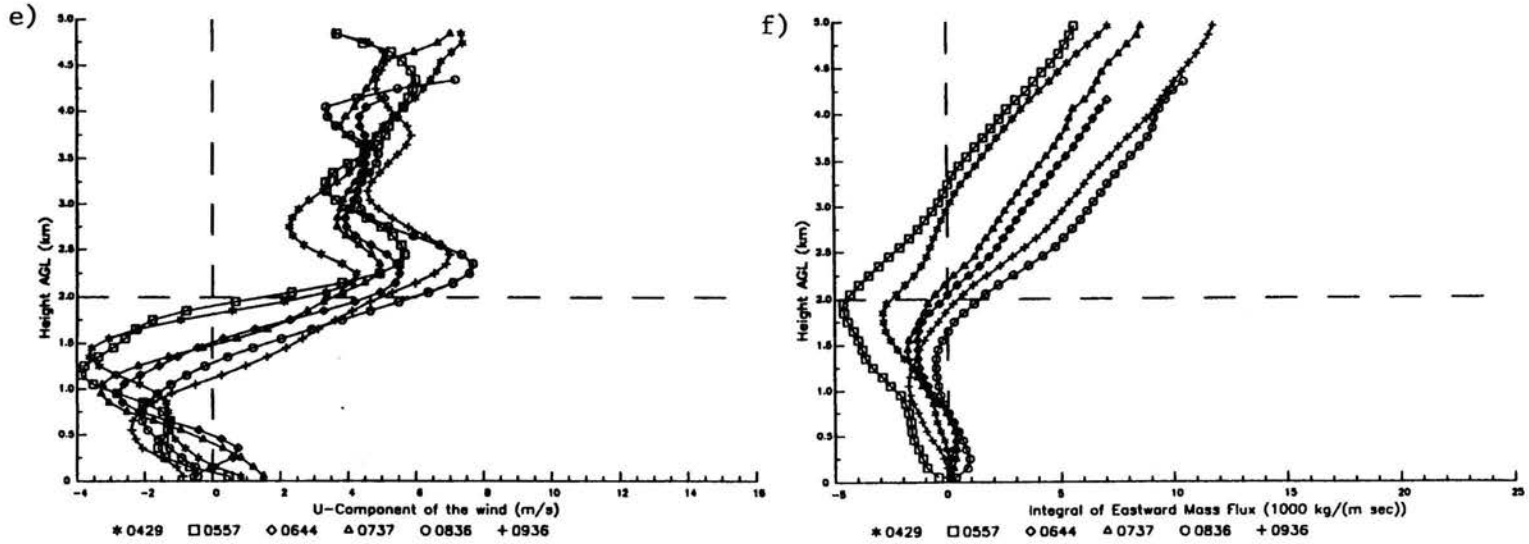

Figure 5.12. U-component of the winds (e) and vertical integral of eastward mass flux (f) at the Fort Collins site on July 5, 1988. The dashed horizontal line is at the height of barrier top.

plains until noon, and November 10, 1987 has a disturbance moving into the region from the west. The other days have smaller changes to the thermal and wind fields above barrier top. The simulations and observations are qualitatively and quantitatively compared in this section. This comparison shows what features in the simulations are evident in the observations, relates the intensity of the simulated circulations to the observed circulation, and discusses where the observations are inconclusive about the presence of simulated features.

5.5.1 Base of the Barrier

The observations at the base of the barrier are taken at Christman Field which is near the Colorado State University Department of Atmospheric Science. The comparison between the observations and simulations at this site are discussed for the sunrise state and each of the three phases of the daytime evolution.

5.5.1.1 Sunrise state

Table 5.2 shows some characteristics of the simulated and observed wind fields at sunrise or one hour before sunrise at the base of the barrier. Four out of six days have a strong jet with October 29, 1987 having missing data. On November 10, 1987 the wind data is missing, but a strong u-component at heights similar to the other days is seen in the tethersonde flights. The observed u-components appear to be about 1-1.5ms^{-1} slower than the simulations, and the elevation of the jet maximums are higher. The first range of foothills is about 600m higher than the Fort Collins site at 5km to the west of the site, and the wind maximum occurs above the top of this first range of foothills. In the model the topography is smoothed to eliminate all terrain features with a wavelength less than 10km. The simulations do not have these separate ranges of foothills, and the model terrain only rises 50m in the first 5km west of the base of the barrier site.

Table 5.2

Speed and height of the maximum u-component in the near surface jet and the height and speed of the minimum u-component at sunrise for the base of the barrier site in all the simulations and for the observations at sunrise or up to 1.5 hours before sunrise at the Fort Collins site.

	Maximum U-component		Minimum U-Component	
Simulation	Speed (ms^{-1})	Height (m)	Speed (ms^{-1})	Height (km)
Baseline	5.5	250	0.8	1.0
June 21	5.6	250	1.1	1.1
Nov. 1	5.7	375	0.8	1.1
Dec. 21	4.8	375	0.8	1.3
WMWP	6.5	250	0.5	1.0
DMWP	6.4	250	0.6	1.0
WMDP	6.2	250	0.5	1.1
Stronger winds	5.0	250	0.7	1.3
No winds	3.0	500	-1.1	1.3
Low CBL	4.8	500	0.8	1.3
Less Stability	5.4	500	1.2	1.1
Half Barrier Height	4.6	150	1.7	0.7
Observations				
Nov. 12, 1990	6.7	1000	3.0	2.0
Oct. 25, 1990	3.9	1000	1.2	1.6
Oct. 29, 1987	Missing	Missing	Missing	Missing
Nov. 3, 1987	3.3	900	-3.7	1.7
Nov. 10, 1987	Missing	Missing	Missing	Missing
July 5, 1988	0.8	0	-3.6	1.4

The difference between actual terrain and model terrain likely produces the difference in height of the jet maximum between the simulations and observations. In the simulations the jet follows the terrain on the east slope of the barrier, and the jet is near the surface at the base of the barrier. In the observations the jet is higher at the base of the barrier site because it flows over the foothills to the west. Tyson and Preston-White (1972) observe nocturnal flows down a 3.0km high escarpment in South Africa. The nocturnal flow down the escarpment towards the ocean to the east passes above the tops of the foothills. Below the crests of the foothills are local flows which appear to be isolated from the larger scale flow down the escarpment. A similar flow pattern likely occurs on the east slope of the Front Range of the Colorado Rockies. The nocturnal jet likely flows above the top of the foothills and is isolated from the local nocturnal flows between the foothills. At the base of the barrier the jet is immediately above the top of the first ridge of foothills to the west of the site, which is 600m at Fort Collins. Table 5.2 also shows that on some of the observation days easterly flow is observed near barrier top, while the simulation only have weak westerly flow in that region.

The observations and simulations have similar depths of the stable core at the base of the barrier. In the observations the depth of the stable core is 1.3 to 2.0km high at the Fort Collins site. The simulations have a 2.0km deep stable core at the base of the barrier site except for a 1.5km deep stable core in the stronger wind run. The modeled wind field and depth of the stable core at sunrise agree well with the observations indicating that the simulations reproduce the major features of the sunrise state.

5.5.1.2 Phase 1

November 12, 1990, November 3, 1987, and November 10, 1987 have warming associated with the weakening jet at 600 to 1000m AGL at the base of the barrier. Similarly, all the simulations, except the no winds and wet mountain - dry plains simulations, have warming with the weakening nocturnal jet. During Fall 1987 the micrometeorological station has negative or weak positive surface sensible heat flux for the first 3 hours after sunrise while significant warming is observed in the lower layers of the soundings. The observed warming is much larger than the local surface sensible heat flux. On October 29, 1987 warming is observed in the lower layers of the soundings, but the observations are inconclusive to the presence or absence of a jet. On October 25, 1990 the jet disappears by two hours after sunrise at the base of the barrier. On July 5, 1988 the jet is absent with mainly easterly winds occurring below 2.0km. Strong warming is still observed early in the day despite a near zero surface sensible heat flux, and no explanation for the warming without the presence of the weakening jet is offered. The presence of warming with the weakening jet on many of the observational days supports the explanation for phase 1 warming described previously. The observations also show that there can be some variability to the evolution during this phase.

5.5.1.3 Phase 2

In the simulations the main features of this phase of the evolution are the easterly upslope flow, westerly return flow, suppressed CBL, and strong warming above the CBL. These features are seen on many of the observation days verifying the existence of the solenoid. Along with the qualitative comparison of the simulations and observations, the thermal and wind fields in this phase are quantitatively compared to further relate the simulations to the observations.

Table 5.3 shows the observed westward mass flux in the upslope flow compared to values obtained from the November 1 heating, baseline, and the dry mountain - wet plains (DMWP) simulations. The upslope flow exists during the day and its magnitude generally increases significantly with time. In the simulations the upslope flow at the base of the barrier generally begins between three and four hours after sunrise. During the Fall 1990 the upslope flow develops between 2 and 4 hours after sunrise. On October 29, 1987 the winds generally still have westerly component winds at about 3.25 hours after sunrise (0946 MST), and the tethersonde data for this day shows fairly weak upslope flow at four hours after sunrise with significant upslope flow by five hours after sunrise. Similarly, November 3, 1987 has significant upslope flow, which is observed by the tethersonde, develop by five hours after sunrise with the speeds being weaker than on October 29, 1987. On November 10, 1987 at about 3 hours after sunrise (0947 MST) easterly upslope flow exists beneath a very weak westerly component flow above 650m. July 5, 1988 has easterly flow throughout the morning and no explanation is offered for this easterly flow. This comparison shows that the observed and simulated times of the beginning of the upslope flow agree well.

The quantitative comparison of the mass flux in the upslope flow shows good agreement on October 29, 1987 between the observations and November 1 heating simulation (which is discussed in section 4.2). On November 10, 1987 the values at 1249 MST agree well with the November 1 heating simulation. For the Fall 1990 the November 1 simulation under predicts the mass flux in the upslope flow at 4 hours after sunrise and overpredict it at 6 and 8 hours after sunrise. The observed mass flux for the Fall 1990 days is about twice as strong as the November 1 heating simulation at 4 hours after sunrise. For 6 and 8 hours after sunrise the observations on November 12, 1990 is about one-quarter to one-third as strong as the November 1 heating simulation, and on October 25, 1990 the observed mass flux at these times is about one-half of the November 1 heating simulation. On November 3, 1987

Table 5.3

The observed mass flux in the upslope flow at the Fort Collins site compared to the simulated mass flux the upslope flow at the base of the barrier site for the baseline, November 1 heating, and DMWP simulations. The model data is for the same time after sunrise as the observations. The number in parenthesis next to the observation time is the approximate number of hours after sunrise.

Observation Date and Time (MST)	Westward Mass Flux ($1000*kgm^{-1}s^{-1}$) Observed	Nov. 1 Run	Baseline Run	DMWP Run
Nov. 12, 1990				
0904 (2)	0.0	0.0	0.0	0.0
1110 (4)	0.8	0.4	1.7	1.3
1305 (6)	0.6	2.4	4.9	4.0
1503 (8)	1.1	3.1	4.4	4.8
Oct. 25, 1990				
0834 (2)	0.0	0.0	0.0	0.0
1035 (4)	0.7	0.4	1.7	1.3
1234 (6)	1.1	2.4	4.9	4.0
1429 (8)	1.9	3.1	4.4	4.8
Oct. 29, 1987				
0946 (3.25)	0.0	0.0	0.2	0.1
1259 (6.5)	2.6	2.6	6.1	4.4
1457 (8.5)	3.2	2.9	4.1	4.7
Nov. 3, 1987				
0946 (3.25)	0.0	0.0	0.2	0.1
1242 (6.25)	0.8	2.4	4.9	4.0
1502 (8.5)	0.5	2.9	4.1	4.7
Nov. 10, 1987				
0947 (3)	0.9	0.0	0.2	0.1
1249 (6)	2.1	2.4	4.9	4.0
1519 (8.25)	Missing	2.9	4.1	4.7
July 5, 1988				
0557 (1.5)	4.6	0.0	0.0	0.0
0644 (2.25)	1.4	0.0	0.0	0.0
0737 (3)	1.9	0.0	0.2	0.1
0836 (4)	0.6	0.4	1.7	1.3
0936 (5)	1.8	1.6	3.2	2.7

shading of the plains and stronger winds aloft may have led to the much lower mass flux in the upslope flow. For all observational days the baseline and DMWP simulations overpredict the mass flux.

Table 5.4 shows the observed depth of the upslope flow compared to the same three simulations as in Table 5.3. For the Fall 1990 observations the November 1 heating simulation under predicts the depth of the upslope flow at 4 hours. The depth of the upslope flow in the November 1 heating simulation is about twice as large as the observations at 6 hours after sunrise, and is about 25% larger than the observations at 8 hours after sunrise. For October 29, 1987 and November 10, 1987 the simulated depth for November 1 heating is about 70% as deep as the observations at 6 and 8 hours after sunrise. For these two days in the Fall 1987 the mass flux in the upslope flow in the November 1 heating simulation agrees well with the observations suggesting that for a given the mass flux in the upslope flow the simulation under predicts the depth of the upslope flow.

Another notable feature of the simulated wind field is the increase in the u-component of the flow above the barrier top. In the observations this return flow is not apparent, and all the vertical integrals of the eastward mass flux for each day do not meet at a particular height as seen in the simulations (as in Figure 3.10). On October 25, 1990 and November 3, 1987 significant increases in the eastward mass flux well above barrier top occurs while on November 12, 1990 the eastward mass flux decreases. On some days (October 29, 1987 and November 10, 1987) missing wind data does not allow for the identification of changes in wind fields above barrier top. These differences in the evolution of the integral of eastward mass flux suggest that other factors may influence the daytime evolution. The November 1 heating simulation has the maximum speed of the u-component of the return flow increase by about $2ms^{-1}$ during the day. This change in speed is fairly small and can be masked by synoptic-scale changes or other aspects of the evolution not identified in the

Table 5.4

The observed depth of the upslope flow at the Fort Collins site compared to the simulated depth of the upslope flow at the base of the barrier site for the baseline, November 1 heating, and DMWP simulations. The model data is for the same time after sunrise as the observations. The number in parenthesis next to the observation time is the approximate number of hours after sunrise.

Observation Date and Time (MST)	Depth of upslope flow (m)			
	Observed	Nov. 1 Run	Baseline Run	DMWP Run
Nov. 12, 1990				
0904 (2)	0	0	0	0
1110 (4)	650	399	705	886
1305 (6)	450	886	1276	1276
1503 (8)	850	1080	1865	1472
Oct. 25, 1990				
0834 (2)	0	0	0	0
1035 (4)	1250	399	705	886
1234 (6)	450	886	1276	1276
1429 (8)	850	1080	1865	1472
Oct. 29, 1987				
0946 (3.25)	0	49	269	153
1259 (6.5)	1150	886	1276	1276
1457 (8.5)	1650	1080	1865	1472
Nov. 3, 1987				
0946 (3.25)	0	49	269	153
1242 (6.25)	550	886	1276	1276
1502 (8.5)	350	1080	1865	1472
Nov. 10, 1987				
0947 (3)	650	49	269	153
1249 (6)	1250	886	1276	1276
1519 (8.25)	Missing	1080	1865	1472
July 5, 1988				
0557 (1.5)	1950	0	0	0
0644 (2.25)	1450	0	0	0
0737 (3)	1450	49	269	153
0836 (4)	1250	399	705	886
0936 (5)	1050	705	886	886

simulations. These observations are inconclusive about the presence or absence of the increase in the return flow speed.

The main features of the thermal fields are the suppressed CBL depth and warming above the CBL. These two features are very apparent in the observations. Table 5.5 quantitatively compares the CBL depths from the observations and the three simulations listed in the other tables. The November 1 heating simulation has a CBL about 75% larger than in the Fall 1990 observations, except for 1503 MST on November 12, 1990 where the simulated CBL is over four times deeper. On October 29, 1987 the simulated CBL depths agree well with the observations, and the observed CBL at 1457 MST is only 25% deeper than the November 1 heating simulation. On November 10, 1987 the November 1 heating simulation overpredicts the CBL depth in the afternoon.

The simulations show that a near neutral layer appears above barrier top in the afternoon. On October 29, 1987 a near neutral layer appears at 8 hours after sunrise from 2.2 to 2.8km with warming in the lower portion of this layer, and the amount of cooling above this elevated neutral layer from one hour before sunrise is about $1.2MJm^{-2}$ ($37Wm^{-2}$). In the November 1 heating simulation the near neutral layer is from 2.2 to 2.8km and has $1.2MJm^{-2}$ ($37Wm^{-2}$) of cooling above it. This simulated near neutral layer is very similar to the October 29, 1987 observations. October 29, 1987 is the only day with any evidence of this near neutral layer. On the other observation days the atmosphere appears to be too disturbed to show this feature. While the one observation day suggests the presence of a near neutral layer above the height of the barrier top, the observations are inconclusive about its existence.

Some qualitative features in the simulated moisture profile in the simulations match the observations. On some of the observation days a moisture inversion is observed during phase 2. The moisture inversion has drying or less moistening in the easterly flow above the CBL and increased moisture in the westerly return flow. The dry mountain - wet plain

Table 5.5

The observed CBL depths at the Fort Collins site compared to the simulated CBL depths at the base of the barrier site for the baseline, November 1 heating, and DMWP simulations. The model data is for the same time after sunrise as the observations. The number in parenthesis next to the observation time is the approximate number of hours after sunrise.

Observation Date and time (MST)	CBL Depth (m) Observed	Nov. 1 Run	Baseline Run	DMWP Run
Nov. 12, 1990				
0904 (2)	0	0	0	0
1110 (4)	200	153	399	49
1305 (6)	300	544	886	399
1503 (8)	200	886	2454	705
Oct. 25, 1990				
0834 (2)	0	0	0	0
1035 (4)	200	153	399	49
1234 (6)	300	544	886	399
1429 (8)	500	866	2454	705
Oct. 29, 1987				
0946 (3.25)	200	49	49	49
1259 (6.5)	700	625	1070	472
1457 (8.5)	1100	886	2454	893
Nov. 3, 1987				
0946 (3.25)	200	49	49	49
1242 (6.25)	100	544	886	399
1502 (8.5)	300	886	2454	893
Nov. 10, 1987				
0947 (3)	0	49	49	49
1249 (6)	300	544	886	399
1519 (8.25)	0	886	2454	893
July 5, 1988				
0557 (1.5)	0	0	0	0
0644 (2.25)	0	0	0	0
0737 (3)	200	49	49	49
0836 (4)	200	153	399	49
0936 (5)	300	269	705	153

simulation has a moisture inversion develop during phase 2 (Figure 5.13). The moisture changes in the simulation are associated with the same wind features as in the observations, and the moisture inversion occurs from 6 to 8 hours after sunrise which agrees well with the observations. This moisture inversion results from the westward movement of drier air in the region above the CBL, while the moisture in the return flow increases during this time.

In this phase the simulations and observations qualitatively agree fairly well. The simulations and observations both have upslope flow beginning at about the same time. During the day the observations and simulations have intensifying and deepening upslope flow. A moisture inversion commonly appears on the observational days., and it is seen in some of the simulations including DMWP. Other features of the evolution, especially those above barrier top, are not clearly evident, and they may be masked by synoptic-scale changes or other factors. The quantitative comparison at the base of the barrier shows generally good agreement between the October 29, 1987 observations and the November 1 heating simulation with the simulation under developing the depth of the upslope flow. The November 10, 1987 observations and the November 1 heating simulation have a similar relationship with the model overdeveloping the CBL depth. Compared to the Fall 1990 observations, the November 1 heating simulation overdevelops the mass flux in the upslope flow, the depth of the upslope flow, and the CBL depth. In the observations synoptic-scale disturbances or other processes are sufficiently strong to mask some features of the evolution seen in the simulations, and the observations are inconclusive about the existence or absence of these features.

5.5.1.4 Phase 3

None of the observations taken in the fall identify phase 3 of the evolution which is not very surprising, because the November 1 heating simulation does not have the leading

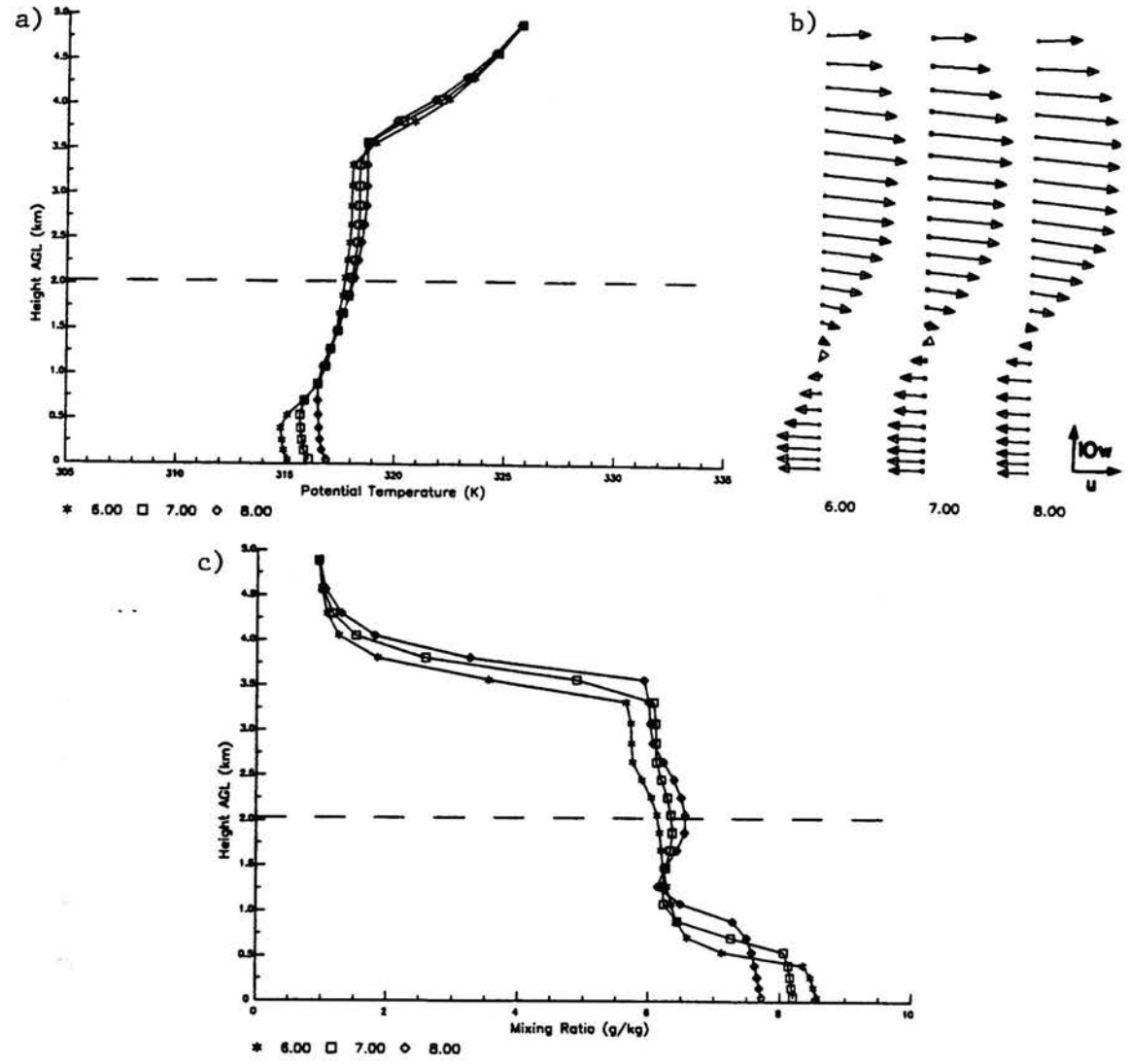

Figure 5.13. The vertical profile of potential temperature (a), winds (b), and mixing ratio (c) at the base of the barrier site for the wet plains – dry mountain simulation at 6, 7, and 8 hours after sunrise. The horizontal component of the winds is the u-component and the vertical component of the winds is 10 times the vertical velocity. The dashed horizontal line is at the height of barrier top.

edge of the cold core moving eastward. This simulation does not have sufficient heating to allow the leading edge of the cold core to move eastward. The observations on July 5, 1988 end before the leading edge of the cold core moves eastward. On this day, cumulus with moderate vertical development appear over the foothills by the end of the observing period and scattered thunderstorms develop later in the day.

5.5.2 Site 30km West of the Base of the Barrier

Table 5.6 shows some characteristics of the observed wind field at sunrise at the site 30km to the west of the base of the barrier (Rustic) compared with most of the simulations. This site is in a 450m deep valley and is 600m higher than the base of the barrier site. The top of this valley is 1050m higher than the Fort Collins site, and in the simulations the elevation difference between the base of the barrier site and the site 30km to its west is nearly the same. The maximum u-component of the simulated jet maximum agrees well with the observations. The heights of the observed u-component maximum are greater than in the simulations which results from the observing site being in a narrow river valley. As in Tyson and Preston-White (1972), the nocturnal flows down the east side of the barrier appear above the tops of the narrow valleys. On November 12, 1990 the maximum is 150m above valley top, and on October 25, 1990 the maximum is 150m below valley top. On October 25 the maximum may be partly influenced by valley flows, but the westerly component winds extend to over 500m above barrier top, indicating westerly flow exists above valley top. Other features of the wind profile at this site are a wind minimum between 1.0 and 2.0km. The speeds of the observed wind minimums are about 1 ms^{-1} faster than the model, and are about 700m higher.

During the day the observations and simulations have many qualitative similarities. The simulated evolution of potential temperature shows a deepening CBL with warming in

Table 5.6

Speed and height of the maximum u-component in the near surface jet and the height and speed of the minimum u-component at sunrise for the site 30km west of the base of the barrier site in all the simulations and the values for the observations at the Rustic site.

	Maximum U-component		Minimum U-Component	
Simulation	Speed (ms^{-1})	Height (m)	Speed (ms^{-1})	Height (km)
Baseline	9.1	275	-0.6	2.3
June 21	6.9	375	-0.2	2.3
Nov. 1	9.4	250	-0.7	1.9
Dec. 21	9.3	300	-0.5	1.9
WMWP	10.0	175	-0.4	1.8
DMWP	9.5	175	-0.5	1.9
WMDP	9.9	125	-0.5	1.9
Stronger winds	3.8	0	2.6	0.4
No winds	5.4	0	-1.3	1.8
Lower CBL	9.3	250	-0.1	1.4
Less Stability	6.5	250	-0.4	2.8
Half Barrier Height	5.6	0	2.6	0.7
Observations				
Nov. 12, 1990	9.4	600	0.9	1.9
Oct. 25, 1990	11.2	300	0.5	1.6

the lower portion of the CBL and cooling in the upper portion (Figure 3.14 shows this site for the baseline run). On November 12, 1990 the Rustic site (see Figure 5.4) has strong warming below 1100m AGL with a nearly neutral layer from 1100m to 1700m (about 1200m above valley top). At six hours after sunrise (1254 MST) a neutral layer is present to about 2.5km AGL, which is about 2.0km above valley top. The November 1 heating simulation has a qualitatively similar evolution to the baseline run, and the CBL is about 800m deep at 4 hours after sunrise and about 1700m deep at 6 hours after sunrise. The CBL depth in the November 1 heating simulation is less than the height **above valley top** of the top of the observed neutral layer, but the simulated and observed heights are fairly close.

The observed u-component decreases below about 1.5km throughout the day with easterly component flow occurring below 900m AGL by 6 hours after sunrise. Above 1.5km the u-component of the flow increases. In the baseline simulation increasing easterly flow near the surface with increasing westerly flow above it occurs at the site 20km west of the base of the barrier, which is east of the lee side convergence zone. The observed vertical integral of eastward mass flux up to at least 5km decreases throughout the day, which is similar to the other sites on this day. Despite the tendency for the eastward mass flux (westerly flow) to decrease throughout the day, the increasing speed in the westerly return flow still appears at this site.

On October 25, 1990 (see Figure 5.7) the cooling in the upper portion of the CBL is not present. Throughout the day strong warming appears at from 2.0 to 2.7km AGL which suppresses the CBL depth. This strong warming is also seen at the Fort Collins and Carpenter sites. Similarly, the strong increase in the vertical integral of eastward mass flux during the day at the Rustic site is seen at the Fort Collins and Carpenter sites. During the day the u-component of the flow weakens below 600m and increases above 600m. In the baseline run the u-component of the flow, which weakens and remains positive throughout

the day, occurs at a site west of the lee side convergence zone. The evolution of the thermal and wind fields differ from November 12, 1990, and during the day it appears to be significantly influenced by increasing winds and a sinking layer both of which occur at the three sites.

At the Rustic site the observations and simulations qualitatively agree well. On November 12, 1990 a deepening CBL with cooling and increasing winds in its upper portion is observed. Observations at the other sites indicate generally weakening of the winds above barrier top on this day. On October 25, 1990 a strong sinking layer, which is observed at the other sites, hampers the CBL growth. With the presence of the deep river valley at the surface, a quantitative comparison is difficult because thermally driven valley circulations can greatly influence the wind and thermal fields near the surface.

5.5.3 Summary of Observations and Observing Methodology

The observing method in this study uses frequent airsonde launches to study the daytime evolution of the atmosphere. This method does not explicitly identify horizontal gradients, but observations at several sites show how the evolution varies horizontally. The integral quantities vertically sum the total influence of the circulations over many levels instead of examining the circulation at only one level, such as the surface. The integrals show how the depth and intensity of the circulation change with time, and they show how the circulation influence the vertical thermal structure. A similar analysis method is used in studying the simulations.

The observations and simulations agree well for the sunrise state of the atmosphere and phase 1 of the evolution at the base of the barrier. At the base of the barrier site the jet down the east side of the barrier and a stable core of 1.5 to 2.0km deep are very common on the six observing days. The weakened jet is frequently observed at 2 to 3 hours after

sunrise. The micrometeorological data shows that the phase 1 warming occurs with a negative or weakly positive surface sensible heat flux which is another consistent feature in the simulations. On the eastern slope of the barrier the observations and simulation also agree well at sunrise and during the early part of the day. This site has the strong westerly flow down the east side of the barrier at sunrise, and during the morning the CBL has significant cooling in its upper portion. This site is located in a deep, narrow river valley while the simulations do not have any valleys on the east slope of the barrier. The river valley complicates the comparison somewhat because the valley influences the wind and thermal fields in the lowest 450m.

During phase 2 of the daytime evolution the observations and simulations agree fairly well. At the site 30km west of the base of the barrier the observations and simulations both have a growing neutral layer with cooling in its upper portion. The u-component of the flow weakens near the surface, and the u-component of the flow above it increases. At the base of the barrier site the simulations and observations show the developing upslope flow, suppressed CBL, and warming above the CBL. The timing of the beginning of the upslope flow is similar for the observations and simulations. Some simulations have a moisture inversion develop in the afternoon similar to the observations. The qualitative comparison of the simulations and observations show that the two-dimensional simulations recreate the main features of the observed evolution well.

Quantitative comparison shows that the November 1 heating simulation agrees well with the observations on October 29, 1987, but the simulation under develops the depth of the upslope flow. Comparison of the same simulation to the Fall 1990 observations shows that the model overdevelops the CBL depth, the mass flux in the upslope flow, and the depth of the upslope flow. The qualitative and quantitative differences between the simulations and observations throughout the daytime evolution may result from many factors including

synoptic-scale changes, improper surface heating in the simulations, three-dimensional effects on the evolution, or the absence of foothills on the eastern slope of the barrier due to the smoothing of the topography in the simulations. Phase 3 of the evolution is not seen in the observations which is not surprising, because most of the observations are taken during the fall and because the observations during the summer end late in the morning.

The analysis of the observations of the daytime evolution show that frequent airsonde launches are very useful as an observational method. This method shows how the atmosphere evolves vertically, and the large number of observational days indicate which features of the evolution commonly occur. The quantitative analysis of the vertical profiles of thermal and wind structure are very useful for comparing the simulated strength of the evolution to the observations. The frequent launching of airsondes at several sites show whether changes in the thermal and wind fields are isolated to one site. During the Fall 1990 similar changes in the wind and thermal fields are seen at the three sites strongly suggesting that the changes are synoptically induced. The frequent airsonde launches do not identify some features of the simulations. The simulations show that these changes are small and likely are masked by other influences including synoptic scale changes. If these changes in the thermal and wind fields are larger, the frequent launching of airsondes are more likely to identify them. Wind profilers and RASS can observe a large population of days. With this large population of observational days the frequency of the occurrence of different features of the evolution can be better determined and the larger data set can show the range of the values of the different quantities describing the diurnal evolution.

CHAPTER 6.
CONCEPTUAL MODEL OF THE EVOLUTION

6.1 Introduction

In this study eleven two-dimensional simulations of the daytime evolution of the atmosphere east of the Front Range of the Colorado Rockies under synoptically undisturbed conditions with clear skies and light winds with a westerly component of around $5ms^{-1}$ are examined. Observations taken on several days at the base of the barrier, on the east slope of the barrier, and on the eastern plains well east of the base of the barrier are presented. The main observing method is the frequent launching of airsondes to study how the atmosphere evolves vertically on these days. The observations show many of the simulated features early in the day, and in the afternoon some of the simulated features are not identified because the atmosphere is somewhat disturbed.

This chapter presents conceptual diagrams of the daytime evolution of the atmosphere east of the crest of the Front Range of the Colorado Rockies under conditions of clear skies, little change in time and space of the synoptic-scale wind and thermal fields, and light ambient winds with a westerly component around $5ms^{-1}$. These diagrams show the major features of the sunrise state of the atmosphere and each of the three phases. The discussion of these conceptual diagrams include showing how the simulations change for the different initial condition and how well the observations and simulations agree.

6.2 Sunrise state: Interaction between Nocturnal Thermal and Ambient Flows

At sunrise the atmosphere is far from horizontally homogeneous. The westerly ambient flow complexly interacts with the thermally driven flows creating the complicated

sunrise state. Before this complex state is examined, a simulation with no ambient winds is first discussed. The no ambient wind simulation shows the thermally driven flows at sunrise. The cooling of the barrier and surrounding terrain creates flow down the east side of the barrier resulting in divergence at the top of the barrier. To replace this lost mass, sinking motion above the barrier occurs with easterly flow to the east of the barrier crest. On the eastern plains the drainage flow slows, creating convergence and rising motion which lifts the cold air to near barrier height at the base of the barrier.

The presence of ambient westerly flow greatly complicates the circulation. Figure 6.1 shows a conceptual diagram of the sunrise state of the atmosphere using an x-z cross-section. A strong jet occurs down the east side of the barrier. This jet is much stronger than the no wind simulation with a maximum u-component of over $9ms^{-1}$ versus $6ms^{-1}$ in the no wind simulation. On the eastern plains the jet slows, and the resulting convergence lifts the cold air creating the stable core. At the base of the barrier the stable core is 2.0km in all the simulations except the stronger winds simulation where it is 1.5km deep. The stable core becomes shallower further east.

The observations have a stable core 1.3 to 2.0km deep at the base of the barrier site, and the jet appears at 600 to 1300m AGL which is immediately above the 600m high ridge of foothills 5km to the west of the Fort Collins site. On the east slope of the barrier the observations show the presence of a jet in and above the narrow river valley in which the Rustic site is located. The observations at Rustic show a nearly zero u-component flow at 1 to 2km AGL, and a similar feature is seen in the simulations.

The nocturnal evolution of the atmosphere influences the atmosphere far above the barrier top. The mountain wave above the barrier develops about 20km further to the west in the baseline run than a run in which there is no diabatic heating. One possible explanation for the retrogression of the mountain wave is the divergence at barrier top forces sinking of

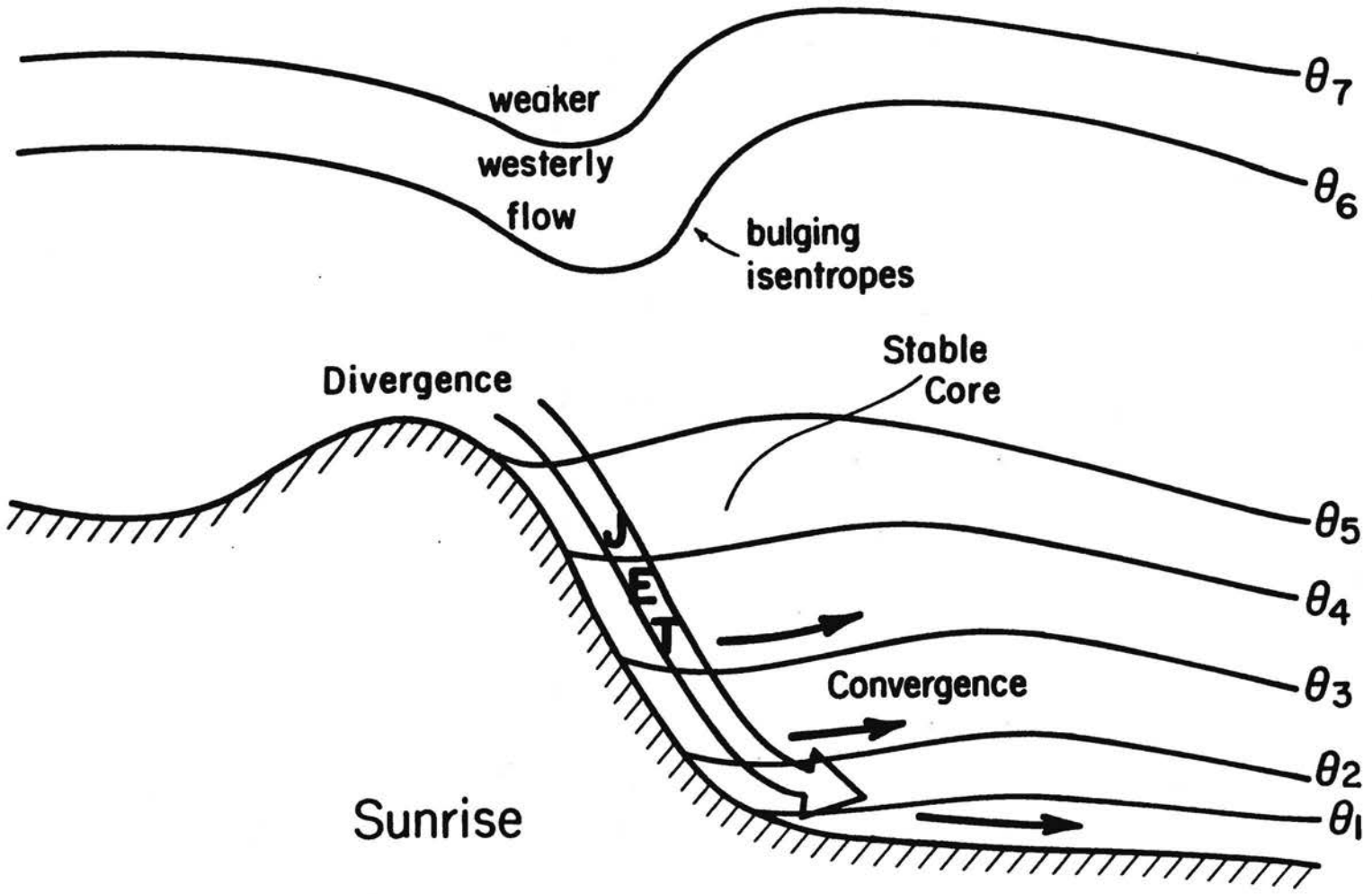

Figure 6.1. Conceptual diagram of the sunrise state of the atmosphere.

the ambient flow further west than if the surface cooling is not present. The change in the ambient stability and wind patterns, especially to the west of the barrier and below 4.0km, caused by the nocturnal cooling may also substantially influence the location of the mountain wave.

Changes to the ambient winds and stability can significantly alter the structure of the jet. On the east slope of the barrier the maximum u-component of the jet is significantly less in the stronger winds and one-quarter stability simulations than in the baseline run, while the maximum u-component of the jet at the base of the barrier is nearly the same for all simulations with westerly ambient winds. In the baseline run (and runs with the same ambient winds and stability) the maximum u-component of the jet down the east side of the barrier occurs near the barrier crest, and all the ambient flow below 3.5km is channeled down the east side of the barrier. However, in the stronger winds and one-quarter stability simulations the jet maximum is closer to the base of the barrier, and less ambient flow is channeled down the east side of the barrier. In the one-quarter and stronger winds simulations the bulging isentropes are weaker and further to the east than in the baseline run.

The differences in the structure of the jet and the bulging isentropes appear to be related to the vertical wavelength of the hydrostatic mountain wave above 3.5km. In the stronger winds and one-quarter stability simulations the vertical wavelength of a hydrostatic mountain wave above 3.5km is twice as large as in the baseline run (and other runs with the same stability and ambient winds), ignoring any changes to the ambient thermal or wind fields induced by diabatic cooling or by mesoscale circulations caused by the cooling of the surface. The jet down the east side of the barrier is located in a pressure trough. In the baseline run the trough extends about half the way down the east slope. In the stronger winds and one-quarter stability runs, a weak trough is seen on the upper portion of the east slope of the barrier, and a stronger pressure trough is located further down the slope. The location of the

stronger trough is the same in the stronger winds and one-quarter stability simulations. In both simulations the maximum u-component of the flow occurs in this stronger pressure trough further down the slope, and this low pressure trough is approximately beneath a region of higher pressure at 3.5km. The location of the pressure ridge at 3.5km is the same in the stronger winds and one-quarter stability simulations, and the ridge is further east in these two simulations than in the baseline run. The similarity of the jet structure for the stronger winds and one-quarter stability simulations and the differences these two simulations have compared the baseline run (and other runs with the same ambient winds and stability) strongly suggest that the hydrostatic mountain wave substantially influences the structure of the jet.

The half barrier height simulation shows that the magnitude of the thermally driven flow can also influence the sunrise state of the atmosphere. The bulging isentropes are weaker than in the baseline run, and much less of the ambient flow is channeled down the east side of the barrier. The very complicated thermal and wind structures, along with the non-linear interactions between the mountain waves and thermally driven flows, make further analysis of the sunrise state very complicated. The interactions of nocturnal flows with mountain waves is an area for future research.

6.3 Phase 1: Weakening Nocturnal Flows Interacting with Surface Heating

Figure 6.2 shows a conceptual diagram for phase 1 of the evolution. This phase occurs until 3-4 hours after sunrise and is characterized by advective warming near the base of the barrier, associated with the weakening nocturnal flow down the east side of the barrier. In the baseline simulation the warming begins at 1.5 hours after sunrise and extends to 20km east of the base of the barrier. At the base of the barrier the warming occurs from 200m to 800m AGL, and this warming does not occur for the no wind, no nighttime phase, and wet

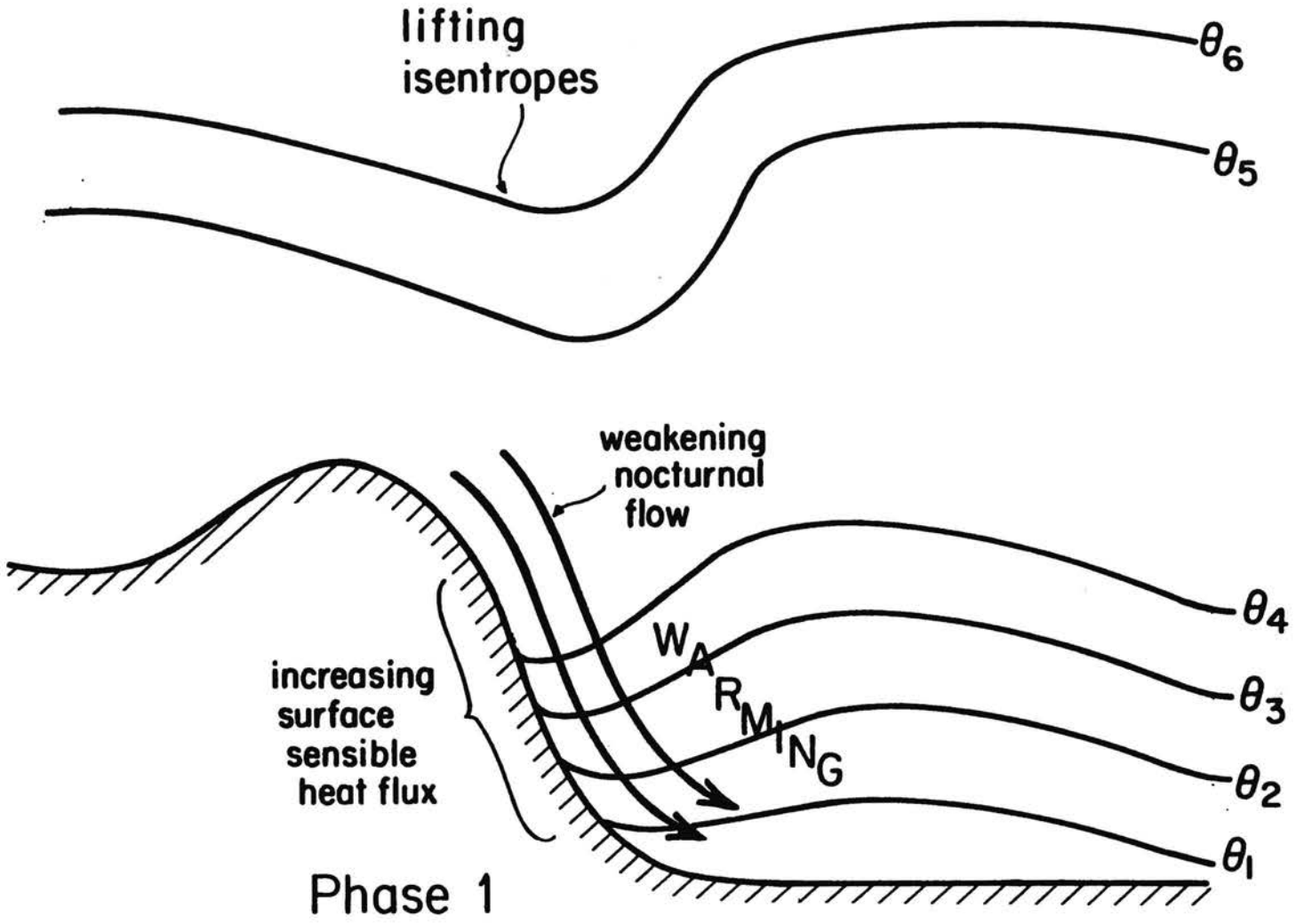

Figure 6.2. Conceptual diagram for phase 1 of the evolution.

mountain-dry plain simulation. The observations and simulations with westerly ambient winds show that the atmosphere warms much more than the local surface sensible heat flux.

In all simulations except the no ambient wind run, the flow down the east side of the barrier is influenced by horizontal pressure gradients established throughout the night which tend to speed the flow down the east side of barrier. As discussed in the last section, some of the ambient westerly flow appears to be channeled down the east side of the barrier. The interaction between the ambient and thermally driven flows creates lower pressure on the east side of the barrier, and the location of trough appears to be influenced by the wavelength of the mountain wave above the barrier crest. These pressure fields do not immediately die when surface heating begins. They gradually weaken forcing flow down the east side of the barrier for the first 3 hours after sunrise despite the absence of surface cooling. The phase 1 warming does not solely result from positive surface sensible heat flux on the eastern slope of the barrier heating the air which is advected eastward. By one hour after sunrise the air along the lower portion of the east slope of the barrier warms despite the surface sensible heat flux at these sites still being negative. At the base of the barrier the source terms for potential temperature show that the vertical advection only weakens slightly during this phase and that the less horizontal advection and diffusion allow the warming to occur. The circulations in phase 1 appear to maintain the warming due to vertical motions while weakening cooling due to horizontal motions. In the wet mountain-dry plain simulation the surface sensible heat flux does not increase after sunrise, and this phase is not present.

During phase 1 the bulging isentropes weaken and the u-component of the flow in and around the bulging isentropes increases. With these changes the strength of the pressure trough in which the jet lies also decreases. With the weakening jet and less of the ambient flow being channeled down the east side of the barrier, the eastward mass flux above the height of the barrier top increases.

6.4 Phase 2: Developing Solenoid

The main feature of this phase is a developing solenoid. The solenoid development is much more complicated than only the forming of the upslope and return flows. Figure 6.3 shows a conceptual model of the early part of this phase. Upslope flow first develops near the base of the barrier and expands eastward. On the east side of the barrier the upslope flow meets the ambient westerly flow in the lee side convergence zone. The rising air in the lee side convergence zone lifts the air into the more stable atmosphere above the barrier creating the cold core. As expected, westerly return flow develops above barrier top, and sinking motion occurs on the eastern plains.

The solenoid is not symmetric, and its evolution is complicated by its interaction with the atmosphere above barrier top. As the cold core builds into the atmosphere, it lifts colder air creating higher pressure. Immediately to the east of the cold core is a region of sinking motion which creates a pressure trough in which the center of the solenoid is located. The strong pressure gradient created by the high pressure in the cold core and pressure trough immediately to its east affects the westerly return flow. The westerly return flow is strongly accelerated by this pressure gradient creating a wind maximum. Deceleration occurs as the exits the east side of the pressure trough. The slowing leads to convergence with strong sinking motion occurring immediately to the east of the solenoid while further east the sinking motion is weaker.

Two distinct stages are seen in the evolution. In the first stage (Figure 6.3) the easterly upslope flow on the eastern plains is confined to the CBL, and a region of weaker winds separates the easterly flow from the westerly return flow above it. At this time the pressure gradient in the stable core is positive (higher pressure to the west). Cold air advection occurs in the upslope flow in the CBL, and warming is present in the stable core above the CBL due to subsidence and horizontal warm air advection. The second stage

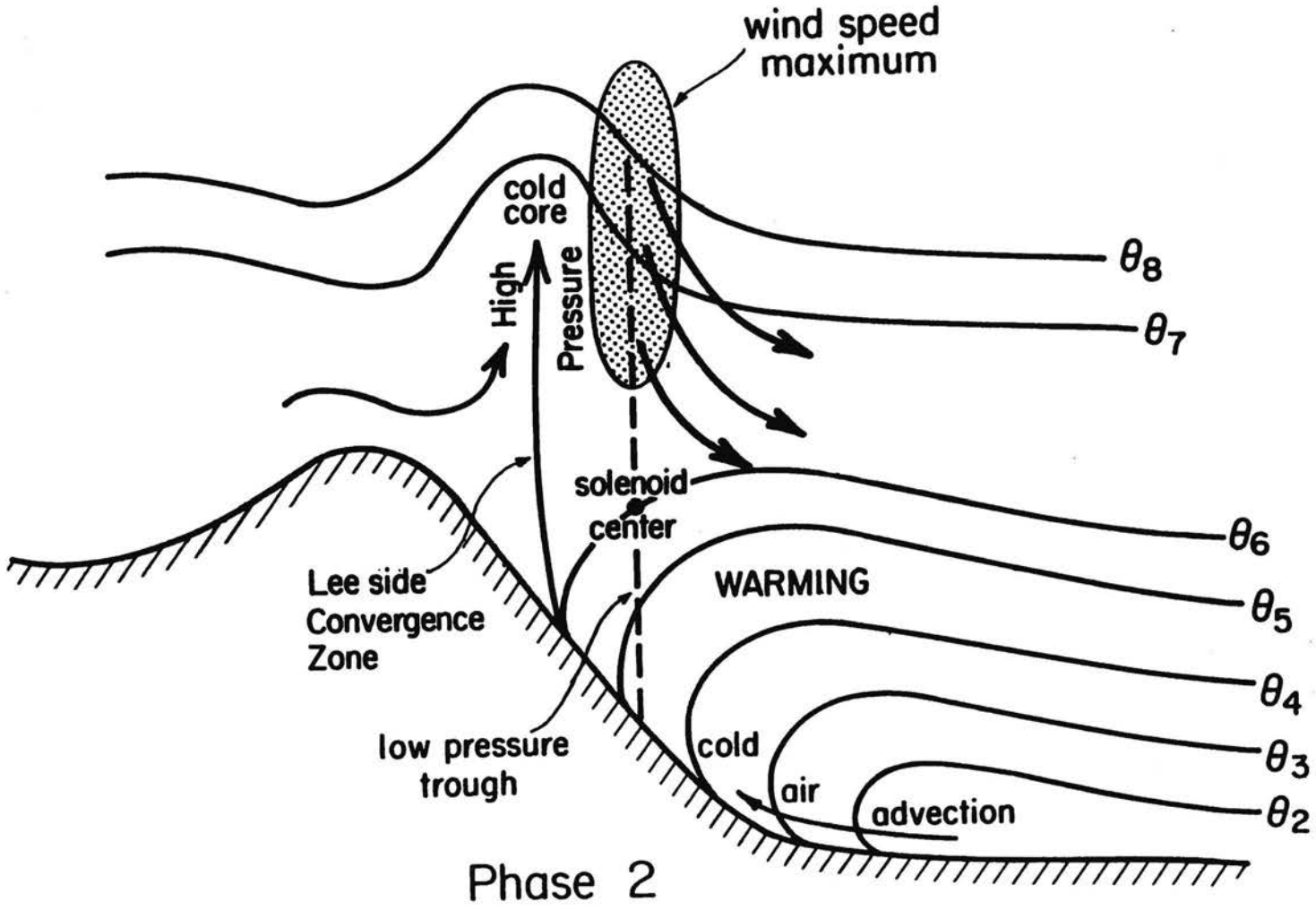

Figure 6.3. Conceptual diagram for the first stage of phase 2 of the evolution.

begins when the pressure gradient in the stable core first becomes negative. Figure 6.4 shows a conceptual model for this stage. Warming in the stable core above the CBL and warming due to the sinking on the leading edge of the cold core lower the pressure near the base of the barrier. When the pressure gradient becomes negative (lower pressure to the west), upslope flow occurs above the CBL, and strong vertical wind shear develops where the upslope and westerly return flow meet. The location where the pressure gradient in the stable core changes from positive to negative is a pressure ridge. A secondary maximum of sinking motion occurs near this pressure ridge, because of increased divergence and convergence associated with the increased mass flux. The pressure ridge in the stable core moves eastward away from the solenoid center. The two stage evolution does not occur for all simulations. In the stronger winds simulation the region of the lower pressure does not have time to develop before the leading edge of the cold core moves eastward. In the half barrier height simulation the barrier does not appear to be high enough to cause heating over a sufficiently deep layer in the stable core to obtain the easterly flow above the CBL.

On the eastern plains cold air advection occurs in the upslope flow in the CBL with warm air advection above the CBL. This pattern of advection leads to the suppression of the CBL on the eastern plains. In the baseline simulations the magnitude of the horizontal cold air advection and heating above the CBL decreases with distance east of the base of the barrier, suggesting that the CBL may be less suppressed further east.

The different simulations show how winds, heating, and thermal structure influence the circulation. For moister soil on the eastern plains the circulations are generally shallower and weaker, and the CBL is shallower on the eastern plains due to less surface sensible heat flux and more horizontal cold air advection. Moister soil west of barrier crest further reduces the strength and depth of the thermally driven circulations. For times of the year closer to the winter solstice the solenoid is generally weaker and shallower, and similarly the CBL

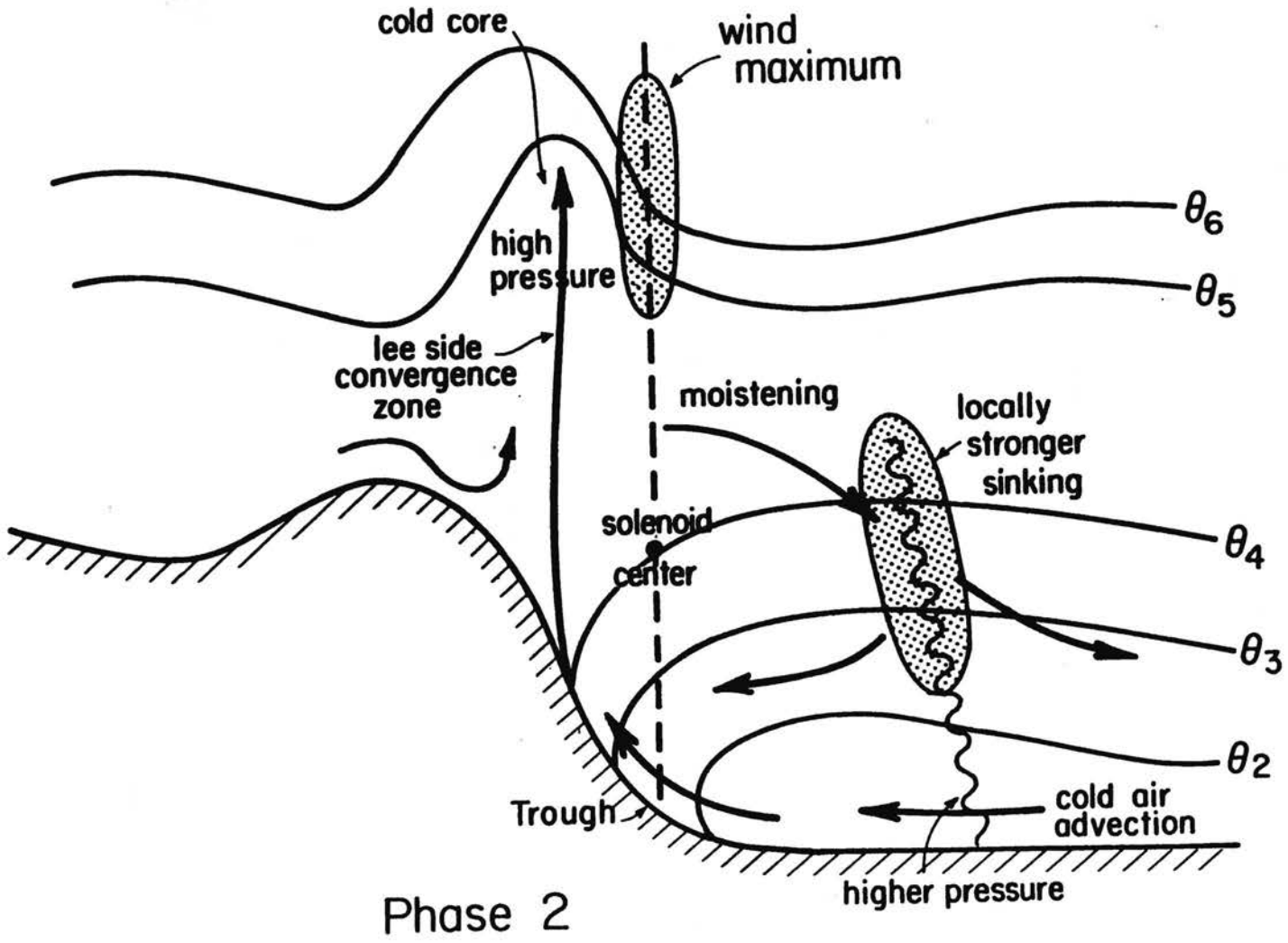

Figure 6.4. Conceptual diagram for the second stage of phase 2 of the evolution.

depth becomes shallower for days closer to the winter solstice. The similarity of baseline and June 21 heating simulation suggests that the intensity and depth of the solenoid in this phase does not increase much above a given value for more heating. For stronger winds the circulation is generally weaker, and the CBL is deeper. For less stability above barrier top the solenoid initially is weaker and more shallow than in the baseline run, and later it is deeper and stronger than the baseline run. The heating above the CBL, however, is the same for the later times of this phase. For the lower initial CBL simulation the circulation is generally shallower and weaker than the baseline run with roughly the same amount of heating above the CBL.

The observations are too disturbed to identify some of the subtle simulated changes above barrier top at the base of the barrier site. Comparison of some of the vertical quantities to the simulations suggests that the model overdevelops the intensity of the circulation (especially in the Fall 1990 regime), under develops the depth of the upslope flow, and over predicts the CBL depth especially for Fall 1990 regime. These differences may result from differences in the surface sensible heat flux, the smooth topography in the simulations which eliminates the foothills, or the synoptic-scale changes.

6.5 Phase 3: Migrating solenoid

Figure 6.5 shows a conceptual diagram for phase 3 of the evolution. The main feature of this phase is the eastward movement of the leading edge of the cold core, and the movement of the solenoid beneath it. As seen in phase 2 the center of the solenoid is located in a pressure trough beneath the leading edge of the cold core. A wind maximum is located in the pressure trough and convergence in the westerly return flow ahead of the trough produces stronger sinking motion towards the surface. Correspondingly, the divergence to the west of the pressure trough produces rising motion towards the surface, and

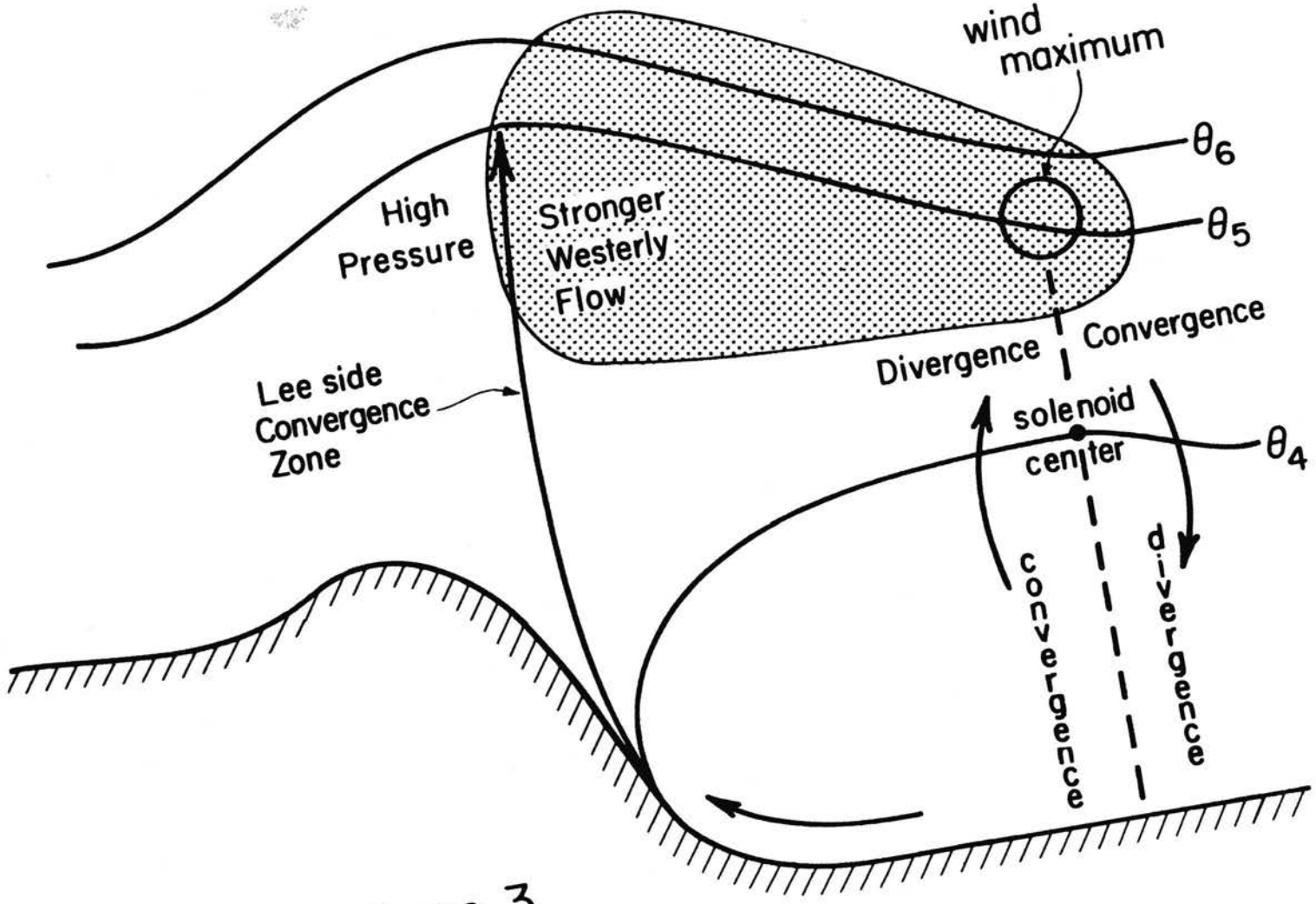

Figure 6.5. Conceptual diagram for phase 3 of the evolution.

in phase 2 this divergence is in the lee side convergence zone. As the pressure trough moves eastward the rising and sinking motions associated with the pressure trough move eastward. The main lee side convergence zone remains stationary over the east side of the barrier.

The eastward movement of the leading edge of the cold core is an advective phenomenon. The model has cold air advection in the leading edge of the cold core. The eastward movement of the cold core influences the winds in the troposphere. The winds above the cold core weaken during the day. The strong horizontal pressure gradient created by the cold core accelerates ambient air into the cold core from its west and from above it. With the movement of air downward into the cold core, weaker horizontal pressure gradients are created above the cold core leading to weaker westerly flow above the cold core. This flow pattern is similar to a return circulation imposed on the ambient westerly flow.

The leading edge of the cold core rotates around a point above the eastern slope of the barrier like a spoke rotating around a wheel. As the leading edge of the cold core becomes less vertical, the pressure trough becomes less vertical, and the trough in which the solenoid is located weakens. Along with less surface heating the eastward moving solenoid weakens and eventually dies with a solenoid redeveloping near the base of the barrier.

As the solenoid passes a site, the CBL grows explosively. In the baseline simulation the CBL grows over 1.0km in a one hour period at the base of the barrier site. For the stronger wind and lower barrier height simulations the leading edge of the cold core starts moving eastward sooner. In the simulation with the moister plains and west side of the barrier, the leading edge of the cold core moves eastward later because of the longer time needed to develop a cold core and establish the pressure gradients to move the leading edge eastward. The solenoid moves eastward faster for stronger ambient winds, more heating, and lower barrier height.

In the wet plain-dry mountain simulation the solenoid does not move eastward beneath the leading edge of the cold core. In this simulation the stability in the stable core is greater than in the baseline simulation. Convergence occurs on the eastern side of the wind maximum beneath the leading edge of the cold core, and divergence occurs on the western side this wind maximum. The convergence produces sinking motion beneath the height of the wind maximum, and divergence produces rising motion. In this simulation the convergence and divergence are not sufficiently strong to cause to the sinking and rising motion extend down to the surface. Explosive CBL growth does not occur on the eastern plains in this simulations.

The solenoid often dissipates later in the day and a wind maximum at 3-4km AGL can be seen continuing to move eastward. The solenoid often redevelops near the base of the barrier if there is sufficient heating. The migrating solenoid results is a disturbance – which can significantly affect the simulation – advected eastward. Throughout the day the main circulation (upslope flow, lee side convergence zone, return flow) remains over the east side of the barrier and the eastern plains near the barrier. In the half barrier height simulation, however, the lee side convergence zone, upslope flow, and westerly return flow move eastward away from the barrier and eastern plains near the barrier, and the evolution has many similarities to Banta (1982).

The observations do not identify phase 3 of the evolution. The November 1 heating simulation indicates the heating is not sufficient to have the leading edge of the cold core move eastward. On July 5, 1988 the observations are terminated late in the morning. On this date thunderstorms which develop in the afternoon likely influence the eastward moving solenoid.

CHAPTER 7
CONCLUSIONS

7.1 Summary and Conclusions

The west-east nature of the daytime evolution of the atmosphere east of the crest of the Front Range of the Colorado Rockies in the vicinity of Fort Collins is studied under conditions of clear skies, little changes in time and space of the synoptic-scale wind and thermal fields, and ambient winds above barrier top with a westerly component around $5ms^{-1}$. This study focuses on the mountain-plains circulation examining the thermal fields and wind fields created by the complex interactions between the thermally induced flows, created by the heating and cooling of the high mountain barrier and eastern plains, and the ambient flows. The daytime evolution is studied using computer simulations and observations mainly consisting of deep airsondes.

A range of two-dimensional simulations using version 2A of the CSU RAMS are run with different patterns of soil moisture (which affects the surface sensible heat flux), time of year, ambient winds, ambient thermal structures, and barrier height. These simulations show which features of the daytime evolution are common for the different initial conditions as well as how the evolution qualitatively and quantitatively changes for the various initial conditions. The utility of using vertical profiles of the thermal and wind fields at several sites in the model domain as a model analysis tool is examined in this study of the daytime evolution. Parameters derived from these vertical profiles quantitatively show the horizontal variation in the evolution and quantitatively show the changes in the evolution between the simulations with different initial conditions.

The observations of the daytime evolution mainly consist of frequent airsonde launches (every 2-3 hours) at sites on the eastern slope of the barrier and on the plains east of the Front Range. The usefulness of frequent airsonde launches as an observational tool is examined in this study. The frequent airsonde launches are compared qualitatively and quantitatively to the simulations to examine how well the various model runs simulate the daytime evolution.

The simulations and observations have many similar features indicating that the two-dimensional simulations identify the major features of the daytime evolution. From the simulations and observations a conceptual model of the daytime evolution is derived, which has a complicated sunrise state and three phases to the evolution. The thermal field, wind field, and important physical processes for the sunrise state and each phase is given in the conceptual model. This conceptual model can be the basis for further two-dimensional and three-dimensional study of the daytime evolution east of a large north-south mountain barrier.

The sunrise state of the conceptual model is not close to horizontally homogeneous. The main features are a jet down the east side of the barrier and a stable core on the eastern plains. The maximum u-component in the jet is 7-10ms^{-1}, and the stable core is 1.5 to 2.0km deep near the base of the barrier. Comparison of the baseline simulation to a simulation without diabatic heating shows that the thermally driven nocturnal circulations can alter the position of the mountain wave above barrier top. The ambient stability and wind speed, which influence the wavelength of a hydrostatic mountain wave, can influence the structure of the jet down the east side of the barrier.

Phase 1 of the evolution lasts until 3-4 hours after sunrise, and the main feature of this phase is heating up to 20km east of the base of the barrier associated with the weakening jet down the east side of the barrier. Since this jet is not purely thermally driven, it does not weaken significantly shortly after sunrise. The weakening jet advects warmer air eastward

from the east slope of the barrier. On the east slope of the barrier the air can warm despite a negative surface sensible heat flux.

Phase 2 begins at 3-4 hours after sunrise and can end as early as 5.5 hours after sunrise, or it can last the entire day. The main feature of this phase is a developing solenoid. The solenoid is not horizontally or vertically symmetric, and it does not develop uniformly with time. The developing solenoid has two stages of its evolution. In the first stage the horizontal pressure gradient in the stable core above the CBL is positive. In the second stage a negative horizontal pressure gradient in the stable core develops next to the barrier, and this region of negative pressure gradient expands eastward. The solenoid circulations suppress the CBL depth on the eastern plains by warming the atmosphere above the CBL through horizontal and vertical advection and by cooling the air in the CBL through horizontal cold air advection. The solenoid circulations are weaker and develop later as the distance east of the base of the barrier increases. The daytime solenoid circulations and the associated movement of energy are evident beyond 50km east of the base of the barrier.

Phase 3 is characterized by the eastward movement of the leading edge of the cold core. Often the solenoid migrates eastward beneath the leading edge of the cold core. This phase does not occur on all days, and the simulations show that days with weak surface heating due to time of year do not have the leading edge of the cold core moving eastward. Beneath the leading edge of the cold core, a pressure trough exists, and associated with this pressure trough is a maximum in the u-component at 3 to 4km above the flat plains to the east. Convergence ahead of the maximum tends to produce sinking motion towards the surface, and divergence behind the maximum tends to produce rising motion towards the surface. This rising and sinking motion produces the solenoid that migrates eastward. As the migrating solenoid passes over a site the CBL depth can explosively increase by over 1km in one hour. If the stable core is sufficiently stable the sinking and rising motions produced by

the convergence and divergence do not reach the surface, and a migrating solenoid does not accompany the eastward moving leading edge of the cold core. In this case the solenoid center remains stationary throughout the day. Throughout this phase the lee side convergence zone remains stationary over the eastern slope of the barrier with significant upslope flow existing east of this zone onto the eastern plains. The migrating solenoid is a disturbance – which can significantly influence the atmosphere – in the main daytime circulation.

Examination of the vertical profiles of the thermal and wind fields at different sites in the simulations is very useful as a model analysis tool. Comparison of the amount of heating vertically to the surface sensible heat flux shows how the mesoscale circulation moves energy laterally and vertically. Vertical integrals of heating show the heights where the circulations are moving energy. The vertical integral of eastward mass flux shows depths and amount of the changes to the u-component of the flow. Quantities, most of which are derived from the vertical integrals, are used to quantitatively describe the horizontal changes in the evolution and the changes in the evolution between the different simulations. The mass flux in the upslope flow and maximum u-component of the return flow are used to quantify the intensity of the circulation. The depth of the upslope flow and a parameter called the top of the solenoid, which is defined as the height where the mass flux towards the barrier equals the mass flux away from the barrier, are used to define the depth of the circulation. The depth of the CBL, amount of heating above the CBL, and horizontal advection of heat in the CBL are used to quantify the changes the circulations have on the thermal fields.

The different initial conditions in the simulations can significantly change the strength and depth of the circulation as well as the thermal fields in phases 2 and 3. Some of the significant changes for phases 2 and 3 include the westward mass flux in the solenoid being up to 60% weaker in the stronger wind simulation than in the baseline run. In the stronger

wind simulation the CBL is 30% to 100% deeper than in the baseline run in phase 2, and phase 3 begins 1.5 hours earlier than in the baseline run. In the wet plain - dry mountain simulation the CBL depth is 50% or less than in the baseline run, and the westerly mass flux in the upslope flow is over 25% smaller than in the baseline simulation. Despite this weaker mass flux, the depth of the upslope flow is nearly the same in the two simulations. For the half barrier height simulation the mass flux in the upslope flow is 10% to 25% as large as in the baseline run while the depth of the upslope flow is 20 to 80% as large as in the baseline run. In the half barrier height simulation, once the solenoid passes the site the westward mass flux is very small and eventually becomes zero because the lee side convergence zone moves eastward with the solenoid.

The comparison between the simulations show the following general conclusions for phases 2 and 3. The circulation is generally weaker and shallower for moister soil on the eastern plains (less surface sensible heat flux), moister soil west of barrier crest, days closer to the winter solstice, stronger winds, and lower CBL the previous day. The circulation is generally deeper and stronger for less stability (after about 5 hours after sunrise) and for times closer to the summer solstice, especially by 5 hours after sunrise. The CBL on the eastern plains is shallower for moister soil on the eastern plains, days closer to the winter solstice, stronger winds, and the lower CBL the previous day (after the solenoid passes).

The frequent airsonde launches are very useful for observing the daytime evolution of the flow. The observations and simulations qualitatively agreed well. At sunrise the observations have a jet down the east side of the barrier and a stable core. The airsondes show the phase 1 warming at the base of the barrier associated with the weakening jet. A micrometeorological station is sometimes collocated with the airsonde launching site, and the station shows very small or negative surface sensible heat flux at the base of the barrier when the phase 1 warming occurs. In phase 2 the observations have many features of the simulated

thermal and wind fields. At the Fort Collins site (at the base of the barrier), the developing upslope flow and suppressed CBL are seen. At the Rustic site (30km west of the base of the barrier), a CBL with cooling in its upper portion is observed, and weakening westerly or easterly winds near the surface with increasing westerly flow above it are seen. Quantitative comparison of the simulations to the observed wind fields show good agreement on one day in October 1987, and the model overdevelops the upslope flow and CBL on two days during Fall 1990.

Some features of the simulated evolution such as the increase in speed of the return flow and a near neutral layer over the eastern plains above the barrier crest height are small and likely are masked by other changes in the observations. The observations do not identify phase 3 of the evolution which is not surprising since the observations are taken in the Fall when heating is weak and daylength is too short to have this phase develop. On days with stronger heating, which would develop stronger return flow and have phase 3, the frequent airsonde observations are very likely to identify these features.

7.2 Future Research

This research explores the west-east nature of the daytime evolution for different initial conditions. One area for further research is to explore the influence of the north-south variation of the topography on the daytime evolution. The height and width of the Front Range changes fairly significantly especially to the north of Fort Collins, and the Cheyenne Ridge and Palmer Divide can affect the daytime evolution as well. Three-dimensional simulations can be run to explore these influences. More complex heating patterns can be included in the simulations including north-south variations to the soil moisture.

The influence of changes in the ambient thermal and wind fields on the daytime evolution is another area for future research. The simulations in this dissertation do not

allow for synoptic-scale changes in the ambient winds and thermal fields. The observations show that the ambient wind and thermal fields change during the day, and the changes in the ambient fields may influence the evolution.

The sunrise state shows a very complicated interaction between mountain waves and thermally driven flow. A study of the transition from the daytime to nighttime phase as well as changes in the atmosphere during the nighttime is another area for future research. The non-linear interactions between mountain waves and thermally induced flows for many different cooling rates, ambient stabilities, and ambient winds is a very interesting research topic.

Observations of the daytime evolution can be taken at more sites to obtain a better understanding of the daytime evolution including the north-south changes in the evolution. With the development of wind profilers and RASS, the evolution for many days can be studied providing a better idea of the universality of some of the observed features and a better understanding of the intensity of the circulations for different atmospheric conditions.

CHAPTER 8.
REFERENCES

Abbs, D.J. and R.A. Pielke, 1986: Thermally Forced Surface Flow and Convergence Patterns over Northeast Colorado. *Mon. Wea. Rev.*, **114**, 2281-2296.

Arritt, R.W. and R.A. Pielke, 1986: Interactions of Nocturnal Slope Flows with Ambient Winds. *Boundary-Layer Meteor.*, **37**, 183-195.

Atkinson, B.W., 1981: *Meso-scale Atmospheric Circulations*. Academic Press, 495 pp.

Bader, D.C. and T.B. McKee, 1983: Dynamic Model Simulations of the Morning Boundary Development in Deep Mountain Valleys. *J. Climate Appl. Meteor.*, **22**, 341-351.

Banta, R.M., 1982: An Observational and Numerical Study of Mountain-Boundary Layer Flow. Atmospheric Science Paper # 350, Colorado State University, Fort Collins, CO.

Banta, R.M., 1984: Daytime Boundary-Layer Evolution over Mountainous Terrain. Part I: Observations of the Dry Circulations. *Mon. Wea. Rev.*, **112**, 340-356.

Banta, R.M., 1986: Daytime Boundary-Layer Evolution over Mountainous Terrain. Part II: Numerical Studies of Upslope Duration. *Mon. Wea. Rev.*, **114**, 1112-1130.

Banta, R.M. and W.R. Cotton, 1981: An Analysis of the Structure of Local Wind Systems in a Broad Mountain Basin. *J. Appl. Meteor.*, **20**, 1255-1266.

Bonner, W.D., 1968: Climatology on the Low-Level Jet. *Mon. Wea. Rev.*, **96**, 833-850.

Bossert, J.E., 1990: Regional-Scale Flows in Complex Terrain: An Observational and Numerical Investigation .Atmospheric Science Paper # 472, Colorado State University, Fort Collins, CO.

Bossert, J.E., J.D. Scheaffer, and E.R. Reiter, 1989: Aspects of Regional-Scale Flows in Mountainous Terrain. *J. Appl. Meteor.*, **28**, 590-601.

Braham, R. and M. Draginis, 1960: Roots of Orographic Cumuli. *J. Meteor.*, **17**, 214-226.

Chen, C. and W. Cotton, 1983: A One-Dimensional Simulation of the Stratocumulus-Capped Mixed Layer. *Boundary-Layer Meteor.*, **25**, 289-321.

Clark, T.L. and R.D. Farley, 1984: Severe Downslope Windstorm Calculations in Two and Three Spatial Dimensions Using Anelastic Grid Nesting: A Possible Mechanism for Gustiness. *J. Atmos. Sci.*, **41**, 329-350.

Cotton, W.R., R.L. George, and K.R. Knupp, 1982: An Intense Quasi-Stationary Thunderstorm over Mountainous Terrain. Part I: Evolution of the Storm-Initiating Mesoscale Circulation. *J. Atmos. Sci.*, **39**, 328-342.

Cotton, W.R., R.L. George, P.J. Wetzel and R.L. McAnelly, 1983: A Long-Lived Mesoscale Convective Complex. Part I: The Mountain-Generated Component. *Mon. Wea. Rev.*, **111**, 1893-1918.

Cotton, W.R., C.J. Tremback, and R.L. Walko, 1988: CSU RAMS-A cloud model goes regional. *Proc. NCAR Workshop on Limited-Area Modeling Intercomparison*, Nov. 15-18, NCAR, Boulder, CO.

Cram, J., 1990: Numerical Simulation and Analysis of the Propagation of a Prefrontal Squall Line. Atmospheric Science Paper # 471, Colorado State University, Fort Collins, CO.

Crook, N.A., T.L. Clark, and M.W. Moncrieff, 1991: The Denver Cyclone. Part II: Interaction with the Convective Boundary Layer. *J. Atmos. Sci.*, **48**, 2109-2126.

Defant, F., 1952: Local Winds. *Compendium on Meteorology*. T.F. Malone, Ed., American Meteorological Society, Boston, pp. 655-672.

Dirks, R.A,, 1969: A Theoretical Investigation of Convective Patterns in the Lee of the Colorado Rockies. Atmospheric Science Paper # 154, Colorado State University, Fort Collins, CO.

Durran, D.R., 1986: Another Look at Downslope Windstorms. Part I: On the Development of Analogs to Supercritical Flow in an Infinitely Deep, Continuous Stratified Fluid. *J. Atmos. Sci.*, **43**, 2527-2543.

Egger, J., 1987: Valley Winds and the Diurnal Circulations over Plateaus. *Mon. Wea. Rev.*, **115**, 2177-2185.

Fast, J.D. and M.D. McCorcle, 1990: A Two-Dimensional Sensitivity Study of the Great Plains Low-Level Jet. *Mon. Wea. Rev.*, **118**, 151-163.

Garrett, A.J., 1980: Orographic Cloud over the Eastern Slopes of Mauna Loa Volcano, Hawaii Related to Insolation and Wind. *Mon. Wea. Rev.*, **108**, 931-941.

Gill, A.E., 1982: *Atmospheric-Ocean Dynamics*, Academic Press, 662 pp.

Hahn, C.J., 1981: A Study of the Diurnal behavior of the Boundary-Layer Winds at the Boulder Atmospheric Observatory. *Boundary-Layer Meteor.*, **21**, 231-245.

Hahn, D.C., 1980: Observed Characteristics of Turbulence in the Atmospheric Boundary Layer over Mountainous Terrain. Atmospheric Science Paper # 320, Colorado State University, Fort Collins, CO.

Helfand, H.M. and J.C. Labraga, 1988: Design of a Nonsingular Level 2.5 Second-Order Closure Model for the Prediction of Atmospheric Turbulence. *J. Atmos. Sci.*, **45**, 113-132.

Henz, J.F., 1974: Colorado High Plains Thunderstorm Systems: A Descriptive Radar-Synoptic Climatology. M.S. Thesis, Department of Atmospheric Science, Colorado State University, Fort Collins, CO.

Hootman, B. and W. Blumen, 1983: Analysis of Nighttime Drainage Winds in Boulder, Colorado during 1980. *Mon. Wea. Rev.*, **111**, 1052-1061.

Hughes, R.L., 1978: A Numerical Simulation of Mesoscale Flow over Mountainous Terrain. Atmospheric Science Paper # 303, Colorado State University, Fort Collins, CO.

Klemp, J.B. and D.K. Lilly, 1975: The Dynamics of Wave-Induced Downslope Winds. *J. Atmos. Sci.*, **32**, 320-339.

Lavoie, R.L., 1967: Air Motions over the Windward Coast of the Island of Hawaii. *Tellus*, **19**, 354-358.

Lee, T.J. and R.A. Pielke, 1992: Estimating the Soil Specific Humidity. To appear in *J. Appl. Meteor.*, April.

Lee T.J., R.A. Pielke, R.C. Kessler, and J. Weaver, 1989: Influence of Cold Pools Downstream of Mountain Barriers on Downslope Winds and Flushing. *Mon. Wea. Rev.*, **117**, 2041-2058.

Liu, J.Y. and H.D Orville, 1969: Numerical Modeling of Precipitation and Cloud Shadow Effects on Mountain-Induced Cumuli. *J. Atmos. Sci.*, **26**, 1283-1298.

Mahrer, Y. and R. Pielke, 1975: A Numerical Study of the Airflow over Mountains Using Two-Dimensional Version of the University of Virginia Mesoscale Model. *J. Atmos. Sci.*, **32**, 2144-2155.

Mahrer, Y. and R. Pielke, 1977: A Numerical Study of the Airflow over Irregular Terrain. *Beitrage zur Physik der Atmopshare*, **50**, 98-113.

Mahrt, L., 1982: Momentum Balance of Gravity Flows. *J. Atmos. Sci.*, **39**, 2701-2711.

McNider, R.T., 1981: Investigation of the Impact of Topographic Circulations on the Transport and Dispersion of Air Pollutants. Ph.D. Dissertation. Department of Environmental Sciences, University of Virginia, Charlottesville, Virginia.

McNider, R.T and R.A. Pielke, 1981: Diurnal Boundary-Layer Development over Sloping Terrain. *J. Atmos. Sci.*, **38**, 2198-2212.

Orville, H.D., 1964: On Mountain Upslope Winds. *J. Atmos. Sci.*, **21**, 622-633.

Orville, H.D., 1965: A Numerical Study of the Initiation of Cumulus Clouds over Mountainous Terrain. *J. Atmos. Sci.*, **22**, 684-699.

Orville, H.D., 1968: Ambient Wind Effects on the Initiation and Development of Cumulus Clouds over Mountains. *J. Atmos. Sci.*, **25**, 385-403.

Orville, H.D. and F.J. Kopp, 1977: Numerical Simulation of the Life History of a Hailstorm. *J. Atmos. Sci.*, **34**, 1596-1618.

Orville, H.D. and L.J. Sloan, 1970: A Numerical Simulation of the Life History of a Rainstorm. *J. Atmos. Sci.*, **27**, 1148-1159.

Pielke, R.A., 1974: A Three-Dimensional Numerical Model of the Sea Breeze over South Florida. *Mon. Wea. Rev.*, **102**, 115-139.

Pielke, R.A., M.D. Moran, M. Segal, D.A. Wesley, and T.B. McKee, 1987: Opportunities for Nowcasting Air Pollution Episodes and Accidental Toxic and Radioactive Releases. *Proc. Symp. Mesoscale Analysis and Forecasting*, 17-19 August, 1987, Vancouver, Canada, 463-470.

Rao, K.S. and H.F. Snodgrass, 1981: A Nonstationary Nocturnal Drainage Flow Model. *Boundary-Layer Meteor.*, **20**, 309-320.

Raymond, D. and M. Wilkening, 1980: Mountain-Induced Convection under Fair Weather Conditions. *J. Atmos. Sci.*, **37**, 2693-2706.

Reiter, E. and M. Tang, 1984: Plateau Effects on Diurnal Circulation Patterns. *Mon. Wea. Rev.*, **112**, 638-651.

Richard, E., P. Mascart, and E. Nicherson, 1988: The Role of Surface Friction in Downslope Windstorms. *J. Appl. Meteor.*, **28**, 241-251.

Sang, J.G. and E.R. Reiter, 1982: Model-Derived Effects of Large-Scale Diurnal Thermal Forcing on Meteorological Fields. *Arch. Met. Geoph. Biokl., Ser. A*, **31**, 185-203.

Schneider, J.M., 1991: Dual Doppler Measurement of a Sheared, Convective Boundary Layer. Ph.D. Dissertation. Department of Meteorology, University of Oklahoma, Norman, OK.

Segal, M., J. Garratt, R. Pielke, and Z. Ye, 1991: Scaling and Numerical Model Evaluation of Snow-Cover Effects on the Generation and Modification of Daytime Mesoscale Circulations. *J. Atmos. Sci.*, **48**, 1024-1042.

Smith, J.K. and T.B. McKee, 1983: Undisturbed Clear Day Diurnal Wind and Temperature Pattern in Northeast Colorado. Atmospheric Science Paper # 365, Colorado State University, Fort Collins, CO.

Smith, R.B., 1979: The Influence of Mountains on the Atmosphere. *Advances in Geophysics*, B. Saltzman, Ed., Volume 21, Academic Press, 87-230.

Smith, R.B., 1989: Hydrostatic Flow over Mountains. *Advances in Geophysics*, Volume 31, Academic Press.

Smolarkiewicz, P. and R. Rotunno, 1989: Low Froude number Flow past Three-Dimensional Obstacles. Part I: Baroclinically Generated Lee Vortices. *J. Atmos. Sci.*, **46**, 1154-1164.

Smolarkiewicz, P. and R. Rotunno, 1990: Low Froude number Flow past Three-Dimensional Obstacles. Part II: Upwind Flow Reversal Zone. *J. Atmos. Sci.*, **47**, 1498-1511.

Tang, M. and E. Reiter, 1984: Plateau Monsoons of the Northern Hemisphere: A Comparison between North America and Tibet. *Mon. Wea. Rev.*, **112**, 617-637.

Toth, J.J. and R.H. Johnson, 1984: Summer Surface Flow Characteristics over Northeast Colorado. *Mon. Wea. Rev.*, **113**, 1458-1649.

Tremback, C.J. 1990: Numerical Simulation of a Mesoscale Convective Complex: Model Development and Numerical Results. Atmospheric Science Paper # 465, Colorado State University, Fort Collins, CO.

Tremback, C.J. and R. Kessler, 1985: A surface temperature and moisture parameterization for use in mesoscale numerical models. Preprints, *7th Conference on Numerical Weather Prediction*, 17-20 June, 1985, Montreal, Canada, Amer. Meteor. Soc.

Tremback, C.J., G.J. Tripoli, R. Arritt, W.R. Cotton, and R.A. Pielke, 1986: The regional atmospheric modeling system. *Proc. Internat. Conf. Development and Application of Computer Techniques to Environmental Studies*, November, Los Angeles, CA; P. Zanetti (ed.), Computational Mechanics Publications, Boston, 601-607.

Tripoli, G.J,, 1986: A Numerical Investigation of an Orogenic Mesoscale Convective System. Atmospheric Science Paper # 401, Colorado State University, Fort Collins, CO.

Tripoli, G.J. and W.R. Cotton, 1982: The Colorado State University Three-Dimensional Cloud/Mesoscale Model-1982. Part I: General Theoretical Framework and Sensitivity Experiments. *Journal de Rech. Atmos.*, **16**, 185-220.

Tripoli, G.J. and W.R. Cotton, 1989a: Numerical Study of an Observed Mesoscale Convective System. Part I: Simulated Genesis and Comparison with Observations. *Mon. Wea. Rev.*, **117**, 273-304.

Tripoli, G.J. and W.R. Cotton, 1989b: Numerical Study of an Observed Mesoscale Convective System. Part II: Analysis of Governing Dynamics. *Mon. Wea. Rev.*, **117**, 305-328.

Tyson, P.D. and R.A. Preston-White, 1972: Observations of Regional Topographically-induced Wind Systems in Natal. *J. Appl. Meteor.*, **11**, 643-650.

Wetzel, P.J., 1973: Moisture Sources and Flow Patterns During the Northeast Colorado Hail Season. M.S. Thesis, Colorado State University Department of Atmospheric Science, Fort Collins, CO.

Whiteman, C.D., 1980: Breakup of Temperature Inversions in Colorado Mountain Valleys. Atmospheric Science Paper # 328, Colorado State University, Fort Collins, CO.

Whiteman, C.D. and T.B. McKee, 1982: Breakup of Temperature Inversions in Deep Mountain Valleys. Part II: Thermodynamic Model. *J. Appl. Meteor.*, **21**, 290-302.

Wilczak, J.M. and J.W. Glendening, 1988: Observations and Mixed-Layer Modeling of a Terrain-Induced Mesoscale Gyre: The Denver Cyclone. *Mon. Wea. Rev.*, **116**, 2688-271.

Yamada, T., 1977: A Numerical Experiment on Pollutant Dispersion in a Horizontally-Homogeneous Atmospheric Boundary Layer. *Atmos. Environ.*, **11**, 1015-1024.

APPENDIX A.
THE EQUATIONS USED IN THE VERTICAL DIFFUSION SCHEME

A modified Mellor-Yamada Level 2.5 closure scheme from Helfand and Labraga (1988) is added to the CSU RAMS[1]. This scheme uses turbulent kinetic energy (TKE) to predict the vertical diffusion coefficients for momentum and scalars (which includes potential temperature). A level 2.5 closure scheme (Yamada, 1977) is used where the turbulence is decaying, and level 2.0 closure is used where the turbulence is growing.

The shear production of TKE is calculated by:

$$K_m \left[\left(\frac{\partial u}{\partial z} \right)^2 + \left(\frac{\partial v}{\partial z} \right)^2 \right] \tag{A.1}$$

where u and v are horizontal wind components and K_m is the coefficient for vertical diffusion of momentum. The buoyant production of TKE is calculated by:

$$-K_h N^2 \tag{A.2}$$

where K_h is the coefficient for vertical diffusion of scalars and N^2 is the Brunt-Vaisala frequency. The dissipation of TKE is calculated by:

$$\frac{q^{3/2}}{l(16.6)} \tag{A.3}$$

where q is TKE and l is a length scale (in meters). The length scale used in this closure scheme is given by:

---

[1] Marek Uliasz and Tsengdar John Lee did much of the initial work of installing this scheme into the CSU RAMS. My major contributions to installing this scheme include detailed debugging, vectorization of the code, removing many "hardwired" features in the original scheme, and testing this scheme in the CSU RAMS.

$$l = \frac{k(z+z_o)}{1+\frac{k(z+z_o)}{l_\infty}} \qquad (A.4)$$

where k is the von Karmen constant (0.35) and z_o is the surface roughness. The length scale l_∞ is given by:

$$l_\infty = 0.1 \frac{\int_0^H z\sqrt{q}\,dz}{\int_0^H \sqrt{q}\,dz} \qquad (A.5)$$

where H is the top of the model domain.

The vertical diffusion coefficients for momentum and scalars are calculated by:

$$K_m = \sqrt{q}\, l\, S_m \qquad K_h = \sqrt{q}\, l\, S_h \qquad (A.6)$$

where S_m and S_h are defined later. The equations used for calculating S_m and S_h are determined by whether level 2.0 or level 2.5 closure is used. Level 2.0 is used for growing turbulence and level 2.5 is used otherwise. The tendency of turbulent kinetic energy is calculated by:

$$\frac{dq}{dt} = \begin{array}{c}\text{advection + horizontal diffusion + vertical diffusion} \\ \text{+ buoyant production (Eq A.1) + shear production (Eq A.2)} \\ \text{- dissipation (Eq A.3)}\end{array} . \qquad (A.7)$$

The equilibrium turbulence kinetic energy (q_r) is calculated by finding the TKE for which the shear production (eq A.1) plus the buoyant production (eq A.2) equals the dissipation (eq A.3). This can be expressed as:

$$K_m\left[\left(\frac{\partial u}{\partial z^2}\right)^2+\left(\frac{\partial v}{\partial z}\right)^2\right] - K_H N^2 = \frac{q_r^{3/2}}{l(16.6)} \qquad (A.8)$$

$$q_r = S_m \left[\left(\frac{\partial u}{\partial z} \right)^2 + \left(\frac{\partial v}{\partial z} \right)^2 \right] - S_h N^2 \qquad \text{(A.9)}$$

since

$$K_m = \sqrt{q_r}\, l S_m \qquad K_h = \sqrt{q_r}\, l S_h \ .$$

When solving for q_r, S_m and S_h are calculated using level 2.0 closure with $q=q_r$. (The equations for level 2.0 closure will be given below). If $q < q_r$, the turbulence is growing because the dissipation is smaller than the sum of buoyant and shear production. For growing turbulence level 2.0 closure is used. For $q \geq q_r$, level 2.5 closure is used.

For level 2.0 closure S_m and S_h are calculated from the following equations:

$$R_i = \frac{N^2}{\left[\left(\frac{\partial u}{\partial z} \right)^2 + \left(\frac{\partial v}{\partial z} \right)^2 \right]} \qquad \text{(A.10)}$$

$$R_f = 0.6588 \left(R_i + 0.1776 - \sqrt{R_i (R_i - 0.3221) + 0.03156} \right) \qquad \text{(A.11)}$$

$$S_h = \sqrt{\frac{q}{q_r}} * 2.583 \, \frac{(R_f - 0.1912)}{(R_f - 1)} \qquad \text{(A.12)}$$

$$S_m = \sqrt{\frac{q}{q_r}} * S_h * 0.7590 * \frac{(R_f - 0.2341)}{(R_f - 0.2231)} \ . \qquad \text{(A.13)}$$

For level 2.5 closure S_m and S_h are calculated from the following system of equations:

$$G_m = \frac{l^2}{q} \left[\left(\frac{\partial u}{\partial z} \right)^2 + \left(\frac{\partial v}{\partial z} \right)^2 \right] \qquad \text{(A.14)}$$

$$G_H = \frac{-l^2}{q} N^2 \qquad \text{(A.15)}$$

$$S_{m_i} = 0.6992 - 9.3395 * G_H \qquad \text{(A.16)}$$

$$S_{m_2} = 1 - (36.7188 - 187.441 * G_H + 88.839 * G_M) * G_M + (5.078 * G_M) \quad \text{(A.17)}$$

$$S_m = \frac{S_{m_1}}{S_{m_2}} \quad \text{(A.18)}$$

$$S_h = \frac{0.74 - 4.0848 * S_m * G_m}{1 - 30.592 * G_H} \quad . \quad \text{(A.19)}$$